Chemical and Physical Instability of Monoclonal Antibodies Induced by Metal-catalyzed Carbonylation

By

Yi Yang

Submitted to the Department of Pharmaceutical Chemistry and the Faculty of the Graduate School of the University of Kansas in partial fulfillment of the requirements for the degree of Doctor of Philosophy.

Dissertation Committee Members

_____
Chairperson: Dr. Christian Schöneich

_____
Dr. John Stobaugh

_____
Dr. David Volkin

_____
Dr. Teruna Siahaan

_____
Dr. Lynn Gennaro

_____
Dr. Heather Desaire

Date Defended: May 7, 2019

The Dissertation Committee for Yi Yang certifies that this is the approved version of the following dissertation:

Chemical and Physical Instability of Monoclonal Antibodies Induced by Metal-catalyzed Carbonylation

_____

Chairperson: Dr. Christian Schöneich

Date approved: May 7, 2019

ABSTRACT

In the pharmaceutical industry, recombinant monoclonal antibodies (mAbs) have become a major focus of therapeutic drug development due to their broad applications in many disease areas. During manufacturing and storage of mAb drug products, metal-catalyzed carbonylation, a post-translational modification referring to the formation of carbonyls (aldehydes and ketones) on proteins after metal-catalyzed oxidation, is a relevant product variant of mAbs, which may impact mAb safety and/or efficacy. However, to date, very little is known about the occurrence of metal-catalyzed carbonylation during mAb manufacturing and storage or the effects of metal-catalyzed carbonylation on chemical and physical stability of mAbs. To answer those questions, this dissertation first focused on developing a new protein carbonylation assay with improved assay precision and robustness over the conventional assays. Using the new protein carbonylation assay, a study was performed to investigate various cell culture and formulation factors, which revealed that iron ion, hydrogen peroxide, and polysorbate 20 can critically impact mAb carbonylation during manufacturing or storage. This study also revealed that metal-catalyzed carbonylation positively correlated with increased acidic charge heterogeneity and aggregation propensity of mAbs. To elucidate the increased acidic charge heterogeneity, the acidic fraction of a model IgG1 mAb after metal-catalyzed oxidation was collected and characterized, which showed that metal-catalyzed carbonylation products (primarily threonine carbonylation products) directly contributed to the increased acidic charge heterogeneity. Several additional oxidation products, such as carboxylic acids (from further oxidation of aldehydes) and pyroglutamate (from oxidation of proline residues in the hinge region), were identified for the first time in mAbs, which provides further explanation to the increased acidic charge heterogeneity. To elucidate the increased aggregation propensity, this dissertation used a model

stress system and anions from the Hofmeister series to investigate the effects of metal-catalyzed carbonylation on physical stability of the model IgG1 mAb. In particular, the investigation applied a site-specific carbonylation analysis, which revealed for the first time that mAb aggregation can be affected by carbonylation location, carbonylation type, and buffer type. These findings showed that effects of metal-catalyzed carbonylation on physical instability of mAbs can be much more complex than what have been previously proposed/suggested in the literature. Finally, this dissertation investigated formation of Schiff base crosslinks as a potential route of chemical instability of the metal-catalyzed carbonylation products. To facilitate the investigation, a new analytical methodology was developed to characterize crosslinked peptides. This new methodology addressed several key analytical challenges for crosslink analysis and successfully identified bissulfosuccinimidyl suberate (BS3)-crosslinked peptides in a BS3-treated mAb sample. Using the new analytical methodology, this study showed that Schiff base formation is a not major degradation pathway of mAbs even under a harsh condition by copper-catalyzed oxidation. In summary, this dissertation provided a comprehensive understanding of the chemical and physical instability of mAbs induced by metal-catalyzed carbonylation, which can help improve mAb stability against metal-catalyzed carbonylation in the future.

This doctoral dissertation is dedicated to:
My parents,
Baohuan Liu & Yunchang Yang

ACKNOWLEDGEMENTS

I would first like to thank my thesis research advisor Dr. Christian Schöneich for his guidance and for his support throughout my graduate study at the Pharmaceutical Chemistry department. It has been an amazing experience and an honor working under his guidance. I greatly appreciate his insight in the field of protein oxidation and his mentorship, which not only shaped my thesis but also helped me develop into an independent researcher. I would like to also thank the graduate students and research staffs in Dr. Schöneich's group, Huan Kang, Indira Prajapati, Natalia Subeizu, and Dr. Björn Peters, for their friendship and scientific discussions.

I would like to thank my dissertation committee members at KU: Dr. John Stobaugh, Dr. David Volkin, Dr.Teruna Siahaan, and Dr. Heather Desaire for their willingness to serve on my dissertation defense committee. I am grateful of their time and interest in evaluating my research, and their constructive feedback. In particular, I would like to thank Dr. John Stobaugh for reading my thesis and providing valuable suggestions and comments. Additionally, I would like to thank Nancy Helm for her support and assistance to my graduate study.

I would like to thank my mentor and dissertation committee member at Genentech: Dr. Lynn Gennaro for her continuous support to my graduate study at KU and for fostering my career development at Genentech. I would also like to thank her for reading my thesis and offering constructive feedback for improvement.

I would like to thank my colleagues and co-workers at Genentech for their collaboration and technical assistance. Dr. Inn Yuk provided constructive input and suggestions to my research. Anna Mah, Yutian Gan, Karina Padilla, and Dr. Huimin Zhang provided technical assistance. Finally, I would like to thank Genentech for the financial support and PAC management David Michels, Matt Kalo, and Pat Rancatore for their support.

Table of Contents

Chapter 1

Introduction

Metal-Catalyzed Antibody Carbonylation

Recombinant monoclonal antibodies (mAbs) are an important class of therapeutics for the treatment of many diseases.[1-2] Compared to small molecule drugs, mAbs are much more complex due to their heterogeneous nature.[3] A major source of the mAb heterogeneity are post translational modifications (PTMs) introduced to mAbs during manufacturing and/or storage.[4] Among the various PTMs, metal-catalyzed oxidation is a highly relevant degradation pathway of mAbs since mAbs are in contact with metal or metal ions during the manufacturing or the storage processes. For example, during cell culture production, iron ions at concentrations of 0.1-0.5 mM are used in the cell culture media to increase mAb production titers.[5] During purification or storage, stainless steel is a common surface contact material.[6] The iron ions present in the cell culture media or leached from the stainless steel can cause methionine[7-8] and histidine oxidation[8] in the Fc region. Other than methionine and histidine oxidation, metal-catalyzed protein carbonylation, referring to the formation of aldehyde/ketone groups, primarily on Arg, Lys, Pro, and Thr,[9-10] is a major degradation pathway caused by metal-catalyzed oxidation reactions.[9] From various studies, the levels of metal-catalyzed carbonylation products were found to be several orders of magnitude greater than those of other oxidation products.[11-12] Metal-catalyzed carbonylation is also widely accepted as a biomarker for oxidative stress,[13-14] because the metal-catalyzed carbonylation is an irreversible and unrepairable PTM in biological systems. Interestingly, in the pharmaceutical industry, the knowledge on metal-catalyzed carbonylation as a degradation product of mAbs is limited. In one study, Bee et al. showed that a significant amount of protein carbonylation, at approximately 0.8 mole of carbonyl per mole of mAb, but no methionine oxidation, was found in the mAbs absorbed to the stainless steel surface,[15] which suggests that metal-catalyzed carbonylation may increase mAb aggregation propensity and thus

can potentially affect mAb product quality and stability. In another study, Purdie et al. showed that cell culture medium composition affected the extent of mAb carbonylation, and also reported a positive correlation between mAb carbonylation and mAb aggregation.[16] However, there is a lack of a comprehensive study on various factors that impact mAb carbonylation and on how mAb carbonylation impacts the physical and chemical stability of mAbs.

Analytical Methods for Quantifying Protein Carbonylation

Many different carbonylation assays have been developed for studying protein carbonylation.[17] Historically, quantitation of protein carbonyls is usually based on the unique characteristics of the hydrazines and the corresponding hydrazones after the derivatization. For example, a widely used spectrophotometric carbonylation assay measures the absorbance of a derived sample at 375 nm, where the derivatization reagent, 2,4-dinitrophenylhydrazine (DNPH), and the resulting hydrazone, strongly absorb.[18] A fluorometric carbonylation assay measures the fluorescence with excitation at 485 nm and emission at 535 nm of a derived sample after the derivatization with fluorescein thiosemicarbazide.[19] An ELISA carbonylation assay uses anti-DNPH antibody for quantification after the derivatization of a sample with DNPH.[20] While different hydrazine/hydrazide reagents have been employed for the derivatization and the quantitation purposes, a common procedure in these protein carbonylation assays is the removal of the unreacted hydrazine/hydrazide after the derivatization step to prevent over-quantification of the carbonylation levels.[21] Typically, the unreacted hydrazine/hydrazide is removed through protein precipitation and washing, which is a labor-intensive process and constitutes a major source of experimental variability.[21] In fact, a study by Matthijssens et al. demonstrated that two additional washing steps during sample preparation reduced the carbonylation result by 15% when using the DNPH spectrophotometric carbonylation assay.[22] The poor assay precision and

labor-intensive nature associated with the sample precipitation and washing steps can make it difficult to broadly apply these carbonylation assays to measure mAb carbonylation for product characterization, development, and quality control. While improved ELISA[23] and DNPH[24] assays have been recently reported, to the best of our knowledge, there has not been a study that comprehensively addresses various assay performance issues inherent to protein carbonylation measurement, particularly issues related to assay robustness.

Factors Influencing the Extent and Specificity of Protein Carbonylation

Based on the mechanism proposed by Stadtman for metal-catalyzed carbonylation,[9] protein carbonylation involves a site-specific Fenton-like reaction, where the hydroxyl radical attacks the side chain of the residue adjacent to a metal binding site to form the carbonyl group. Presumably, metal ions, oxidants (such as hydrogen peroxide), and protein structure/conformation may all affect the extent and specificity of carbonylation. However, from the protein formulation perspective, how various formulation factors, such as buffer species, formulation excipients, and surfactants, affect protein carbonylation is still not well understood. In a study by Arai et al., the effects of bicarbonate and phosphate buffers on metal-catalyzed oxidation of low-density lipoprotein (LDL) were studied[25]. Under the same stress condition, a greater extent of protein carbonylation of LDL was observed in the bicarbonate buffer than in the phosphate buffer, for which the authors suggested that a complex interaction between bicarbonate and iron ions may be responsible and that intermediary formation of a carbonate radical may result in much more selective oxidation reactions. In recent studies by Rao et al.[23, 26], several narrowly specified stress conditions were tested for their effects on the extent of protein carbonylation of β-glucosidase, rabbit IgG, and transferrin. These experiments suggest that the extent of carbonylation is Fe^{2+} concentration dependent; however, the effects of other factors,

such as the protein type and the addition of mannitol, were found to vary from case to case.[23] Clearly, more studies are needed to understand how the various factors affect the extent and specificity of carbonylation of mAbs, particularly under the relevant manufacturing and storage conditions, which can help us develop better manufacturing processes and stable protein formulations against oxidative carbonylation.

For the site specificity of oxidative carbonylation, our previous work showed that the common carbonylation sites on three different mAbs were solvent-exposed.[27] However, not all solvent-exposed lysine, arginine, proline, and threonine residues are prone to oxidative carbonylation. Apparently, the occurrence and distribution of oxidative carbonylation sites on proteins are not random. One observation is that the protein carbonylation sites tend to "cluster together".[28] This observation suggests an autoxidation type of mechanism, i.e. self-propagation of carbonylation sites.[28] Another theory suggested that protein sequence regions that are enriched with Arg, Lys, Pro, and Thr residues are oxidative carbonylation hot spots.[29] However, it is unclear if we can use these empirical observations to predict carbonylation hot spots on mAbs. In this work, we will identify carbonylation hot spots on mAbs by characterizing highly carbonylated mAb samples, and understand if there are any sequence motifs that dictate site-specific antibody carbonylation.

Effects of Metal-Catalyzed Carbonylation on Protein Stability

As the result of the oxidative carbonylation, the positive charge on lysine and arginine side chains and the steric constrains from proline residues are lost. Those changes could lead to increased protein aggregation propensity. Based on molecular dynamics simulation results, Petrov and Zagrovic proposed that the carbonylation of lysine and arginine residues are equivalent to introducing charge-neutral and hydrophobic mutations.[30] However, this theoretical

model does not provide a comprehensive picture of how various carbonylation species impact the physical stability of mAbs. For example, it is not known if lysine and arginine carbonylation products play a more dominant role than proline and threonine carbonylation products in driving the formation of aggregates. To elucidate the detailed effects and mechanisms at the site-specific level, we will apply stress conditions to carbonylated mAbs and characterize the induced aggregation/precipitation to investigate if certain carbonylation species are preferentially enriched in the aggregates.

From the chemical stability perspective, the aldehyde products (amino-adipic semialdehyde and glutamic semialdehyde) from the carbonylation of lysine, arginine, and proline residues may undergo further reactions. One of the reactions is the oxidation of the aldehydes to the respective carboxylic acids (2-aminoadipic acid and glutamic acid), which leads to a decreased isoelectric point of proteins. This mechanism has been hypothesized by Stadtman to explain the formation of more acidic forms, observed on the isoelectric focusing gel images of *E. Coli.* glutamine synthetase after metal-catalyzed oxidation.[9, 31] However, to the best of our knowledge, to date, no report has directly investigated these potential carboxylic acid species to understand the acidic charge variants induced by metal-catalyzed oxidation. Therefore, it will be interesting to investigate if these carboxylic acid products constitute a significant degradation pathway for the induced acidic charge variants on mAbs. Another reaction is the formation of a Schiff base between an aldehydes and a primary amine, which generates intra- or inter-peptide crosslinks, which could contribute to the formation of aggregates.[32] For mAbs, formation of these potential crosslink products has not been well studied, particularly after metal-catalyzed oxidation.

Significance

In the pharmaceutical industry, metal-catalyzed carbonylation represents a relatively new product variant of mAbs. Recently, this product variant is gaining more interest from both the pharmaceutical industry and the FDA, since metal-catalyzed carbonylation may pose safety, immunogenicity, or efficacy concerns about protein therapeutics. For example, using transgenic mouse models, Filipe et al. showed that mAbs stressed with metal-catalyzed oxidation were more immunogenic than mAbs stressed with other conditions.[33] This finding suggests that carbonylation, a major degradation product of metal-catalyzed oxidation, may critically impact the immunogenicity of mAbs. However, to date, very little is known about the mechanisms for the occurrence of metal-catalyzed carbonylation or the effect of this type of PTM on therapeutic mAb products. This thesis seeks to establish analytical methods to characterize carbonylation and related degradation products on mAbs and to obtain in-depth understandings of how various factors during mAb manufacturing and storage may impact mAb carbonylation. This knowledge will be valuable for the industry to develop manufacturing processes or formulations to control mAb carbonylation. In addition, this thesis seeks to elucidate the impact of oxidative carbonylation on the physical and chemical stability of mAbs, which will be useful for designing mAbs with improved stability against metal-catalyzed carbonylation in the future.

Specific Aim 1: **to develop an improved analytical method for quantifying protein carbonylation (Chapter 2)**.

The existing assays for quantifying protein carbonylation suffer from rather crude performance issues,[21] which have been attributed to protein precipitation and washing used in the sample preparation procedures. Given that the performance issues with current assays may hinder progress on our study of mAb carbonylation, this work developed an improved analytical method to address the analytical challenges/drawbacks with the conventional protein

carbonylation assays. This work first focused on identifying a new reagent for the derivatization and quantitation of protein carbonyls that does not require protein precipitation or washing. This work then developed the derivatization and sample preparation conditions to achieve optimal assay performance. Finally, an extensive set of experiments to evaluate the performance of the new method was performed, which showed that the new protein carbonylation assay has excellent assay precision, linearity, reproducibility, and robustness for quantifying total protein carbonylation of mAbs. These assessments demonstrated that the new assay represents a significant improvement over the commonly used assays.

Specific Aim 2: **to understand bioprocessing and formulation factors that critically impact mAb carbonylation during manufacturing and storage (Chapter 2).**

From the mAb bioprocessing prospective, the level of iron ions in cell culture media may play a critical role in generating mAb carbonylation. This study will perform cell culture experiments with various levels of iron ions to understand the effect of iron on mAb carbonylation during cell culture production. From the formulation perspective, this study will investigate how the presence of iron ions and polysorbate 20 in the formulations impact mAb carbonylation under long term storage, which can help identify critical formulation factors for mAb carbonylation and the related mAb instability during storage. Additionally, this study will evaluate relative effects of iron (II) and hydrogen peroxide on mAb carbonylation to explain the findings from the cell culture and the storage experiments. Finally, this study will investigate the relationship between carbonylation and mAb product quality, such as size and charge heterogeneity, from all the experiments, to gain an initial understanding of the effects of mAb carbonylation on physical and chemical instability of mAbs.

Specific Aim 3: **to elucidate the effect of oxidative carbonylation on acidic charge heterogeneity of mAbs after metal-catalyzed oxidation (Chapter 3).**

The findings from Chapter 2 revealed a positive correlation between metal-catalyzed carbonylation and formation of acidic charge heterogeneity in mAbs. This chapter describes a study on the mechanism and the related degradation products to explain the observed correlation between mAb carbonylation and the induced acidic charge variants after metal-catalyzed oxidation. This study will induce the formation of acidic charge variants on a model IgG1 mAb by iron (II) and hydrogen peroxide, and then fraction collect the acidic and the main peak regions from an ion exchange chromatography column. Subsequently, an extended characterization of mAb carbonylation products will be performed to address the following questions: 1) are carbonylation products enriched in the acidic fraction? 2) what types of carbonylation products are enriched in the acidic region? 3) is there any further oxidation of aldehydes (to carboxylic acid), and if so, are these products a major component in the acidic fraction? 4) does mAb conformation play a critical factor in the induced acidic charge variants? To facilitate these investigations, the study will also optimize the site-specific carbonylation analysis method for relative quantitation of site-specific carbonylation products by LC-MS/MS analysis.

Specific Aim 4: **to elucidate the effect of oxidative carbonylation on physical stability of mAbs (Chapter 4).**

The findings from Chapter 2 suggested that metal-catalyzed carbonylation may contribute to mAb aggregation. To elucidate the effect of oxidative carbonylation on physical stability of mAbs, this chapter will compare the aggregation/precipitation of oxidized and unstressed mAb samples under a commonly used stir stress condition.[8, 34] This comparison will help differentiate the effects of oxidation products (including oxidative carbonylation) from those of intrinsic mAb

aggregation factors. This chapter will then describe an investigation aimed at determining if there is any preferential enrichment of carbonylation products in the aggregates or in the supernatants. In particular, from a site-specific perspective, it will be interesting to understand if carbonylation type or location plays a role in the aggregation/precipitation of the tested mAb samples, and if there are any carbonylation hotspots that drive mAb aggregation/precipitation. In addition, the chapter will probe the effect of oxidative carbonylation on the physical stability of mAbs by studying the aggregation/precipitation behaviors in buffers that contains various Hofmeister anions. This will aid in determining if the effect of oxidative carbonylation may be influenced by specific interactions with the anions. The knowledge gained from these studies will be useful for designing mAbs with improved stability against metal-catalyzed carbonylation in the future.

Specific Aim 5: **to develop a new analytical method to investigate formation of Schiff base and other crosslinks in mAbs after metal-catalyzed carbonylation (Chapter 5).**

Formation of Schiff base crosslinks between aldehydes (as generated from carbonylation of Arg, Lys, and Pro residues) and primary amines (such as N-terminus and lysine side chain) could represent a mechanism for the increase of acidic charge variants and aggregates in mAbs after metal-catalyzed oxidation. To investigate this potential mechanism for the induced chemical and physical instability of mAbs after metal-catalyzed oxidation, this chapter describes the development of a new analytical method using Strong cation exchange Enrichment and Enzymatic MS^2 ($SEEMS^2$) to enrich and identify crosslinked peptides. The main goal for developing this new method is to reduce the difficulty and complexity with crosslink analysis. Specifically, crosslinked peptides are often in low abundance;[35] and the MS^2 spectra of crosslinked peptides are often very complex to interpret.[36] To demonstrate the feasibility of the new method, this work will include characterization of crosslinked peptides in a BS3-crosslinked

model mAb sample. Subsequently, this method will be applied to investigate mAb crosslinks after copper-catalyzed oxidation. The rationale for selecting copper-catalyzed oxidation instead of iron-catalyzed oxidation is threefold. First, copper-catalyzed oxidation is more effective than iron-catalyzed oxidation in generating carbonylation on mAbs and other proteins.[26, 37] Potential Schiff base crosslink products are, therefore, expected to be more abundant in mAbs after copper-catalyzed oxidation than after iron-catalyzed oxidation, which would be beneficial to the investigation. Second, copper-catalyzed oxidation was found to be more effective than iron-catalyzed oxidation in generating dityrosine crosslinks in lens proteins.[38] It will be interesting to understand if any dityrosine crosslink products in mAbs can be identified after copper-catalyzed oxidation. Third, after stressed by copper-catalyzed oxidation, mAbs were found to induce immunogenicity in transgenic mice.[33] It will be interesting to identify oxidation-induced mAb crosslink products, which may help elucidate the observed immunogenicity. By applying the SEEMS[2] method to investigate potential crosslink products in a model mAb after copper-catalyzed oxidation, this study seeks to determine if formation of Schiff base crosslinks is a major degradation pathway related to oxidative carbonylation, and if the Schiff base crosslinks are a major factor for the chemical and physical instability of mAbs induced after metal-catalyzed oxidation. Additionally, this study seeks to identify other types of crosslinks, such as di-tyrosine crosslinks, which can help better understand the nature of chemical and physical instability of mAbs induced after metal-catalyzed oxidation.

Reference

1. Reichert, J. M., Monoclonal antibodies as innovative therapeutics. *Curr Pharm Biotechnol* **2008,** *9* (6), 423-30.

2. Laffly, E.; Sodoyer, R., Monoclonal and recombinant antibodies, 30 years after. *Hum Antibodies* **2005,** *14* (1-2), 33-55.

3. Liu, H.; Gaza-Bulseco, G.; Faldu, D.; Chumsae, C.; Sun, J., Heterogeneity of monoclonal antibodies. *J Pharm Sci* **2008,** *97* (7), 2426-47.

4. Wang, W.; Singh, S.; Zeng, D. L.; King, K.; Nema, S., Antibody structure, instability, and formulation. *J Pharm Sci* **2007,** *96* (1), 1-26.

5. Bai, Y.; Wu, C.; Zhao, J.; Liu, Y. H.; Ding, W.; Ling, W. L., Role of iron and sodium citrate in animal protein-free CHO cell culture medium on cell growth and monoclonal antibody production. *Biotechnol Prog* **2011,** *27* (1), 209-19.

6. Vazquez-Rey, M.; Lang, D. A., Aggregates in monoclonal antibody manufacturing processes. *Biotechnol Bioeng* **2011,** *108* (7), 1494-508.

7. Lam, X. M.; Yang, J. Y.; Cleland, J. L., Antioxidants for prevention of methionine oxidation in recombinant monoclonal antibody HER2. *J Pharm Sci* **1997,** *86* (11), 1250-5.

8. Luo, Q.; Joubert, M. K.; Stevenson, R.; Ketchem, R. R.; Narhi, L. O.; Wypych, J., Chemical modifications in therapeutic protein aggregates generated under different stress conditions. *J Biol Chem* **2011,** *286* (28), 25134-44.

9. Stadtman, E. R., Metal ion-catalyzed oxidation of proteins: biochemical mechanism and biological consequences. *Free Radic Biol Med* **1990,** *9* (4), 315-25.

10. Yang, Y.; Stella, C.; Wang, W.; Schoneich, C.; Gennaro, L., Characterization of oxidative carbonylation on recombinant monoclonal antibodies. *Anal Chem* **2014,** *86* (10), 4799-806.

11. Dean, R. T.; Fu, S.; Stocker, R.; Davies, M. J., Biochemistry and pathology of radical-mediated protein oxidation. *Biochem J* **1997,** *324 (Pt 1)*, 1-18.

12. Stadtman, E. R., Protein oxidation and aging. *Free Radic Res* **2006,** *40* (12), 1250-8.

13. Dalle-Donne, I.; Rossi, R.; Giustarini, D.; Milzani, A.; Colombo, R., Protein carbonyl groups as biomarkers of oxidative stress. *Clin Chim Acta* **2003,** *329* (1-2), 23-38.

14. Dalle-Donne, I.; Giustarini, D.; Colombo, R.; Rossi, R.; Milzani, A., Protein carbonylation in human diseases. *Trends Mol Med* **2003,** *9* (4), 169-76.

15. Bee, J. S.; Davis, M.; Freund, E.; Carpenter, J. F.; Randolph, T. W., Aggregation of a monoclonal antibody induced by adsorption to stainless steel. *Biotechnol Bioeng* **2010,** *105* (1), 121-9.

16. Purdie, J. L.; Kowle, R. L.; Langland, A. L.; Patel, C. N.; Ouyang, A.; Olson, D. J., Cell culture media impact on drug product solution stability. *Biotechnol Prog* **2016,** *32* (4), 998-1008.

17. Yan, L. J.; Forster, M. J., Chemical probes for analysis of carbonylated proteins: a review. *J Chromatogr B Analyt Technol Biomed Life Sci* **2011,** *879* (17-18), 1308-15.

18. R.L.Levine, D. G., C.N.Oliver**,** A.Amici, I.Climent, A.G.Lenz, B.W.Ahn, S. Shaltiel, E.R.Stadtman, *Determination of Carbonyl Content in Oxidatively Modified Proteins*. Methods in Enzymology: Methods in Enzymology, 1990; Vol. 186, p 464–478.

19. Mohanty, J. G.; Bhamidipaty, S.; Evans, M. K.; Rifkind, J. M., A fluorimetric semi-microplate format assay of protein carbonyls in blood plasma. *Analytical biochemistry* **2010,** *400* (2), 289-94.

20. Buss, H.; Chan, T. P.; Sluis, K. B.; Domigan, N. M.; Winterbourn, C. C., Protein carbonyl measurement by a sensitive ELISA method. *Free radical biology & medicine* **1997,** *23* (3), 361-6.

21. Rogowska-Wrzesinska, A.; Wojdyla, K.; Nedic, O.; Baron, C. P.; Griffiths, H. R., Analysis of protein carbonylation--pitfalls and promise in commonly used methods. *Free Radic Res* **2014,** *48* (10), 1145-62.

22. Matthijssens, F. B., Bart P.; Vanfleteren, Jacques R., Evaluation of Different Methods for Assaying Protein Carbonylation. *Current Analytical Chemistry* **2007,** *3* (2), 93-102.

23. Uehara, H.; Rao, V. A., Metal-mediated protein oxidation: applications of a modified ELISA-based carbonyl detection assay for complex proteins. *Pharm Res* **2015,** *32* (2), 691-701.

24. Mesquita, C. S.; Oliveira, R.; Bento, F.; Geraldo, D.; Rodrigues, J. V.; Marcos, J. C., Simplified 2,4-dinitrophenylhydrazine spectrophotometric assay for quantification of carbonyls in oxidized proteins. *Analytical biochemistry* **2014,** *458*, 69-71.

25. Arai, H.; Berlett, B. S.; Chock, P. B.; Stadtman, E. R., Effect of bicarbonate on iron-mediated oxidation of low-density lipoprotein. *Proc Natl Acad Sci U S A* **2005,** *102* (30), 10472-7.

26. Kryndushkin, D.; Rao, V. A., Comparative Effects of Metal-Catalyzed Oxidizing Systems on Carbonylation and Integrity of Therapeutic Proteins. *Pharm Res* **2016,** *33* (2), 526-39.

27. Yang, Y.; Stella, C.; Wang, W.; Schoneich, C.; Gennaro, L. A., Characterization of Oxidative Carbonylation on Recombinant Monoclonal Antibodies. *Analytical chemistry* **2014**.

28. Rao, R. S.; Moller, I. M., Pattern of occurrence and occupancy of carbonylation sites in proteins. *Proteomics* **2011,** *11* (21), 4166-73.

29. Maisonneuve, E.; Ducret, A.; Khoueiry, P.; Lignon, S.; Longhi, S.; Talla, E.; Dukan, S., Rules governing selective protein carbonylation. *PLoS One* **2009,** *4* (10), e7269.

30. Petrov, D.; Zagrovic, B., Microscopic analysis of protein oxidative damage: effect of carbonylation on structure, dynamics, and aggregability of villin headpiece. *J Am Chem Soc* **2011,** *133* (18), 7016-24.

31. Rivett, A. J.; Levine, R. L., Metal-catalyzed oxidation of Escherichia coli glutamine synthetase: correlation of structural and functional changes. *Arch Biochem Biophys* **1990,** *278* (1), 26-34.

32. Usui, K.; Hulleman, J. D.; Paulsson, J. F.; Siegel, S. J.; Powers, E. T.; Kelly, J. W., Site-specific modification of Alzheimer's peptides by cholesterol oxidation products enhances aggregation energetics and neurotoxicity. *Proc Natl Acad Sci U S A* **2009,** *106* (44), 18563-8.

33. Filipe, V.; Jiskoot, W.; Basmeleh, A. H.; Halim, A.; Schellekens, H.; Brinks, V., Immunogenicity of different stressed IgG monoclonal antibody formulations in immune tolerant transgenic mice. *MAbs* **2012,** *4* (6), 740-52.

34. Telikepalli, S. N.; Kumru, O. S.; Kalonia, C.; Esfandiary, R.; Joshi, S. B.; Middaugh, C. R.; Volkin, D. B., Structural characterization of IgG1 mAb aggregates and particles generated under various stress conditions. *J Pharm Sci* **2014,** *103* (3), 796-809.

35. Tinnefeld, V.; Venne, A. S.; Sickmann, A.; Zahedi, R. P., Enrichment of Cross-Linked Peptides Using Charge-Based Fractional Diagonal Chromatography (ChaFRADIC). *J Proteome Res* **2017,** *16* (2), 459-469.

36. Giese, S. H.; Fischer, L.; Rappsilber, J., A Study into the Collision-induced Dissociation (CID) Behavior of Cross-Linked Peptides. *Mol Cell Proteomics* **2016,** *15* (3), 1094-104.

37. Kryndushkin, D.; Wu, W. W.; Venna, R.; Norcross, M. A.; Shen, R. F.; Rao, V. A., Complex Nature of Protein Carbonylation Specificity After Metal-Catalyzed Oxidation. *Pharm Res* **2017,** *34* (4), 765-779.

38. Kato, Y.; Kitamoto, N.; Kawai, Y.; Osawa, T., The hydrogen peroxide/copper ion system, but not other metal-catalyzed oxidation systems, produces protein-bound dityrosine. *Free Radic Biol Med* **2001,** *31* (5), 624-32.

Chapter 2

Investigation of Metal-Catalyzed Antibody Carbonylation with an Improved Protein Carbonylation Assay

INTRODUCTION

As previously reviewed in Chapter 1, metal-catalyzed protein carbonylation results in the formation of carbonyl species from lysine, arginine, proline, and threonine residues[1] (Figure 1). These carbonylation products could potentially have detrimental effects on mAb product quality. Therefore, it is important to understand how the metal-catalyzed carbonylation occurs during mAb production and storage. However, the current understanding of mAb carbonylation during bioprocess development (e.g., cell culture production) and pharmaceutical development (e.g., formulation and storage) is very limited. From the bioprocess development perspective, Purdie et al. showed that lowering the content of cysteine and ferric ammonium citrate in cell culture media reduced the extent of mAb carbonylation.[2] However, their study reported only relative levels of mAb carbonylation. From the pharmaceutical development perspective, Uehara and Rao showed that iron content, buffer type, and storage temperature affected the extent of carbonylation of rabbit IgG and other proteins.[3] Nevertheless, the underlying mechanisms for the interaction between iron ions and various formulation excipients to induce mAb carbonylation, and the physicochemical consequence of mAb carbonylation during storage remain poorly understood.

An analytical challenge for investigating mAb carbonylation is that conventional protein carbonylation assays have various assay performance issues. For example, the coefficient of variation (CV) of the commonly used 2,4-dinitrophenylhydrazine (DNPH) spectrophotometric assay exceeded 20%.[4] The large CV was attributed to the inconsistent removal of excess derivatization reagent, DNPH, during the protein precipitation and washing steps.[5-6] Another commonly used assay quantifies the carbonyl content by enzyme-linked immunosorbent assay (ELISA) with anti-dinitrophenylhydrazone (DNP) antibodies.[7] One limitation of the ELISA-

based carbonylation assay is that the assay requires a standard with a known protein carbonylation level. Given that it is difficult to know how accurate the predetermined carbonylation level was for the assay standard, significant assay error can be introduced, particularly when different assay standards are used by different laboratories.[5]

To overcome the assay performance issues with the commonly used carbonylation assays, we developed a protein **C**arbonylation **A**ssay using **L**ucifer **Y**ellow carbohydrazide (CALY) as the derivatization reagent. Like DNPH, Lucifer Yellow carbohydrazide (LY CH)[8] contains a hydrazide group, which reacts selectively with aldehydes and ketones on proteins.[9] Unlike DNPH, LY CH has significantly higher solubility in water,[10] which supports a simpler sample preparation without protein precipitation. To demonstrate the suitability of CALY for use in mAb bioprocess and pharmaceutical development, we evaluated the robustness, linearity, precision, accuracy, detection and quantitation limits of the assay.

After demonstrating suitable assay performance, we applied CALY to investigate mAb carbonylation under pharmaceutically relevant production, storage, and stress conditions. In the cell culture production study, we investigated the effect of iron concentration in a chemically-defined background. In the storage study, we investigated the effects of polysorbate 20 and iron during long-term storage. In the stress study, we investigated the effect of iron and hydrogen peroxide, key factors identified to control protein carbonylation.[1] These studies highlighted bioprocess and pharmaceutical conditions during production and storage that could increase mAb carbonylation. Finally, we also investigated the relationship between carbonylation and size or charge heterogeneity of mAbs. These investigations led to novel insights into the impact of metal-catalyzed carbonylation on mAb product quality.

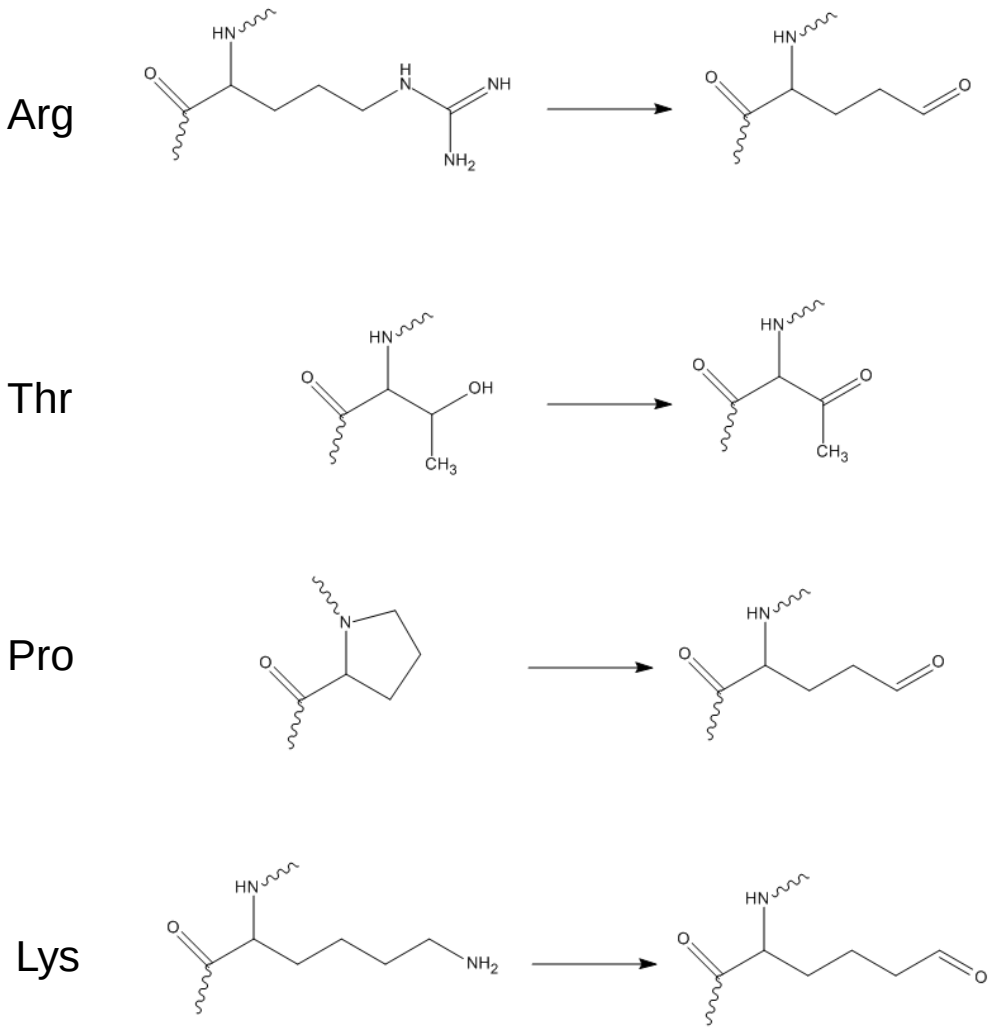

Figure 1. Oxidative carbonylation products of arginine (Arg), threonine (Thr), proline (Pro), and lysine (Lys).

MATERIALS AND METHODS

Materials

All mAbs are IgG1 and were manufactured by Genentech: mAb A was used for CALY development, the storage study, and the stress study; mAb B was used for the production study; mAbs C and D were used for additional stress studies. Lucifer Yellow carbohydrazide dilithium salt (Lucifer Yellow CH or LY CH), ferrous sulfate ($FeSO_4$), hydrogen peroxide solution (30% in H_2O, w/w), methionine, ethylenediaminetetraacetic acid (EDTA), sodium succinate, succinic acid, sodium phosphate (dibasic and monobasic), sodium chloride, sodium acetate, acetic acid, sodium hydroxide solution (1M in H_2O), 2-(N-morpholino)ethanesulfonic acid (MES), lithium hydroxide, reduced Triton X-100, and Polysorbate 20 (PS20) were purchased from Sigma-Aldrich (St. Louis, MO, USA). Amicon Ultra-15 30 kDa filter units were purchased from EMD Millipore (Billerica, MA, USA). The TSK G3000 SWXL (7.8x300mm) size exclusion column was purchased from Tosoh Bioscience (King of Prussia, PA, USA). The ProPac WCX 10 column was purchased from Dionex (Sunnyvale, CA, USA). The OxiSelect™ protein carbonyl assay kit was purchased from Cell Biolabs (San Diego, CA, USA). Carboxypeptidase B (CpB) was purchased from Roche Diagnostics (Mannheim, Germany).

Preparation of mAb Samples for the Development of CALY

For the development of CALY, two batches of a highly oxidized mAb A (batch 1 and batch 2) were prepared using the condition described previously.[11] Briefly, mAb A was mixed with ferrous sulfate and hydrogen peroxide to a final concentration of 5 mg/mL, 2 mM, and 10 mM, respectively, in 50 mM sodium succinate, pH 6.5. The reaction mixture was incubated at room temperature for 1.5 hours and the reaction subsequently stopped by adding excess methionine and EDTA.

Determination of Protein Carbonylation Levels by CALY

The workflow of CALY is shown in Figure 2. The mAb samples were derivatized by LY CH in 50 mM MES, 0.05% reduced Triton X-100, pH 6.0 (titrated with lithium hydroxide). The LY CH-to-mAb molar ratio was 8,000:1, where the final mAb concentration was 0.5 mg/mL. The derivatization was carried out at 37°C in the dark for 18 hours. After the derivatization, the mAb samples (500 µL) were buffer-exchanged three times into a buffer containing 200 mM potassium phosphate, 250 mM potassium chloride, pH 6.2, using Amicon Ultra-15 30 kDa filters to remove the excess LY CH (with a dilution factor of ~30 for each round of buffer exchange). Subsequently, the LY CH-derivatized mAbs were analyzed by size exclusion chromatography (SEC), where 25 µL of the mAb material (approximately 25 µg of protein) was injected onto a TSK G3000 SWXL (7.8x300 mm) size exclusion column. The mobile phase was 200 mM potassium phosphate, 250 mM potassium chloride, pH 6.2. The column temperature was controlled at 25°C and the HPLC autosampler temperature was controlled at 8°C. An isocratic flow of 0.5 ml/min was employed. The effluent was monitored by UV absorbance at 280 and 428 nm. Manual integration of all the peaks from approximately 10 to 22 minutes was performed to determine the total peak areas at 280 and 428 nm (A_{280} and A_{428}) for the LY CH-derivatized mAb sample as shown in Figure 3.

To quantify carbonylation levels, mAb (not derivatized by LY CH) and LY CH were used as the standards. The mAb standard curves were prepared by SEC analysis of 25 µL of a mAb standard at various protein concentrations (0.25, 0.5, 1, 2, and 3 mg/mL), as shown in Figures 4-A and 4-B. The LY CH standard curves were prepared similarly by SEC analysis of 25 µL of LY CH at various concentrations (1, 5, 10, 15, and 20 uM), as shown in Figures 4-C and 4-D. Carbonylation levels (z/x) were determined by solving the two-variable (x and z) linear

equations: A280=m1x+b1+m3z+b3 and A428=m2x+b2+m4z+b4, where x is the protein concentration (mg/mL) and z is the molar concentration (μM = nmol/mL) of carbonyl groups; A280 is the integrated peak area of the LY CH-derived mAb at 280 nm (Figure 3A); A428 is the integrated peak area of the LY CH-derived mAb at 428 nm (Figure 3B); m1 to m4 and b1 to b4 are constants obtained from linear regression fitting of the standard curves (Figure 4).

The carbonylation level of a mAb sample was reported in nmol/mg as a ratio of the molar concentration of carbonyl groups (z) to the protein concentration (x), and can be determined using the following equations (derived by solving the two-variable linear equations):

$$x = [m4*A280 - m3*A428 - m4*(b1+b3) + m3*(b2+b4)] / (m4*m1 - m2*m3)$$

$$z = [m2*A280 - m1*A428 - m2*(b1+b3) + m1*(b2+b4)] / (m2*m3 - m1*m4)$$

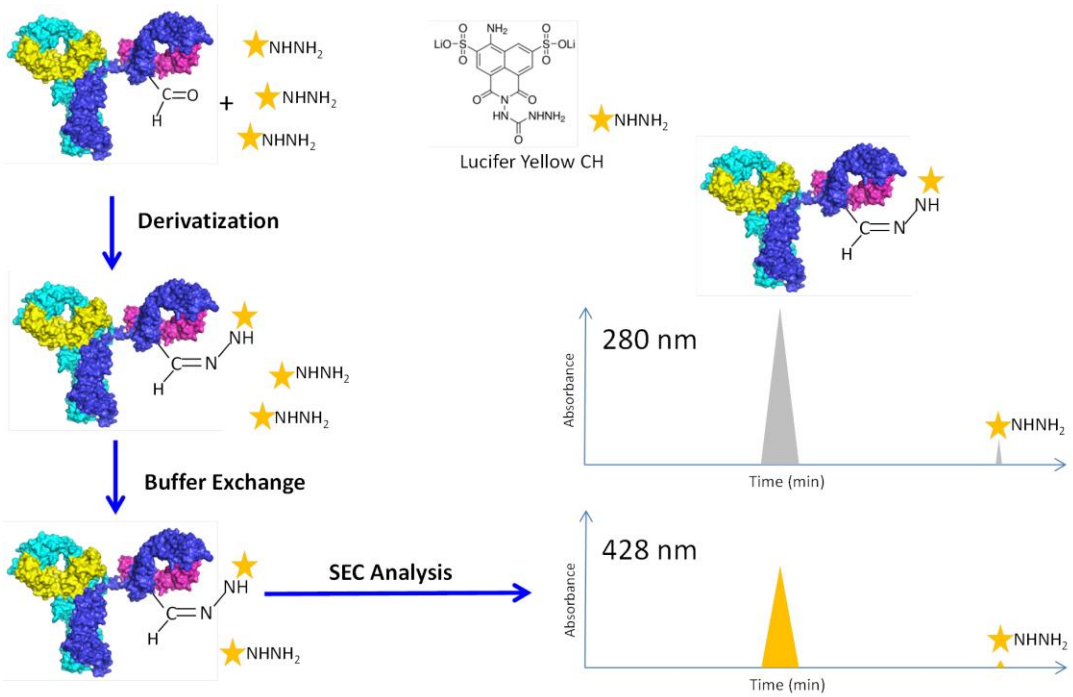

Figure 2. Illustration of the workflow of CALY, which includes derivatization, buffer exchange, and size exclusion chromatography analysis.

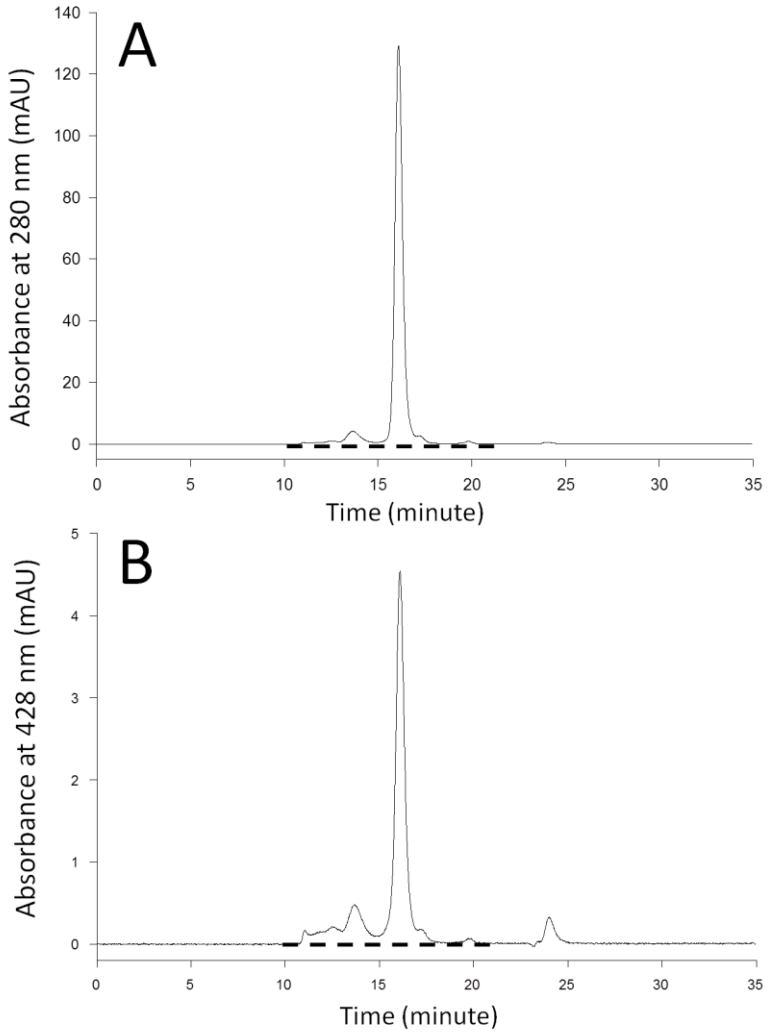

Figure 3. Typical size exclusion chromatograms, with absorbance at 280 nm (A) and 428 nm (B), of a derivatized and buffer-exchanged mAb sample. Peak integration is illustrated with the dashed lines.

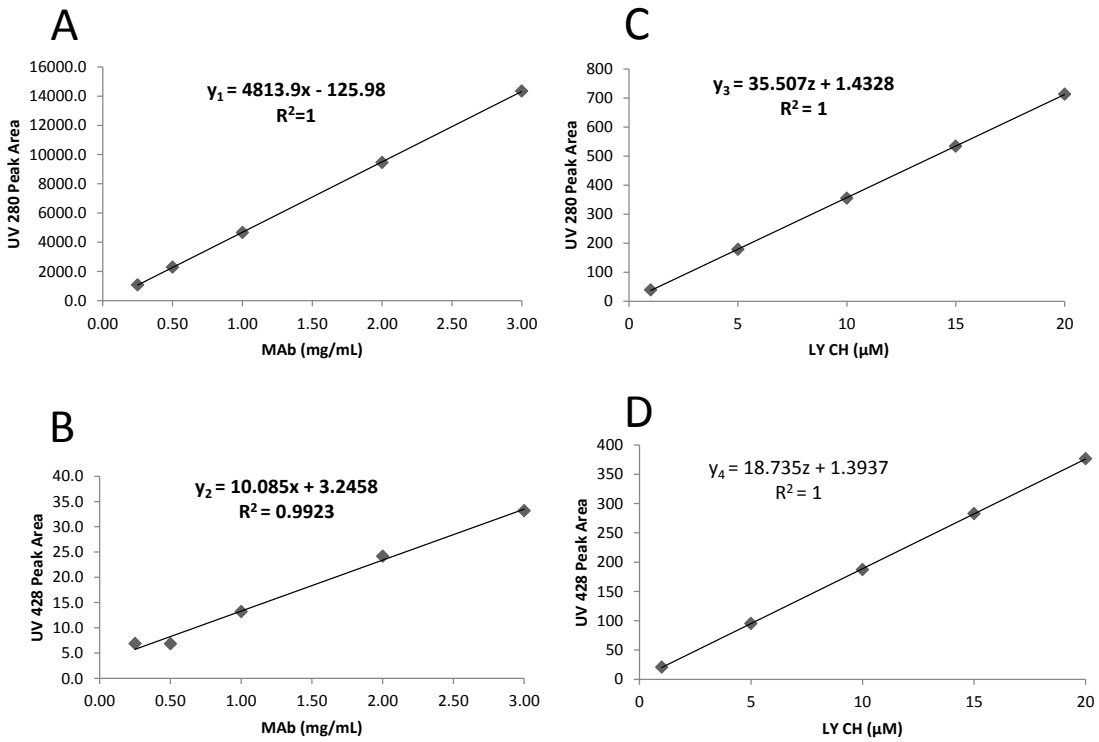

Figure 4. Standard curves for the CALY reagents: mAb and LY CH at 280 nm and 428 nm. **A**: Standard curve 1 (mAb at 280 nm): y1=m1x+b1; **B**: Standard curve 2 (mAb at 428 nm): y2=m2x+b2; **C**: Standard curve 3 (LY CH at 280 nm): y3=m3z+b3; **D**: Standard curve 4 (LY CH at 428 nm): y4=m4z+b4; x is the mAb protein concentration (mg/mL) and z is the molar concentration (μM = nmol/mL) of carbonyl groups. Carbonylation level (z/x) is determined by solving the two-variable (x and z) linear equations: A280=m1x+b1+m3z+b3; A428=m2x+b2+m4z+b4.

Determination of Protein Carbonylation Levels by DNPH Spectrophotometric Assay

The carbonylation levels of some mAb samples were quantified by the DNPH assay using the OxiSelect^{TM} Protein Carbonyl Spectrophotometric Assay Kit (Cell Biolabs, Inc., San Diego, CA). Briefly, 1 mL of DNPH solution (2 mg/mL) was mixed with 250 µL mAb solution (5 mg/mL). The mixture was incubated at room temperature in the dark for 45 minutes. After the derivatization, the mAb samples were precipitated. The pellets were washed 5 times to remove the excess DNPH. The mAb samples were subsequently re-solubilized. The carbonyl concentration was then determined by measuring the absorbance at 375 nm and using the DNPH extinction coefficient (22,000 M^{-1} cm^{-1}). The protein concentration was determined by the bicinchoninic acid assay (BCA). The protein carbonylation level of a mAb was reported in nmol/mg as a ratio of the carbonyl concentration (uM) to the protein concentration (mg/mL).

Cell Culture Study

The study used two Chinese hamster ovary (CHO) cell lines derived from a CHO-K1 host, that were stably transfected to produce mAb B, and are referred to as cell lines 1 and 2. The cryogenically frozen ampoules of these recombinant cell lines were first thawed and expanded before starting the cell culture experiment. To start the study, production cultures for cell lines 1 and 2 were inoculated at ~10^6 viable cells/mL in 250-mL shake flasks. For each cell line, 6 production cultures were initiated in the same chemically-defined basal media but were supplemented with different initial concentrations of iron (10, 25, 50, 100, 150, and 200 µM ferrous sulfate). The 12 production cultures were agitated (150 rpm, 25 mm throw) in Multitron incubation shakers (INFORS USA Inc) with a 5% CO_2 overlay. The cultures were maintained at 37°C for the first 3 days, and at 33°C thereafter. On days 3, 6, and 9, the production cultures were supplemented with the same chemically-defined concentrated nutrient feed at 1:10 (v/v).

On day 12, the production cultures were harvested by centrifugation and filtration. Protein A chromatography was then used to purify mAb B from the harvested cell cultured fluid for the subsequent characterization.

In the cell culture study, several parameters reflecting cell growth and metabolism were monitored. The viable cell concentration and viability were analyzed by Vi-Cell XR Cell Counter (Beckman Coulter, Brea, CA). Glucose, lactate, ammonium, and culture pH were measured using a Bioprofile 400 (Nova Biomedical, Waltham, MA). On days 0, 7, 10, and 12, the cell culture fluid was sampled to measure iron concentration by inductively coupled plasma mass spectrometry (ICP-MS) using a Thermo Electron X series II instrument (Thermo Scientific, Waltham, MA). In addition, mAb B product titer was measured by protein A chromatography for cell culture fluid samples on days 7, 10, and 12.

Storage Study

Antibody samples were prepared by mixing mAb A (5 mg/mL, final concentration) with ferrous sulfate (Low: 0.1 µM or High: 0.8 µM, final concentration) and PS20 (Low: 0.02%, w/v or High: 0.16%, w/v, final concentration) in 50 mM sodium succinate (pH 6.0), as shown in Table 1. A 5 mg/mL mAb A in 50 mM sodium succinate (pH 6.0) was used as the control. These samples were stored at room temperature in the dark for 4, 8, and 16 weeks. At each time point, methionine and EDTA were added to the samples to a final concentration of 1 mM and 50 µM, respectively, to quench carbonylation reactions. Subsequently, these samples were stored at -80°C until further analysis.

Sample Label	mAb A Concentration	Ferrous Sulfate Concentration	PS20 Concentration
Control	5 mg/mL	0 µM	0% (w/v)
Fe (Low)/ PS20 (Low)		0.1 µM	0.02% (w/v)
Fe (Low)/ PS20 (High)		0.1 µM	0.16% (w/v)
Fe (High)/ PS20 (Low)		0.8 µM	0.02% (w/v)
Fe (High)/ PS20 (High)		0.8 µM	0.16% (w/v)

Table 1. The iron and PS20 concentrations for the storage study.

Stress Study

Antibody samples were prepared by mixing mAb A (5 mg/mL, final concentration) with ferrous sulfate (4, 20, 100, or 500 µM) and hydrogen peroxide (8, 40, 200, or 1000 µM) in 50 mM sodium succinate (pH 6.5), as shown in Table 2. These samples were incubated at room temperature in the dark for 2 hours. Subsequently, excess methionine and EDTA were added to these samples to quench carbonylation reactions. Additionally, mAb B and mAb C (5 mg/mL, final concentration) were mixed with ferrous sulfate (4, 20, 100, or 500 µM) and hydrogen peroxide (1000 µM) in 50 mM sodium succinate (pH 6.5). These samples were incubated at room temperature in the dark for 2 hours. Subsequently, excess methionine and EDTA were added to the samples to quench carbonylation reactions.

Size Heterogeneity Analysis

The size heterogeneity of the mAb samples was evaluated by size exclusion chromatography (SEC) using a TSK G3000 SWXL (7.8x300 mm) size exclusion column with the same chromatography conditions as used for CALY, except that the effluent was only monitored at 280 nm. Integration of the High Molecular Weight Species (HMWS), Main Peak, and Low Molecular Weight Species (LMWS) for each sample was performed manually.

Sample Label	mAb A Concentration	Ferrous Sulfate Concentration	Hydrogen Peroxide Concentration
A1	5 mg/mL	500 µM	1000 µM
A2			200 µM
A3			40 µM
A4			8 µM
A5		100 µM	1000 µM
A6			200 µM
A7			40 µM
A8			8 µM
A9		20 µM	1000 µM
A10			200 µM
A11			40 µM
A12			8 µM
A13		4 µM	1000 µM
A14			200 µM
A15			40 µM
A16			8 µM

Table 2. The oxidation conditions used to generate the stressed mAb A samples.

Charge Heterogeneity Analysis

The charge heterogeneity of mAb samples was evaluated by ion exchange chromatography (IEC) or imaged capillary isoelectric focusing (iCIEF), as noted. Before the analysis, all of the mAb samples were mixed with carboxypeptidase B (CpB) at an enzyme-to-mAb ratio of 1 to 100 (weight to weight). These mixtures were incubated at 37ºC for 30 minutes, which reduces the basic charge heterogeneity of mAb samples by removing the heavy chain C-terminal lysine residues.

For the IEC analysis, the CpB-treated mAb samples were injected onto a Dionex ProPac WCX 10 column (4x250 mm) using an Agilent HPLC system. Mobile phase A was 25 mM sodium phosphate, pH 6.6. Mobile phase B was 0.2 M sodium chloride in mobile phase A. The mAb charge variants were separated by applying a linear gradient of 0% to 45% B in 52 minutes. The column temperature was controlled at 40°C and the autosampler temperature was controlled at 8°C. The flow rate was 0.5 mL/min. The column effluent was monitored at 280 nm. Integration of the acidic, main, and basic charge variants for each sample was performed manually.

For the iCIEF analysis, the CpB-treated mAb samples were diluted to 0.5 mg/mL and added to the ampholyte mixture containing the carrier ampholytes and pI markers. The mixtures were briefly vortexed and centrifuged before the analysis. The mAb samples were then focused inside the capillary for 1 minute at 1,500 volts and then for 6 minutes at 3,000 volts using an iCE280 Analyzer (Protein Simple, San Jose, CA, USA). The separation of the acidic, main, and basic charge variants was monitored by UV absorbance at 280 nm.

Site-Specific Carbonylation Analysis

The site-specific reactivity of LY CH against mAb carbonylation was indirectly assessed using a mass spectrometry (MS)-based approach,[11] where we looked for residual carbonylation sites that can be derivatized by Girard's reagent T, after the sample has been first derivatized by LY CH. The highly oxidized mAb A (batch 2) was used as a model mAb. This model mAb sample was incubated with LY CH under the derivatization condition of CALY; a control sample was prepared under the same condition but without LY CH treatment. After the incubation, the two samples were buffer-exchanged into 50 mM sodium acetate buffer (pH 4.5), derivatized by Girard's reagent T, reduced by sodium borohydride, digested by trypsin, and analyzed by MS as described previously.[11] Subsequently, mAb carbonylation sites for the two samples were evaluated by database search using the Proteome Discover software (Waltham, MA, USA) and manual investigation of the MS data.

RESULTS

Optimization of the Derivatization Condition for CALY

In this work, we developed an improved protein carbonylation assay, CALY, for quantifying mAb carbonylation (Figure 2). To establish an optimal derivatization condition for CALY, we first focused on identifying a suitable buffer system. Using the highly oxidized mAb A (batch 1) as the test sample, we evaluated several buffers in the pH range of 4.0 to 6.5. At or below pH 5.0, we observed some degree of sample precipitation during the derivatization. We then selected pH 6.0 as the derivatization pH because no precipitation was observed at pH values greater than 5.0 and the derivatization becomes significantly slower at pH values greater than 7.0. Based on the same consideration, we selected MES, which has a pKa of 6.13, as the buffer. To further reduce the risk of sample precipitation during the derivatization procedure, we included reduced Triton X-100, a surfactant that does not have any significant UV absorbance at

280 or 428 nm, in the buffer. In all the subsequent analyses, no sample precipitation was observed using 50 mM lithium MES, 0.05% (w/v) reduced Triton X-100, pH 6.0, as the derivatization buffer.

For the derivatization reaction, we evaluated LY CH-to-mAb molar ratios from 100:1 to 10,000:1 with a reaction time of 18 hours. Based on the corresponding carbonylation levels (Figure 5A) of the highly oxidized mAb A (batch 1), the derivatization started to reach a plateau at a molar ratio of 6000:1. To ensure a robust derivatization condition, we selected 8000:1 as the appropriate reagent-to-mAb molar ratio for CALY. The derivatization time was optimized using a similar approach, and a reaction time of 18 hours was selected (Figure 5B).

A

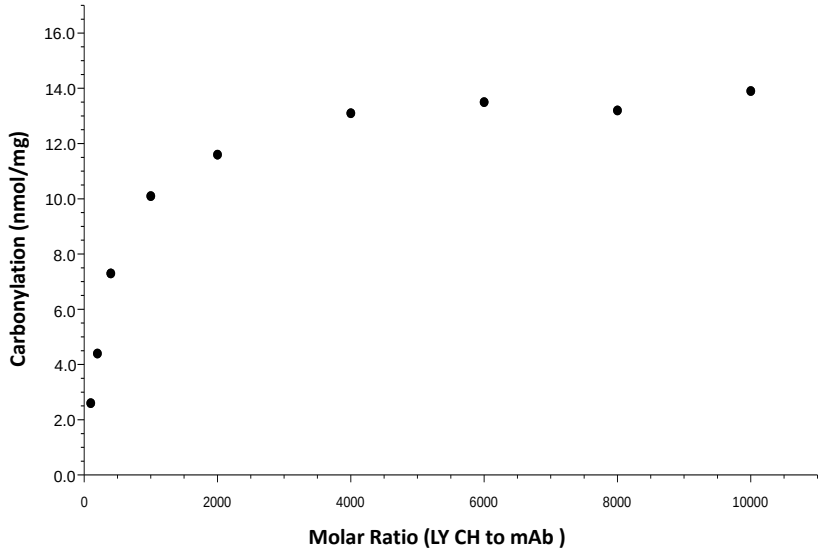

B

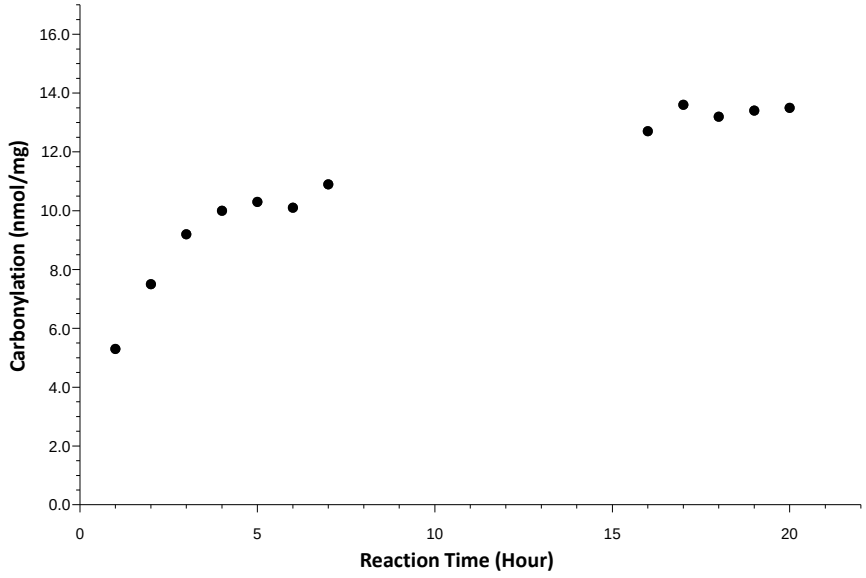

Figure 5. (A) Optimization of the LY CH-to-mAb molar ratio for the CALY derivatization reaction; (B) optimization of the reaction time for the CALY derivatization reaction.

Site-Specific Reactivity of LY CH

LY CH contains a hydrazide group, a type of derivative that reacts specifically with carbonyls.[8-9] In the literature, LY CH has been used as the derivatization reagent to quantify antibody glycan aldehydes generated by periodate oxidation.[12-13] To demonstrate site-specific reactivity of LY CH against carbonyls generated by metal-catalyzed oxidation, we applied a mass spectrometry (MS) based approach (Supplemental Methods). In this approach, we derivatized an oxidized mAb sample first with LY CH and then with Girard's Reagent T (GRT), while a control sample was generated by derivatizing the oxidized mAb sample only with GRT. This derivatization scheme was employed to overcome a challenge with detecting LY CH-derivatized carbonyl peptide ions by MS (sulfate groups on LY CH suppress ionization, data not shown). GRT, a hydrazide reagent that contains a permanently-charged quaternary ammonium group, was used to allow sensitive detection of carbonyl peptides by MS.[11] Therefore, investigating the presence of any GRT-derivatized carbonyl peptides (after the mAb sample has first been derivatized by LY CH) allows an indirect assessment of specific reactivity and derivatization efficiency of LY CH. This assessment revealed that no carbonyl peptide was observed from the mAb sample (pre-treated with LY CH), while 22 carbonyl peptides were observed from the control sample (not pre-treated with LY CH). These MS data indirectly demonstrated selective reactivity of LY CH with mAb carbonyls, generated by metal-catalyzed oxidation.

CALY Performance Assessment

The robustness of CALY was evaluated by assessing the effect of various assay conditions, such as mAb concentration for the derivation (0.45, 0.50, and 0.55 mg/mL), LY CH-to-mAb molar ratio (7000:1, 8000:1, and 9000:1), derivatization buffer pH (5.9, 6.0, and 6.1),

number of buffer exchange steps (2, 3, and 4), injection volume (20, 25, and 30 µL), number of freeze/thaw cycles (0 and 1), and time in the HPLC autosampler (1 to 15 hours at 8ºC) on quantification. The highly oxidized mAb A (batch 1) was used as the test sample. As shown in Figures 6 and 7, very little variation in the measured carbonylation level was observed for most of the assay conditions. In particular, the measured carbonylation levels were similar with two, three, and four rounds of buffer exchange; this finding demonstrates that CALY is robust against variable amounts of unconsumed LY CH (ranging from ~0.033 µM to ~30 µM) in the samples, and supports that exhaustive removal of LY CH is not required. The greatest variation was observed for the different derivatization pHs (with a CV of 5.1%); this suggests that a tight control of the derivatization buffer pH may be necessary for optimal robustness. Overall, a total of 25 measurements from the robustness assessment showed an average carbonylation level of 13.0 nmol/mg with an overall CV of 2.4%. CV values for each individual robustness experiment did not exceed 5.1%. The relatively small CV from these assessments supports that CALY is robust.

The linearity and precision of CALY was evaluated by measuring the carbonylation levels of serially-diluted samples, which were prepared by mixing the highly oxidized mAb A (batch 2) with the unstressed mAb A at 0-to-100, 25-to-75, 50-to-50, 75-to-25, and 100-to-0 (weight-to-weight) ratios. These samples were analyzed by two analysts, on two instruments, with two columns. Three independent preparations were made by each analyst on three different days. A total of six independent measurements were performed for each sample. As shown in Figure 8, a linear relationship was observed between the carbonylation level and the percentage of highly oxidized mAb A in the sample mixture, with coefficient of determination (R^2) of 0.997. The

coefficient of variation of the measurement for each mixed sample was lower than 15%. These results demonstrate the linearity and precision of CALY.

The accuracy of CALY was evaluated by comparing the carbonylation levels of the serially-diluted samples measured by CALY and by the DNPH spectrophotometric assay, which is considered to be a standard assay for quantifying protein carbonylation. As shown in Figure 9, the difference between the mean carbonylation levels determined by CALY and by the DNPH assay was within the coefficient of variation of the DNPH assay (illustrated by the error bars in Figure 9), except for the highly oxidized mAb A. These results support that CALY and the DNPH assay provide similar quantitation of mAb carbonylation with levels up to 7 nmol/mg.

The limit of detection (LOD) and limit of quantitation (LOQ) were calculated as 3 times and 10 times of the standard deviation of the carbonylation levels of the negative control, respectively. Using the unstressed mAb A as the negative control, which was not derivatized by LY CH, we performed 30 independent measurements by CALY and the standard deviation from these measurements was 0.03 nmol/mg (Table 3). The LOD and LOQ of CALY were then determined to be 0.1 and 0.3 nmol/mg, respectively.

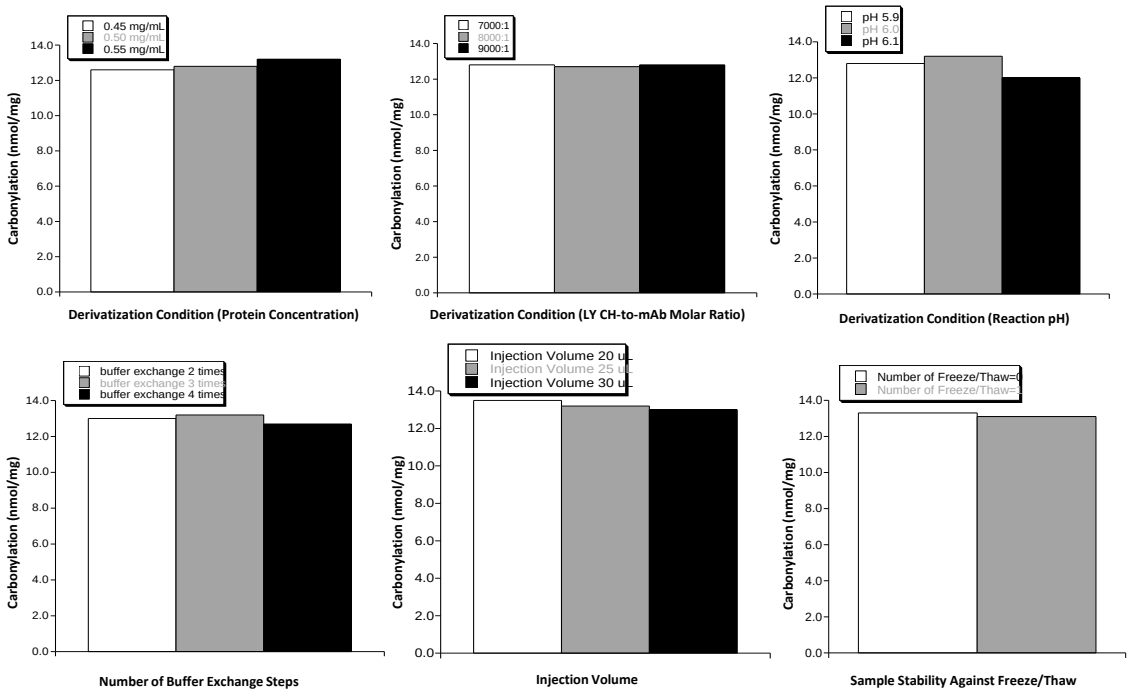

Figure 6. Robustness assessment for CALY: mAb concentration for the derivatization reaction; molar ratio for the derivatization reaction; pH for the derivatization reaction; number of buffer exchange steps; injection volume; and sample stability against freeze/thaw.

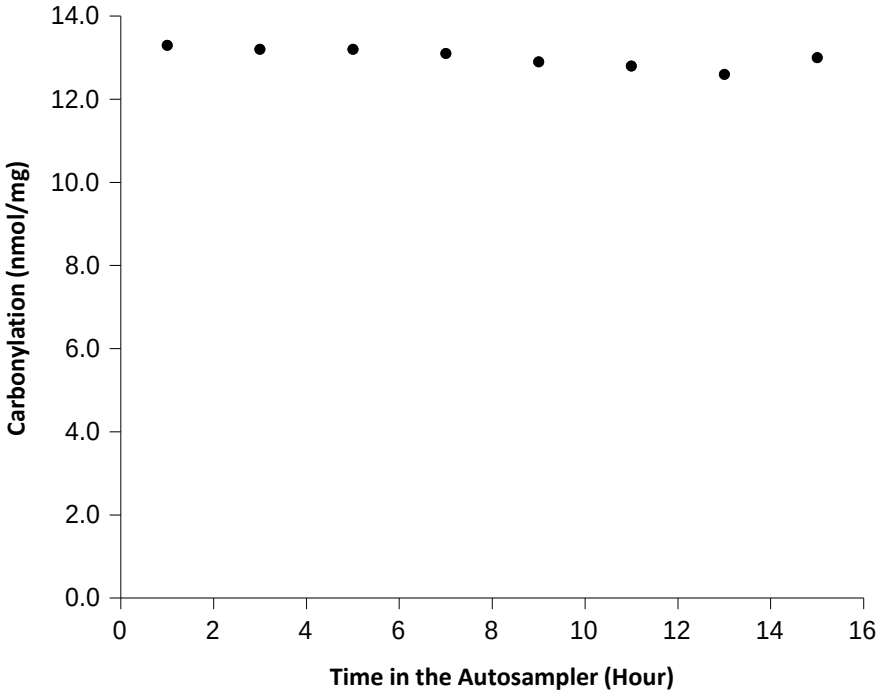

Figure 7. Robustness assessment for CALY: stability of the LY CH-derived mAb A sample in the HPLC autosampler at 8°C.

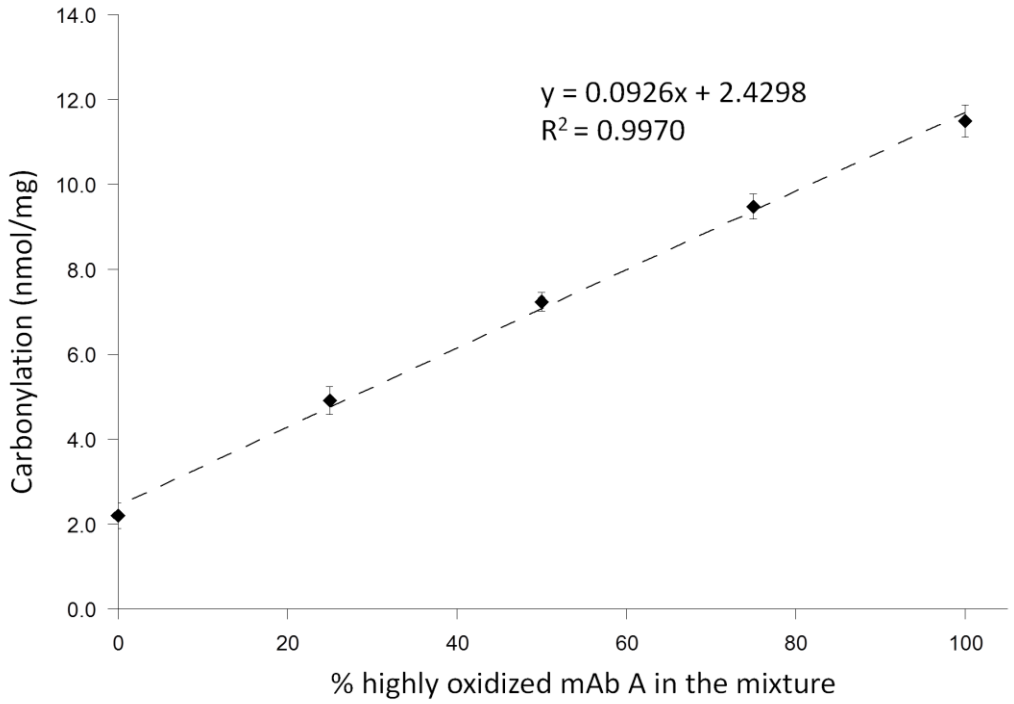

Figure 8. Carbonylation levels of the mixed mAb A samples as determined by CALY (six independent measurements for each sample). Error bars represent the standard deviation of the independent measurements.

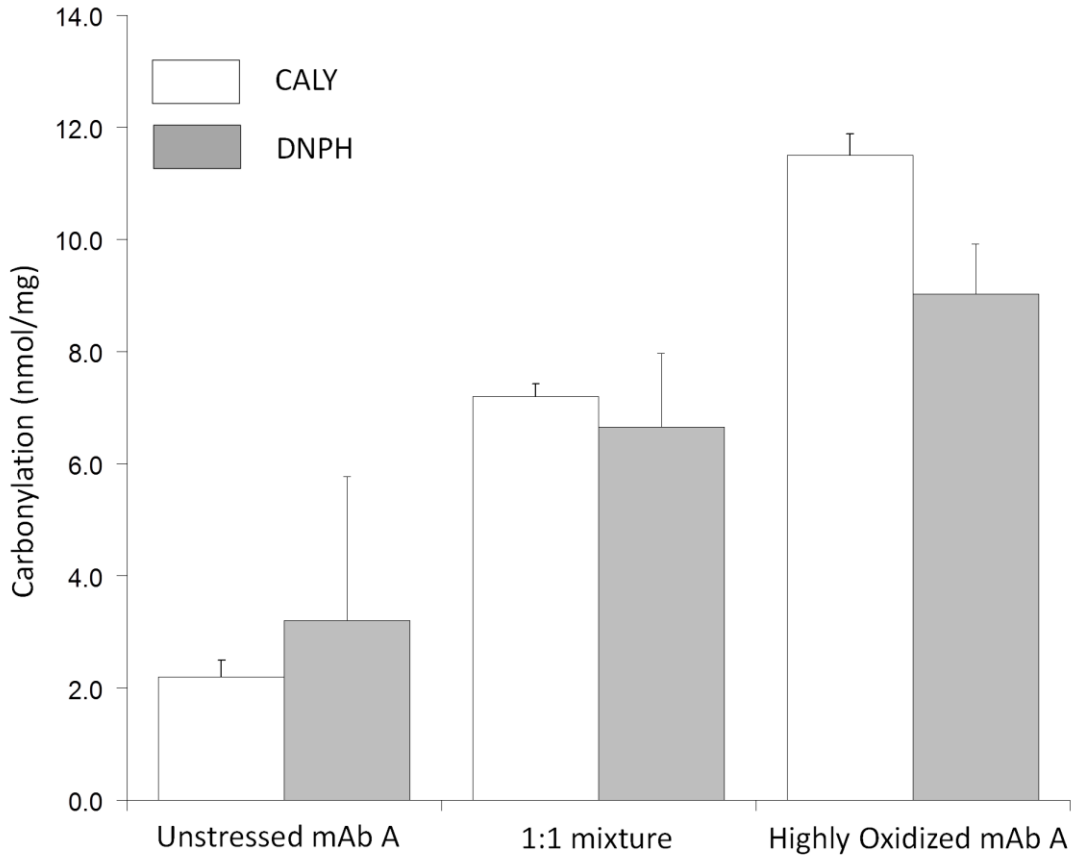

Figure 9. Carbonylation levels of the unstressed, the 1-to-1 mixed, and the highly oxidized mAb A samples as determined by CALY (six independent measurements for each sample) and the DNPH method (three independent measurements for each sample). Error bars represent the standard deviation of the independent measurements.

No.	Carbonylation (nmol/mg)
1	0.18
2	0.10
3	0.20
4	0.13
5	0.19
6	0.17
7	0.17
8	0.10
9	0.18
10	0.13
11	0.17
12	0.16
13	0.14
14	0.12
15	0.15
16	0.14
17	0.16
18	0.15
19	0.11
20	0.16
21	0.17
22	0.16
23	0.17
24	0.12
25	0.14
26	0.15
27	0.15
28	0.17
29	0.15
30	0.14

Table 3. The carbonylation levels of the negative control (i.e., mAb A that was not derivatized by LY CH or exposed to stress conditions). These data were generated from 30 independenat measurements. The standard deviation (SD) from these data, 0.03 nmol/mg, was used to determine the LOD and LOQ of CALY.

Cell Culture Study

Iron is a required nutrient in cell culture media for mAb production.[14-15] However, iron can also catalyze the formation of carbonyl groups on proteins.[16] To understand the effect of iron on mAb carbonylation during cell culture production, we used chemically defined cell culture media supplemented with 6 different levels of iron (10, 25, 50, 100, 150, and 200 µM). These levels were based on the iron concentrations commonly used for mAb production.[14-15, 17] We observed that, as the initial iron concentration increased from 10 to 200 µM, the carbonylation level of mAb B increased from 1.0 to 1.8 nmol/mg with cell line 1 and from 0.9 to 2.2 nmol/mg with cell line 2 (Figure 10). This observation demonstrates that iron in cell culture media critically influences mAb carbonylation during cell culture production.

The relationship between mAb B carbonylation level and the initial iron concentration was not linear: the carbonylation level increased more rapidly as the initial iron concentration increased from 10 to 50 µM than from 100 to 200 µM. Considering that the extracellular iron concentration is expected to decrease due to the consumption of iron by CHO cells, we investigated the relationship between mAb B carbonylation level and the iron concentration in the extracellular cell culture fluid at days 0, 7, 10, and 12. As shown in Figure 11, the extracellular iron concentration decreased almost linearly over time. When plotting mAb B carbonylation levels against the respective extracellular iron concentrations at day 0, 7, 10, or 12, we observed similar non-linear relationships (figures not shown). The lack of a linear relationship between mAb B carbonylation level and the extracellular iron concentration suggests that iron is likely not the only factor that influences mAb carbonylation during cell culture production. We next investigated cell culture growth (Figure 12), metabolism (Figures 13

and 14), and mAb production (Figure 15) profiles, but did not observe any trends or relationships that could explain the non-linear increase in mAb B carbonylation.

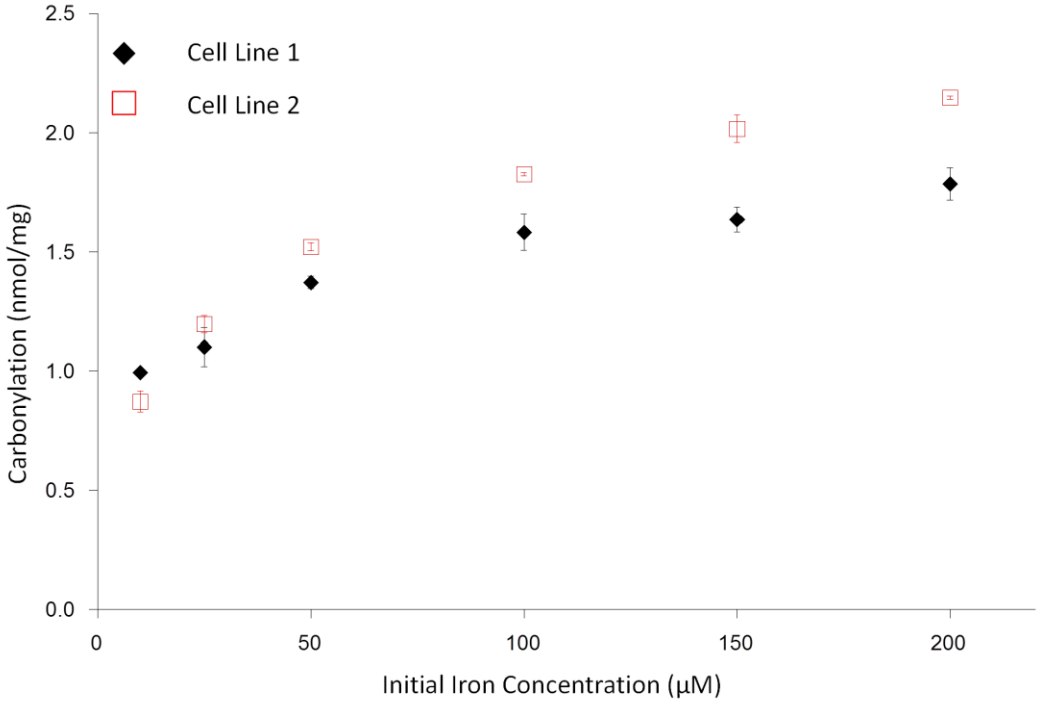

Figure 10. Carbonylation levels of mAb B produced under different initial iron concentrations in the cell culture study (error bars represent the standard deviation of three independent measurements).

A

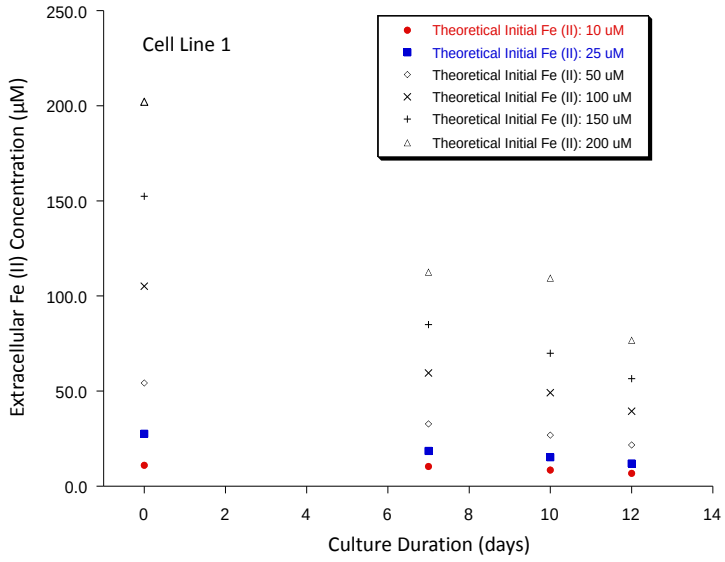

B

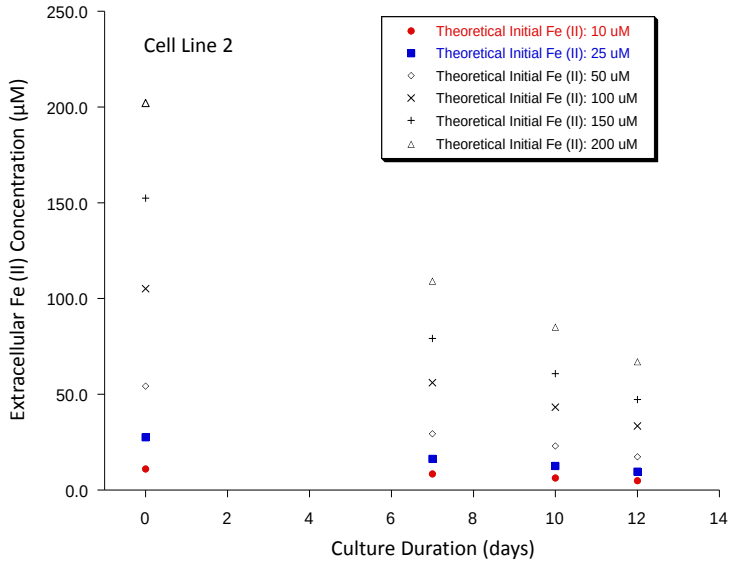

Figure 11. Extracellular iron concentration for (A) cell line 1 and (B) cell line 2.

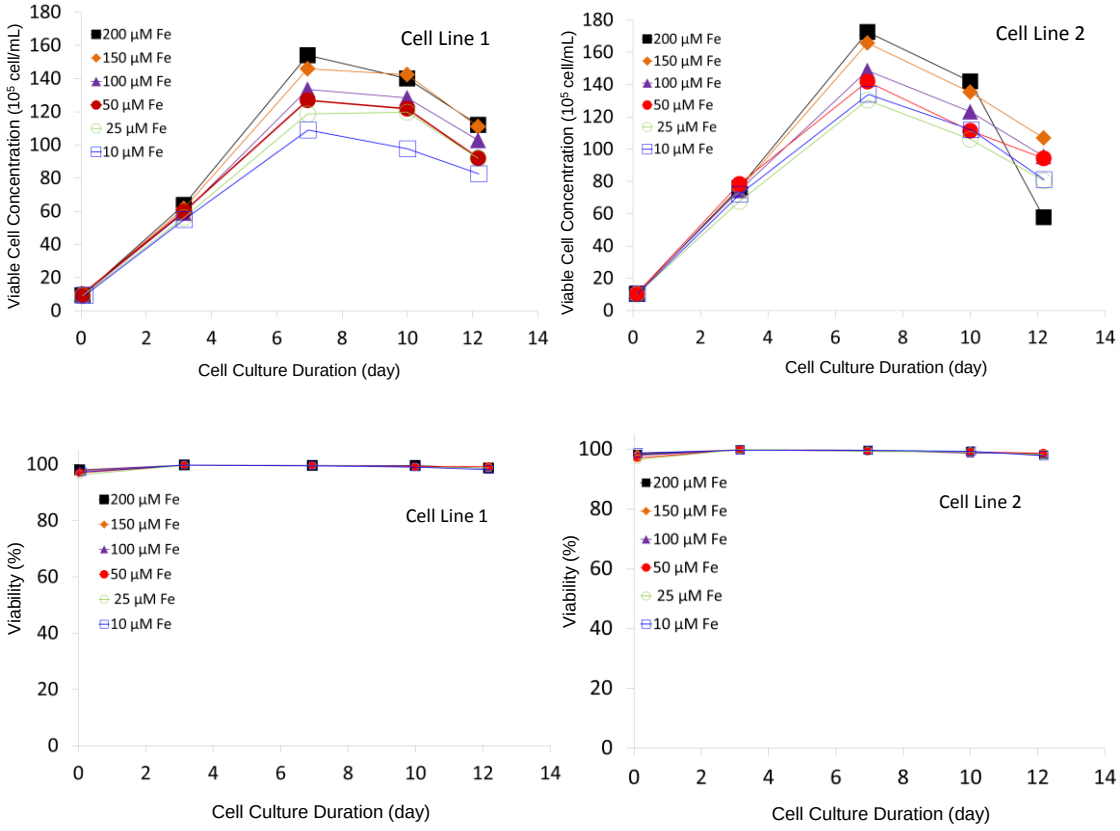

Figure 12. Culture viability and viable cell concentration profiles for the cell culture study using chemically-defined media supplemented with different iron concentrations. The viable cell concentration increased as the initial iron concentration increased, while the culture viability (%) essentially remained the same.

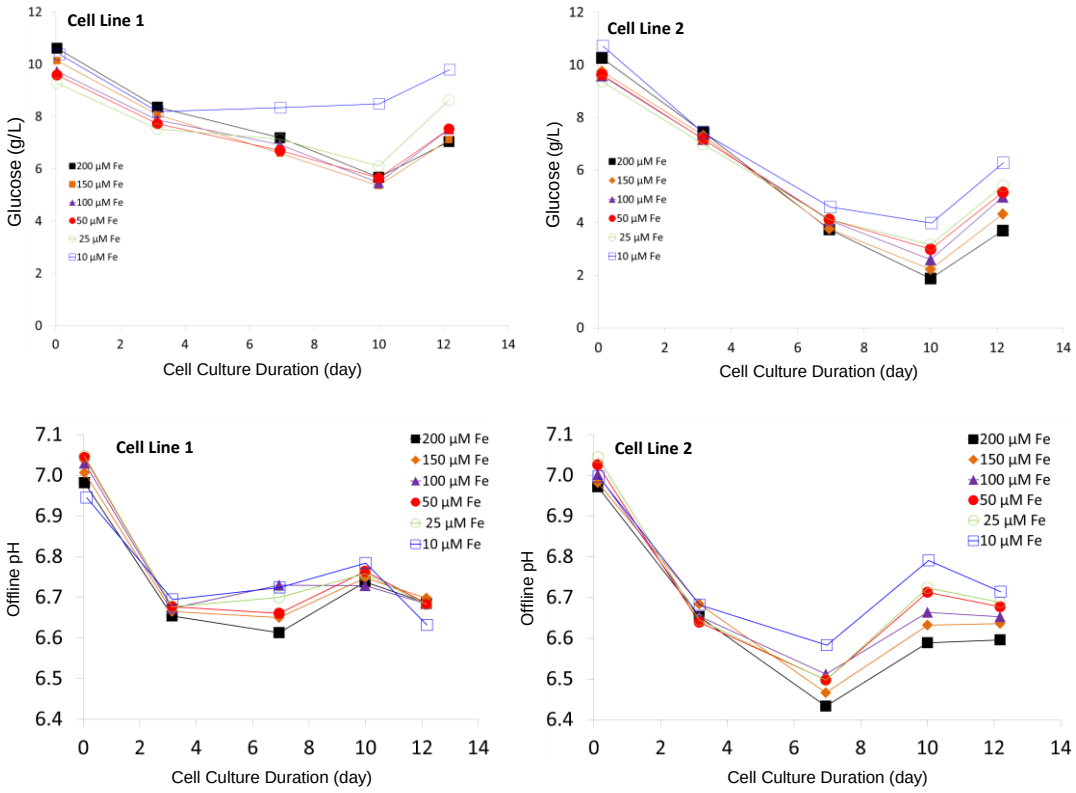

Figure 13. Glucose (upper panel) and offline pH (lower panel) profiles for the cell culture study using chemically-defined media supplemented with different iron concentrations. For cell line 2, a faster glucose consumption and lower culture pH were observed as the initial iron concentration increased. However, for cell line 1, these trends were less clear.

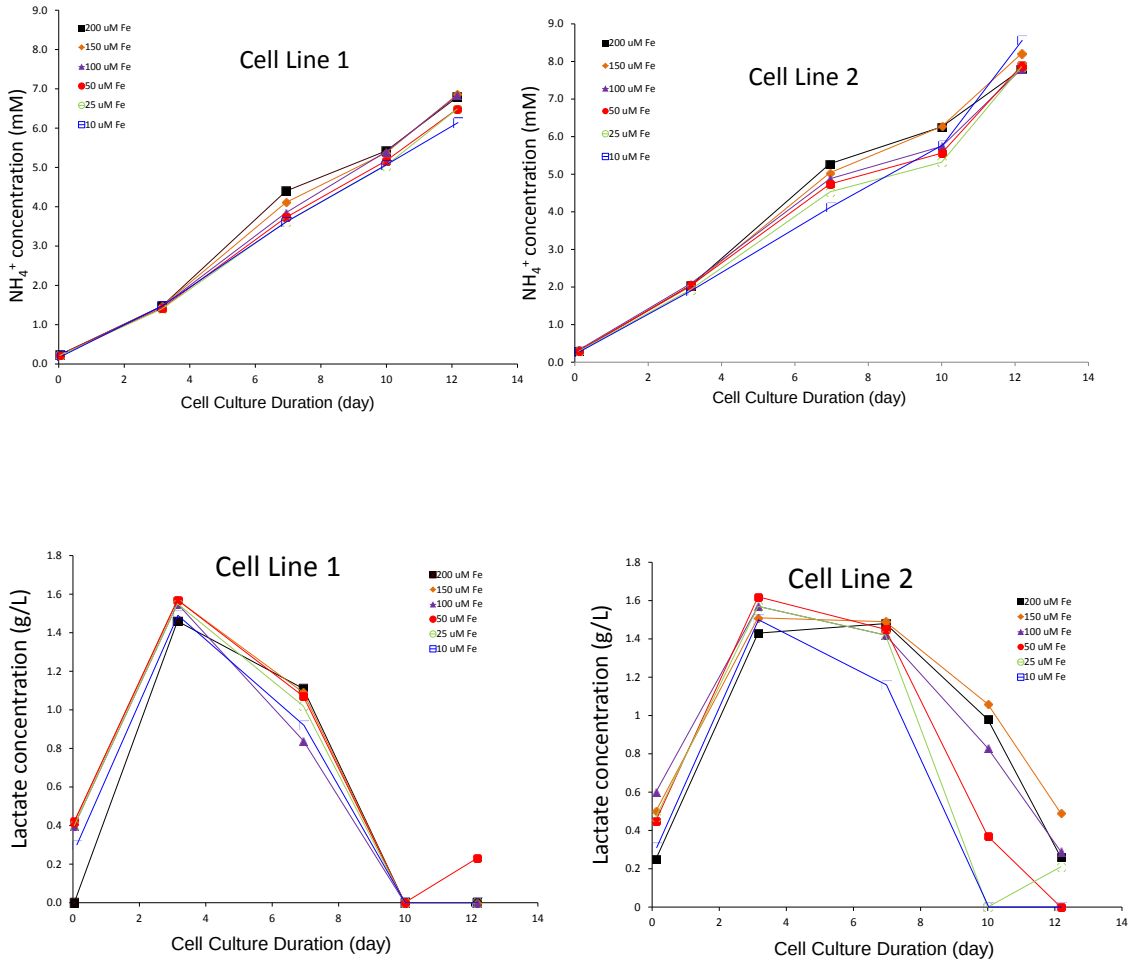

Figure 14. Ammonium (upper panel) and lactate (lower panel) profiles for the cell culture study using chemically-defined media supplemented with different iron concentrations. For both cell lines, no clear trend was observed in the ammonium and lactate profiles as the initial iron concentration increased.

A

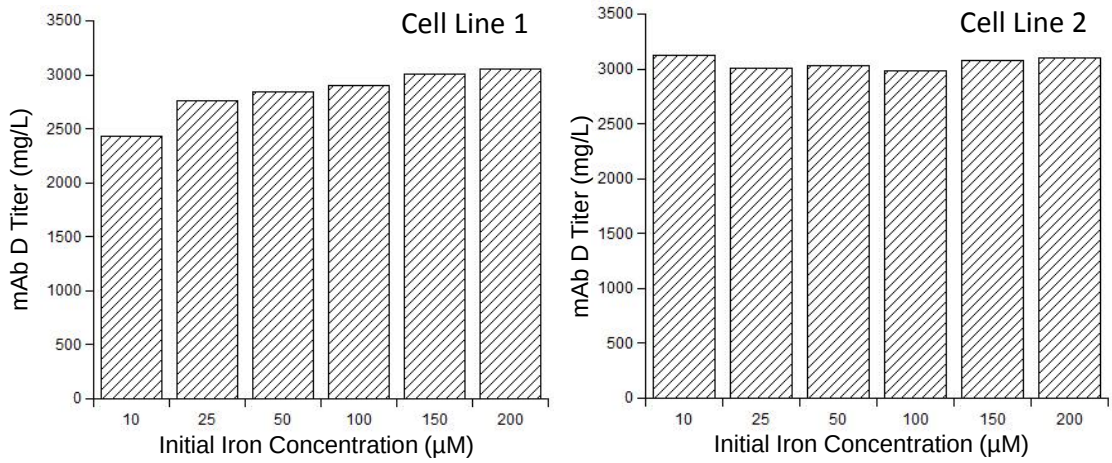

B

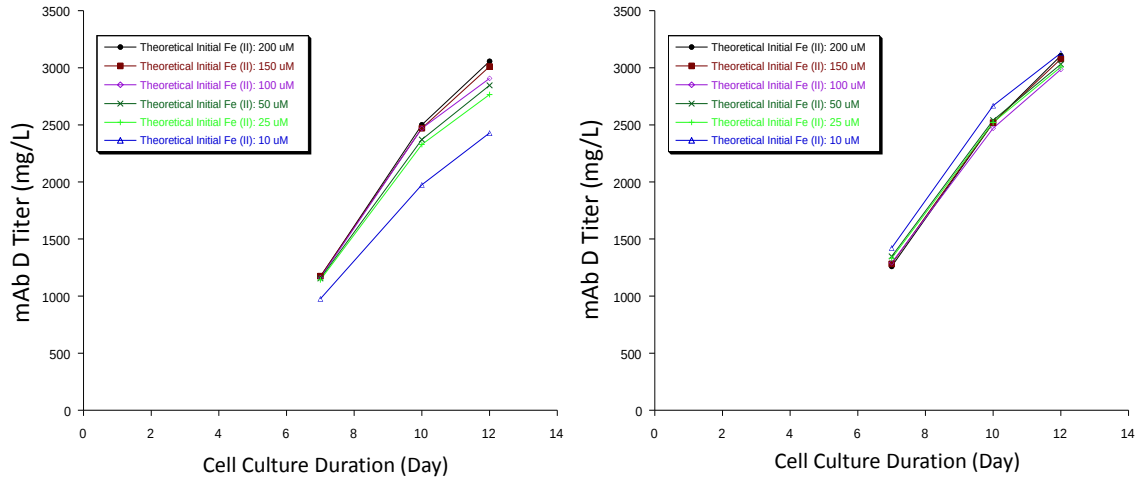

Figure 15. Relationship between the initial iron concentration in chemically-defined media and (A) mAb B titer at day 12; (B) mAb B titer at days 7, 10, and 12.

Storage Study

The mAbs produced and purified after bioprocessing would subsequently be stored. During storage, the mAbs can be exposed to low levels of iron ions leached from stainless steel surfaces or container closure materials.[18-20] Polysorbate 20 (PS20), a surfactant in mAb formulations commonly used to minimize aggregation during storage,[21] is known to contain peroxides.[22] Therefore, the peroxides from PS20 could react with iron ions to induce mAb carbonylation during storage. To understand this potential route of mAb carbonylation, we prepared mAb A samples in 50 mM sodium succinate buffer (pH 6.0) with a combination of low or high levels of iron and PS20 (Table 1). An unstressed mAb A with a relatively low level of carbonylation, 1.1 nmol/mg, was used as the control. The iron concentrations (0.1 μM and 0.8 μM) were based on the concentrations of the leached iron ions reported by Zhou et al.[18] The PS20 concentrations (0.02% and 0.16%, w/v) were based on the PS20 concentrations reported in mAb formulations.[23] Considering that mAb carbonylation could be a slow process in such a storage study, we measured mAb A carbonylation level at 4, 8, and 16 weeks.

As shown in Figure 16, compared to mAb A control, whose carbonylation level essentially stayed unchanged at 1.1 nmol/mg during storage, all four mAb A samples showed increased levels of carbonylation, which ranged from 1.3 to 2.1 nmol/mg. This observation demonstrates that mAbs in PS20 formulations are indeed susceptible to metal-catalyzed carbonylation during storage when low levels of iron ions are present. Interestingly, the carbonylation levels of the mAb A samples formulated with the high level of PS20 (0.16%, w/v) were consistently higher than those with the low level of PS20 (0.02%, w/v) at 4, 8, and 16 weeks, regardless of the iron concentrations. In addition, mAb A carbonylation products were not stable: a decrease in the

carbonylation level was observed between week 8 and week 16 for the two samples formulated with the high level of PS20 (0.16%, w/v).

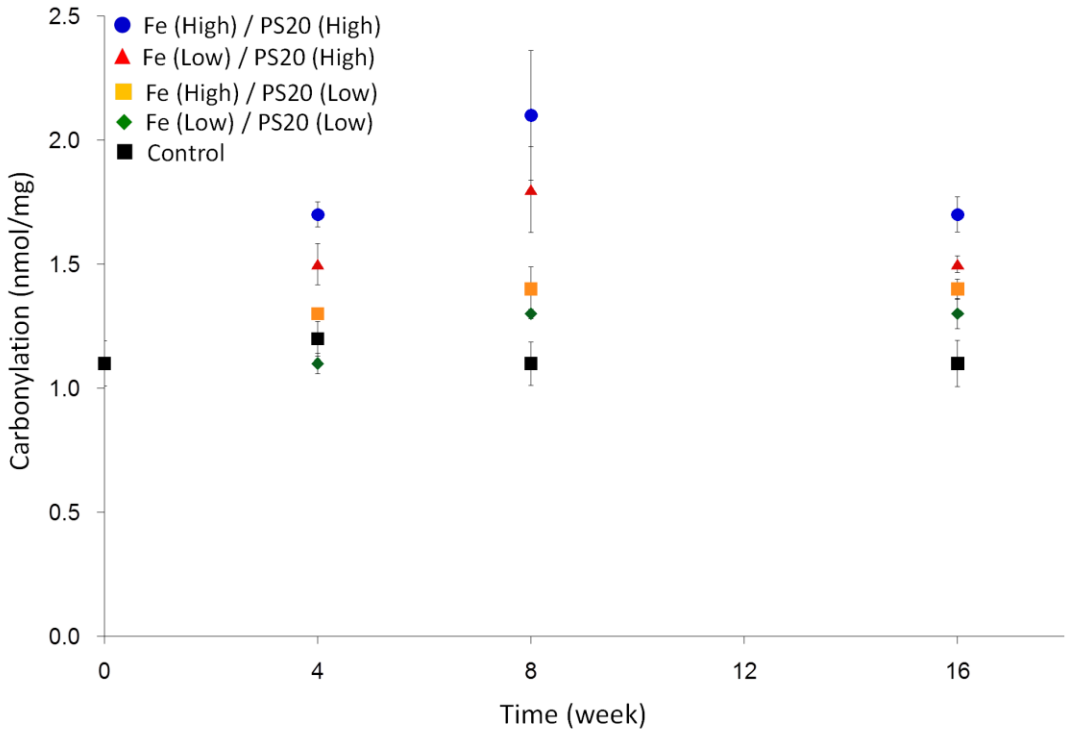

Figure 16. Carbonylation levels of mAb A samples stored at room temperature in the dark for 4, 8, and 16 weeks in the storage study (error bars represent the standard deviation of three independent measurements).

Stress Study

In light of the findings from the cell culture and storage studies, we hypothesized that peroxides could also be a critical factor that influences mAb carbonylation. To understand the effect of iron and peroxides on mAb carbonylation, we performed a stress study using various concentrations of iron (4 µM, 20 µM, 100 µM, or 500 µM) and hydrogen peroxide (8 µM, 40 µM, 200 µM, or 1000 µM), as shown in Table 2. These concentrations were based on the reported values from cell culture studies.[15, 24-25]

The carbonylation levels of the stressed mAb A samples varied from 2.5 to 13.0 nmol/mg (Figure 17). These data showed that a wide range of carbonylation levels can be generated when mAbs are exposed to iron and hydrogen peroxide at the pharmaceutically relevant concentrations. More importantly, these data showed that hydrogen peroxide critically influenced mAb A carbonylation. For example, with 500 µM iron, an increase in hydrogen peroxide concentration from 8 to 1000 µM resulted in an increase of the carbonylation level from 4.3 to 13.0 nmol/mg. Additionally, these data showed that iron and hydrogen peroxide had different impacts on mAb A carbonylation. Iron appeared to be a more dominant factor as mAb A carbonylation levels did not further increase when excess hydrogen peroxide (in relationship to iron) was present. Taken together, the stress study demonstrated a complex dependence of mAb carbonylation on both iron and hydrogen peroxide, which could provide a potential mechanism for the observed mAb carbonylation during production and storage.

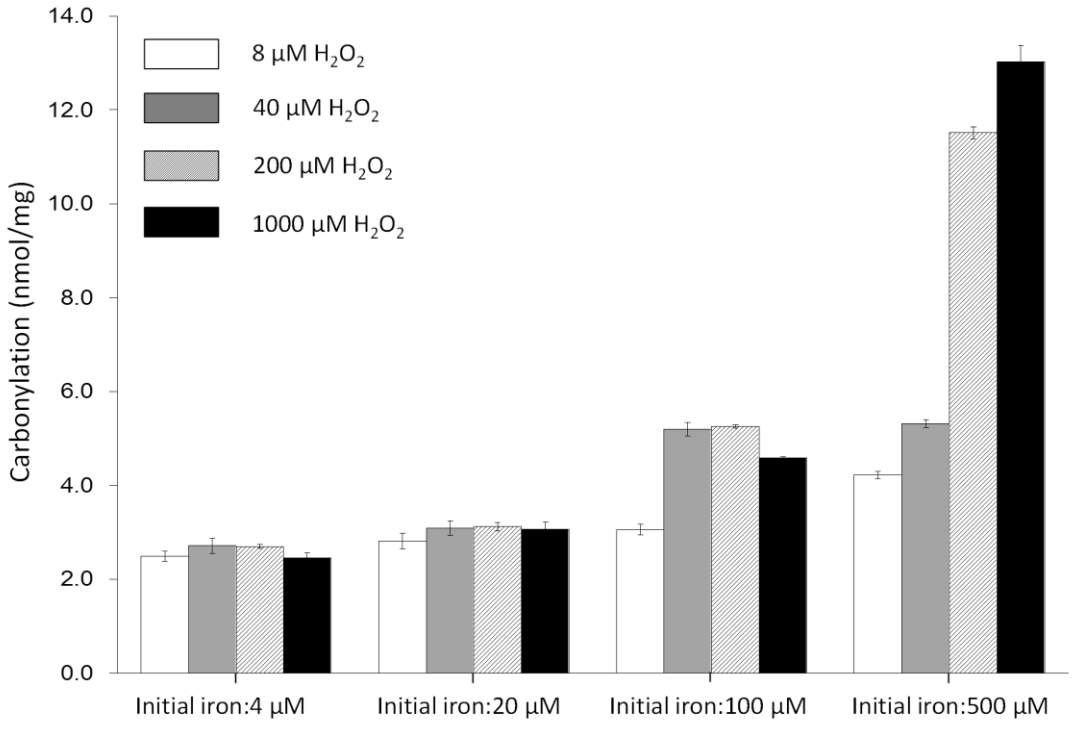

Figure 17. Carbonylation levels of mAb A samples stressed with different iron and hydrogen peroxide concentrations (error bars represent the standard deviation of three independent measurements).

Product Quality Correlations

Metal-catalyzed carbonylation has been linked to the formation of antibody aggregates.[3, 19] To gain a more comprehensive understanding of the effect of metal-catalyzed carbonylation on mAb product quality, we investigated the relationship between carbonylation and mAb product quality on size and charge variants. In the cell culture study, no apparent correlation was observed between the levels of high molecular weight species (HMWS), low molecular weight species (LMWS), or basic variants and the levels of mAb B carbonylation (Figure 18). In contrast, a positive correlation was observed between the levels of acidic variants and the levels of mAb B carbonylation (R^2 =0.96 for both cell lines, Figure 18).

In the storage study, we investigated the relationship between the rate of formation of the size or charge variants and mAb A carbonylation. As shown in Figures 19 and 20, formation of the size and charge variants appeared to largely follow zero-order kinetics. The rates of formation were therefore determined by linear regression analysis of the respective size and charge data (Figure 21). Since mAb A carbonylation profiles were quite complex over the storage time course (Figure 16), for simplicity, we used the average carbonylation levels at 4, 8, and 16 weeks to represent the overall extent of carbonylation during storage. As shown in Figure 22, positive correlations were observed between the average carbonylation levels and the rates of formation of HMWS (R^2=0.97), LMWS (R^2=0.97), and acidic variants (R^2=0.88), but not basic variants (R^2=0.17).

In the stress study, positive correlations were observed (Figure 23) between the levels of carbonylation and size variants (R^2=0.85 for both HMWS and LMWS). Positive correlations were also observed between the levels of carbonylation and charge variants (R^2=0.97 for acidic charge variants; R^2=0.96 for basic charge variants). To understand if a positive correlation may

generally exist between metal-catalyzed carbonylation and acidic charge heterogeneity for mAbs, we further evaluated two more mAbs (mAb C and mAb D), which share only 76% sequence similarity, with a subset of the stress conditions. As shown in Figure 24, a positive correlation (R^2>0.99) was observed between the levels of carbonylation and acidic variants for both mAbs. In contrast, while a positive correlation between the levels of carbonylation and basic variants was observed for mAb D (R^2 =0.97), no such correlation was observed for mAb C (Figure 24), as is the case for mAb B in the cell culture study (Figure 18) and mAb A in the storage study (Figure 22). The consistent correlations between the level of carbonylation and the level of acidic variants for all four mAbs support that a general degradation mechanism may exist that links metal-catalyzed oxidation with formation of acidic charge variants. It should be also pointed out that the linear regression slopes of these correlations differ, which suggests that the degradation mechanism may be sequence- or molecule-specific in response to metal-catalyzed oxidation.

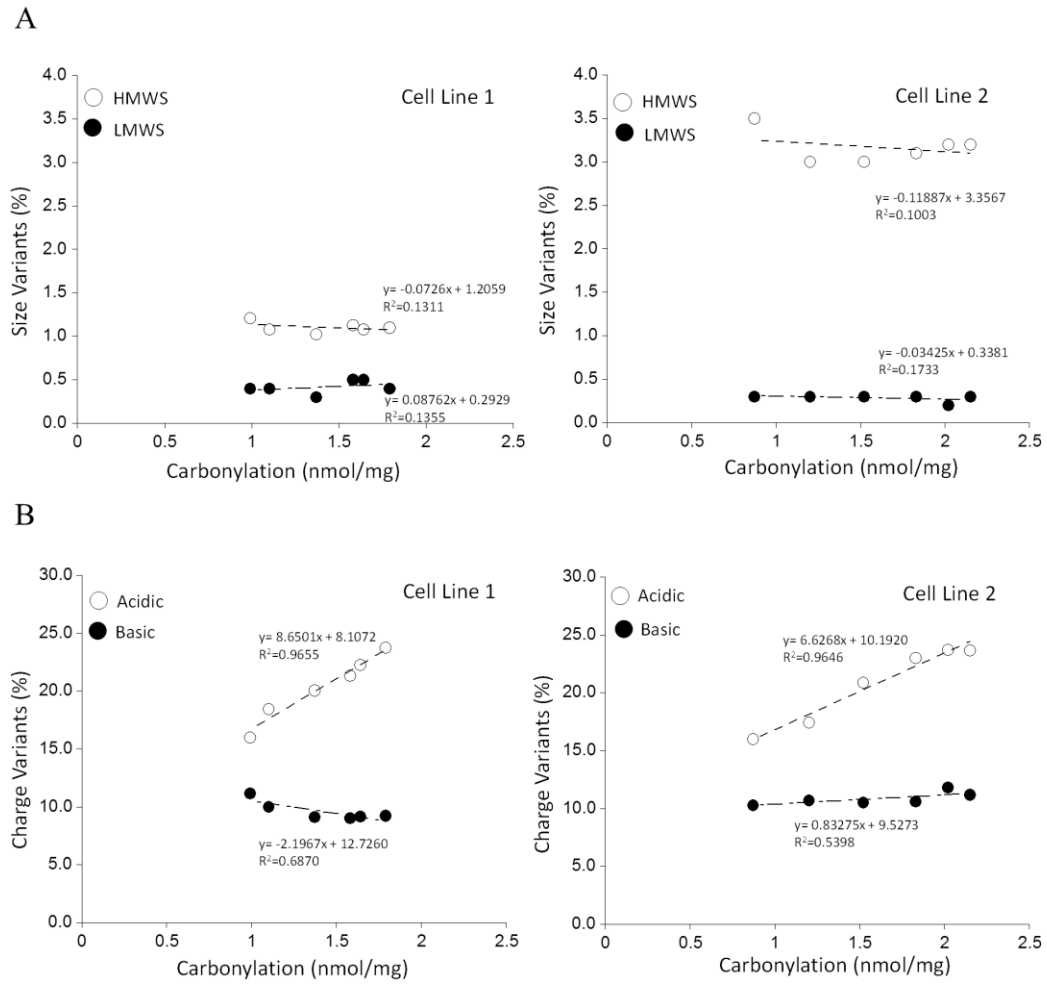

Figure 18. (A) the relationship between the levels of carbonylation and size variants, i.e., High Molecular Weight Species (HMWS) and Low Molecular Weight Species (LMWS) of mAb B samples from the cell culture study; (B) the relationship between the levels of carbonylation and charge variants, i.e., acidic and basic species of mAb B samples from the cell culture study.

A

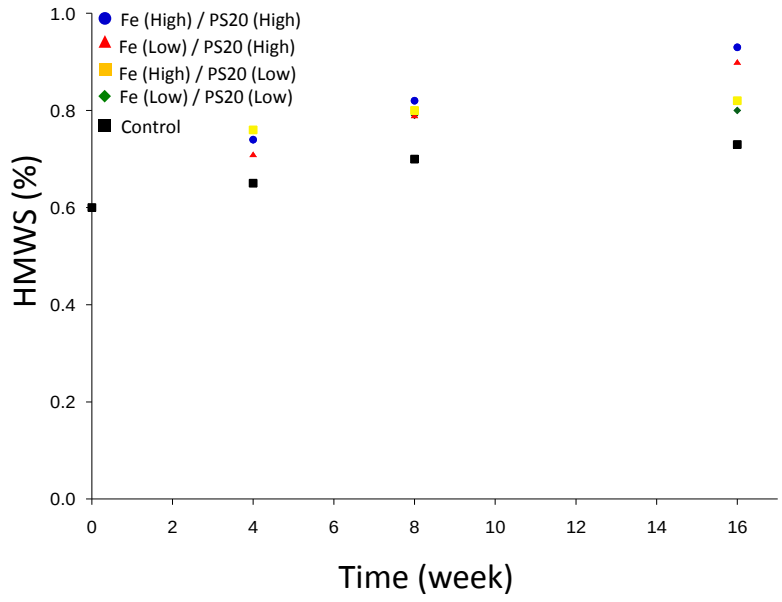

B

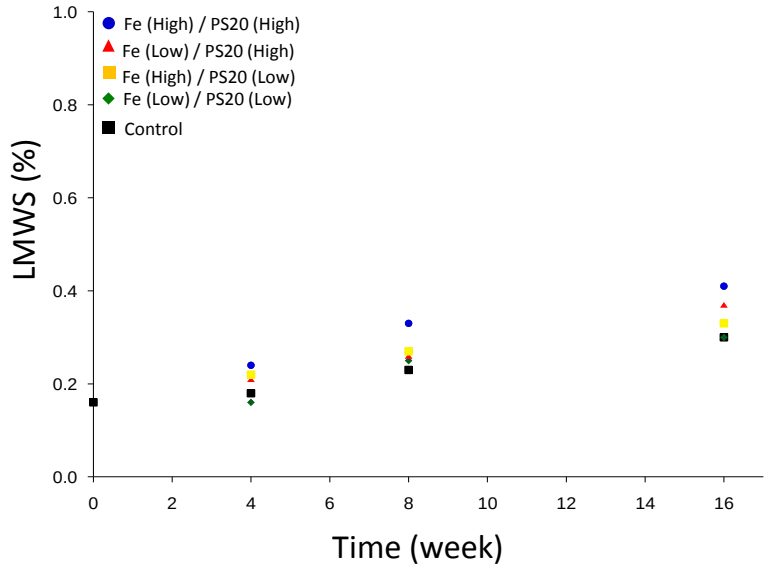

Figure 19. (A) The levels of HMWS; (B) the levels of LMWS of the mAb A samples from the storage study.

A

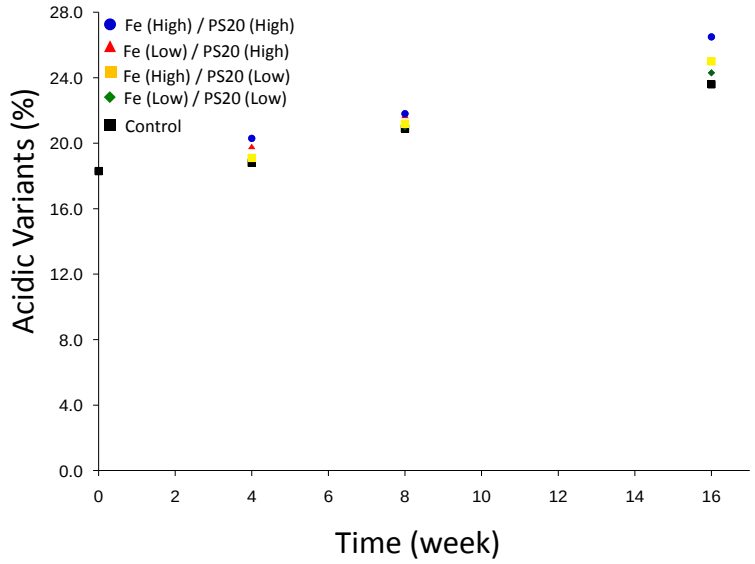

B

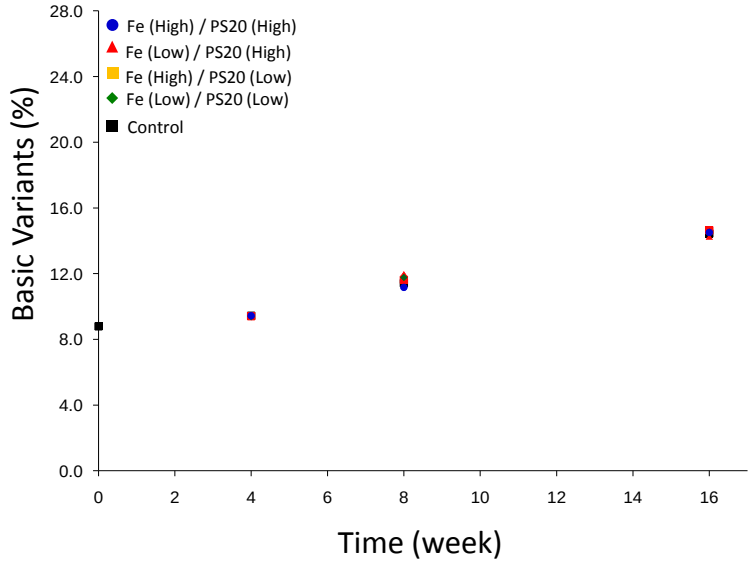

Figure 20. (A) The levels of acidic variants; (B) the levels of basic variant of the mAb A samples from the storage study.

A

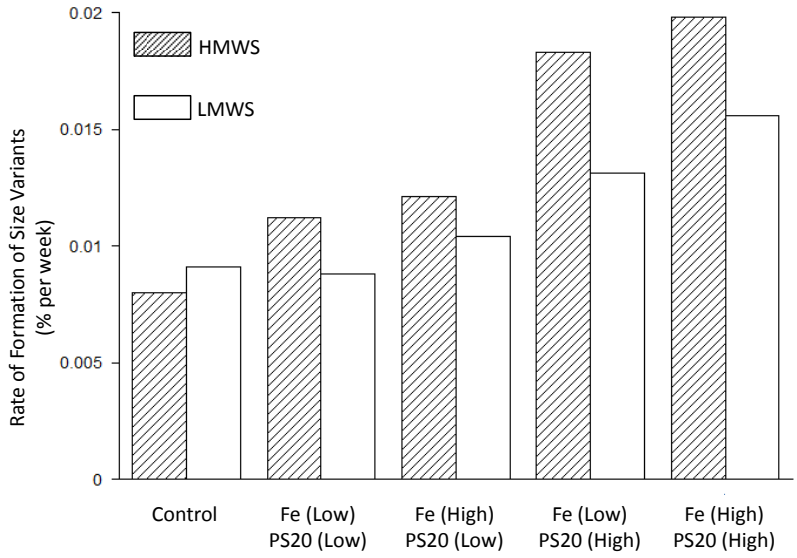

B

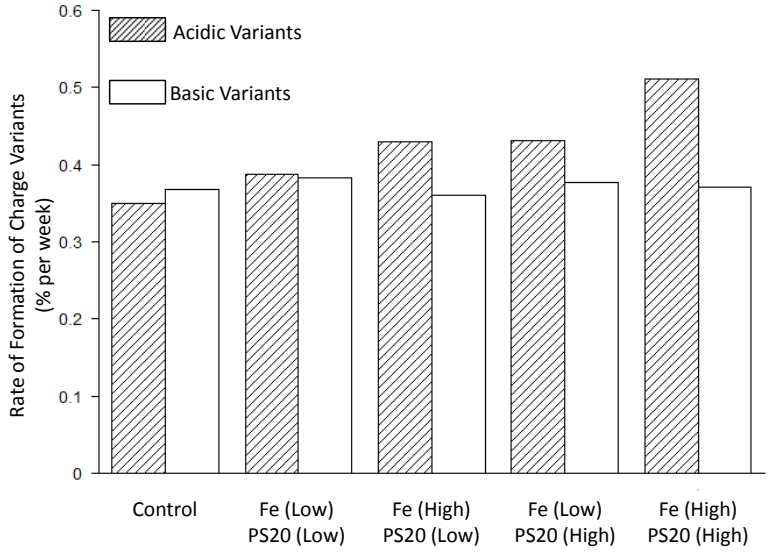

Figure 21. (A) The rate of formation of size variants; (B) the rate of formation of charge variants of the mAb A samples from the storage study.

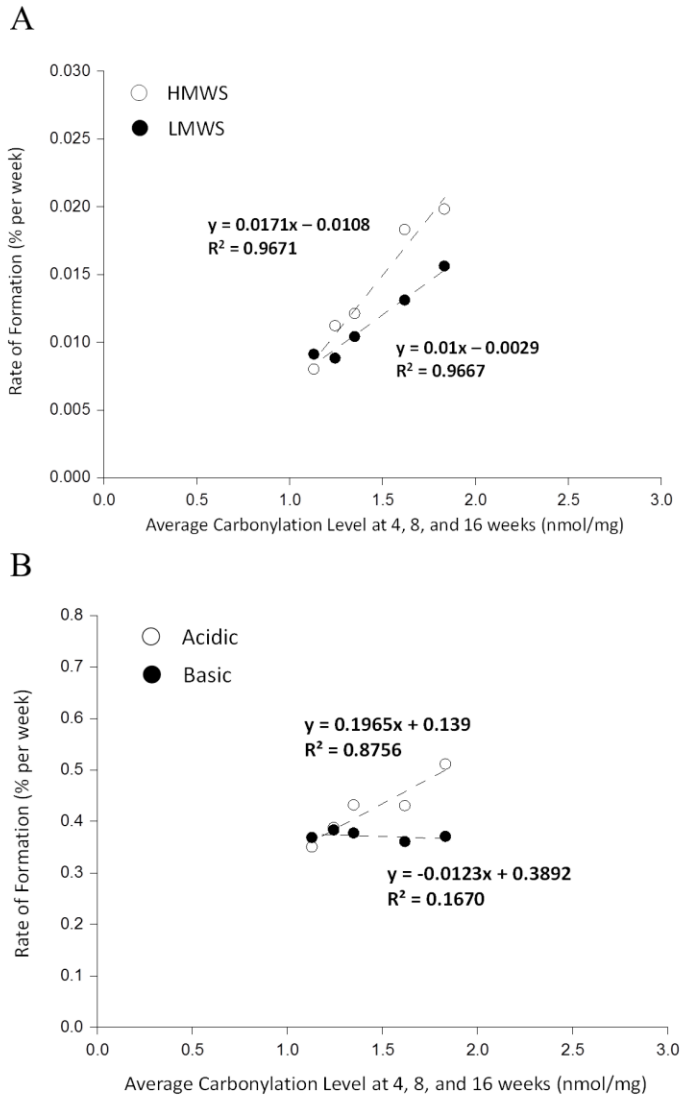

Figure 22. (A) The relationship between the average level of carbonylation at 4, 8, and 16 weeks and the rate of formation of the size variants (i.e., HMWS and LMWS) of mAb A samples from the storage study; (B) the relationship between the average level of carbonylation at 4, 8, and 16 weeks and the rate of formation of the charge variants (i.e., acidic or basic variants) of mAb A samples from the storage study.

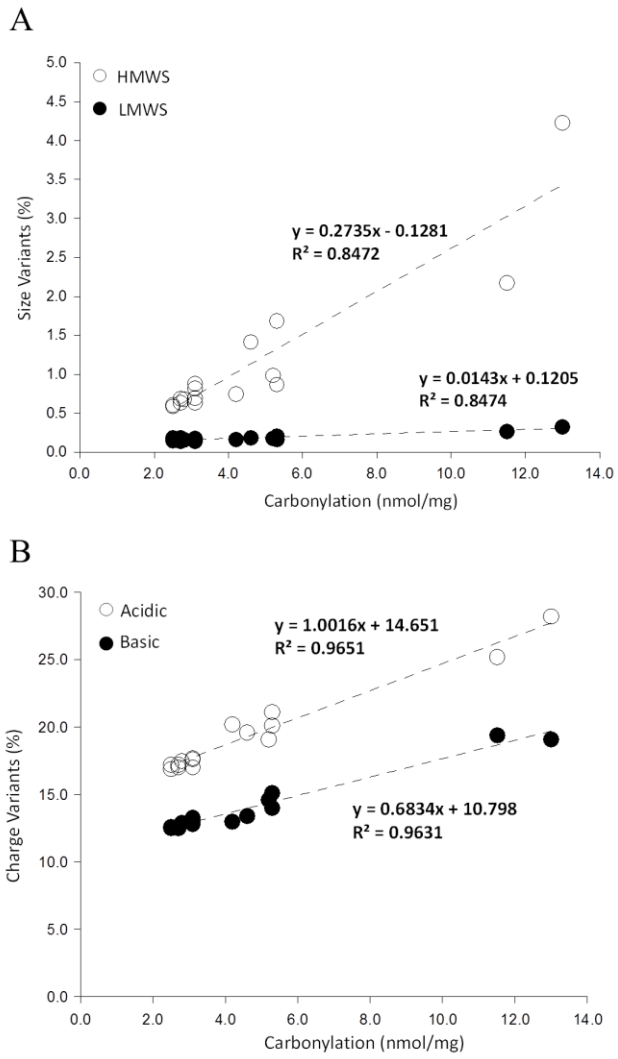

Figure 23. (A) The relationship between the levels of carbonylation and size variants, i.e., High Molecular Weight Species (HMWS) and Low Molecular Weight Species (LMWS) of mAb A samples from the stress study; (B) the relationship between the levels of carbonylation and charge variants, i.e., acidic and basic species of mAb A samples from the stress study.

A

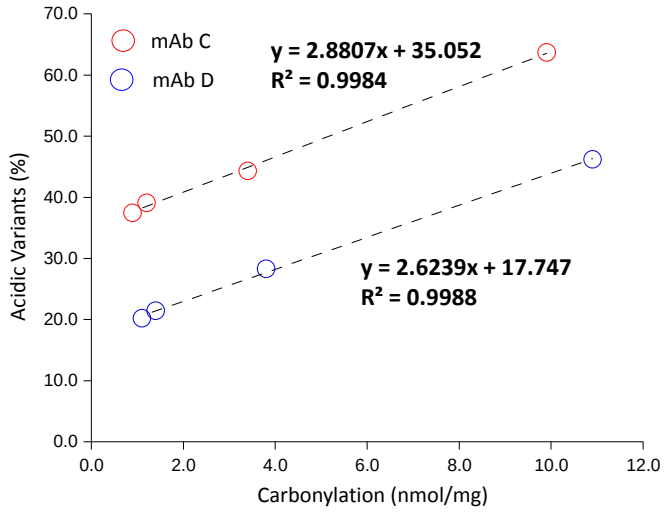

B

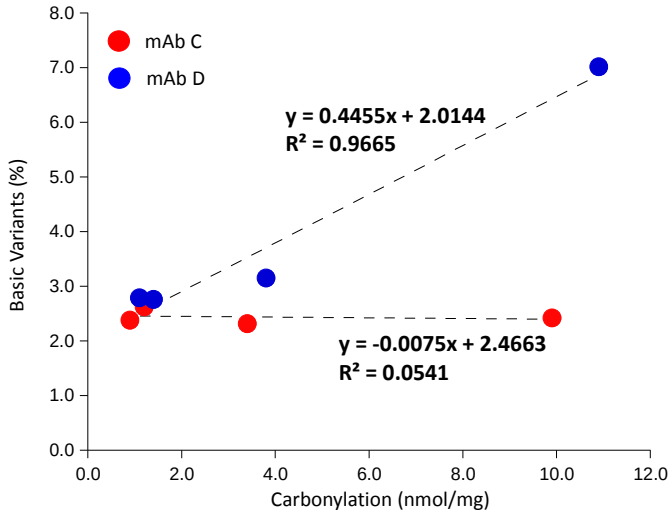

Figure 24. (A) The relationship between the levels of carbonylation and acidic variants of the stressed mAb C and mAb D samples; (B) the relationship between the levels of carbonylation and basic variants of the stressed mAb C and mAb D samples.

DISCUSSION

To develop a robust and precise assay for the investigation of mAb carbonylation, we selected LY CH as the derivatization reagent based on the following considerations. First, LY CH reacts specifically with carbonyls via the hydrazide group. This type of derivatization reaction is widely adopted in many different carbonylation assays.[9] In addition, the site-specific reactivity of LY CH against metal-catalyzed carbonylation was confirmed in our study by an MS-based approach. Second, LY CH has relatively high solubility in water.[10] Taking advantage of the high solubility of LY CH, we designed a workflow that does not require protein precipitation (Figure 2). Third, LY CH strongly absorbs at 428 nm,[8] which differs from the maximum absorbance wavelength (~280 nm) of an mAb. This difference in wavelength allows us to apply the absorbance-based quantitation strategy that has been adopted to determine drug-to-antibody ratios (DARs) for many antibody drug conjugates (ADCs).[26] Namely, the quantitation with CALY is based on the absorbance at 280 nm and 428 nm of an LY CH-derivatized mAb sample (Figure 3), where the individual concentrations of mAb and LY CH can be determined by solving the two equations that account for the absorbance at 280 and 428 nm.

We demonstrated that CALY is more robust and precise than the conventional DNPH assay. A key feature contributing to the improved performance is that LY CH-derivatized mAb species are baseline separated from the unconsumed LY CH on SEC (Figure 3). Therefore, the quantitation does not require exhaustive and reproducible removal of LY CH, which was supported by the robustness assessment data from 2-4 rounds of buffer exchange. By contrast, the commonly used DNPH assay requires protein precipitation, which is believed to cause the observed larger CV of the measurement.[4]

In the accuracy assessment, we observed that the DNPH assay generated a lower carbonylation level for the highly oxidized mAb A than CALY. A similar observation was reported by Soglia et al.,[27] where the DNPH assay generated lower carbonylation levels for oxidized muscle and meat proteins than a modified DNPH assay. Protein unfolding and solubilization were suggested to be the cause.[27] While future studies will be needed to understand if protein unfolding and solubilization contributed to the under-quantification by the DNPH assay for the highly oxidized mAb A in our case, CALY and the DNPH assay provided similar quantitation of mAb carbonylation at levels up to 7 nmol/mg, which covers the carbonylation levels observed in our cell culture and storage studies, as well as a majority of the reported protein carbonylation levels from other studies.[3, 5, 19, 28-30]

We established the LOD and LOQ for CALY as 0.1 nmol/mg and 0.3 nmol/mg, respectively. The LOQ of 0.3 nmol/mg, equivalent to only 0.05 mole carbonyls per mole of a 150 KDa mAb, is approximately 6-10 times lower than the reported normal level of plasma protein carbonylation of 2-3 nmol/mg.[5] The LOQ of CALY is higher than that of a recently modified ELISA-based method, which was established as 0.2 nmol/mg.[3] This is not surprising since ELISA is inherently more sensitive than spectrophotometric methods. Nevertheless, compared to the ELISA-based carbonylation method, CALY has a simpler sample preparation procedure and is, therefore, less tedious/labor-intensive than the ELISA method. In addition, the ELISA assay requires a protein standard with a known carbonylation level for its use in different laboratories,[5] while CALY does not require such a protein carbonylation standard.

The benefit of improved assay robustness and precision with CALY is readily reflected in our cell culture, storage, and stress studies, where less precision with the DNPH assay would make it more difficult to identify the trends and relationships as clearly. The cell culture study

established a link between iron levels in cell culture media and mAb carbonylation. In the literature, a similar iron titration experiment has been performed by Bai et al. [15] However, carbonylation levels were not provided for the produced mAbs in their study. Recently, Purdie et al. provided relative levels of carbonylation for mAbs produced in two chemically defined media and showed relative reduction in mAb carbonylation with the media containing less cysteine and ferric ammonium citrate.[2] Compared to the study by Purdie et al., our results provided a direct and more complete understanding of the effect of iron on mAb carbonylation, where we showed that the relationship between the iron concentration and mAb B carbonylation was not linear. Additionally, we showed that the commonly observed cell culture parameters did not seem to be useful indicators for mAb carbonylation. These findings identified iron as a critical factor, but also suggested that it may be necessary to understand additional factors, such as hydrogen peroxide level in cell cultures[25] and/or cell line-specific defense mechanisms against reactive oxygen species[31], to enable a robust control of mAb carbonylation in cell culture.

The storage study showed that PS20 and iron, at pharmaceutically relevant concentrations, induced mAb carbonylation during storage. The peroxides from PS20 were likely a critical factor for mAb carbonylation during storage. Thus, mAb A samples containing 0.16% PS20, which should contain more peroxides because of the higher PS20 concentration, showed consistently higher levels of carbonylation. With longer storage times, we observed decreases in the carbonylation levels. While this observation has not been previously reported for mAbs, a decrease in the carbonylation levels was observed for myofibrillar proteins during 10-day incubation with iron (III) and hydrogen peroxide.[32] For myofibrilar proteins, the so-called decarbonylation was attributed to the formation of Schiff-bases between aldehydes and lysine residues.[32] Such a decarbonylation process could occur in our storage study, since Schiff-bases

are formed at mildly acidic pHs,[33] such as pH 6.0 of the storage buffer. In addition, other processes, such as formation of insoluble aggregates or formation of carboxylic acids from further oxidation of aldehydes, could also contribute to the observed decreases in mAb carbonylation during storage.

The stress study demonstrated a complex effect of iron and hydrogen peroxide on mAb carbonylation, where the existing knowledge is limited. For example, in the report by Uehara and Rao,[3] the effects of iron content, buffer type, and storage temperature on protein carbonylation were studied at a fixed hydrogen peroxide concentration. In another report by Kryndushkin and Rao,[34] the oxidation reactions were carried out with excess amounts of hydrogen peroxide. Using the 16 stress conditions over a wide range of iron and hydrogen peroxide concentrations, our study more extensively mimicked the oxidative environment that mAbs may be exposed to during cell culture. It should be pointed out that Fenton and Fenton-like reactions are expected to occur under these stress conditions. In the Fenton reactions, ferrous ion is oxidized by hydrogen peroxide to form ferric ion, while hydrogen peroxide decomposes to form a hydroxyl radical and a hydroxyl ion. The hydroxyl radical is highly reactive and can abstract a hydrogen atom from an adjacent carbon-hydrogen bond to form a carbon-centered radical, which initiates the carbonylation process and ultimately leads to the carbonyls detected by CALY. In this sense, formation of these carbonyl products appears to be primarily catalyzed by ferrous ion but not ferric ion. However, in the Fenton-like reactions, ferric ion can react, although at a much slower rate[35], with hydrogen peroxide to generate ferrous ion, hydroperoxyl radical, and proton. The regenerated ferrous ion can then participate in protein carbonylation. Therefore, considering the cyclic nature of these reactions, we focused on the total iron concentration instead of the respective concentration of ferrous or ferric ion. As shown in Figure 17, the observed effect of

iron and hydrogen peroxide is consistent with the proposed mechanism for protein carbonylation,[1] where ferrous ion (which can be regenerated from ferric ion) acts as a catalyst and hydrogen peroxide is consumed in the process. Importantly, the stress study showed that hydrogen peroxide also plays a critical role in mAb carbonylation, which has not been emphasized in the literature. Furthermore, the stress study lends support to our hypotheses and proposed mechanisms that implicate peroxides in the cell culture and storage studies.

From the storage and stress studies, we observed positive correlations between metal-catalyzed carbonylation and the formation of HMWS and LMWS. While correlation does not imply causation, the observed correlation with the HMWS in our studies adds to the growing evidence in the literature supporting that carbonylation may promote the formation of protein aggregates,[3, 19, 36-37] where the cause-effect relationship has been largely attributed to the increased protein hydrophobicity.[36] For the observed correlation with the LMWS, it is unlikely that metal-catalyzed carbonylation directly generated the LMWS. Instead, the carbonylation levels likely parallel the extent of metal-catalyzed mAb fragmentation, probably caused by protein backbone radicals, generated via Fenton reaction (the Fenton reaction cannot only lead to carbonylation but also other radical-mediated processes).[38] From the cell culture studies, surprisingly no correlation was observed between carbonylation and the formation of HMWS or LMWS in mAb B samples. This result suggests that carbonylation cannot be used as a general indicator for mAb aggregation or fragmentation propensity. It is possible that mechanisms [39-40] not related to metal-catalyzed reactions contributed to the formation of HMWS and LMWS under the cell culture conditions.

Our studies revealed a positive correlation between metal-catalyzed carbonylation and formation of acidic variants in mAbs. To the best of our knowledge, this correlation has not been

previously reported for mAbs. The consistent correlations in all of our studies suggests that metal-catalyzed oxidation may represent a degradation pathway for inducing acidic charge heterogeneity of mAbs. This highlights a new direction for investigating acidic charge heterogeneity of mAbs during production and storage. It should be noted that the observed product quality correlations in our studies cannot be satisfactorily explained by deamidation or glycation, two common degradation pathways for inducing acidic variants during production[41] or storage.[42] For example, in the stability study, different mAb A samples should essentially deamidate at the same rate as suggested by the deamidation mechanism,[43-44] since these samples were exposed to the same buffer and temperature. In the cell culture study, the glucose or the offline pH profiles (Figure 13) differed only slightly or were in an opposite trend compared to those of the acidic charge variants.

Carbonylation of lysine and arginine residues directly forms acidic charge species due to the loss of the positive charge on their side chains, and therefore a cause-effect relationship can at least be partially established to explain the correlations. It is possible that, other than lysine and arginine carbonylation, formation of Schiff bases (between aldehydes and primary amines) or carboxylic acids (by further oxidation of aldehyde groups), could contribute to acidic charge heterogeneity, although formation of these products results in a decrease in mAb carbonylation level. In the stability study, formation of Schiff bases or carboxylic acids could potentially explain why the decrease in carbonylation level from 8 to 16 weeks in some samples did not cause a decrease in the level of acidic variants. Further characterization, such as by peptide mapping analysis of enriched acidic fractions, will be performed in the future to elucidate these acidic charge species.

In summary, this work presents an improved protein carbonylation assay, CALY, which addressed several key analytical challenges with commonly used protein carbonylation assays. The method performance of CALY was extensively evaluated and the utility of CALY was demonstrated by several case studies under cell culture, storage, and stress conditions. More importantly, through the use of CALY, we acquired new insights into both the mechanism and the effects of metal-catalyzed carbonylation of mAbs. These insights place us in a better position to address product quality risks associated with metal-catalyzed carbonylation during mAb production and storage.

Reference

1. Stadtman, E. R., Metal ion-catalyzed oxidation of proteins: biochemical mechanism and biological consequences. *Free Radic Biol Med* **1990,** *9* (4), 315-25.

2. Purdie, J. L.; Kowle, R. L.; Langland, A. L.; Patel, C. N.; Ouyang, A.; Olson, D. J., Cell culture media impact on drug product solution stability. *Biotechnol Prog* **2016,** *32* (4), 998-1008.

3. Uehara, H.; Rao, V. A., Metal-mediated protein oxidation: applications of a modified ELISA-based carbonyl detection assay for complex proteins. *Pharm Res* **2015,** *32* (2), 691-701.

4. Matthijssens, F. B., Bart P.; Vanfleteren, Jacques R., Evaluation of Different Methods for Assaying Protein Carbonylation. *Current Analytical Chemistry* **2007,** *3* (2), 93-102.

5. Rogowska-Wrzesinska, A.; Wojdyla, K.; Nedic, O.; Baron, C. P.; Griffiths, H. R., Analysis of protein carbonylation--pitfalls and promise in commonly used methods. *Free Radic Res* **2014,** *48* (10), 1145-62.

6. Luo, S.; Wehr, N. B., Protein carbonylation: avoiding pitfalls in the 2,4-dinitrophenylhydrazine assay. *Redox report : communications in free radical research* **2009,** *14* (4), 159-66.

7. Buss, H.; Chan, T. P.; Sluis, K. B.; Domigan, N. M.; Winterbourn, C. C., Protein carbonyl measurement by a sensitive ELISA method. *Free radical biology & medicine* **1997,** *23* (3), 361-6.

8. Stewart, W. W., Functional connections between cells as revealed by dye-coupling with a highly fluorescent naphthalimide tracer. *Cell* **1978,** *14* (3), 741-59.

9. Fedorova, M.; Bollineni, R. C.; Hoffmann, R., Protein carbonylation as a major hallmark of oxidative damage: update of analytical strategies. *Mass Spectrom Rev* **2014,** *33* (2), 79-97.

10. Hanani, M., Lucifer yellow - an angel rather than the devil. *J Cell Mol Med* **2012,** *16* (1), 22-31.

11. Yang, Y.; Stella, C.; Wang, W.; Schoneich, C.; Gennaro, L. A., Characterization of Oxidative Carbonylation on Recombinant Monoclonal Antibodies. *Analytical chemistry* **2014**.

12. Keener, C. R.; Wolfe, C. A.; Hage, D. S., Optimization of oxidized antibody labeling with lucifer yellow CH. *Biotechniques* **1994,** *16* (5), 894-7.

13. Hage, D. S., Periodate oxidation of antibodies for site-selective immobilization in immunoaffinity chromatography. *Methods Mol Biol* **2000,** *147*, 69-82.

14. Zhang, J.; Robinson, D.; Salmon, P., A novel function for selenium in biological system: selenite as a highly effective iron carrier for Chinese hamster ovary cell growth and monoclonal antibody production. *Biotechnol Bioeng* **2006,** *95* (6), 1188-97.

15. Bai, Y.; Wu, C.; Zhao, J.; Liu, Y. H.; Ding, W.; Ling, W. L., Role of iron and sodium citrate in animal protein-free CHO cell culture medium on cell growth and monoclonal antibody production. *Biotechnol Prog* **2011,** *27* (1), 209-19.

16. Stadtman, E. R., Oxidation of free amino acids and amino acid residues in proteins by radiolysis and by metal-catalyzed reactions. *Annu Rev Biochem* **1993,** *62*, 797-821.

17. Franek, F.; Dolnikova, J., Hybridoma growth and monoclonal antibody production in iron-rich protein-free medium: effect of nutrient concentration. *Cytotechnology* **1991,** *7* (1), 33-8.

18. Zhou, S.; Schoneich, C.; Singh, S. K., Biologics formulation factors affecting metal leachables from stainless steel. *AAPS PharmSciTech* **2011,** *12* (1), 411-21.

19. Bee, J. S.; Davis, M.; Freund, E.; Carpenter, J. F.; Randolph, T. W., Aggregation of a monoclonal antibody induced by adsorption to stainless steel. *Biotechnol Bioeng* **2010,** *105* (1), 121-9.

20. Bee, J. S.; Chiu, D.; Sawicki, S.; Stevenson, J. L.; Chatterjee, K.; Freund, E.; Carpenter, J. F.; Randolph, T. W., Monoclonal antibody interactions with micro- and nanoparticles: adsorption, aggregation, and accelerated stress studies. *J Pharm Sci* **2009,** *98* (9), 3218-38.

21. Kerwin, B. A., Polysorbates 20 and 80 used in the formulation of protein biotherapeutics: structure and degradation pathways. *J Pharm Sci* **2008,** *97* (8), 2924-35.

22. Jaeger, J.; Sorensen, K.; Wolff, S. P., Peroxide accumulation in detergents. *J Biochem Biophys Methods* **1994,** *29* (1), 77-81.

23. Hawe, A.; Filipe, V.; Jiskoot, W., Fluorescent molecular rotors as dyes to characterize polysorbate-containing IgG formulations. *Pharm Res* **2010,** *27* (2), 314-26.

24. Mallaney, M.; Wang, S. H.; Sreedhara, A., Effect of ambient light on monoclonal antibody product quality during small-scale mammalian cell culture process in clear glass bioreactors. *Biotechnol Prog* **2014,** *30* (3), 562-70.

25. Halliwell, B.; Clement, M. V.; Ramalingam, J.; Long, L. H., Hydrogen peroxide. Ubiquitous in cell culture and in vivo? *IUBMB Life* **2000,** *50* (4-5), 251-7.

26. Wakankar, A.; Chen, Y.; Gokarn, Y.; Jacobson, F. S., Analytical methods for physicochemical characterization of antibody drug conjugates. *MAbs* **2011,** *3* (2), 161-72.

27. Soglia, F.; Petracci, M.; Ertbjerg, P., Novel DNPH-based method for determination of protein carbonylation in muscle and meat. *Food Chem* **2016,** *197* (Pt A), 670-5.

28. Stadtman, E. R., Protein oxidation and aging. *Free Radic Res* **2006,** *40* (12), 1250-8.

29. Weber, D.; Davies, M. J.; Grune, T., Determination of protein carbonyls in plasma, cell extracts, tissue homogenates, isolated proteins: Focus on sample preparation and derivatization conditions. *Redox Biol* **2015,** *5*, 367-80.

30. Shacter, E., Quantification and significance of protein oxidation in biological samples. *Drug Metab Rev* **2000,** *32* (3-4), 307-26.

31. Thorpe, G. W.; Fong, C. S.; Alic, N.; Higgins, V. J.; Dawes, I. W., Cells have distinct mechanisms to maintain protection against different reactive oxygen species: oxidative-stress-response genes. *Proc Natl Acad Sci U S A* **2004,** *101* (17), 6564-9.

32. Rysman, T.; Utrera, M.; Morcuende, D.; Van Royen, G.; Van Weyenberg, S.; De Smet, S.; Estevez, M., Apple phenolics as inhibitors of the carbonylation pathway during in vitro metal-catalyzed oxidation of myofibrillar proteins. *Food Chem* **2016,** *211*, 784-90.

33. Cordes, E. H.; Jencks, W. P., On the Mechanism of Schiff Base Formation and Hydrolysis. *Journal of the American Chemical Society* **1962,** *84* (5), 832-837.

34. Kryndushkin, D.; Rao, V. A., Comparative Effects of Metal-Catalyzed Oxidizing Systems on Carbonylation and Integrity of Therapeutic Proteins. *Pharm Res* **2016,** *33* (2), 526-39.

35. Hong, J.; Schoneich, C., The metal-catalyzed oxidation of methionine in peptides by Fenton systems involves two consecutive one-electron oxidation processes. *Free radical biology & medicine* **2001,** *31* (11), 1432-41.

36. Petrov, D.; Zagrovic, B., Microscopic analysis of protein oxidative damage: effect of carbonylation on structure, dynamics, and aggregability of villin headpiece. *J Am Chem Soc* **2011,** *133* (18), 7016-24.

37. Purdie, J.; Kowle, R.; Langland, A.; Patel, C. N.; Ouyang, A.; Olson, D., Cell culture media impact on drug product solution stability. *Biotechnol Prog* **2016**.

38. Vlasak, J.; Ionescu, R., Fragmentation of monoclonal antibodies. *MAbs* **2011,** *3* (3), 253-63.

39. Gomez, N.; Subramanian, J.; Ouyang, J.; Nguyen, M. D.; Hutchinson, M.; Sharma, V. K.; Lin, A. A.; Yuk, I. H., Culture temperature modulates aggregation of recombinant antibody in cho cells. *Biotechnol Bioeng* **2012,** *109* (1), 125-36.

40. Dorai, H.; Ganguly, S., Mammalian cell-produced therapeutic proteins: heterogeneity derived from protein degradation. *Curr Opin Biotechnol* **2014,** *30*, 198-204.

41. Yuk, I. H.; Zhang, B.; Yang, Y.; Dutina, G.; Leach, K. D.; Vijayasankaran, N.; Shen, A. Y.; Andersen, D. C.; Snedecor, B. R.; Joly, J. C., Controlling glycation of recombinant antibody in fed-batch cell cultures. *Biotechnol Bioeng* **2011,** *108* (11), 2600-10.

42. Diepold, K.; Bomans, K.; Wiedmann, M.; Zimmermann, B.; Petzold, A.; Schlothauer, T.; Mueller, R.; Moritz, B.; Stracke, J. O.; Molhoj, M.; Reusch, D.; Bulau, P., Simultaneous

assessment of Asp isomerization and Asn deamidation in recombinant antibodies by LC-MS following incubation at elevated temperatures. *PLoS One* **2012,** *7* (1), e30295.

43. Patel, K.; Borchardt, R. T., Chemical pathways of peptide degradation. II. Kinetics of deamidation of an asparaginyl residue in a model hexapeptide. *Pharm Res* **1990,** *7* (7), 703-11.

44. Song, Y.; Schowen, R. L.; Borchardt, R. T.; Topp, E. M., Effect of 'pH' on the rate of asparagine deamidation in polymeric formulations: 'pH'-rate profile. *J Pharm Sci* **2001,** *90* (2), 141-56.

Chapter 3

Characterization of Acidic Charge Heterogeneity Induced by Metal-Catalyzed Oxidation in a Recombinant Monoclonal Antibody

INTRODUCTION

Recombinant monoclonal antibodies (mAbs) are an important class of therapeutic drugs[1] and have broad applications in many disease areas.[2-3] Compared to small molecule drugs, mAb drugs are immensely more complex not only because mAbs have a much larger molecule weight (~150kDa) but also because a large variety of mAb product variants can be generated during mAb manufacturing.[4-6] These product variants could potentially impact mAb safety and efficacy profiles.[7-8] Therefore, it is necessary to thoroughly characterize mAb product variants during mAb development. In fact, health authorities have recently introduced a quality-by-design paradigm, which emphasizes building process and product quality understandings into a control strategy.[9-10]

Charge variants are a common type of mAb product variants.[11-14] Formation of mAb charge variants often involves changes in the isoelectric point or net charge of mAbs.[11] These charge variants are typically monitored by ion exchange chromatography or imaged capillary isoelectric focusing in a control system.[15-16] During mAb development, it is highly desirable to have consistent charge heterogeneity profiles that meet product quality acceptance criteria for therapeutic use.[17] To help achieve that goal, significant amount of knowledge has been acquired in recent years on the source of mAb charge heterogeneity and the relevant manufacturing factors.[5] For example, a major basic charge variant was identified as C-terminal lysine variant.[18] The source of this variant was attributed to the incomplete enzymatic removal of mAb heavy chain C-terminal lysine residue, which contains a positive charge from the primary amine group on the lysine side chain.[18] Zinc, a cofactor of the enzyme responsible for the removal of the C-terminal lysine residues, was identified as a cell culture factor that can help control this basic variant in mAb products.[19] For the acidic charge variants, a commonly observed acidic charge

variant was asparagine deamidation to aspartate, which contains a negative charge from the carboxylic acid group on aspartate side chain.[20] For the deamidation reaction, multiple factors, such as protein sequence, pH, temperature, and higher order structure, have been identified to explain the formation of these acidic charge variant in mAbs.[20] Based on these understandings, temperature and pH downshifts were implemented in cell culture processes to lower acidic charge variant content in mAbs.[21]

Existing literature points out that mAb acidic charge variants are often more heterogeneous than basic charge variants.[22] This is likely because many possible reactions can occur on lysine or arginine residues, which leads to the loss of the positive charges on mAbs. Quan et. al. reported that glycation, a reaction between lysine and reducing sugars, led to increased acidic charge heterogeneity in a model mAb.[23] This was explained by the formation of a ketoamine Amadori product, which removes the positive charge from lysine.[23] Chumsae et. al. reported that arginine residues can react with methylglyoxal, a cell culture metabolite, to form dihydroxyimidazolidine and hydroimidazolone products, which removes the positive charge from arginine.[24] Interestingly, methionine oxidation, which does not change the net charge of mAbs, was reported in the acidic fractions of an IgG1 mAb.[22] It was hypothesized that conformational changes induced by methionine oxidation promoted the formation of deamidation products, which co-localized with methionine oxidation in the acidic fractions.[22] This may also be explained by methionine oxidation-induced unfolding,[25] which could change pKa values of various residues on proteins.[26]

We previously reported that metal-catalyzed oxidation can induce the formation of acidic charge variants in mAbs.[27] However, to date, the induced acidic charge variants have not been characterized. Several degradation pathways are likely involved in the formation of these acidic

variants. First, metal-catalyzed oxidation can generate protein carbonyls (such as aldehydes and ketones) on lysine, arginine, threonine, and proline residues.[28] When lysine and arginine are converted to their respective aldehyde product (adipic semialdehyde and glutamic semialdehyde), the positive charge on the side chain is lost. While our previous study has confirmed the presence of these two aldehyde products in mAbs after metal-catalyzed oxidation,[29] it is not known if the aldehyde products constitute a major component of the oxidation-induced acidic variants. Second, the aldehyde products can be further oxidized to carboxylic acid (adipic acid or glutamic acid) or react with primary amines on mAbs to form a Schiff base. These additional degradation products can contribute to the acidic charge heterogeneity due to addition of a negative charge (from carboxylic acid) or removal of a positive charge (from primary amine). Third, metal-catalyzed oxidation has been known to convert additional neutral or basic residues to acidic species in proteins.[30] For example, cysteine can be oxidized to cysteic acid; histidine can be oxidized to aspartate; proline can be oxidized to glutamate.[30] For mAbs, it has been reported that cysteine residues in the hinge region can be oxidized to cysteic acid after metal-catalyzed oxidation.[31] However, very little is known about the location and relative abundance of the other acidic oxidation products (if they exist) in mAbs. Considering that these various types of acidic variants may have different impacts on mAb product quality, it is critical to provide a detailed characterization of mAb acidic variants induced by metal-catalyzed oxidation.

This study reports a comprehensive characterization of the acidic variants of a model IgG1 mAb after metal-catalyzed oxidation. The acidic and main peak fractions from the unstressed and highly stressed mAb A were collected to high purity by ion exchange chromatography. Subsequently, these fractions were characterized by a wide range of analytical

methods, such as size exclusion chromatography, intact/reduced molecular mass analysis, peptide mapping, and hydrogen-deuterium exchange mass spectrometry.[32-35] It was found that conventional peptide mapping provided only limited information on the product variants, in particular, the protein carbonyls. To facilitate the characterization of these carbonylation products, an existing site-specific carbonylation peptide mapping method was optimized to for relative quantitation of site-specific carbonyls in mAb A fractions. We showed that, contrary to the common belief, threonine carbonylation products, but not lysine or arginine carbonylation products, are a major component in the acidic fractions. Additionally, we identified a large number of acidic degradation products. Many of these acidic degradation products are reported in mAbs for the first time. The detailed characterization provides a better understanding on how metal-catalyzed oxidation induces acidic charge variants on mAbs. The characterization of these degradation products better informs mAb product quality assessment, which aligns with expectations from health authorities on implementing quality-by-design to ensure the safety and efficacy of mAb products.

MATERIALS AND METHODS

Materials

The recombinant monoclonal antibody, mAb A, was manufactured at Genentech (South San Francisco, CA). Lucifer Yellow carbohydride dilithium salt (Lucifer Yellow CH), ferrous sulfate, hydrogen peroxide solution (30% in H_2O, w/w), methionine, ethylenediaminetetraacetic acid (EDTA), sodium succinate, succinic acid, sodium phosphate (dibasic and monobasic), sodium chloride, sodium acetate, acetic acid, sodium hydroxide solution (1M in H_2O), 2-(N-morpholino)ethanesulfonic acid (MES), lithium hydroxide, reduced Triton X-100, TCEP (tris(2-carboxyethyl)phosphine), (Carboxymethyl)trimethylammonium chloride hydrazide (Girard's

Reagent T, GRT), dithiothreitol (DTT), formic acid, iodoacetic acid (IAA), calcium chloride, tris(hydroxymethyl) aminomethane (Tris), deuterium water, urea, and trifluoroacetic acid (TFA) were purchased from Sigma-Aldrich (St. Louis, MO, USA). TSK G3000 SWXL (7.8x300mm) size exclusion column was purchased from Tosoh Bioscience (King of Prussia, PA, USA). ProPac WCX 10 column was purchase from Thermo Fisher Scientific (Waltham, MA, USA). Carboxypeptidase B was purchased from Roche Diagnostics (Mannheim, Germany). Acetonitrile (ACN) was purchased from Burdick & Jackson (Muskegon, MI, USA). Sequencing-grade trypsin was purchased from Promega (Madison, WI, USA). ACQUITY UPLC Peptide CSH C18 Column (130 Å, 1.7 µm, 2.1x150 mm), Waters ACQUITY BEH C18 VanGuard Pre-column (2.1x5 mm), BEH C18 column (1.0 × 50 mm), and BEH C18 (300 Å, 1.7 um, 2.1x150mm) column were purchased from Waters (Milford, MA, USA). An immobilized protease XIII/pepsin column (2.0 × 30 mm) was purchased from NovaBioAssays (Woburn, MA, USA).

Metal-catalyzed oxidation of mAb A

The oxidized mAb A sample was prepared by metal-catalyzed oxidation, where mAb A was mixed with ferrous sulfate and hydrogen peroxide to a final concentration of 5 mg/mL, 2 mM, and 2 mM, respectively. The oxidation reaction was carried out at the room temperature in 50 mM sodium succinate buffer (pH 6.5) for 2 hours, and was subsequently stopped by addition of excess amounts of methionine and EDTA.

Charge Heterogeneity Analysis

The mAb A samples were analyzed by ion exchange chromatography (IEC) using a Dionex ProPac WCX 10 column (4x250 mm). Before the analysis, the mAb A samples were mixed with Carboxypeptidase B at an enzyme-to-substrate ratio of 1:100 (weight to weight). These samples were then incubated at 37ºC for 30 minutes to remove heavy chain C-terminal lysine on mAb A.

For the IEC analysis, the mobile phase A was 20 mM MES, pH 6.50 ± 0.05. The mobile phase B was 100 mM sodium chloride in mobile phase A. A linear gradient of 0% solvent B to 100% solvent B in 50 minutes was applied to separate mAb A charge variants. The column temperature was controlled at 40°C and the autosampler temperature was controlled at 8°C. The flow rate was 0.5 mL/min. The column effluent was monitored by UV absorbance at 280 nm. Integration of the acidic, main peak, and basic regions was performed manually using Agilent Chemstation software.

Size Heterogeneity Analysis

The mAb A samples were analyzed by size exclusion chromatography (SEC) using a TSK G3000 SWXL (7.8x300 mm) size exclusion column. For the SEC analysis, the mobile phase was 200 mM potassium phosphate, 250 mM potassium chloride, pH 6.2. The column temperature was controlled at 25°C and the HPLC autosampler temperature was controlled at 8°C. An isocratic flow of 0.5 ml/min was employed. The effluent was monitored by UV absorbance at 280 nm. Integration of the High Molecular Weight Species (HMWS), Main Peak, and Low Molecular Weight Species (LMWS) was performed manually using Agilent Chemstation software.

Total Protein Carbonylation Analysis

Total protein carbonylation levels of mAb A samples were measured using Lucifer Yellow CH as the derivatization reagent. As previously described in Chapter 2, for the analysis, mAb A samples (to a final concentration of 0.2 mg/mL) were mixed with Lucifer Yellow CH at a Lucifer Yellow CH-to-mAb molar ratio of 8,000:1. The derivatization reaction was carried out in 50 mM lithium MES buffer, 1% Triton X-100, pH 6.0, at 37°C for 16 hours. After the derivatization, these samples (500 µL) were buffer-exchanged three times into the SEC buffer

using 15mL Amicon Ultra-15 30 kDa filters. Subsequently, the total protein carbonylation levels was determined by the peak areas from 280 and 428 nm absorbance of the Lucifer Yellow CH-derived mAb A on the size exclusion chromatograms.

Peptide Mapping

The mAb A samples were analyzed by the conventional tryptic peptide mapping method, where the samples were denatured, reduced, and S-carboxymethylated before being digested by trypsin. For the tryptic digestion, the trypsin-to-substrate ratio was 1:50 (weight to weight), and the digestion was carried out in 25 mM Tris-HCl, 2 mM $CaCl_2$, pH 8.2, at 37°C for 5 hours. Subsequently, the digestion was stopped by addition of TFA to a final concentration of 0.3% (v/v). The digested samples were separated on a CSH C18 column (130 Å, 1.7 µm, 2.1x150 mm). Solvent A was 0.1% formic acid in water. Solvent B was 0.1% formic acid in acetonitrile. For the separation, a step gradient was used as follows: 1-13% B in 5 minutes and then 13-35% B in 35 minutes. Flow rate was 0.2 ml/min. Column temperature was controlled at 55°C. The eluted peptides were introduced to an OrbiTrap Velos for mass spectrometry analysis.

Additionally, the mAb A samples were analyzed by a site-specific carbonylation peptide mapping method as previously described.[29] Briefly, the carbonyls were derivatized by Girard's Reagent T (GRT). The hydrozones formed after the derivatization were then reduced by sodium borohydride (to a final concentration of 100 µM). Subsequently, the samples were reduced (by DTT), S-carboxymethylated, and digested with trypsin at a trypsin-to-substrate ratio of 1:50 (weight to weight). The digestion was carried out in 25 mM Tris-HCl, 2 mM $CaCl_2$, pH 8.2, at 37°C for 4 hours, and was stopped by addition of TFA to a final concentration of 0.3% (v/v). The digested samples were separated on a BEH C18 column (300 Å, 1.7 µm, 2.1x150 mm). Solvent A was 0.1% TFA in water. Solvent B was 0.09% TFA in acetonitrile. For the separation, a step

gradient was used as follows: 1-20% B in 16 minutes, 20-40% B in 35 minutes, and then 40-57% B in 15 minutes. Flow rate was 0.3 ml/min. Column temperature was controlled at 60°C. The eluted peptides were introduced to an OrbiTrap Velos for mass spectrometry analysis.

The mass spectrometry analysis was performed in positive mode with an electrospray voltage of 4.0 kV and a capillary temperature of 250°C. The MS data acquisition was in a data-dependent mode, where a full MS survey scan was followed by MS2 scans of the 9 most intense ions in the full MS spectrum. To acquire MS^2 spectra, the normalized collision energy was 35 with an activation time of 10 milliseconds. To identify oxidation products, the mass spectrometry data were analyzed by database searching using the Proteome Discover software. The search results were then manually investigated to confirm the identification of the oxidation products. The relative quantification of these oxidation products was performed by extracted ion chromatography as previously described.

Hydrogen Deuterium Exchange Mass Spectrometry (HDX-MS)

Samples were prepared in 20 mM histidine acetate buffer, pH 6.2 ± 0.2, at a concentration of 3 mg/mL. HDX-MS experiments were performed with a fully automated LEAP RTC system (Leap Technologies, Carr, NC) coupled with an Orbitrap Elite mass spectrometer (Thermo Fisher Scientific, San Jose, CA). For deuterium labeling, three samples were incubated in deuterium buffer (20 mM histidine acetate buffer in D_2O, pH 6.2 ± 0.2) at 20°C. For blank control, each sample was diluted into H_2O buffer instead of D_2O. Duplicate data points were taken after 0.5, 1, 10, 60, 240 minutes of deuterium incubation. The exchange reaction was quenched by reducing the pH to 2.2 with 8 M urea and 1 M TCEP·HCl. Each quenched sample was immediately injected onto an immobilized protease XIII/pepsin column (2.0 × 30 mm) for on-line digestion in 0.1 % formic acid and 0.04 % TFA in H_2O (pH 2.3) at 100 µL/min. Then,

the digested peptides were desalted on a trapping column (Waters ACQUITY BEH C18 VanGuard Pre-column 2.1x5 mm) and further separated on an analytical column (BEH C18 column 1.0 × 50 mm). A separation gradient from 5% to 50% B (A: 0.1 % formic acid and 0.04 % TFA in H_2O; B: 0.1 % formic acid, 0.04 % TFA in acetonitrile) over 12 minutes was provided by a Thermo Ultimate 3000 HPLC (Thermo Fisher Scientific, San Jose, CA). On-line digestion and separation were performed at 0°C to minimize back-exchange. The eluate was introduced into an Orbitrap Elite for measurement. Mass spectra were collected over a range of m/z 300 ~ 1800 at a resolving power setting of 60,000 at m/z 400. Peptides identifications were based on accurate masses together with MS/MS fragmentation by Mascot search.[36] Deuterium incorporation was determined by use of EXMS.[37] Averaged deuterium uptake difference (ARDD) was calculated by a modified python script[38] and mapped onto homologous crystal structures to visualize overall HDX results. No back-exchange corrections were made. All deuterium uptake levels are reported in relative values.

RESULTS

Charge Heterogeneity of the Unstressed and Oxidized mAb A Samples

The unstressed and oxidized mAb A samples were analyzed by ion exchange chromatography to evaluate the impact of metal-catalyzed oxidation on the charge heterogeneity profile. As shown in Figure 1 and Table 1, compared to the unstressed mAb A, the oxidized mAb A showed increased acidic and basic variants and a decreased main peak. The decrease in the main peak (by ~40%) in the oxidized mAb A appeared to be largely due to the increase in the acidic variants. Interestingly, despite the large change in the relative distribution, the overall charge profiles of the two mAb A samples are similar. No distinctive new peak was observed in the oxidized mAb A. To characterize the oxidation-induced acidic charge variants in the oxidized

mAb A, we collected the acidic and main peak fractions from the unstressed and the oxidized mAb A samples. Subsequently, the collected fractions were re-analyzed by ion exchange chromatography and shown to be highly purified (Figure 2).

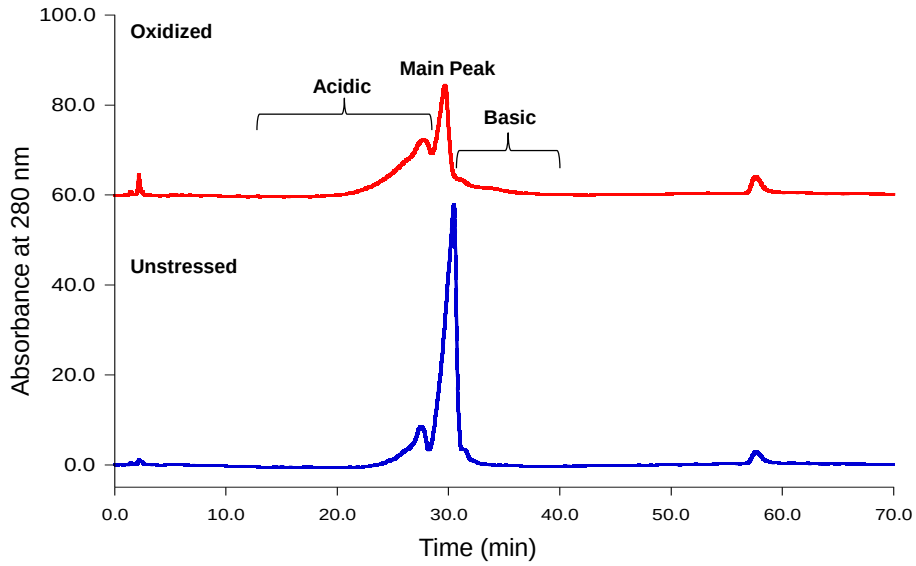

Figure 1. Ion exchange chromatograms of the unstressed and the oxidized mAb A samples

mAb A	Acidic (%)	Main Peak (%)	Basic (%)
Unstressed	18.2	77.6	4.2
Oxidized	51.3	39.8	8.9

Table 1. Charge distribution of the unstressed and the oxidized mAb A samples

A

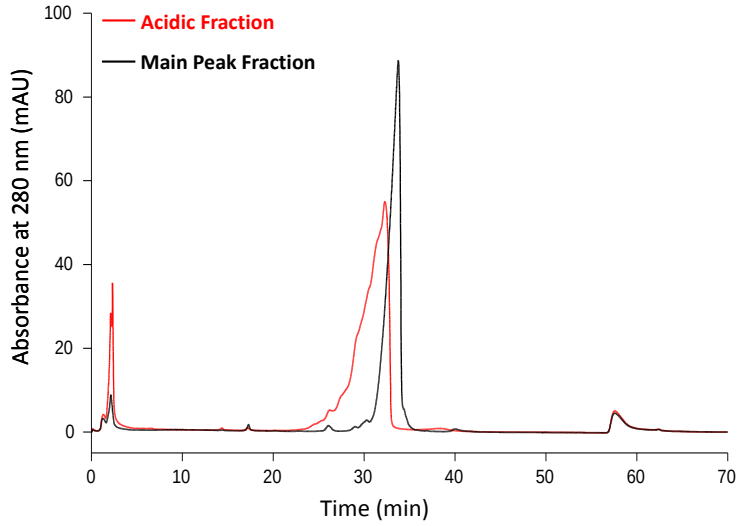

B

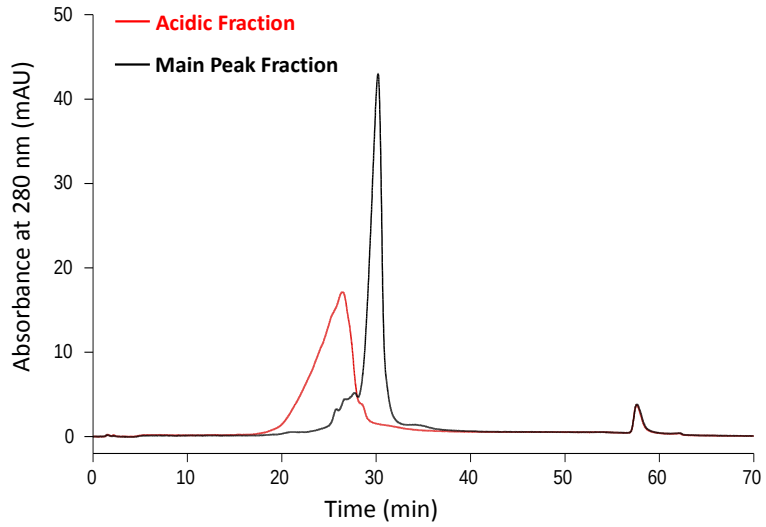

Figure 2. Ion exchange chromatogram of the acidic and main peak fractions from (A) the unstressed and (B) the oxidized mAb A samples.

Size Heterogeneity of mAb A Fractions

Metal-catalyzed oxidation is known to generate size variants, such as low- and high-molecular weight species (LMWS and HMWS), on mAbs.[39-42] These size variants could affect antibody charge heterogeneity since their charge and/or hydrophobicity characteristics may be different from those of the main peak species. We therefore characterized the collected mAb A fractions by SEC (Figures 3 and 4). For the LMWS, a higher level of LMWS was observed in the acidic fraction than in the main peak fraction, for both the unstressed and the oxidized mAb A, which suggests a preferential enrichment of LMWS in the acidic region. Interestingly, one of the LMWS (the shoulder peak eluted at ~16 minutes) was more abundant in the acidic fraction of the oxidized mAb A than in the acidic fraction of the unstressed mAb A. This LMWS was likely des-Fab (an antibody form that contains Fc and one Fab),[43] which could come from metal-catalyzed antibody fragmentation.[42] For the HMWS, a similar level of HMWS was observed in the acidic and the main peak fractions of the unstressed mAb A. By contrast, a lower level of HMWS was observed in the acidic fraction than in the main peak fraction of the oxidized mAb A. The distribution pattern of the HMWS suggests that the oxidation-induced HMWS is unlikely a source of the increased acidic charge heterogeneity.

Quantitatively, as shown in Figure 4, for the oxidized mAb A, the increase in the level of LMWS in the acidic fraction over that in the main peak fraction is relatively small (less than 4%, Figure 4), which cannot fully explain the relatively large increase in the level of acidic charge variants (greater than 30%, table 1) after metal-catalyzed oxidation. In addition, for the oxidized mAb A, the effects of the increased LMWS and decreased HMWS are cancelled out between the acidic and main peak fractions, which suggests that the changes in mAb A size heterogeneity

after metal-catalyzed oxidation are not a major factor for the increased acidic charge heterogeneity.

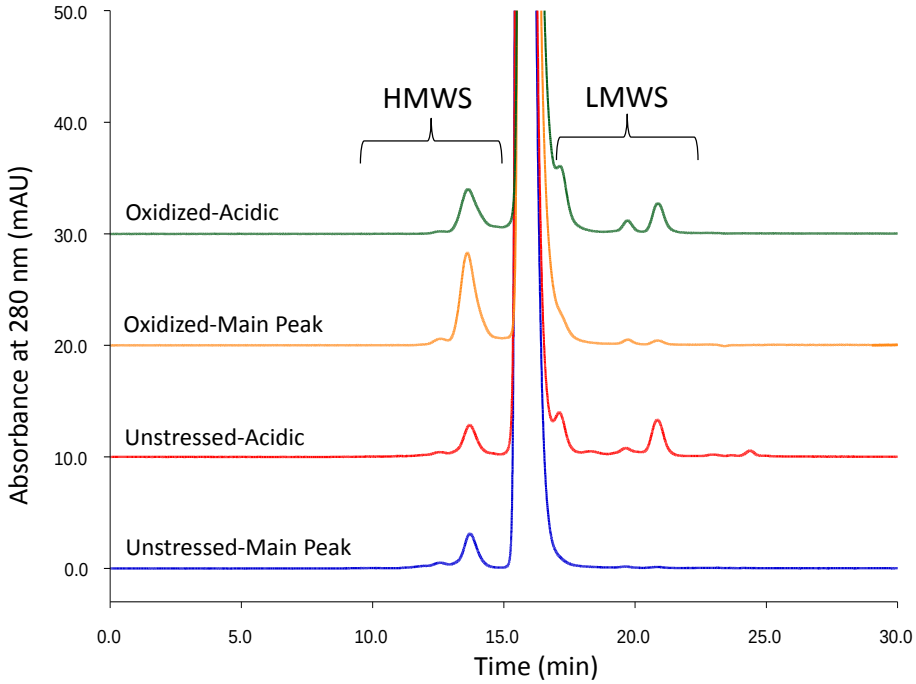

Figure 3. Size exclusion chromatograms of the acidic and main peak fractions of the oxidized and the unstressed mAb A samples

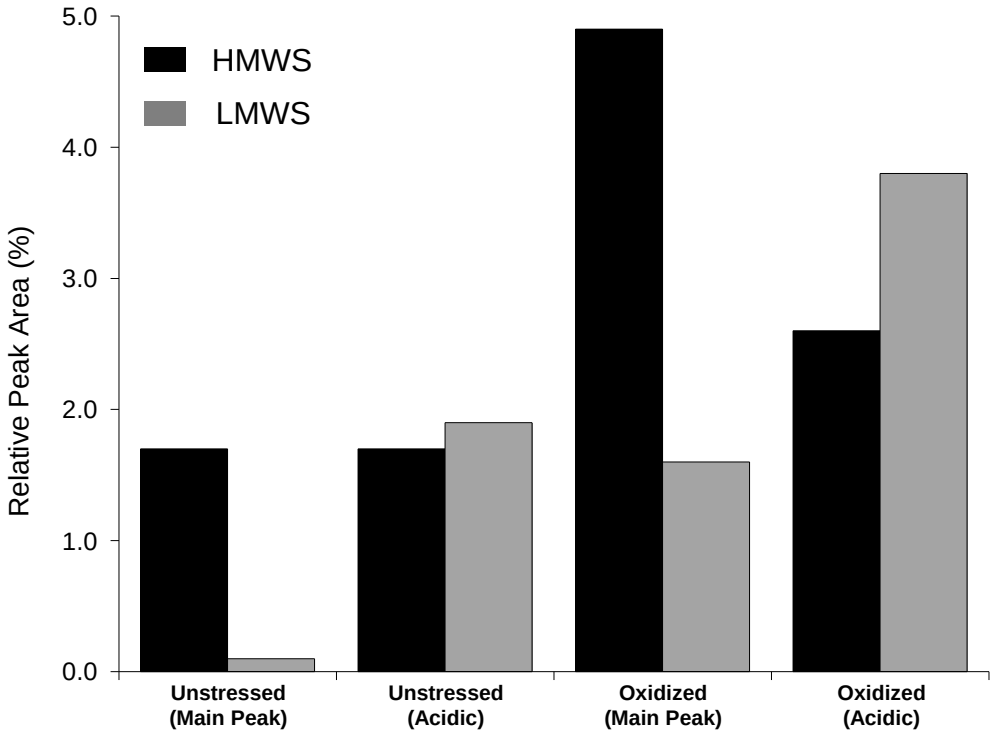

Figure 4. Relative peak areas of the HMWS and LMWS in the acidic and main peak fractions of the oxidized and the unstressed mAb A samples

Molecular Mass of mAb A Fractions

The collected fractions were characterized by intact/reduced molecular mass analysis to identify species that may explain the increased acidic charge heterogeneity. In the deconvoluted mass spectra of intact mAb A samples (Figure 5), the unstressed mAb A fractions have four major species, corresponding to masses of 145,743, 145,905, 146,066, and 146,225 Da, respectively, which are consistent with the theoretical masses of various glycan forms (G0/G0, G0/G1, G1/G1 or G0/G2, and G1/G2, respectively) of intact mAb A. It is worth noting that, compared to the mass spectrum of the unstressed main peak fraction, the mass spectrum of the unstressed acidic fraction showed an elevated baseline, where a large unstructured peak appears to be present. This indicates that more species may be present in low abundance. For the oxidized acidic and main peak fractions, the four major species became much less prominent. In particular, for the oxidized acidic fraction, it appears that only the unstructured baseline peak was present. It is possible that some of the species observed in the oxidized acidic fraction may also be present in the unstressed acidic fraction. However, it is difficult to accurately determine the masses of these species due to poor MS resolution.

In the deconvoluted mass spectra of reduced mAb A samples (Figure 6), the unstressed mAb A fractions have three major mass species, 22400, 50486, 50648, and 50809 Da, which are consistent with the theoretical masses of the reduced light chain and heavy chain (in three glycan forms, G0, G1, and G2) of mAb A. It should be noted that while the three heavy chain glycan forms could theoretically lead to six combinations of glycan forms for the intact mAb A, only four of the glycan forms are the major species observed in the intact mAb A (Figure 5). The oxidized mAb A fractions contain additional species with one or multiple additions of +16 Da to the light chain or heavy chain, suggesting that various oxidation products may be present.

However, these additional species appear to be present in similar relative intensities in the acidic and main peak fractions of the oxidized mAb A (Figure 6).

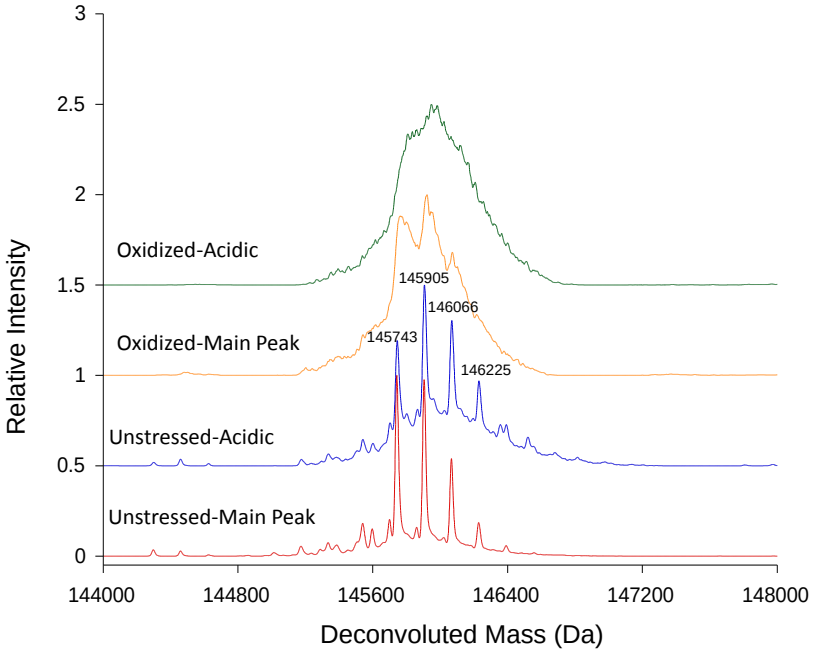

Figure 5. Deconvoluted mass spectra of the intact mAb A fractions

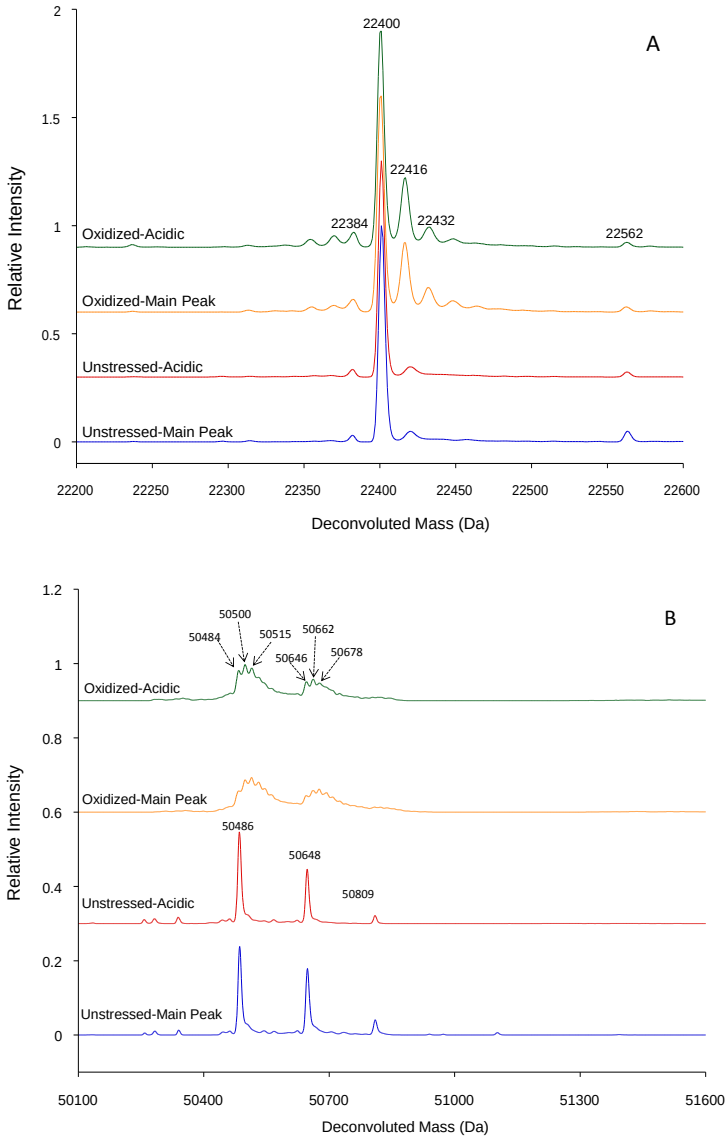

Figure 6. Deconvoluted mass spectra of the reduced light chain (A) and heavy chain (B) of mAb A fractions

Peptide Mapping of Reduced and S-Carboxymethylated mAb A Fractions

To identify the chemical modifications or degradation products that contributed to the increased acidic charge heterogeneity, mAb A fractions were analyzed by conventional tryptic peptide mapping. The peptide map UV profiles of the acidic fraction from the oxidized mAb A and the main peak fraction from the unstressed mAb A (as a control) were compared. As shown in Figure 7 and Table 2, a total of 21 peaks showed different absorbance intensity between the two peptide maps. The peaks that showed decreased peak intensity in the acidic fraction are identified as peptide fragments or digest artifacts, which are unlikely the source of the increased acidic charge heterogeneity. The peaks that showed increased peak intensity in the acidic fraction are identified as oxidation products of methionine (HC M256 and HC M432), tryptophan (HC W53), and threonine (HC T28) residues, or digest artifacts, as summarized in Table 2. Identification of the HC T28 threonine carbonylation product, a ketone, was based a characteristic mass shift of -2 Da at HC T28, where a consistent loss of 2 Da was observed in the y ions starting from y4 and in the b ions starting from b11 in the MS^2 spectrum (Figure 8).

The levels of the identified methionine, tryptophan, and threonine oxidation products in the respective mAb A fractions were subsequently quantified by using the extracted ion chromatograms As shown in Figure 9, relatively small increases were observed in M256 or M432 oxidation levels between the acidic and main peak fractions of the unstressed or the oxidized mAb A. By contrast, relatively large increases were observed in Trp53 oxidation (+16 Da and +4 Da products) levels between the acidic and main peak fractions of the unstressed or the oxidized mAb A (Figure 10). For example, the level of oxindolyalanine product (+16 Da) is almost five-fold higher in the acidic fraction than in the main peak fraction of the oxidized mAb A. A similar distribution pattern was observed for HC T28 carbonylation, where a higher level

was found in the acidic fraction than in the main peak fraction of oxidized mAb A (Figure 11). While these oxidation products showed various degrees of enrichment in the acidic fraction, these oxidation products do not provide satisfactory explanation for the oxidation-induced acidic charge heterogeneity, since these oxidation products are neutral in charge and are not expected to change the net charge of mAbs.

Several types of degradation products from metal-catalyzed oxidation, such as aspartic acid from the oxidation of histidine and cysteic acid from the oxidation of cysteine, can introduce negative charges into mAbs. These degradation products were investigated for their presence in mAb A acidic fractions. Based on tryptic peptide mapping, we found a Cys-to-Cysteic acid product at Cys230 in the hinge region and three His-to-Asp products in the Fc region (Table 3). Identification of the His-to-Asp products was based on a characteristic mass shift of -22 Da at the respective histidine residues. For example, for the HC H289-to-Asp product, a consistent loss of 22 Da was observed in the y ions starting from y4 and in the b ions starting from b11 in the MS^2 spectrum (Figure 12). These unique changes in the fragmentation ion masses allow unambiguous identification of the His-to-Asp product, considering also that no other histidine modification produces a mass shift of -22 Da. Identification of the C230-to-Cysteic acid product was based on a characteristic mass shift of +48 Da, which started from y23 ion in the MS^2 spectrum (Figure 13). After identification of these acidic degradation products, we quantified the relative level of these products in the acidic and main peak fractions by using the extracted ion chromatograms. As shown in Table 3, we found that these acidic products were preferentially localized in the acidic fraction of the oxidized mAb A. However, these levels were considerably lower than those of the methionine, tryptophan, and threonine oxidation products.

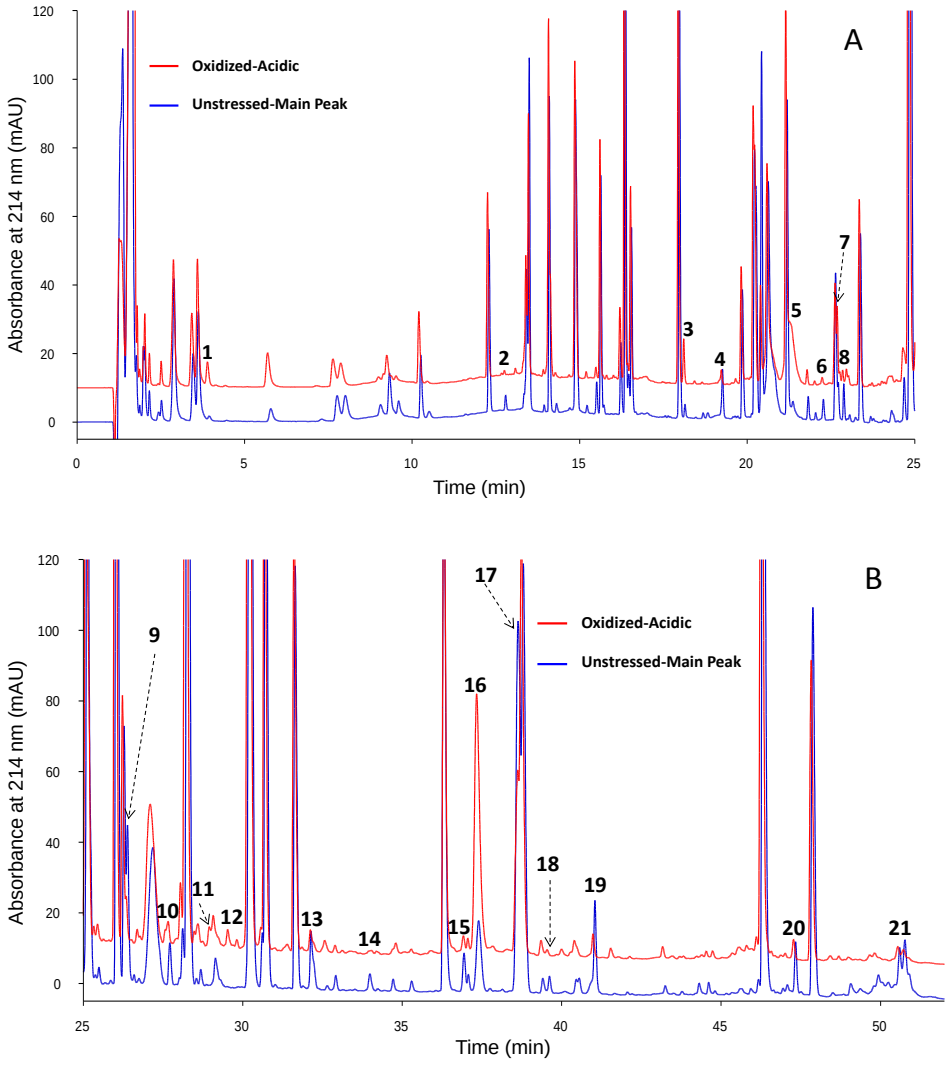

Figure 7. Comparison of the tryptic peptide maps of the oxidized acidic fraction and the unstressed main peak fraction (as a control). (A) 0 to 25 minutes; (B) 25 to 50 minutes.

No.	Retention Time (min)	Observed Mass (m/z)	Theoretical Mass (m/z)	Peptide ID	Comment
1	3.90	656.3842	656.3838	K.AKGQPR.E	Missed Cleavage (HC K344/HC G345)
2	12.80	586.3308	586.3307	R.PGGSLR.L	Tryptic Cleavage before Proline
3	18.14	851.4291	851.4291	K.DTLM(ox)ISR.T	HC M256 Oxidation
4	19.29	1357.7057	1357.7070	EVQLVQSGGGVER.P	Tryptic Cleavage before Proline
5	21.41	952.9763	952.9748	R.EPQVYTLPPSREEMTK.N	Missed Cleavage
6	22.31	655.8461	655.8462	L.TVLHQDWLNGK.E	Nonspecific cleavage (HC L310/HC T311)
7	22.76	1409.6274	1409.6267	R.WQQGNVFSCSVM(ox)HEALHNHYTQK.S	HC M432 Oxidation
8	22.93	1094.9992	1094.9988	N.VFSCSVMHEALHNHYTQK.S	Nonspecific cleavage (HC N425/HC V426)
9	26.42	1146.1162	1146.1164	K.PGQAPVLVIYGANNRPSGIPDR.F	Tryptic Cleavage before Proline
10	27.70	682.8174	682.8171	K.FNWYVDGVEVH.N	Nonspecific cleavage (HC H289/HC N290)
11	28.99	1164.0507	1164.0534	K.GLEWVSGINW(ox)QGGSTGYADSVK.G	HC W53 Oxidation (+16 Da)
12	29.56	1158.0519	1158.0509	K.GLEWVSGINW(ox)QGGSTGYADSVK.G	HC W53 Oxidation (+4 Da)
13	32.15	1302.1509	1302.1501	R.SYYASWYQQKPGQAPVLVIYGAN.N	Nonspecific cleavage (LC N50/LC N51)
14	34.03	1019.9672	1019.9661	K.THTCPPCPAPELLGGPSVF.L	Nonspecific cleavage (HC F245/HC L246)
15	36.99	829.9015	829.9011	K.TTPPVLDSDGSFFLY.S	Nonspecific cleavage (HC Y411/HC S412)
16	37.44	1669.3005	1669.3007	K.SCDKTHTCPPCPAPELLGGPSVFLFPPKPK.D	Missed Cleavage (HC K226/HC T227)
16	37.48	1091.9667	1091.9646	R.LSCAASGFT(-2H)FDDYAMSWVR.Q	HC T28 Carbonylation (-2 Da)
17	38.65	1423.7168	1423.7164	K.THTCPPCPAPELLGGPSVFLFPPKPK.D	Hinge Tryptic Peptide
18	39.66	1651.1672	1651.1643	H.TFPAVLQSSGL------ICNVNHKPSNTK.V	Nonspecific cleavage (HC H172/HC T173)
19	41.08	1760.5548	1760.5558	N.SGA------ICNVNHKPSNTK.V	Nonspecific cleavage (HC N163/HC S164)
20	47.32	1547.5137	1547.5125	K.DYFPE------VNHK.P	Tryptic Cleavage before Proline
21	51.33	N/A	N/A	N/A	Poor MS data

Table 2. Assignment of the peaks identified on the tryptic peptide maps of the acidic and main peak fractions (as shown in Figure 6).

A

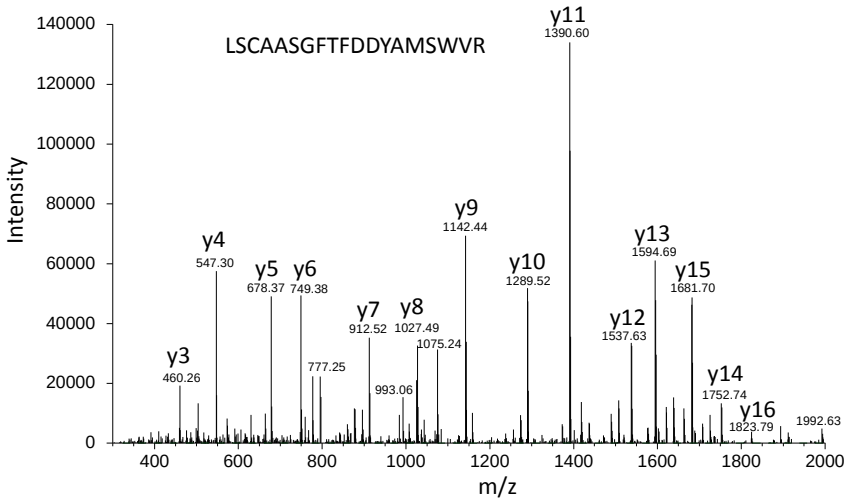

B

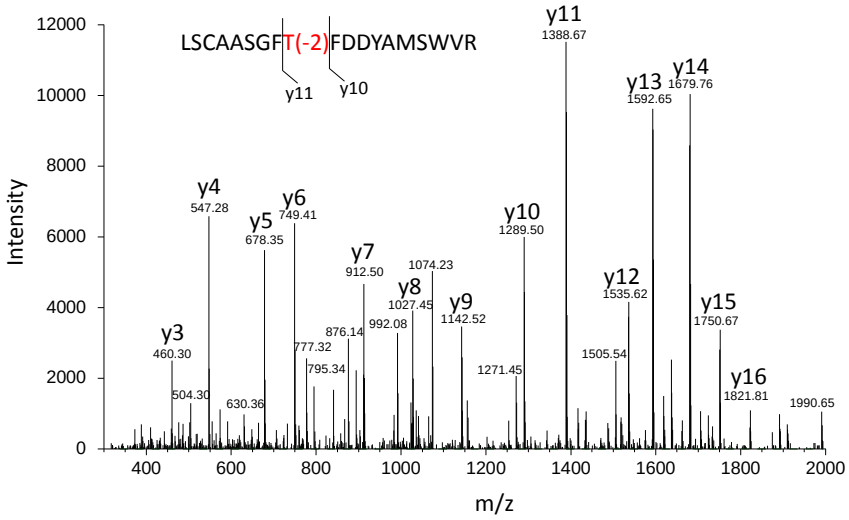

Figure 8. MS2 spectra of (A) a threonine containing peptide and (B) its oxidation product and assignment of the fragment ions

A

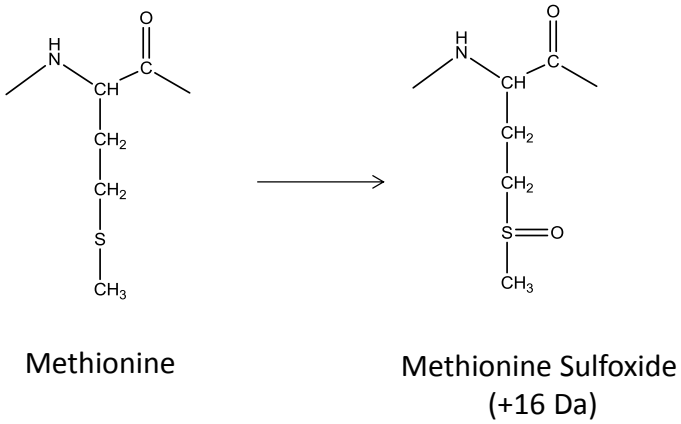

B

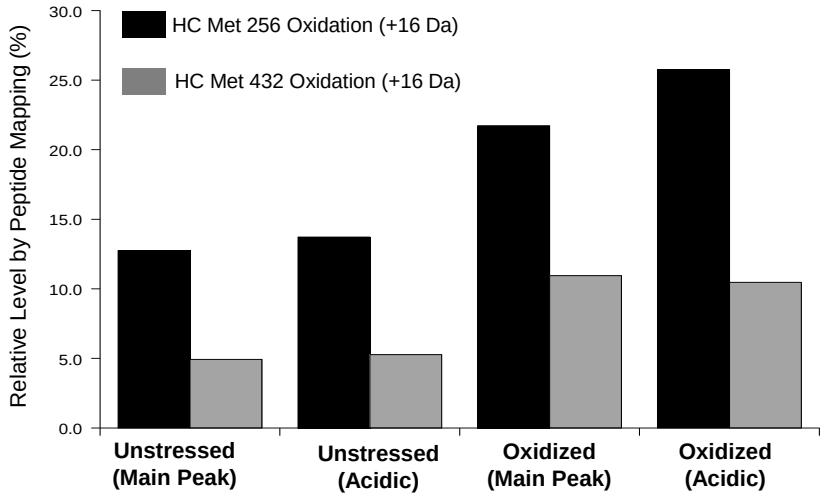

Figure 9. (A) Methionine and its oxidation product (methionine sulfoxide); (B) relative levels of methionine oxidation products in mAb A fractions based on the extracted ion chromatograms

A

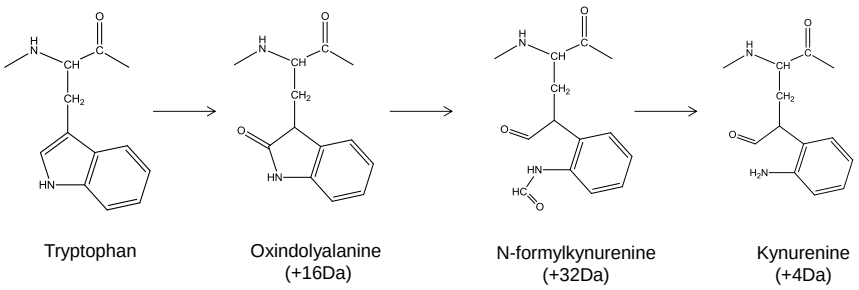

B

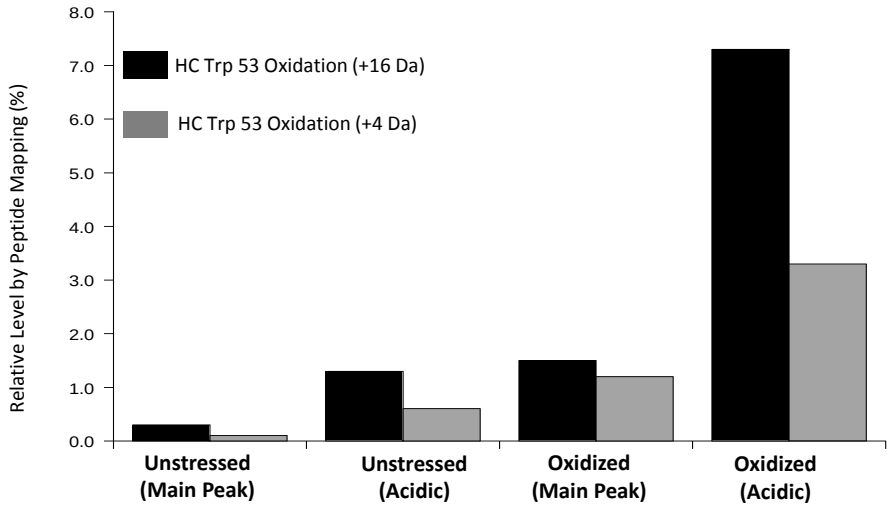

Figure 10. (A) Tryptophan and its oxidation products; (B) relative levels of tryptophan oxidation products in mAb A fractions based on the extracted ion chromatograms (note: +32Da oxidation products were not detected)

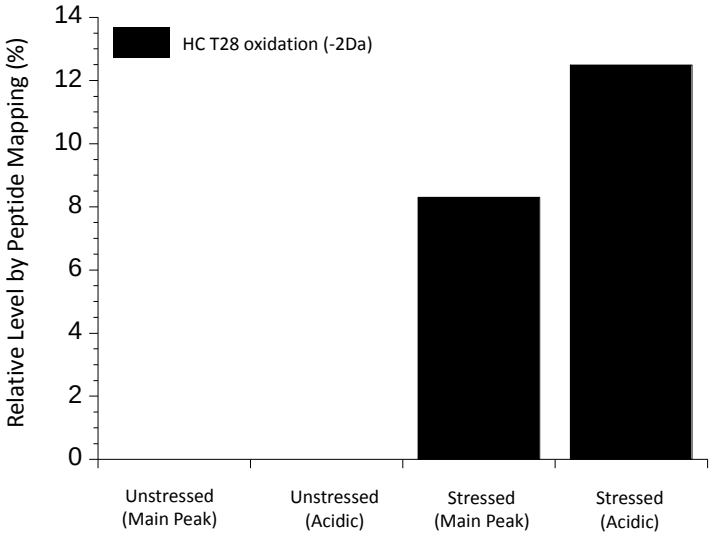

Figure 11. Relative levels of threonine oxidation product (-2Da, ketone) in mAb A fractions based on the extracted ion chromatograms

A

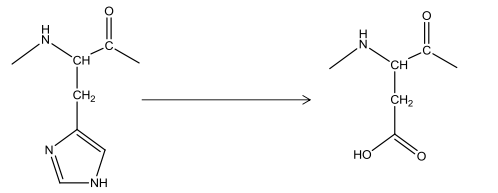

B

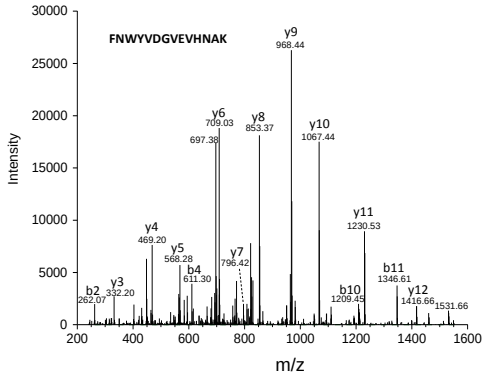

C

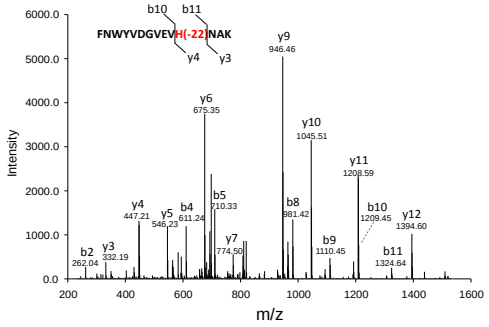

Figure 12. (A) Histidine and one of its oxidation products (aspartic acid); (B) MS2 spectrum of a His containing peptide (HC His289); (C) MS2 spectrum of the oxidized peptide containing a His-to-Asp (-22Da) modification and assignment of the fragment ions

A

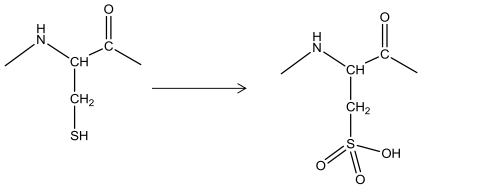

B

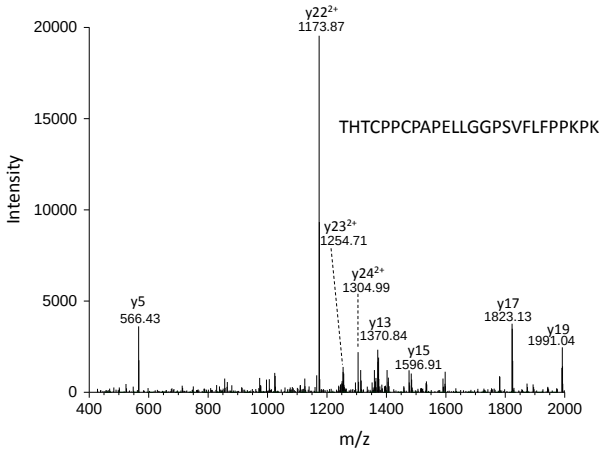

C

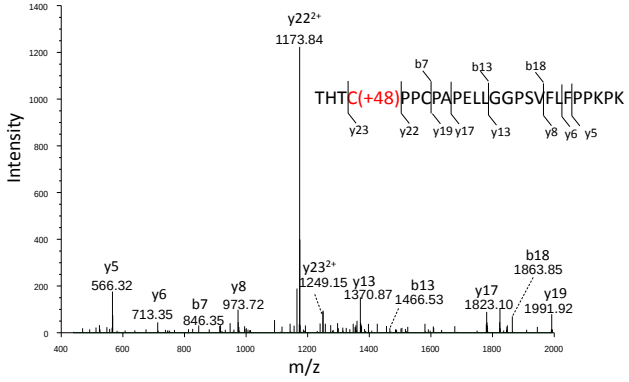

Figure 13. (A) Cysteine and one of its oxidation products (cysteic acid); (B) MS2 spectrum of a Cys containing peptide (HC Cys230); (C) MS2 spectrum of the oxidized peptide containing a Cys-to-Cysteic Acid (+48Da) modification and assignment of the fragment ions

Oxidation Products	Level (%) in the Unstressed (Main Peak)	Level (%) in the Unstressed (Acidic)	Level (%) in the Oxidized (Main Peak)	Level (%) in the Oxidized (Acidic)
HC C230-to-Cysteic Acid	0.0	0.0	0.4	1.1
HC H228-to-D	0.0	0.0	0.1	0.2
HC H289-to-D	0.0	0.0	0.2	0.8
HC H437-to-D	0.4	0.4	0.4	1.7

Table 3. Relative levels of histidine-to-aspartic acid oxidation in the collected fractions by peptide map (based on extracted ion chromatograms)

Total Protein Carbonylation Level of mAb A Fractions

Enrichment of HC T28 carbonylation product, a ketone, in the acidic fraction of the oxidized mAb A suggests that protein carbonylation could be a source of the oxidation-induced acidic charge heterogeneity. We therefore measured the protein carbonylation content of mAb A fractions using a total protein carbonylation assay (CALY).[27] As shown in Figure 14, the protein carbonylation level is consistently higher in the acidic fraction than in the main peak fraction for both the unstressed and the oxidized mAb A. This observation supports that metal-catalyzed carbonylation contributes to the oxidation-induced acidic charge heterogeneity. Interestingly, compared to the unstressed mAb A, oxidized mAb A showed highly increased protein carbonylation content in both the acidic and the main peak fractions, whose levels greatly exceeded that of HC T28 carbonylation product quantified by peptide mapping. This observation suggests that carbonylation products formed at other residues may be present, and that these products may not be readily detected by the conventional tryptic peptide mapping analysis. Therefore, efforts aimed at optimization of a peptide map for relative quantitation of site-specific carbonylation is described in the following sections.

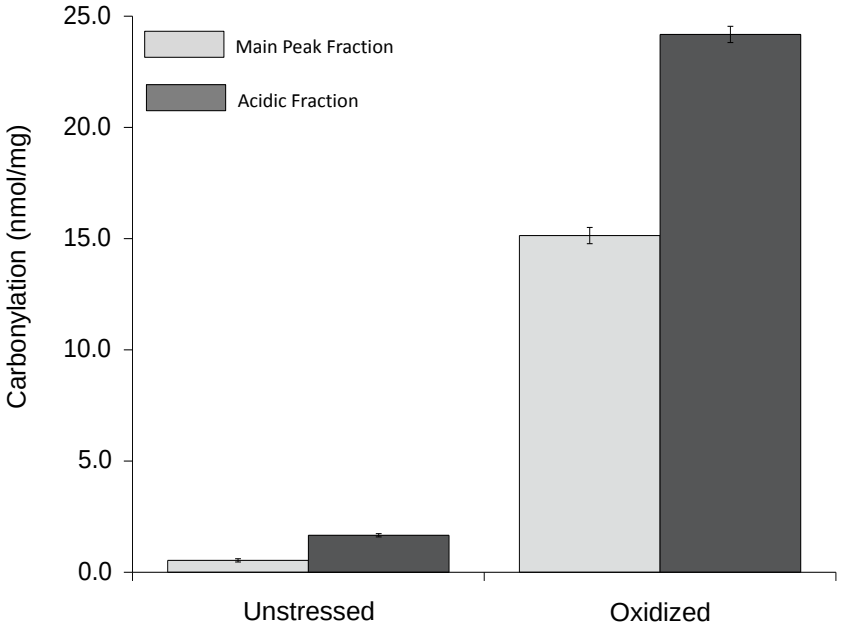

Figure 14. Protein carbonylation level of the acidic and main peak fractions from the unstressed and the oxidized mAb A samples (error bars represent the standard deviation from three measurements)

Optimization of a Peptide Mapping Method for Relative Quantitation of Site-Specific Carbonylation

A peptide mapping method was previously developed to identify site-specific carbonylation on mAbs.[29] In this method (Figure 15), Girard's Reagent T (GRT), a hydrazide that contains a permanently charged quaternary ammonium, was used to derivatize carbonyl groups (aldehydes and ketones) and to enhance the detection and identification of carbonyl peptides.[29] However, it is not known if the method condition is optimal for relative quantitation purposes. We therefore investigated several method conditions that could affect relative quantitation of site-specific carbonylation.

We first investigated peptide mapping digestion pH and digestion time since the potential hydrolysis of the quaternary ammonium group of GRT (to form a tertiary amine) at pH 8.2[44] during enzymatic digestion can lead to under-quantification of site-specific carbonylation. The concern over the quaternary ammonium hydrolysis is based on the observed pH-rate profiles of several quaternary ammonium salts amines in basic solutions.[44] Therefore, two digestion buffers, 25 mM Tris-HCl, 2 mM $CaCl_2$, pH 8.2 and 20 mM MOPS buffer, pH 7.0, were evaluated. The digestion was carried out at 37ºC for 2, 4, and 17 hours, respectively, in both buffers. A highly oxidized mAb A was used as a test sample, and six carbonylation sites were evaluated for their relative carbonylation levels against the different digestion times and pHs.

As shown in Figure 16, for each buffer, very minor differences were observed in the relative level of carbonylation for all six peptides after 2, 4, and 17 hours of digestion, respectively. This suggests that the quaternary ammonium of GRT is relatively stable in the digestion buffers at 37ºC for up to 17 hours. With different digestion buffers (pH 8.2 vs pH 7.0), very minor differences were observed in the relative levels of carbonylation, respectively, for

five of the peptides. However, higher levels of carbonylation were observed for carbonylation peptide LC K157 with Tris buffer (pH 8.2) than with MOPS buffer (pH 7.0) for all digestion times. This observation is not consistent with quaternary ammonium hydrolysis since the hydrolysis rate is usually greater with higher pHs.[44] Therefore, it is unlikely that quaternary ammonium hydrolysis led to the observed differences in LC K157 carbonylation level between pH 8.2 and pH 7.0. Overall, relative quantitation of site-specific carbonylation appeared to be minimally affected by the suspected hydrolysis of the quaternary ammonium of GRT. We subsequently selected 25 mM Tris-HCl, 2 mM $CaCl_2$ (pH 8.2) as the digestion buffer and 4 hours as the digestion time.

We next investigated the sodium borohydride reduction conditions. This investigation is based on two considerations. First, the hydrazides formed after GRT derivatization are not stable under the chromatographic condition (low pH and high temperature) of peptide mapping. Second, sodium borohydride reduction is a necessary step that converts hydrazides to amines (more stable than hydrazides). Incomplete reduction of the hydrazides by sodium borohydride can therefore lead to under-quantification of site-specific carbonylation. In the method that we previously developed,[29] the optimal sodium borohydride concentration for reduction is not known. In this investigation, in order to identify an optimal sodium borohydride concentration, we evaluated 0, 10, 40, 100, and 150 μM sodium borohydride for their effect on the relative carbonylation level at the six carbonylation sites.

As shown in Figure 17, the sodium borohydride concentrations used in the reduction step critically affected relative quantitation of site-specific carbonylation. The relative level of carbonylation at HC R19 appeared to plateau as the sodium borohydride concentration reached 10 μM; for the other five carbonylation sites, their relative levels appeared to plateau as the

sodium borohydride concentration reached 100 μM. Therefore, we selected 100 μM sodium borohydride as a final condition for the reduction of hydrazides formed after GRT derivatization.

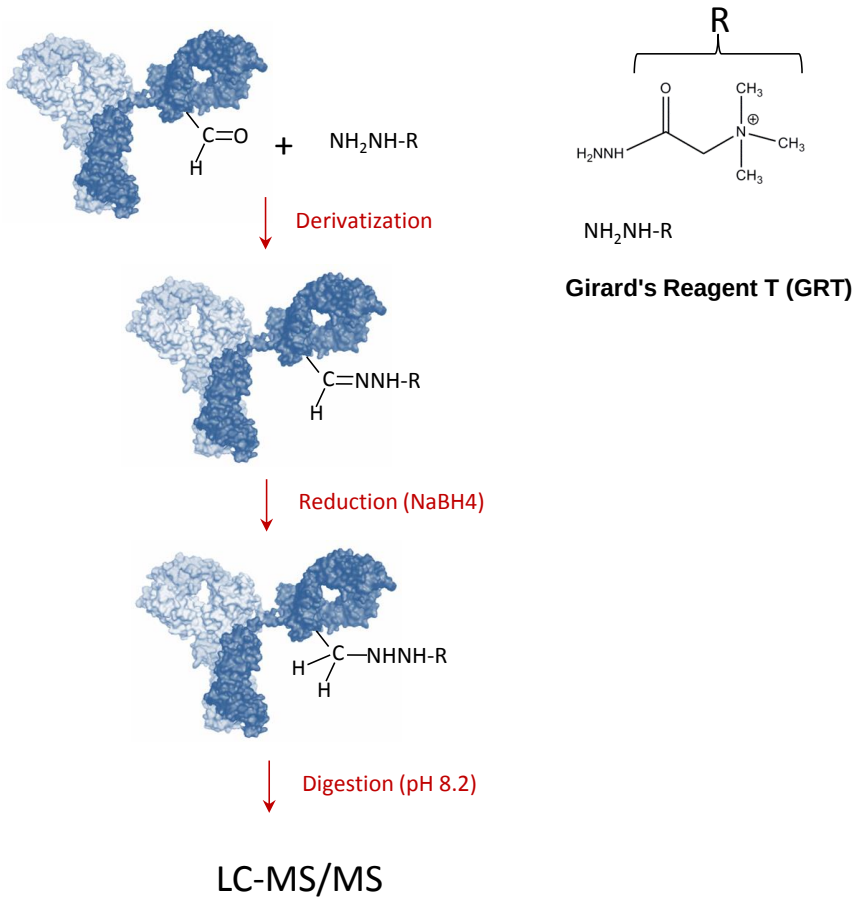

Figure 15. The workflow for characterizing site-specific carbonylation by peptide mapping

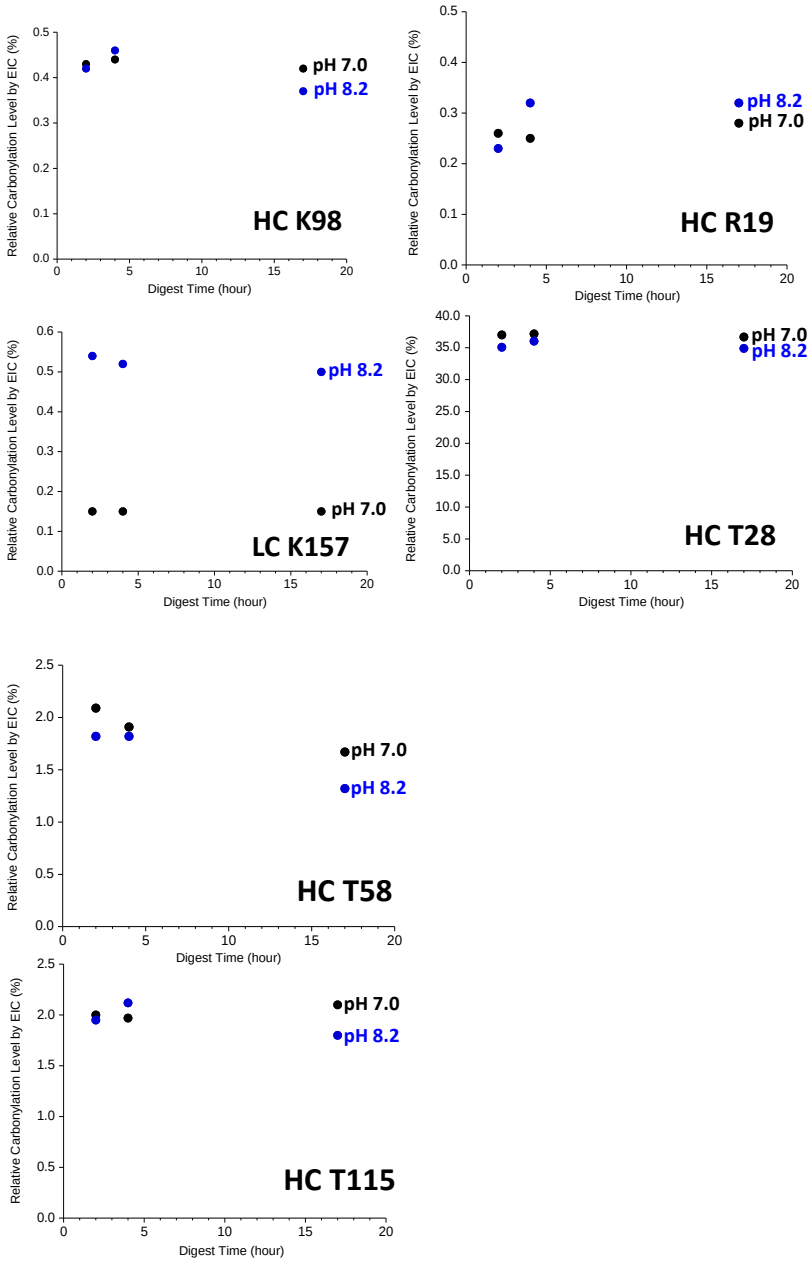

Figure 16. Effects of digestion pH and time on relative quantitation of carbonylation

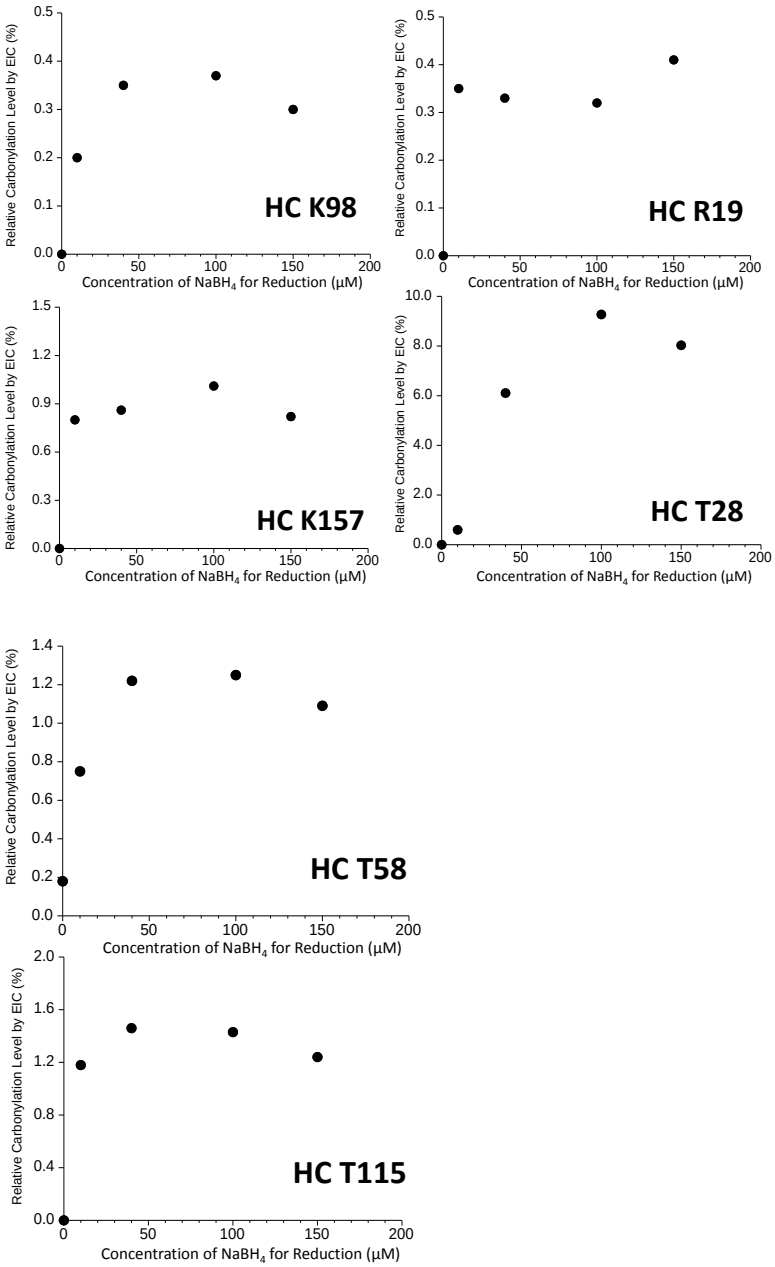

Figure 17. Effect of sodium borohydride reduction on the relative quantitation of carbonylation

Characterization of Site-Specific Carbonylation Products

Using the optimized carbonylation peptide mapping method, we identified the carbonylation sites on mAb A by database searching and manual interpretation of the MS data. For example, database searching indicated that HC K98 was a carbonylation site. The full MS of the observed carbonylation peptide showed an increase of +114 Da in mass compared to that of the unmodified peptide. The mass shift of +114 Da is consistent with GRT derivatization at HC K98, which also results in a trypsin miscleavage site. Additionally, the MS^2 data (Figure 18) showed a mass shift of +114 Da in the y ions starting from y9, while no such mass shift was observed in y4, y5, and y6. Based on the MS^2 data, the +114 Da modification can only occur at HC C96, HC A97, or HC K98. Given that there is no known +114 Da modification of Cys (carboxymethylated) or Ala residue, HC K98 was therefore assigned as a carbonylation site. As shown in Table 4, a total of 16 carbonylation sites were identified on mAb A, which include 4 arginine sites, 3 lysine sites, 8 threonine sites, and 1 proline site. Arginine and lysine carbonylation result in loss of positive charges on their side chains, which can be a source for the oxidation-induced acidic charge variants.

We investigated the distribution of site-specific carbonylation products in mAb A fractions by extracted ion chromatography. As shown in Table 4, for the oxidized mAb A, all of the site-specific carbonylation products showed a higher level in the acidic fraction than in the main peak fraction. The enrichment of the carbonylation products in the acidic fraction does not seem to depend on the type (aldehyde vs. ketone) or the location of these products on mAb A. Surprisingly, threonine carbonylation is the predominant carbonylation product enriched in the acidic fractions, while arginine and lysine carbonylation products are significantly less abundant. In the acidic fraction of oxidized mAb A, the total level of lysine and arginine carbonylation

products is ~ 2%, while the total level of threonine carbonylation products is 39%. This distribution pattern for the different carbonylation products indicates that threonine carbonylation is a major source of the induced acidic charge heterogeneity after metal-catalyzed oxidation.

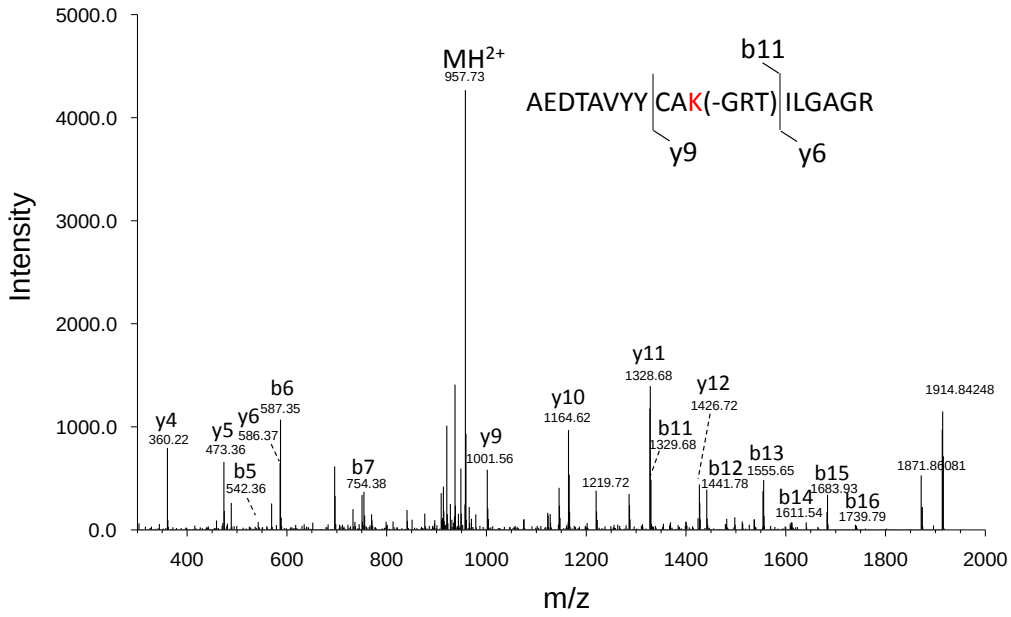

Figure 18. MS^2 spectrum of a GRT-derivatized carbonylation peptide (HC K98) and assignment of the fragment ions

Identified Carbonylation Site	Carbonylation level (%) in the Unstressed (Main Peak)	Carbonylation level (%) in the Unstressed (Acidic)	Carbonylation level (%) in the Oxidized (Main Peak)	Carbonylation level (%) in the Oxidized (Acidic)
HC R13	0.0	0.0	0.0	0.2
HC R19	0.0	0.0	0.0	0.1
HC T28	0.0	0.1	11.8	18.7
HC T58	0.0	0.0	2.2	2.7
HC K65	0.0	0.0	0.0	0.1
HC R87	0.0	0.0	0.0	0.3
HC K98	0.0	0.1	0.1	0.7
HC R104	0.0	0.0	0.0	0.1
HC T115	0.1	0.3	5.3	6.4
HC T139	0.0	0.2	0.6	2.5
HC T227	0.0	0.0	1.7	3.7
LC T4	0.0	0.0	1.2	1.7
LC P7	0.0	0.0	0.1	0.2
LC T117	0.0	0.0	1.0	2.0
LC T132	0.0	0.0	1.0	1.3
LC K157	0.0	0.0	0.0	0.2

Table 4. Relative levels of site-specific carbonylation in mAb A fractions by peptide map (based on extracted ion chromatograms)

Characterization of Additional Oxidation Products

Aldehydes generated by metal-catalyzed oxidation can be further oxidized to carboxylic acids. For example, glutamic semialdehyde (proline- and arginine-derived carbonyl product) can be oxidized to glutamic acid;[45] adipic semialdehyde (lysine-derived carbonyl product) can be oxidized to adipic acid.[45] Formation of these carboxylic acids can increase acidic charge heterogeneity of proteins. Therefore, we further characterized mAb A fractions to understand if these carboxylic acid products could be a source of the induced acidic charge heterogeneity.

From peptide mapping of the reduced and S-carboxymethylated mAb A fractions, we observed formation of glutamic acid but not adipic acid (Table 5). Identification of an arginine-to-glutamic acid product at HC R13 was based on the MS^2 spectrum of a doubly charged peptide ion of m/z 949.4828, which showed a mass shift of -27 Da (to that of the unmodified peptide) in the y ions starting from y7 and in the b ions starting from b13 (Figure 19). The unique mass shifts allow us to pinpoint the arginine-to-glutamic acid modification at HC R13. Similarly, identification of a proline-to-glutamic acid product at LC P7 was based on the MS^2 spectrum of a doubly charged ion of m/z 951.9915, where a mass shift of +32 Da (in comparison to those from the unmodified peptide) was observed in the y ions starting from y11 (Figure 20), allowing us to pinpoint the proline-to-glutamic acid at LC P7.

Interestingly, multiple proline-to-pyroglutamic acid (but not proline-to-glutamic acid) products were observed on mAb A hinge peptide, THTC**PP**C**P**A**P**ELLGGPSVFLFPPKPK (proline-to-pyroglutamic acid sites are underlined/bold). Identification of these oxidation products was supported by their MS^2 spectra (Figure 21), which have the same y ions from y5 to y14. In addition, a terminal or penultimate y ion (from the N-terminal side) was present in the MS^2 mass spectra, which allows the assignment of the mass shift/modification to the proline

residue at the N-termini of these peptides (Figure 21). Formation of these proline-to-pyroglutamic acid products requires cleavage of the hinge peptide (between the proline residue and its preceding residue). Given that the preceding residues (Cys230, Pro231, Cys233, and Ala235, respectively) are not lysine or arginine, it was likely that these products were generated by metal-catalyzed oxidation. It should be pointed out that the proline-to-pyroglutamic acid modification does not introduce a change in the net charge at the modification site. However, the oxidation-induced cleavage introduces a C-terminal carboxylic acid to the preceding residue, which is expected to increase acidic charge heterogeneity of mAb A.

Relative quantitation by using the extracted ion chromatogram shows that the glutamic acid products are not a major source of the induced acidic charge heterogeneity (Table 5), as their levels are not more than 0.1% in the main peak or the acidic fractions of unstressed and oxidized mAb A. By contrast, up to 0.7% proline-to-pyroglutamic acid product was observed in the acidic fraction of the oxidized mAb A. Furthermore, for the oxidized mAb A, higher levels of proline-to-pyroglutamic acid products were consistently observed in the acidic fraction than in the main peak fraction (Table 5).

A

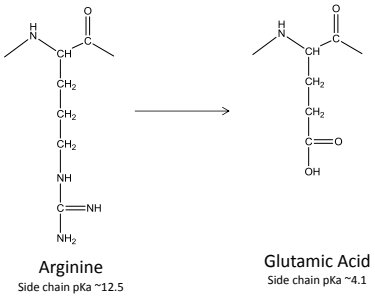

B

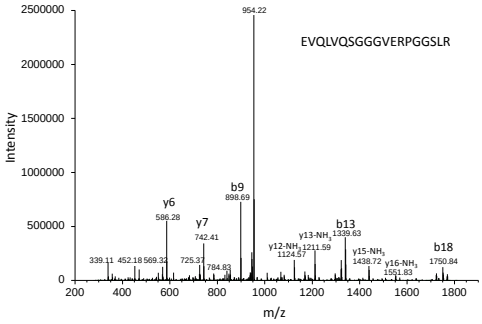

C

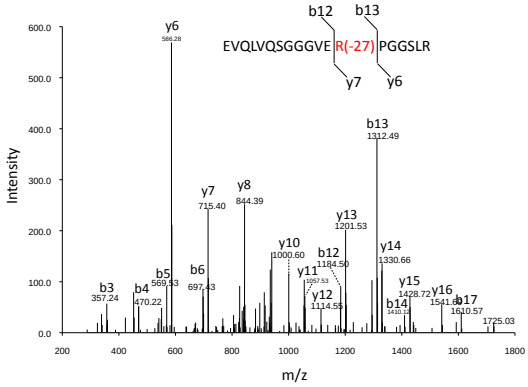

Figure 19. (A) Arginine and one of its oxidation products (glutamic acid); (B) MS^2 spectrum of an Arg containing peptide (HC R13); (C) MS^2 spectrum of the oxidized peptide containing an Arg-to-Glu (-27 Da) modification and assignment of the fragment ions

A

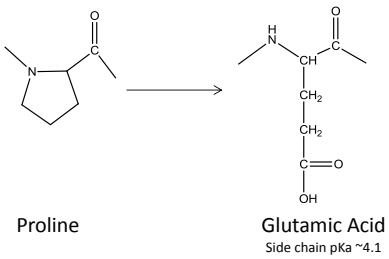

B

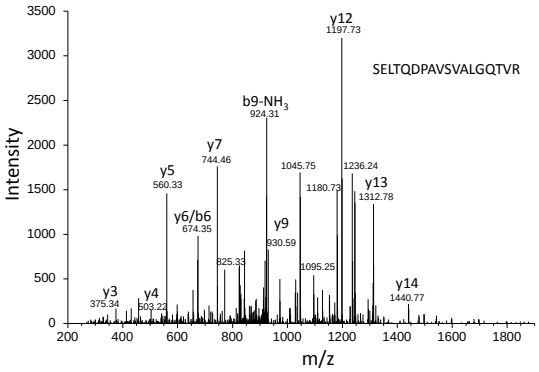

C

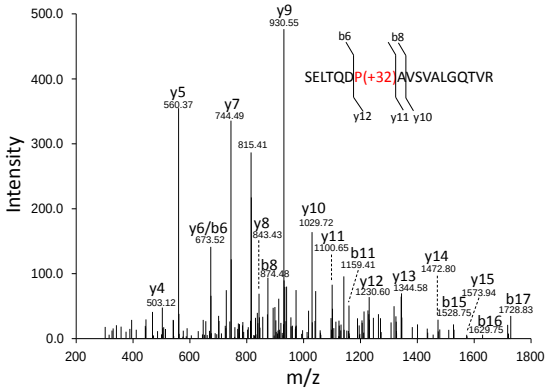

Figure 20. (A) Proline and one of its oxidation products (glutamic acid); (B) MS^2 spectrum of a Pro containing peptide (LC P7); (C) MS^2 spectrum of the oxidized peptide containing a Pro-to-Glu (+32 Da) modification and assignment of the fragment ions

A

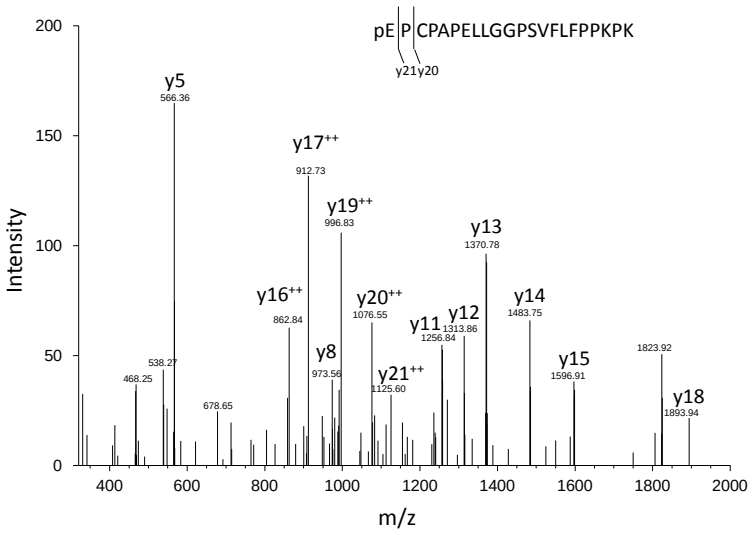

B

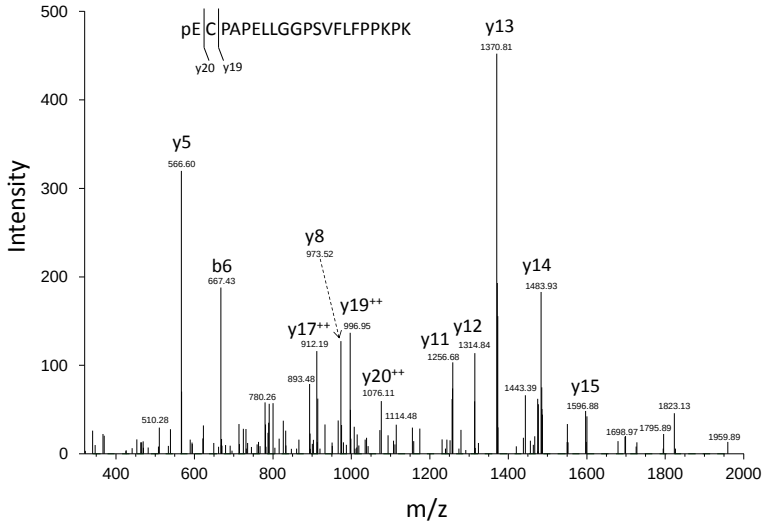

Figure 21. MS^2 spectra of hinge region peptides that contain a P-to-pE oxidation product (A: HC P231; B: HC P232) and assignment of the fragment ions

C

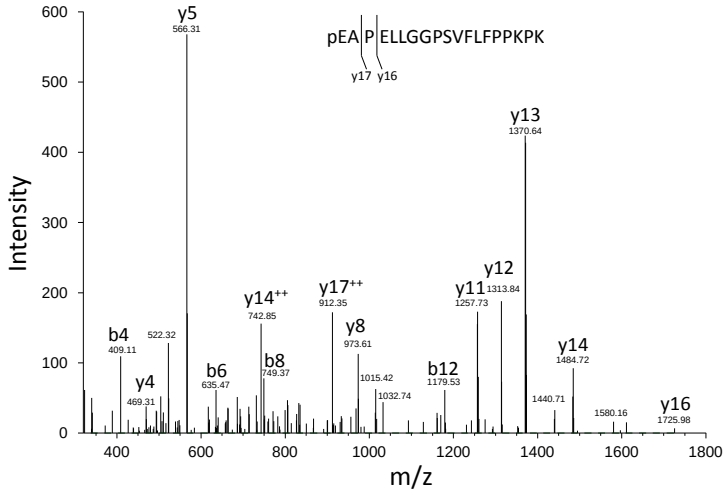

D

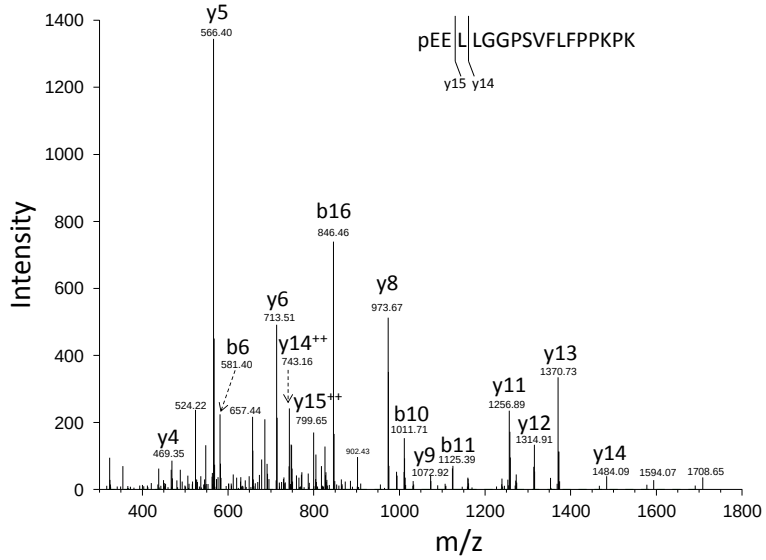

Figure 21. MS^2 spectra of hinge region peptides that contain a P-to-pE oxidation product (C: HC P234; D: HC P236) and assignment of the fragment ions

Oxidation Products	Level (%) in the Unstressed (Main Peak)	Level (%) in the Unstressed (Acidic)	Level (%) in the Oxidized (Main Peak)	Level (%) in the Oxidized (Acidic)
HC R13-to-E	0.0	0.0	0.0	0.1
HC R104-to-E	0.1	0.1	0.0	0.1
HC P231-to-pE	0.0	0.0	0.2	0.4
HC P232-to-pE	0.0	0.0	0.3	0.5
HC P234-to-pE	0.0	0.0	0.2	0.4
HC P236-to-pE	0.0	0.0	0.5	0.7
LC P7-to-E	0.0	0.0	0.1	0.1

Table 5. Relative level of additional oxidation products in mAb A fractions by peptide map (based on extracted ion chromatograms)

Analysis of Conformational Dynamics of mAb A Fractions by HDX-MS

We investigated the conformational dynamics of the mAb fractions by H/D exchange experiments. As shown in Figure 22, minor differences were observed in deuterium uptakes near the HC M256 site, i.e., HC245-255 and HC248-255. Both peptides displayed increased dynamics in the acidic fraction of the stressed mAb A than the main peak fraction of the unstressed mAb A (as a control). However, no significant conformational difference was detected for peptides near HC T28, HC W53, HC T115, HC N319 (deamidation site located within an NG motif), HC N388 (deamidation site located within an NG motif), and HC M432. Therefore, our data indicate that it is unlikely that conformational factors play a major role in the oxidation-induced acidic charge heterogeneity.

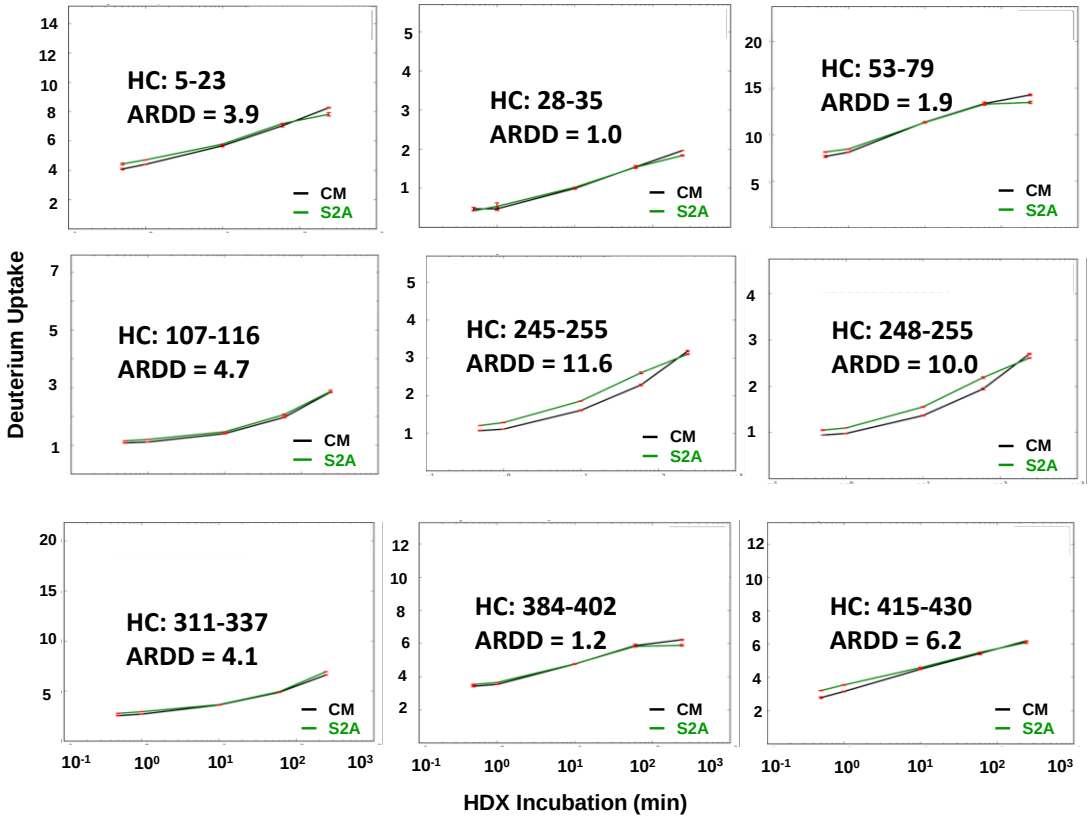

Figure 22. Plots of deuterium uptake as a function of time for the unstressed main peak fraction (Black, as the control) *versus* the stressed acidic fraction of mAb A (Green), for near the following sites HC T28, HC W53, HC T115, HC M256, HC N319 (NG motif), HC N388 (NG motif) and HC M432.

DISCUSSION

This study applied a large array of analytical characterization methods to gain an in-depth understanding of the acidic charge heterogeneity induced by metal-catalyzed oxidation on a model IgG1 mAb. During the characterization, we found that the commonly used analytical characterization methods, such as molecular mass analysis, size exclusion chromatography, and peptide mapping after reduction and S-carboxymethylation, provided limited information on the oxidation-induced acidic charge variants. For example, from the molecular mass analysis, the deconvoluted mass spectra of the acidic and main peak fractions are almost identical (Figures 5 and 6), making it difficult to link/attribute the oxidation-induced acidic charge heterogeneity to a particular species. From size exclusion chromatography, the increase in the LMWS levels and the decrease in the HMWS levels essentially cancelled out, which suggests that these changes in the size variants cannot be a major source for the oxidation-induced acidic charge heterogeneity. Based on conventional tryptic peptide mapping, two of the predominant degradation products enriched in the acidic fractions were identified as Fc methionine sulfoxide and oxidized tryptophan in the CDR. Since methionine and tryptophan oxidation products are not expected to affect the net charge of mAbs, these oxidation products do not provide a satisfactory explanation for the oxidation-induced acidic charge heterogeneity. Specifically, for the Fc methionine oxidation products, conflicting observations have been reported on their distribution in mAb charge variant fractions. Chumsae et al. showed that Fc methionine oxidation products induced by tert-butyl hydroperoxide (tBHP) localized to the basic fraction.[46] By contrast, Ponniah et al. reported higher levels of Fc methionine oxidation products in the enriched acidic fraction [47] Hintersteiner et al. hypothesized that conformational changes could affect interactions between

the column and the charge residues/species adjacent to these oxidation products.[48] However, to date, no conformational data are available to support this hypothesis.

To gain a better understanding of the nature of the oxidation-induced acidic charge variants, we took a targeted approach and investigated acidic degradation products[45] from metal-catalyzed oxidation that could be present in the acidic fraction. A cysteine-to-cysteic acid product (HC C230) and a histidine-to-aspartic acid product (HC H228) were identified in the hinge region, which are consistent with the degradation products reported in a human IgG1 under similar oxidation conditions.[31] Two additional histidine-to-aspartic acid products were identified in the CH2 (HC H289) and CH3 (HC H437) domains. These two histidine oxidation sites were previously reported in a human IgG1 under light stress conditions, where +32 Da oxidation products were observed.[49] Interestingly, no histidine-to-aspartic acid product was reported under the light stress condition.[49] Additionally, while HC H289 was found to be the predominant oxidation (+32 Da) site under light stress,[49] our study showed that HC H437 was the predominant histidine-to-aspartic acid degradation site. Our observation indicates that metal-catalyzed oxidation shows different site preferences than light stress for histidine oxidation. It should be noted that cysteine-to-cysteic acid and the histidine-to-aspartic acid products are located in the conserved regions of IgG1. Formation of these products, therefore, may represent a general degradation pathway for the increased acidic charge heterogeneity of mAbs observed after metal-catalyzed oxidation.

Oxidative carbonylation is another degradation pathway that is expected to contribute to the acidic charge heterogeneity after metal-catalyzed oxidation, as formation of lysine- and arginine-derived carbonylation products (2-aminoadipic semialdehyde and glutamic semialdehyde) result in a loss of the positive charge on lysine and arginine side chains. On the

other hand, formation of threonine- and proline-derived carbonylation products (2-amino-3-ketobutyrate and glutamic semialdehyde) should not change the net charge of a protein, and, therefore, these carbonylation products are not expected to be enriched in the acidic charge variants of mAbs. However, to date, no study has investigated the distribution of these carbonyl products in mAb charge variants.

It should be pointed out that the conventional peptide mapping analysis can readily detect the threonine carbonylation product (2-amino-3-ketobutyrate) but not the lysine/argining/proline carbonylation products (aminoadipic semialdehyde and glutamic semialdehyde). It is possible that these aldehyde products may not be as stable as the ketone product under the peptide mapping conditions. Thus, as previously discussed,[29] identification of site-specific protein carbonyls (especially aldehyde products) often requires the derivatization of the carbonyl groups before the enzyme digestion. The commonly used derivation reagents are hydrazides, which react with carbonyls on proteins. The derivatization products are further stabilized by sodium borohydride reduction to form amines. However, for relative quantitation of site-specific carbonyls, an analytical challenge that has not been previously noted in the literature is the efficiency of the sodium borohyride reduction. As illustrated by this study, incomplete reduction of hydrazides resulted in underestimation of the relative levels, which is not ideal for characterizing the distribution of the carbonylation products in mAb A fractions. We therefore improved the sodium borohyride reduction condition to enable a consistent reduction of the hydrazides after the GRT derivatization. With the optimized reduction condition, the relative levels of threonine-derived carbonylation products obtained from the conventional peptide mapping and the GRT-derivitization peptide mapping methods were found to be similar (data not shown).

By measuring the extent of mAb A carbonylation in the acidic and main peak fractions, we found that carbonylation products are enriched in the acidic fractions (Figure 14 and Table 4). The total protein carbonylation level correlated well with the sum of site-specific carbonylation levels (Figure 23). The orthogonal measurements further support that metal-catalyzed carbonylation contributes to the induced acidic charge heterogeneity. For the distribution of the carbonylation products, it is surprising that the predominant carbonylation products localized in the acidic fractions are threonine-derived carbonylation products but not lysine- or arginine-derived carbonylation products, as commonly expected based on the literature.[50-54] Given that threonine carbonylation is not expected to change the net charge of a protein, one hypothesis for the observed enrichment of threonine-derived carbonylation products in the acidic region could be due to concurrent formation of threonine-derived carbonylation products with lysine- and arginine-derived carbonylation products during metal-catalyzed oxidation, and subsequent co-localization of these carbonyls in the acidic region. This hypothesis is based on the existing reports on the distribution pattern of protein carbonylation sites by Lv et.al.,[55] which showed that carbonylation sites tend to cluster together, presumably near metal binding sites. However, not all threonine-derived carbonylation sites are close to a lysine- or arginine-derived carbonylation site on mAb A. Furthermore, lysine- and arginine-derived carbonylation products constitute only a small fraction of the total carbonyls (Table 4). Finally, all eight threonine-derived carbonylation products are found to be preferably localized in the acidic fraction regardless of their locations on mAb A. Thus, the concurrent formation hypothesis provides only a partial explanation. Clearly, further study will be necessary to fully understand the mechanism for the preferential enrichment of threonine-derived carbonylation products. Nevertheless, this study demonstrates that, at least for mAb A, threnonine-derived carbonylation products are a major

component of the oxidation-induced acidic charge heterogeneity after metal-catalyzed oxidation. It should be also pointed out that, different from the cysteine and histidine oxidation products, only a small portion of the carbonylation products are located in the conserved regions. This suggests that formation of these carbonylation products may be a molecule- or sequence- specific degradation pathway for the oxidation-induced acidic charge heterogeneity.

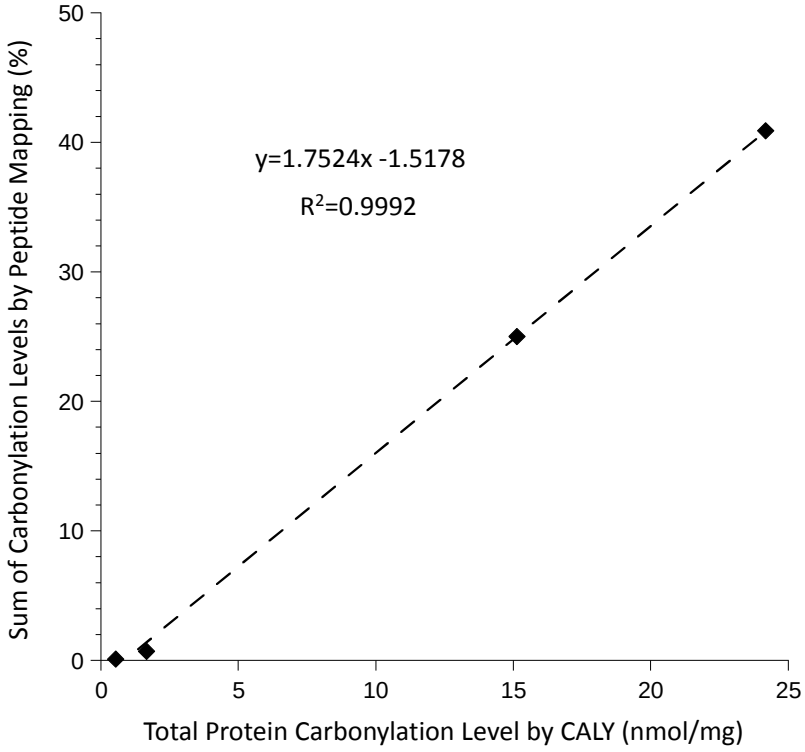

Figure 23. Correlation between the total protein carbonylation levels and the sum of site-specific carbonylation levels of the collected mAb A fractions.

This study detected formation of glutamic acid from arginine and proline residues. The arginine- and proline-derived carbonylation products (glutamic semialdehyde) are likely the precursors, which are further oxidized to carboxylic acid. This study also detected formation of pyroglutamate from proline residues in the mAb A hinge region. To the best of our knowledge, these hinge fragmentation products have not been previously described. Surprisingly, no proline-to-glutamic semialdehyde or proline-to-glutamic acid products were detected at these hinge proline sites. Three degradation mechanisms that do not involve oxidative carbonylation were therefore proposed, as illustrated in Figures 24-26 to explain the formation of these pyroglutamate products, where oxidation of pyrrolidine ring to pyroglutamate (via at least three possible oxidation mechanisms) is followed by hydrolysis of the peptide bond between pyroglutamate and the preceding residue. Considering that the hinge sequence is conserved for IgG1, formation of these pyroglutamate products should represent a general degradation pathway for the oxidation-induced acidic charge heterogeneity of mAbs after metal-catalyzed oxidation. It should be pointed out that the proposed mechanisms (Figures 24-26) are different from a mechanism for oxidative cleavage of prolyl peptides suggested by Uchida et al.,[56] where a 2-pyrrolidone product was formed at the C-terminus of a proline residue following the peptide bond cleavage (induced by the hydroxyl radical), and no pyroglutamate product was reported.[56]

In summary, this study presents for the first time a detailed characterization of the acidic charge variants induced by metal-catalyzed oxidation on mAbs. From the perspective of mAb product variant characterization, this study identified multiple degradation pathways and related degradation products as the source of the oxidation-induced acidic charge heterogeneity. To the best of our knowledge, many of the degradation products, such as histidine-to-aspartic acid, proline-to- pyroglutamate, and arginine-to-glutamic acid, are reported in mAbs for the first time.

More importantly, this study discovered that metal-catalyzed carbonylation directly contributes to the formation of acidic charge variants of mAbs. This study also revealed that threonine-derived carbonylation but not lysine- or arginine-derived carbonylation can be the predominant carbonylation product enriched in mAb acidic fractions. Identification and further characterization of these degradation products should help address increasing expectations from health authorities on physiochemical characterization of mAb product variants. Additionally, the findings from this study should help develop a targeted analytical control strategy to ensure the safety and efficacy of mAb products. Finally, from a bioprocessing perspective, this study further confirms our previous claim that metal-catalyzed oxidation represents a general degradation mechanism (like deamidation or glycation) that leads to increased acidic charge heterogeneity of mAbs. Therefore, this study points to a new area of product quality investigation/root cause analysis to assist mAb bioprocess development, where maintaining consistent mAb charge heterogeneity profile is highly desirable.

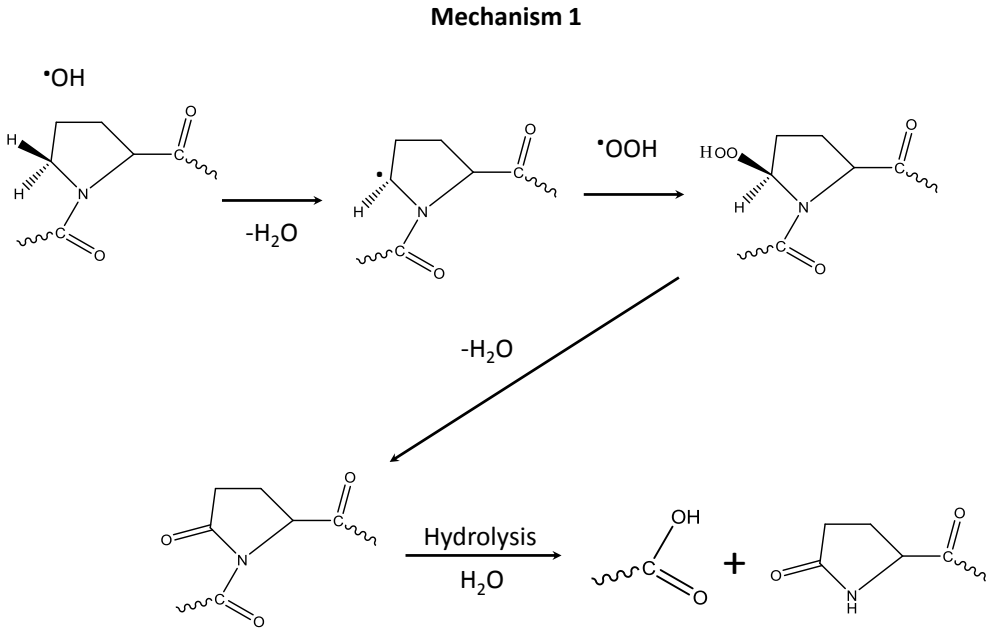

Figure 24. A proposed mechanism (#1) for the formation of proline-to-pyroglutamate product: oxidation of proline to pyroglutamate is followed by hydrolysis of the peptide bond between the preceding residue and pyroglutamate.

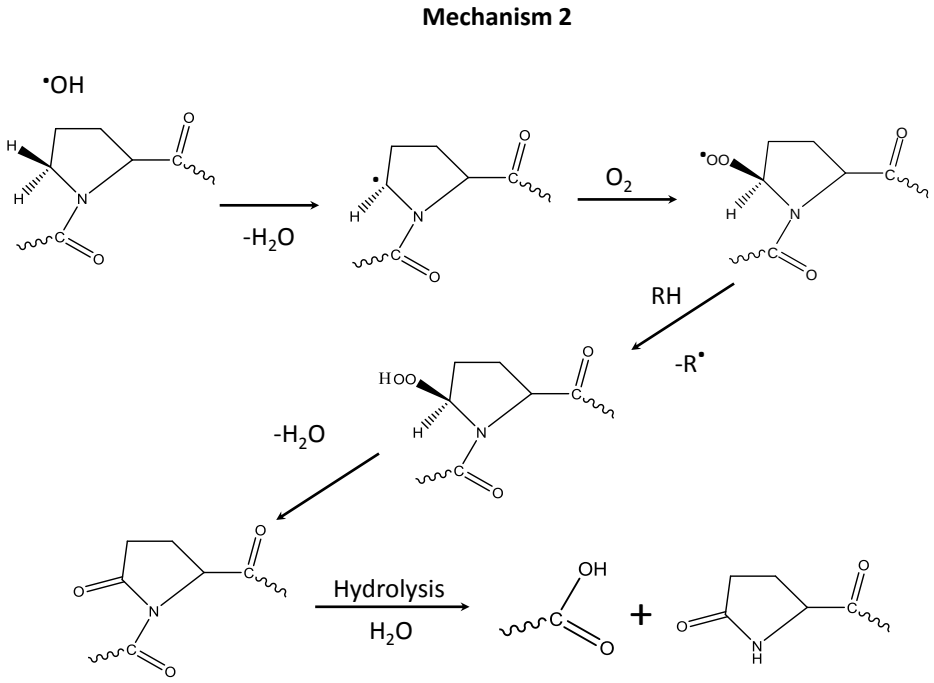

Figure 25. A proposed mechanism (#2) for the formation of proline-to-pyroglutamate product: oxidation of proline to pyroglutamate is followed by hydrolysis of the peptide bond between the preceding residue and pyroglutamate.

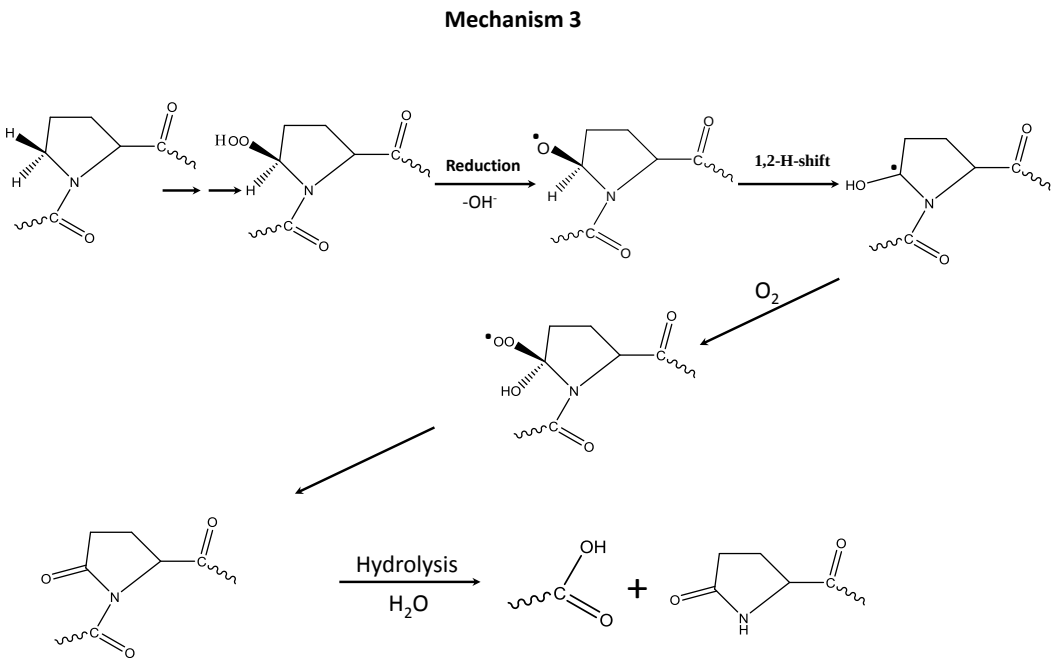

Figure 26. A proposed mechanism (#3) for the formation of proline-to-pyroglutamate product: oxidation of proline to pyroglutamate is followed by hydrolysis of the peptide bond between the preceding residue and pyroglutamate.

Reference

1. Leavy, O., Therapeutic antibodies: past, present and future. *Nat Rev Immunol* **2010,** *10* (5), 297.

2. Chan, A. C.; Carter, P. J., Therapeutic antibodies for autoimmunity and inflammation. *Nat Rev Immunol* **2010,** *10* (5), 301-16.

3. Weiner, L. M.; Surana, R.; Wang, S., Monoclonal antibodies: versatile platforms for cancer immunotherapy. *Nat Rev Immunol* **2010,** *10* (5), 317-27.

4. Liu, H.; Gaza-Bulseco, G.; Faldu, D.; Chumsae, C.; Sun, J., Heterogeneity of monoclonal antibodies. *J Pharm Sci* **2008,** *97* (7), 2426-47.

5. Chung, S.; Tian, J.; Tan, Z.; Chen, J.; Lee, J.; Borys, M.; Li, Z. J., Industrial bioprocessing perspectives on managing therapeutic protein charge variant profiles. *Biotechnol Bioeng* **2018,** *115* (7), 1646-1665.

6. Chirino, A. J.; Mire-Sluis, A., Characterizing biological products and assessing comparability following manufacturing changes. *Nat Biotechnol* **2004,** *22* (11), 1383-91.

7. Goetze, A. M.; Schenauer, M. R.; Flynn, G. C., Assessing monoclonal antibody product quality attribute criticality through clinical studies. *MAbs* **2010,** *2* (5), 500-7.

8. Alt, N.; Zhang, T. Y.; Motchnik, P.; Taticek, R.; Quarmby, V.; Schlothauer, T.; Beck, H.; Emrich, T.; Harris, R. J., Determination of critical quality attributes for monoclonal antibodies using quality by design principles. *Biologicals* **2016,** *44* (5), 291-305.

9. Yu, L. X.; Amidon, G.; Khan, M. A.; Hoag, S. W.; Polli, J.; Raju, G. K.; Woodcock, J., Understanding pharmaceutical quality by design. *AAPS J* **2014,** *16* (4), 771-83.

10. Finkler, C.; Krummen, L., Introduction to the application of QbD principles for the development of monoclonal antibodies. *Biologicals* **2016,** *44* (5), 282-90.

11. Vlasak, J.; Ionescu, R., Heterogeneity of monoclonal antibodies revealed by charge-sensitive methods. *Curr Pharm Biotechnol* **2008,** *9* (6), 468-81.

12. Du, Y.; Walsh, A.; Ehrick, R.; Xu, W.; May, K.; Liu, H., Chromatographic analysis of the acidic and basic species of recombinant monoclonal antibodies. *MAbs* **2012,** *4* (5), 578-85.

13. Gramer, M. J., Product quality considerations for mammalian cell culture process development and manufacturing. *Adv Biochem Eng Biotechnol* **2014,** *139*, 123-66.

14. Beyer, B.; Walch, N.; Jungbauer, A.; Lingg, N., How Similar Is Biosimilar? A Comparison of Infliximab Therapeutics in Regard to Charge Variant Profile and Antigen Binding Affinity. *Biotechnol J* **2018**, e1800340.

15. Fekete, S.; Beck, A.; Veuthey, J. L.; Guillarme, D., Ion-exchange chromatography for the characterization of biopharmaceuticals. *J Pharm Biomed Anal* **2015,** *113*, 43-55.

16. Wu, G.; Yu, C.; Wang, W.; Wang, L., Interlaboratory method validation of icIEF methodology for analysis of monoclonal antibodies. *Electrophoresis* **2018,** *39* (16), 2091-2098.

17. International Conference on Harmonization. Q6B, S. t. p. a. a. c. f. b. b. p. G., Switzerland; 1999., Q6B, Specifications: test procedures and acceptance criteria for biotechnological/biological products. **1999**.

18. Harris, R. J., Processing of C-terminal lysine and arginine residues of proteins isolated from mammalian cell culture. *J Chromatogr A* **1995,** *705* (1), 129-34.

19. Luo, J.; Zhang, J.; Ren, D.; Tsai, W. L.; Li, F.; Amanullah, A.; Hudson, T., Probing of C-terminal lysine variation in a recombinant monoclonal antibody production using Chinese hamster ovary cells with chemically defined media. *Biotechnol Bioeng* **2012,** *109* (9), 2306-15.

20. Yan, Q.; Huang, M.; Lewis, M. J.; Hu, P., Structure Based Prediction of Asparagine Deamidation Propensity in Monoclonal Antibodies. *MAbs* **2018**, 1-12.

21. Xie, P.; Niu, H.; Chen, X.; Zhang, X.; Miao, S.; Deng, X.; Liu, X.; Tan, W. S.; Zhou, Y.; Fan, L., Elucidating the effects of pH shift on IgG1 monoclonal antibody acidic charge variant levels in Chinese hamster ovary cell cultures. *Appl Microbiol Biotechnol* **2016,** *100* (24), 10343-10353.

22. Ponniah, G.; Kita, A.; Nowak, C.; Neill, A.; Kori, Y.; Rajendran, S.; Liu, H., Characterization of the acidic species of a monoclonal antibody using weak cation exchange chromatography and LC-MS. *Anal Chem* **2015,** *87* (17), 9084-92.

23. Quan, C.; Alcala, E.; Petkovska, I.; Matthews, D.; Canova-Davis, E.; Taticek, R.; Ma, S., A study in glycation of a therapeutic recombinant humanized monoclonal antibody: where it is, how it got there, and how it affects charge-based behavior. *Anal Biochem* **2008,** *373* (2), 179-91.

24. Chumsae, C.; Gifford, K.; Lian, W.; Liu, H.; Radziejewski, C. H.; Zhou, Z. S., Arginine modifications by methylglyoxal: discovery in a recombinant monoclonal antibody and contribution to acidic species. *Anal Chem* **2013,** *85* (23), 11401-9.

25. Mo, J.; Yan, Q.; So, C. K.; Soden, T.; Lewis, M. J.; Hu, P., Understanding the Impact of Methionine Oxidation on the Biological Functions of IgG1 Antibodies Using Hydrogen/Deuterium Exchange Mass Spectrometry. *Anal Chem* **2016,** *88* (19), 9495-9502.

26. Lindman, S.; Bauer, M. C.; Lund, M.; Diehl, C.; Mulder, F. A.; Akke, M.; Linse, S., pK(a) values for the unfolded state under native conditions explain the pH-dependent stability of PGB1. *Biophys J* **2010,** *99* (10), 3365-73.

27. Yang, Y.; Mah, A.; Yuk, I. H.; Grewal, P. S.; Pynn, A.; Cole, W.; Gao, D.; Zhang, F.; Chen, J.; Gennaro, L.; Schoneich, C., Investigation of Metal-Catalyzed Antibody Carbonylation With an Improved Protein Carbonylation Assay. *J Pharm Sci* **2018**.

28. Amici, A.; Levine, R. L.; Tsai, L.; Stadtman, E. R., Conversion of amino acid residues in proteins and amino acid homopolymers to carbonyl derivatives by metal-catalyzed oxidation reactions. *J Biol Chem* **1989,** *264* (6), 3341-6.

29. Yang, Y.; Stella, C.; Wang, W.; Schoneich, C.; Gennaro, L., Characterization of oxidative carbonylation on recombinant monoclonal antibodies. *Anal Chem* **2014,** *86* (10), 4799-806.

30. Stadtman, E. R., Oxidation of free amino acids and amino acid residues in proteins by radiolysis and by metal-catalyzed reactions. *Annu Rev Biochem* **1993,** *62*, 797-821.

31. Yan, B.; Yates, Z.; Balland, A.; Kleemann, G. R., Human IgG1 hinge fragmentation as the result of H2O2-mediated radical cleavage. *J Biol Chem* **2009,** *284* (51), 35390-402.

32. Zhang, H. M.; Li, C.; Lei, M.; Lundin, V.; Lee, H. Y.; Ninonuevo, M.; Lin, K.; Han, G.; Sandoval, W.; Lei, D.; Ren, G.; Zhang, J.; Liu, H., Structural and Functional Characterization of

a Hole-Hole Homodimer Variant in a "Knob-Into-Hole" Bispecific Antibody. *Anal Chem* **2017,** *89* (24), 13494-13501.

33. Zhang, H. M.; Kazazic, S.; Schaub, T. M.; Tipton, J. D.; Emmett, M. R.; Marshall, A. G., Enhanced digestion efficiency, peptide ionization efficiency, and sequence resolution for protein hydrogen/deuterium exchange monitored by Fourier transform ion cyclotron resonance mass spectrometry. *Anal Chem* **2008,** *80* (23), 9034-41.

34. Wales, T. E.; Engen, J. R., Hydrogen exchange mass spectrometry for the analysis of protein dynamics. *Mass Spectrom Rev* **2006,** *25* (1), 158-70.

35. Zhang, Z.; Smith, D. L., Determination of amide hydrogen exchange by mass spectrometry: a new tool for protein structure elucidation. *Protein Sci* **1993,** *2* (4), 522-31.

36. Perkins, D. N.; Pappin, D. J.; Creasy, D. M.; Cottrell, J. S., Probability-based protein identification by searching sequence databases using mass spectrometry data. *Electrophoresis* **1999,** *20* (18), 3551-67.

37. Kan, Z. Y.; Mayne, L.; Chetty, P. S.; Englander, S. W., ExMS: data analysis for HX-MS experiments. *J Am Soc Mass Spectrom* **2011,** *22* (11), 1906-15.

38. Zhang, Q.; Willison, L. N.; Tripathi, P.; Sathe, S. K.; Roux, K. H.; Emmett, M. R.; Blakney, G. T.; Zhang, H. M.; Marshall, A. G., Epitope mapping of a 95 kDa antigen in complex with antibody by solution-phase amide backbone hydrogen/deuterium exchange monitored by Fourier transform ion cyclotron resonance mass spectrometry. *Anal Chem* **2011,** *83* (18), 7129-36.

39. Glover, Z. K.; Basa, L.; Moore, B.; Laurence, J. S.; Sreedhara, A., Metal ion interactions with mAbs: Part 1. *MAbs* **2015,** *7* (5), 901-11.

40. Narhi, L. O.; Luo, Q.; Wypych, J.; Torosantucci, R.; Hawe, A.; Fujimori, K.; Nashed-Samuel, Y.; Jawa, V.; Joubert, M. K.; Jiskoot, W., Chemical and Biophysical Characteristics of Monoclonal Antibody Solutions Containing Aggregates Formed during Metal Catalyzed Oxidation. *Pharm Res* **2017,** *34* (12), 2817-2828.

41. Joubert, M. K.; Luo, Q.; Nashed-Samuel, Y.; Wypych, J.; Narhi, L. O., Classification and characterization of therapeutic antibody aggregates. *J Biol Chem* **2011,** *286* (28), 25118-33.

42. Vlasak, J.; Ionescu, R., Fragmentation of monoclonal antibodies. *MAbs* **2011,** *3* (3), 253-63.

43. Cordoba, A. J.; Shyong, B. J.; Breen, D.; Harris, R. J., Non-enzymatic hinge region fragmentation of antibodies in solution. *J Chromatogr B Analyt Technol Biomed Life Sci* **2005,** *818* (2), 115-21.

44. Bogardus, J. B.; Higuchi, T., Kinetics and mechanism of hydrolysis of labile quaternary ammonium derivatives of tertiary amines. *J Pharm Sci* **1982,** *71* (7), 729-35.

45. Stadtman, E. R., Metal ion-catalyzed oxidation of proteins: biochemical mechanism and biological consequences. *Free Radic Biol Med* **1990,** *9* (4), 315-25.

46. Chumsae, C.; Gaza-Bulseco, G.; Sun, J.; Liu, H., Comparison of methionine oxidation in thermal stability and chemically stressed samples of a fully human monoclonal antibody. *J Chromatogr B Analyt Technol Biomed Life Sci* **2007,** *850* (1-2), 285-94.

47. Ponniah, G.; Nowak, C.; Neill, A.; Liu, H., Characterization of charge variants of a monoclonal antibody using weak anion exchange chromatography at subunit levels. *Anal Biochem* **2017,** *520*, 49-57.

48. Hintersteiner, B.; Lingg, N.; Zhang, P.; Woen, S.; Hoi, K. M.; Stranner, S.; Wiederkum, S.; Mutschlechner, O.; Schuster, M.; Loibner, H.; Jungbauer, A., Charge heterogeneity: Basic antibody charge variants with increased binding to Fc receptors. *MAbs* **2016,** *8* (8), 1548-1560.

49. Amano, M.; Kobayashi, N.; Yabuta, M.; Uchiyama, S.; Fukui, K., Detection of histidine oxidation in a monoclonal immunoglobulin gamma (IgG) 1 antibody. *Anal Chem* **2014,** *86* (15), 7536-43.

50. Purdie, J. L.; Kowle, R. L.; Langland, A. L.; Patel, C. N.; Ouyang, A.; Olson, D. J., Cell culture media impact on drug product solution stability. *Biotechnol Prog* **2016,** *32* (4), 998-1008.

51. Stadtman, E. R., Role of oxidized amino acids in protein breakdown and stability. *Methods Enzymol* **1995,** *258*, 379-93.

52. Yang, Y.; Mah, A.; Yuk, I. H.; Grewal, P. S.; Pynn, A.; Cole, W.; Gao, D.; Zhang, F.; Chen, J.; Gennaro, L.; Schoneich, C., Investigation of Metal-Catalyzed Antibody Carbonylation With an Improved Protein Carbonylation Assay. *J Pharm Sci* **2018,** *107* (10), 2570-2580.

53. Yi, Y.; Zang, L., High-throughput Carbonyl Content Method of Therapeutic mAb using size-exclusion chromatography with ultraviolet and fluorescence detection. *Anal Biochem* **2019,** *571*, 25-36.

54. Rivett, A. J.; Levine, R. L., Metal-catalyzed oxidation of Escherichia coli glutamine synthetase: correlation of structural and functional changes. *Arch Biochem Biophys* **1990,** *278* (1), 26-34.

55. Lv, H.; Han, J.; Liu, J.; Zheng, J.; Liu, R.; Zhong, D., CarSPred: a computational tool for predicting carbonylation sites of human proteins. *PLoS One* **2014,** *9* (10), e111478.

56. Uchida, K.; Kato, Y.; Kawakishi, S., A novel mechanism for oxidative cleavage of prolyl peptides induced by the hydroxyl radical. *Biochem Biophys Res Commun* **1990,** *169* (1), 265-71.

Chapter 4

Effects of Oxidative Carbonylation on Physical Stability of a Recombinant Monoclonal Antibody

INTRODUCTION

During pharmaceutical development of recombinant monoclonal antibody (mAb) drug products, a major focus is identification of mAb candidates and formulations that provide suitable physical stability characteristics.[1] In particular, it is necessary to control the formation of mAb aggregates in the products, since the aggregates could pose a safety risk to patients.[2-3] The safety risk of mAb aggregates is often attributed to adverse immune responses potentially induced by the aggregates.[4] Both innate and adaptive immune pathways could be involved.[5] For the innate immune response, mAb aggregates may have repetitive structure motifs or patterns, which can directly activate B1 cells to generate low-affinity antibodies (such as IgM) against the aggregates.[5-6] For the adaptive immune response, mAb aggregates may be recognized by antigen presenting cells and are then internalized, processed, and presented to the major histocompatibility complex (MHC).[5, 7] The peptide epitope presented in the MHC activates naive T cells to form antigen-specific helper T cells, which subsequently trigger B cell activation and production of antigen-specific antibodies against the aggregates.[7] To date, the exact factors that could lead to an immune response against mAb aggregates are not well understood. For example, in a study by Boll et al., mAb particles/aggregates with low levels of chemical modifications were not immunogenic in a transgenic mouse model.[8] These particles/aggregates broke immune tolerance when extensive chemical modifications were present.[8] However, many of these modifications are yet to be identified.[8] It is therefore important to understand the nature and underlying mechanism of mAb aggregation, and to correlate the understandings with clinical experience or immunogenicity model system data, which will enable better assessment and control of the safety risk from mAb aggregates.

Existing studies show that mAb aggregates can be generated by a large variety of stress conditions.[9-10] The resulting aggregates often have different physicochemical properties and morphologies. Joubert et al. reported that among the 14 tested stress conditions, harsh mechanical stress generated the greatest number of subvisible particles, while thermal stress generated the greatest number of visible particles.[9] From FTIR analysis, almost all aggregates displayed a certain degree of changes in secondary structure, where 90ºC treated mAb samples showed the greatest perturbation of the folded-β sheet structure.[9] The 90ºC samples also showed the highest degree of change in tertiary structures, indicating that proteins were mostly unfolded in the aggregates from the 90ºC stress.[9] Finally, these aggregates demonstrated different surface hydrophobicity and reversibility.[9] Using similar stress conditions, Telikepalli et al. provided additional characterization of IgG1 mAb aggregates, and found that shaking stress generated mostly fibrillar particles, while stirring stress generated mostly spherical particles.[11] Interestingly, the aggregates generated by shaking and freeze–thaw did not display many differences in the biophysical characteristics compared with the unstressed mAb.[11] The aggregates generated by stirring and heating, however, contained non-native disulfide cross-links, intermolecular beta sheet content, and elevated surface hydrophobicity.[11] Using a transgenic mouse model, Filipe et al. discovered that the different types of aggregates had different immunogenic potential.[4] The aggregates produced by freeze-thaw are not immunogenic.[4] However, the aggregates produced by metal-catalyzed oxidation are most immunogenic,[4] which suggests that oxidative modifications may generate neo-epitopes on mAbs. Kijanka et al. reported that submicron size particles of a murine antibody are more immunogenic than its soluble oligomers or micron size particles, which shows that mAb aggregate size can

affect the immunogenic potential.[12] These studies highlight the complexity of mAb aggregation and the importance to understand the nature of mAb aggregates.

Various mechanisms, including mAb self-association, interactions between unfolded or partially unfolded intermediates, and chemical degradations/crosslinks, have been proposed to explain mAb aggregation.[2, 13-14] Through these mechanisms, intrinsic and extrinsic factors could influence the mAb physical stability profile. For the intrinsic factors, aggregation-prone motifs or hot-spots have been identified in mAb variable and constant domains.[15-17] In particular, the complementarity determining regions (CDRs) could contribute to aggregation since the CDRs often contain hydrophobic and charged/polarizable residues required for antigen binding.[18] The light chain CDR3 contains a glutamine/asparagine rich motif, that was also found in the aggregation prone regions on prion and amyloid proteins.[17] In the constant domains, C_L and C_{H2} have conserved sequences (VVCLL and VVSVLTVL) rich in β-branched aliphatic residues (valine, leucine, isoleucine), which could contribute to aggregation.[17] Chemical degradation/crosslinks, such as methionine oxidation in the Fc domain, intra- or inter-molecular disulfide scrambling, histidine oxidation/co-valent crosslinks, could alter antibody structure and thus lead to increased aggregation propensity.[10, 17] For the extrinsic factors, various mAb formulation parameters, such as buffer type, ionic strength, and surfactant type/concentration, can influence mAb physical stability profiles.[14, 19] For example, in an agitation study, with three IgG2 mAbs, Fesinmeyer et al. showed that the extent of mAb aggregation increased as the buffer anion size increased, while the cation size did not have any effect.[20] Using several stress conditions, Telikepalli et al. showed that presence of sodium chloride in mAb solutions enhanced mAb aggregation.[11] Under a shaking stress condition, Wang et al. showed that the effects of surfactants on two IgG1 mAbs depended on the surfactant type/concentration.[21] At the lower

concentrations, these surfactants reduced the extent of mAb aggregation.[21] However, at the higher concentrations, certain surfactants induced structural perturbation and were found to destabilize the mAbs.[21]

Considering that mAb aggregates generated by metal-catalyzed oxidation could potentially pose an immunogenic risk[4] and that oxidation products themselves could contribute to immunogenicity, it is necessary to gain an in-depth understanding of the nature and mechanism of metal-catalyzed mAb aggregation. In particular, understanding the effects of chemical degradation products from metal-catalyzed oxidation on mAb aggregation could help to elucidate and address the potential immunogenicity risks. Among the various degradation products, oxidative carbonylation products, which primarily consist of aminoadipic semialdehyde (from lysine), glutamic semialdehyde (from arginine/proline), and 2-amino-3-ketobutyric acid (from threonine),[22] attracted a lot of interest since oxidative carbonylation products themselves can be immunogenic.[23-24] Zafar et al. reported increased binding of carbonylated human serum albumin over unstressed human serum albumin by autoantibodies from systemic lupus erythematosus patients, and suggested that oxidative carbonylation could trigger autoantibody production.[24] Oxidative carbonylation products have also been implicated in protein/mAb aggregation. Bee et al. reported that protein carbonylation levels in mAb aggregates generated on stainless steel microparticle surfaces increased four-fold.[25] Interestingly, no methionine oxidation was observed in the aggregates.[25] In a storage study, Purdie et al. reported a positive correlation between the relative extent of mAb carbonylation and mAb aggregation rate.[26] From a theoretical perspective, Petrov and Zagrovic applied molecular dynamics simulations to understand the effect of oxidative carbonylation to protein structure and dynamics, and suggested that carbonylation of lysine and arginine residues can significantly increase the

protein intrinsic aggregation propensity.[27] While these studies support that oxidative carbonylation can contribute to protein aggregation, to date, a detailed understanding of the effects of oxidative carbonylation on mAb physical stability is still lacking.

This study investigates the effects of oxidative carbonylation on the physical stability of a model IgG1 antibody (mAb A) in several buffers. A commonly used stir stress system[9, 11] was employed to compare the aggregation propensity between the unstressed and the carbonylated mAb A, which provided an initial assessment of the effects. The carbonylated mAb A samples were further analyzed for the extents of total protein carbonylation and site-specific carbonylation in the supernatants, after the mAb solutions were stirred for 1 day and 3 days (and subsequently centrifuged). This analysis helps understand if there is any preferential aggregation/precipitation of carbonylation products, which could reveal aggregation-prone carbonylation spots on mAb A. Other degradation products generated by metal-catalyzed oxidation, such as methionine sulfoxide and hydroxytryptophan,[28] were also analyzed to understand their contributions to physical instability of mAb A in relation to oxidative carbonylation. From an extrinsic perspective, buffer ion types and ion strength in the mAb A solutions were studied to understand if these factors exacerbate or alleviate the effects of oxidative carbonylation. Specifically, three different anions, SO_4^{2-}, I^-, and Cl^-, from the Hofmeister series,[29] were used to probe potential interactions between these anions and site-specific carbonylation that may impact the physical stability of mAb A. Furthermore, the unstressed and the carbonylated mAb A were analyzed by differential scanning calorimetry (DSC) to identify any correlations between mAb A thermal stability and oxidative carbonylation, which provided a more comprehensive view on the effect of oxidative carbonylation.

MATERIALS AND METHODS

Materials

The recombinant humanized IgG1 monoclonal antibody, mAb A, was produced at Genentech (South San Francisco, CA). Lucifer Yellow carbohydride dilithium salt (Lucifer Yellow CH), hydrogen peroxide solution (30% in water, w/w), ferrous sulfate, methionine, ethylenediaminetetraacetic acid (EDTA), sodium succinate, sodium borohydride, methanol, succinic acid, sodium phosphate (dibasic and monobasic), sodium chloride, sodium acetate, sodium sulfate, sodium iodide, acetic acid, sodium hydroxide solution (1 M in water), 2-(N-morpholino)ethanesulfonic acid (MES), lithium hydroxide, reduced Triton X-100, (Carboxymethyl)trimethylammonium chloride hydrazide (Girard's Reagent T, GRT), dithiothreitol (DTT), iodoacetic acid (IAA), calcium chloride, tris(hydroxymethyl) aminomethane (Tris), trifluoroacetic acid (TFA), potassium phosphate, and glycine were purchased from Sigma-Aldrich (St. Louis, MO, USA). guanidinium hydrochloride (8 M in water) was purchased from Thermo Scientific (Waltham, MA, USA). TSK G3000 SWXL (7.8x300 mm) size exclusion column was purchased from Tosoh Bioscience (King of Prussia, PA, USA). Acetonitrile (ACN) was purchased from Burdick & Jackson (Muskegon, MI, USA). Sequencing-grade trypsin was purchased from Promega (Madison, WI, USA). ACQUITY UPLC Peptide BEH C18 (300 Å, 1.7 um, 2.1x150mm) column were purchased from Waters (Milford, MA, USA).

Preparation of Carbonylated mAb A by Metal-catalyzed Oxidation

The carbonylated mAb A sample was prepared by metal-catalyzed oxidation as previously described.[30] The oxidation reaction mixture consisted of mAb A, ferrous sulfate, and hydrogen peroxide at final concentrations of 5 mg/mL, 2 mM, and 10 mM, respectively. The mixture was

incubated at room temperature for 2 hours in 50 mM sodium succinate buffer (pH 6.5). Excess amounts of methionine and EDTA were subsequently added to the mixture to stop the oxidation reactions. The carbonylated mAb A sample was then buffer exchanged into 10 mM sodium acetate (pH 5.0) with a 30 kDa Amicon filter (EMD Millipore, Burlington, MA, USA).

Aggregation of mAb A by Stirring

A commonly used stir stress condition[9, 11] was employed to generate mAb aggregates. The unstressed and carbonylated mAb A were buffer-exchanged into four different buffers: A) 10 mM sodium acetate, 1 mM EDTA, pH 5.0; B) 150 mM sodium chloride, 10 mM sodium acetate, 1 mM EDTA, pH 5.0; C) 150 mM sodium sulfate, 10 mM sodium acetate, 1 mM EDTA, pH 5.0; D) 150 mM sodium iodide, 10 mM sodium acetate, 1 mM EDTA, pH 5.0. The final mAb protein concentration was 2 mg/mL. These mAb solutions were stirred at a speed setting of 7 on a Corning stirring plate (Corning, NY, USA) with a magnetic stir bar (10 mm x 6 mm, Fisher Scientific, Hampton, NH, USA). After stirring for 1 and 3 days at room temperature, the mAb samples were centrifuged at 10,000 rpm for 10 minutes using a Beckman Coulter Centrifuge. For each sample, the supernatant was transferred to another tube for subsequent analyses.

Analysis of mAb A Size Variants by Size Exclusion Chromatography

The size variants of mAb A samples were separated on a TSK G3000 SWXL (7.8x300 mm) size exclusion column with an isocratic flow of 0.5 mL/min. The SEC mobile phase was 200 mM potassium phosphate, 250 mM potassium chloride, pH 6.2. The column temperature was set at 25°C and the HPLC autosampler temperature was at 8°C. The elution was monitored by UV absorbance at 280 nm. Sample injection volume was 40 µL. The relative peak areas as well as the total peak area of mAb A size variants were determined by manual integration of the size exclusion chromatograms using Agilent Chemstation software.

Total Protein Carbonylation Assay

Total protein carbonylation levels were determined using a previously described assay.[30] Briefly, for the analysis, mAb A samples were derivatized by Lucifer Yellow CH at a Lucifer Yellow CH-to-mAb molar ratio of 8,000:1. The derivatization reaction mixture was incubated at 37°C for 16 hours in 50 mM lithium MES buffer, 1% Triton X-100, pH 6.0. After the derivatization, the mAb A samples were buffer-exchanged into 200 mM potassium phosphate, 250 mM potassium chloride, pH 6.2. Subsequently, the Lucifer Yellow CH-derived mAb A samples were analyzed by size exclusion chromatography, and the total protein carbonylation levels were determined by the total peak areas from 280 and 428 nm absorbance.

Differential Scanning Calorimetry (DSC)

DSC analysis was performed to assess the overall conformational stability of unstressed and stressed mAb A in the four different buffers. The analysis was conducted on a MicroCal VP-Capillary instrument (Malvern Panalytical, Malvern, UK). A temperature ramp from 20°C to 100°C with a scan rate of 60°C per hour was used for the scanning. A volume of 300 µl of mAb solutions was injected through setting the cell filling volume. A clean cycle step was applied between each sample run. DSC data analysis was conducted with Origin 7.0 software, where the corresponding buffer signal was subtracted and the thermograms were fitted into a 3-transition model with T_m of CH2, CH3, and Fab regions.

Characterization of Site-Specific Carbonylation

The site-specific carbonylation analysis was based on a previously described peptide mapping method.[31] The carbonyls were derivatized by Girard's Reagent T (GRT) at a GRT-to-protein molar ratio of 20,000:1. After the derivatization, the mAb A samples were buffer-exchanged to 10 mM sodium acetate, pH 5.0. Subsequently, each mAb A sample (200 µL) was

mixed with 1 M sodium borohydride (100 µL, prepared in methanol) and 400 mM sodium phosphate buffer (200 µL, pH 8.0) to a final volume of 500 µL. The reduction by sodium borohydride was carried out at room temperature for 30 minutes. These samples were then reduced (by DTT), S-carboxymethylated (by IAA), and buffer exchanged to 25 mM Tris, 1 mM calcium chloride, pH 8.2, for tryptic digestion. The digestion was carried out at 37°C for 4 hours with a trypsin-to-substrate ratio of 1:50 (weight to weight), and was stopped by the addition of TFA to a final concentration of 0.3% (v/v). The digested mAb A samples were separated on a BEH C18 column (300 Å, 1.7 µm, 2.1x150 mm), where solvent A was 0.1% TFA in water and solvent B was 0.09% TFA in acetonitrile. A step gradient was employed: 1-20% B in 16 minutes, 20-40% B in 35 minutes, and 40-57% B in 15 minutes. Column temperature was 60°C. Flow rate was 0.3 mL/min.

Mass spectrometry analysis was performed on an OrbiTrap Velos in the positive mode with an electrospray voltage of 4.0 kV and a capillary temperature of 250°C. A data-dependent mode was used to acquire the mass spectrometry data, where the top 9 most intense ions in the full MS spectrum were selected for MS^2 analysis. For the MS^2 analysis, the normalized collision energy was 35%, and the activation time was 10 milliseconds. Identification of carbonylation and other oxidation products was based on database searching using the Proteome Discover software. The relative quantification of these oxidation products was performed by using extracted ion chromatograms as previously described.[31]

RESULTS

Formation of Precipitates or Insoluble Aggregates

After 1 day and 3 days of stirring, extensive protein precipitation was observed in all mAb A samples. The amount of precipitates or insoluble aggregates was indirectly evaluated by the

relative total peak areas (normalized to that of the T0 sample) of mAb A supernatants from the SEC analysis, where a decrease in the relative total peak area of a supernatant sample reflects an increase in the amount of precipitates or insoluble aggregates (based on mass balance). As shown in Figure 1, the relative total peak area for all mAb A supernatants decreased over the time course of stirring. Interestingly, in each buffer, after 1 day of stirring, no significant difference was observed in the relative total peak area between the unstressed and stressed mAb A samples. By contrast, after 3 days of stirring, the relative total peak area of the stressed mAb A was lower than that of the unstressed mAb A. Chemical or physical changes induced by metal-catalyzed oxidation may be responsible for the increased formation of precipitates or insoluble aggregation. The effects of the chemical or physical changes induced by metal-catalyzed oxidation, however, were not apparent with the first day of stirring. When comparing the effects from the four different buffers, we found that buffer type also impacted the formation of precipitates or insoluble aggregates. Among the four buffers, buffer A generated the least amount of precipitates/insoluble aggregates, respectively, for the unstressed and the stressed mAb A, at day 1 and day 3. This observation suggests that the presence of the additional 150 mM sodium salts in buffers B, C, and D exacerbated mAb A precipitation/aggregation. Between buffers B, C, and D, the extent of precipitation or aggregation follows an order of D>B>C, where the greatest amount of precipitates/insoluble aggregates after 3 days of stirring was observed with buffer D. Given that the pI of mAb A is 8.2 (and thus mAb A is positively charged in the pH 6.5 buffers), the order of D>B>C is consistent with a reversed order of the Hofmeister series for the effects of the three anions (I^->Cl^->SO_4^{2-}), which is commonly observed for positively charged proteins.[32-33]

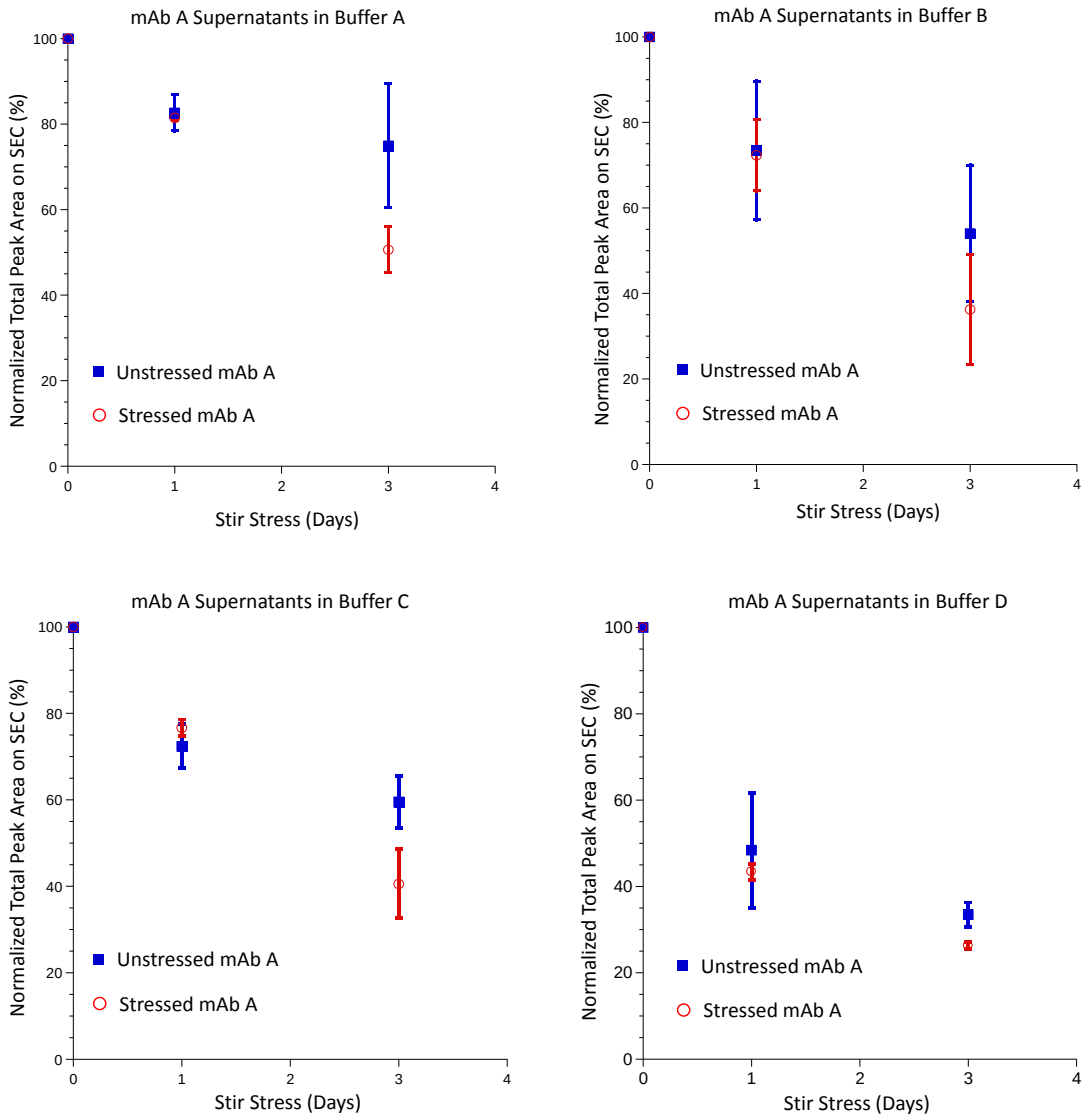

Figure 1. Relative total peak area (normalized to that of T0 sample) of mAb A supernatants on size exclusion chromatograms. Buffer A is 10 mM sodium acetate, 1 mM EDTA, pH 5.0. Buffer B is 150 mM sodium chloride, 10 mM sodium acetate, 1 mM EDTA, pH 5.0. Buffer C is 150 mM sodium sulfate, 10 mM sodium acetate, 1 mM EDTA, pH 5.0. Buffer D is 150 mM sodium iodide, 10 mM sodium acetate, 1 mM EDTA, pH 5.0.

Soluble Aggregates

The soluble aggregates in mAb A supernatants were characterized by size exclusion chromatography. As shown in Figures 2 and 3 and Table 1, for buffer A, B, or C, the levels of soluble aggregates in the supernatants of both unstressed and stressed mAb A decreased over the time course of stirring. By contrast, for buffer D, the levels of soluble aggregates increased after 1 day of stirring, and subsequently decreased after 3 days of stirring. In addition, for buffer D, the soluble aggregates were more heterogeneous than those from buffer A, B, or C (Figures 2 and 3). In particular, a peak eluted at ~11 minutes, presumably a very large oligomer of mAb A, was present only in mAb A supernatants from buffer D (Figure 3). These differences indicate that the effect of buffer D on the formation of soluble aggregates may differ significantly from that of buffer A, B, or C. It should also be pointed out that although the highest levels of precipitates and soluble aggregates were found in buffer D, the formation of soluble aggregates does not correlate with the formation of the precipitates or insoluble aggregates as shown in Figure 1.

For mAb A supernatant samples, the levels of LMWS (i.e. mAb A fragments, eluted at ~19.5 minutes) consistently increased over the time course of stirring, for all four buffers. The enrichment of LMWS in the supernatants regardless of the buffer type suggests that LMWS may not be a major component that drives the formation of the precipitates or insoluble aggregates.

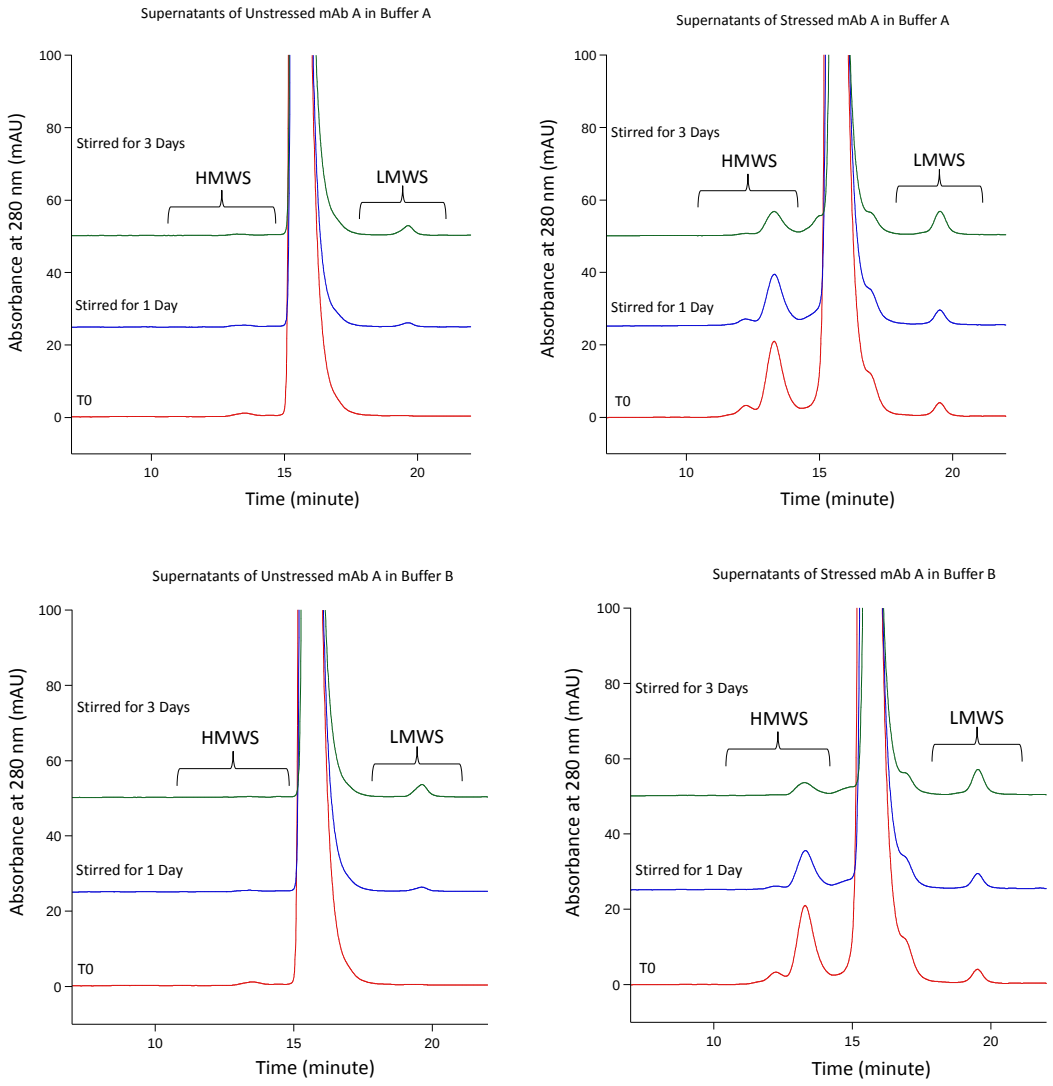

Figure 2. Size exclusion chromatograms of the mAb A supernatants after mAb A samples were stirred for 0, 1, and 3 days in buffer A (10 mM sodium acetate, 1 mM EDTA, pH 5.0) and buffer B (150 mM sodium chloride, 10 mM sodium acetate, 1 mM EDTA, pH 5.0).

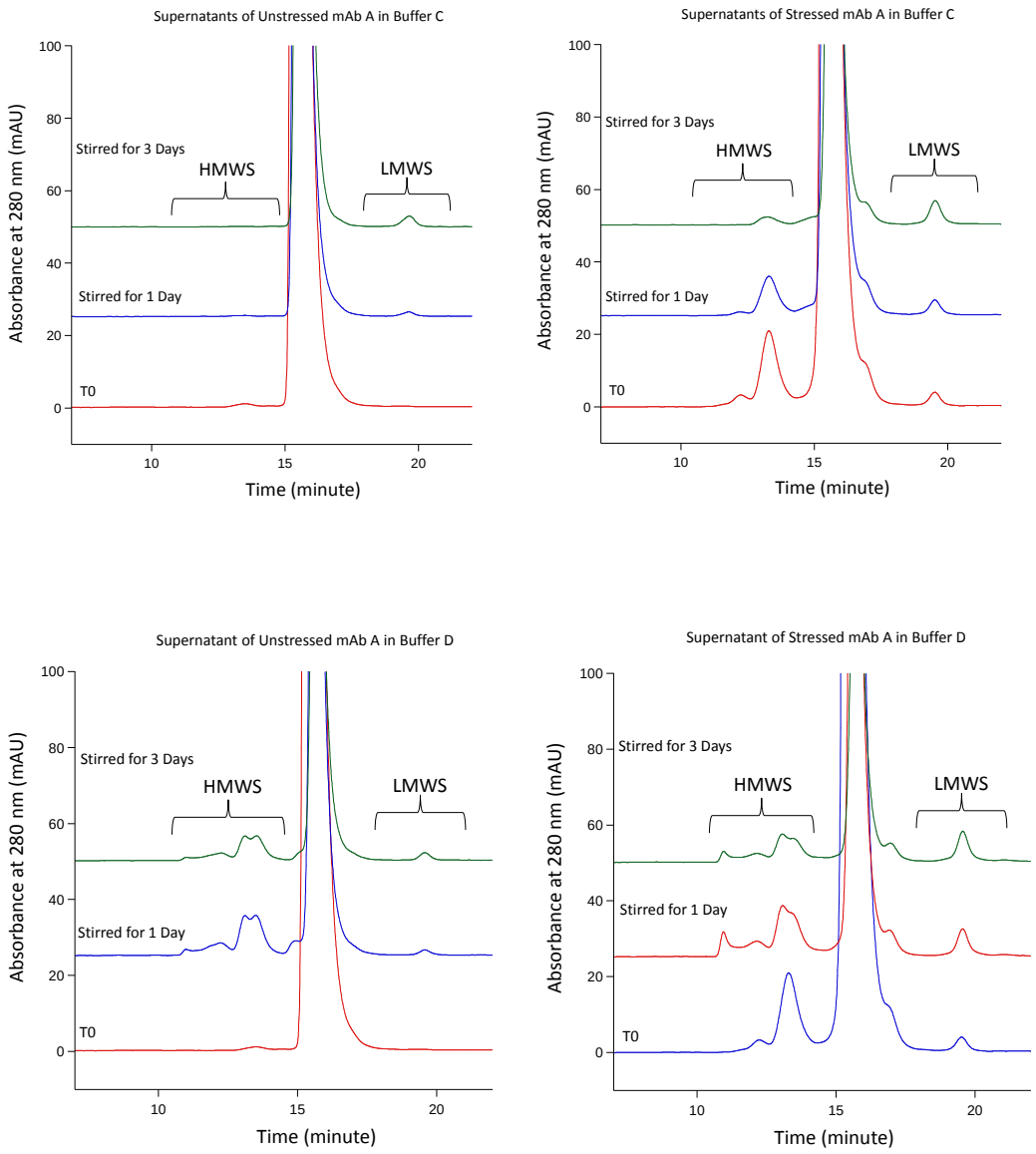

Figure 3. Size exclusion chromatograms of mAb A supernatants after mAb A samples were stirred for 0, 1, and 3 days in buffer C (150 mM sodium sulfate, 10 mM sodium acetate, 1 mM EDTA, pH 5.0) and buffer D (150 mM sodium iodide, 10 mM sodium acetate, 1 mM EDTA, pH 5.0)

mAb A		% HMWS	% Main Peak	% LMWS
Unstressed	T0	0.3 ± 0.0	98.6 ± 0.0	1.1 ± 0.0
	Stirred for 1 Day in Buffer A	0.3 ± 0.1	97.9 ± 0.3	1.8 ± 0.2
	Stirred for 3 Days in Buffer A	0.2 ± 0.1	97.3 ± 0.7	2.5 ± 0.7
	Stirred for 1 Day in Buffer B	0.2 ± 0.0	98.0 ± 0.0	1.8 ± 0.4
	Stirred for 3 Days in Buffer B	0.1 ± 0.0	96.9 ± 1.0	3.0 ± 1.1
	Stirred for 1 Day in Buffer C	0.1 ± 0.1	98.2 ± 0.1	1.7 ± 0.1
	Stirred for 3 Days in Buffer C	0.2 ± 0.0	97.0 ± 0.7	2.9 ± 0.8
	Stirred for 1 Day in Buffer D	11.8 ± 0.6	86.2 ± 0.9	2.0 ± 0.3
	Stirred for 3 Days in Buffer D	7.1 ± 4.3	87.2 ± 1.0	5.7 ± 5.1
Stressed	T0	6.9 ± 0.0	90.4 ± 0.0	2.7 ± 0.0
	Stirred for 1 Day in Buffer A	5.8 ± 0.2	90.8 ± 0.2	3.3 ± 0.1
	Stirred for 3 Days in Buffer A	5.2 ± 0.2	89.7 ± 0.4	5.2 ± 0.4
	Stirred for 1 Day in Buffer B	4.6 ± 0.2	92.0 ± 0.1	3.3 ± 0.3
	Stirred for 3 Days in Buffer B	2.6 ± 0.6	90.2 ± 1.8	7.2 ± 2.3
	Stirred for 1 Day in Buffer C	4.4 ± 0.1	92.1 ± 0.1	3.5 ± 0.2
	Stirred for 3 Days in Buffer C	2.2 ± 0.4	91.7 ± 0.6	6.2 ± 1.0
	Stirred for 1 Day in Buffer D	15.3 ± 0.3	78.3 ± 0.4	6.4 ± 0.2
	Stirred for 3 Days in Buffer D	14.3 ± 0.2	76.1 ± 0.3	9.6 ± 0.2

Table 1. Relative levels of HMWS, Main Peak, and LMWS in mAb A supernatants from the SEC analysis. The error represents the standard deviation from three independent analyses.

Extent of mAb A Carbonylation in the Supernatants

To understand the relationship between oxidative carbonylation and the formation of mAb A precipitates or insoluble aggregates, we planned to measure the extent of mAb A carbonylation in the precipitates and in the supernatants by CALY. However, for the precipitates, poor solubility/recovery of the precipitates caused significant sample loss (greater than 90%) at the buffer exchange step of CALY, which prevented a reliable measurement of mAb A carbonylation. For the supernatants, no sample solubility or recovery issue was observed for CALY measurement. We therefore focused on studying the relationship between mAb A carbonylation level in the supernatants and the formation of precipitates. It is worth noting that a modified DNPH assay which used urea and SDS for sample solubilization was recently developed to measure protein and cell wall polysacharide carbonyl content.[34] In the future, it will be interesting to investigate if the modified DNPH assay could provide a reliable measurement of the carbonylation content for the precipitates.

As shown in Figure 4, for buffers A, B, and C, mAb A carbonylation levels in the supernatant followed a similar pattern against time: after 1 day of stirring, the carbonylation level decreased by approximately 1.5 nmol/mg; subsequently, the carbonylation level remained essentially unchanged. For buffer D, after 1 day of stirring, the carbonylation level decreased by approximately 4.3 nmol/mg, almost three times the decrease observed in buffers A, B, and C; subsequently, after 3 days of stirring, the carbonylation level further decreased by 0.9 nmol/mg.

The relationship between mAb A carbonylation in the supernatants and the amount of precipitates/insoluble aggregates appeared to depend on buffer type. For buffers A, B, and C, the levels of mAb A carbonylation in the supernatants decreased in almost the same way (Figure 4), while the amounts of precipitates/insoluble aggregates were different with the three buffers

(Figure 1). In particular, the amount of soluble mAb A in the supernatants continued to decrease after 1 day of stirring for all three buffers (Figure 1). However, mAb A carbonylation level in the supernatants remained essentially unchanged after 1 day of stirring for all three buffers (Figure 4). These data indicate that, for buffers A, B, and C, mAb A carbonylation was likely not a major factor that led to the formation of mAb A precipitates/insoluble aggregates. By contrast, for buffer D, the change in the level of mAb A carbonylation in the supernatants (Figure 4) mirrors the change in the amount of the precipitates/insoluble aggregates (Figure 1). These data indicate that mAb A carbonylation may have a more prominent effect on the formation of precipitates/insoluble aggregates in buffer D than in buffers A, B, and C.

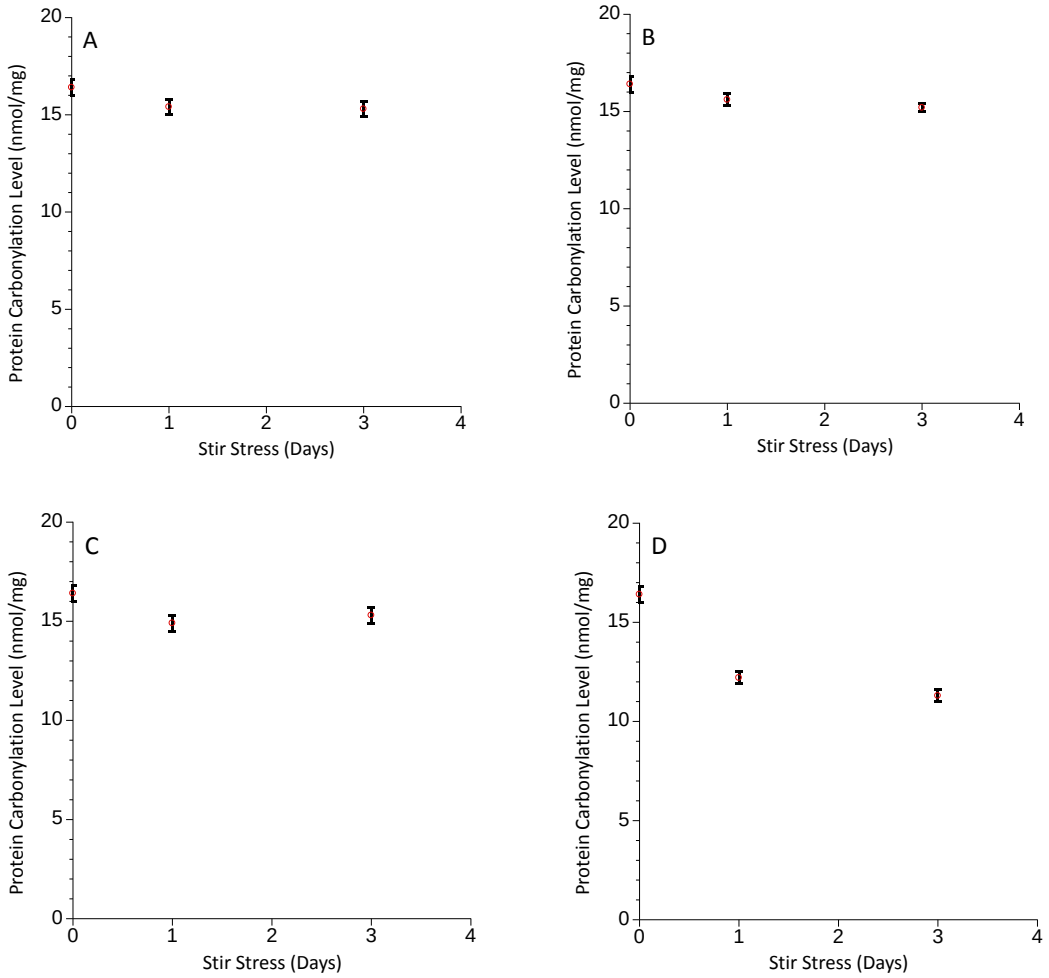

Figure 4. Total protein carbonylation levels of mAb A in the supernatants after the oxidized mAb A samples were stirred for 0, 1, and 3 days in buffers A, B, C, and D.

Characterization of Site-Specific Carbonylation in mAb A Supernatants

To further understand the effect of oxidative carbonylation on the formation of precipitates/insoluble aggregates, we characterized site-specific carbonylation products in mAb A samples by peptide mapping. For the precipitates, similar to the CALY analysis, we observed significant sample losses during sample preparation, which prevented reliable analysis of site-specific carbonylation products in the precipitates. We therefore focused on characterizing site-specific carbonylation products in the supernatants, and differences in these levels between 0, 1 and 3 days of stirring. This characterization indirectly reveals the carbonylation products that are preferentially localized/enriched in the precipitates under the stir stress condition. Using the peptide mapping method previously described[31] and optimized (Chapter 3) for relative quantitation of site-specific carbonylation on mAbs, we identified a total of 15 carbonylation products/sites (Table 2) in mAb A supernatants. The relative levels of these carbonylation products were subsequently determined by extracted ion chromatograms.

Preferential localization or enrichment of a site-specific carbonylation product in the precipitates leads to a decrease in the relative level of this product in the supernatants. Therefore, we looked for the carbonylation products that decreased in the supernatants over the time course of stirring. Interestingly, as shown in Table 2, not all carbonylation products decreased in the supernatants over the time course of stirring. In addition, certain carbonylation products decreased only in buffer D. To differentiate the various carbonylation products, we categorized these carbonylation products to three types based on how their levels changed in the four different buffers (Table 3). The carbonylation products that did not decrease significantly in any of the buffers were assigned as type 1. The carbonylation products that decreased only in buffer

D, but not in buffer A, B, or C, were assigned as type 2. The carbonylation products that decreased in all four buffers were assigned as type 3.

Carbonylation Sites		Buffer A		Buffer B		Buffer C		Buffer D	
	T0	1 day	3 days	1 day	3 days	1 day	3 days	1 day	3 days
HC K98	1.2±0.1%	1.1±0.2%	1.2±0.1%	1.0±0.1%	1.2±0.4%	1.2±0.2%	1.1±0.2%	1.5±0.2%	1.3±0.2%
HC R13	0.2±0.0%	0.1±0.0%	0.0±0.0%	0.1±0.0%	0.0±0.0%	0.1±0.0%	0.0±0.0%	0.1±0.0%	0.0±0.0%
HC T58	1.9±0.1%	1.9±0.1%	2.0±0.0%	1.9±0.1%	2.0±0.2%	1.9±0.1%	2.0±0.0%	0.0±0.0%	0.0±0.0%
HC R104	1.2±0.1%	1.5±0.1%	1.4±0.1%	1.4±0.1%	1.4±0.2%	1.4±0.0%	1.4±0.2%	1.4±0.1%	1.4±0.1%
HC T115	5.2±0.2%	5.1±0.5%	5.9±0.2%	6.0±0.2%	6.0±0.2%	5.8±0.1%	6.1±0.4%	1.4±0.2%	1.4±0.1%
HC T139	1.9±0.1%	1.9±0.1%	1.9±0.1%	1.8±0.2%	2.0±0.1%	1.9±0.1%	1.7±0.1%	0.0±0.0%	0.0±0.0%
LC T4	1.9±0.1%	1.8±0.1%	1.8±0.1%	1.8±0.2%	1.8±0.3%	1.7±0.1%	1.9±0.2%	1.6±0.2%	1.4±0.1%
LC P7	0.2±0.0%	0.2±0.1%	0.2±0.0%	0.2±0.1%	0.2±0.1%	0.2±0.1%	0.2±0.1%	0.1±0.0%	0.1±0.0%
LC K157	0.1±0.0%	0.1±0.0%	0.1±0.0%	0.1±0.0%	0.1±0.0%	0.1±0.0%	0.1±0.0%	0.1±0.0%	0.1±0.0%
HC R19	0.1±0.0%	0.1±0.0%	0.1±0.0%	0.1±0.0%	0.1±0.0%	0.1±0.0%	0.1±0.0%	0.1±0.0%	0.1±0.0%
HC T28	10.3±0.1%	9.9±0.4%	10.3±0.5%	10.1±0.4%	10.2±0.1%	10.2±0.2%	10.4±0.5%	3.7±0.2%	3.2±0.2%
LC T117	1.0±0.0%	1.0±0.1%	1.0±0.1%	0.9±0.1%	0.9±0.1%	0.9±0.1%	1.0±0.1%	0.3±0.0%	0.2±0.0%
LC T132	1.2±0.1%	1.1±0.1%	1.1±0.1%	1.1±0.1%	1.2±0.2%	1.2±0.1%	1.1±0.1%	1.1±0.1%	1.1±0.1%
HC R87	0.1±0.0%	0.1±0.0%	0.1±0.0%	0.1±0.0%	0.1±0.0%	0.1±0.0%	0.1±0.0%	0.1±0.0%	0.1±0.0%
HC T227	2.1±0.1%	2.1±0.1%	2.1±0.1%	2.1±0.1%	2.1±0.1%	2.3±0.1%	2.2±0.0%	0.0±0.0%	0.0±0.0%

Table 2. Relative levels (mean ± standard deviation) of site-specific carbonylation products in mAb A control and supernatants (determined by extracted ion chromatograms). The mean and standard deviation were obtained from three independent measurements.

Carbonylation Site	Type	Location
HC K98	1	CH1
HC R13	3	VH
HC T58	2	VH
HC R104	1	CH1
HC T115	2	CH1
HC T139	2	CH1
LC T4	2	VL
LC P7	1	VL
LC K157	1	CL
HC R19	1	VH
HC T28	2	VH
LC T117	2	CL
LC T132	1	CL
HC R87	1	VH
HC T227	2	Hinge

Table 3. The type and location of identified carbonylation products on the stressed mAb A. Over the time course of stirring, the product that did not show any significant decrease in the supernatants is assigned as Type 1; the product that showed decreased levels in supernatants with buffer D but not with the other buffers is assigned as Type 2; the product that showed decreased levels in supernatants with all four buffers is assigned as Type 3.

An example of type 1 carbonylation product was LC T132 carbonylation. Identification of this product was supported by the MS^2 data. As shown in Figure 5, for the b ions, when comparing the LC T132 carbonylation peptide and the unmodified wild type tryptic peptide, we observed a mass shift of +113 Da at the b5 ion. The mass shift of +113 Da is consistent with the theoretical mass increase introduced by the derivatization of a threonine carbonylation product (2-amino-3-ketobutyric acid).[31] Given that no known modification of +113 Da occurs on alanine, leucine, valine, or cysteine of the sequence covered by the b5 ion, the MS^2 data support the assignment of threonine carbonylation on LC T132. Relative levels of LC T132 carbonylation were determined by extracted ion chromatograms (Figure 6), which showed very little difference between T0, 1-day stir, and 3-day stir supernatant samples, in all four buffers. It should be noted that reduction of the hydrazide formed between GRT and the ketone group (2-amino-3-ketobutyric acid) by sodium borohydride, as a part of the peptide mapping procedure, can generate up to 4 chiral centers. These stereoisomers could be separated as two or more peaks on the extracted ion chromatograms (as shown in Figure 6). In contrast, no chiral center is generated from reduction of the hydrazide formed between GRT and the aldehyde group (glutamic semialdehyde and adipic semialdehyde), which leads to a single peak on the extracted ion chromatograms.

An example of a type 2 carbonylation product was HC T28 carbonylation, a predominant carbonylation product of mAb A (Table 2). Identification of this product was supported by the MS^2 data. As shown in Figure 7, when comparing HC T28 carbonylation peptide and the unmodified wild type tryptic peptide, we observed a mass shift of +113 Da that started at the y11 ion (but not at the y10 ion). The unique mass shifts allowed an unambiguous assignment of carbonylation on HC T28. On the extracted ion chromatograms (Figure 8), the HC T28

carbonylation product was separated into four peaks. As previously explained, the four peaks likely came from the four stereoisomers introduced after GRT derivatization and sodium borohydride reduction. Importantly, the relative level of HC T28 carbonylation did not change significantly in buffers A, B, and C, over the time course of stirring (Table 2). By contrast, the relative level of HC T28 carbonylation decreased by more than 50% in buffer D (Figure 8 and Table 2). Furthermore, for buffer D, the decrease in the relative level of HC T28 carbonylation followed a similar pattern to that observed in the overall mAb A carbonylation level (Figure 4D). Interestingly, the same pattern was observed for all type 2 carbonylation products: a larger decrease occurred during the first day of stirring than during the second and the third days of stirring. These observations suggest that type 2 carbonylation products likely contributed to the increased mAb A precipitation/aggregation in buffer D.

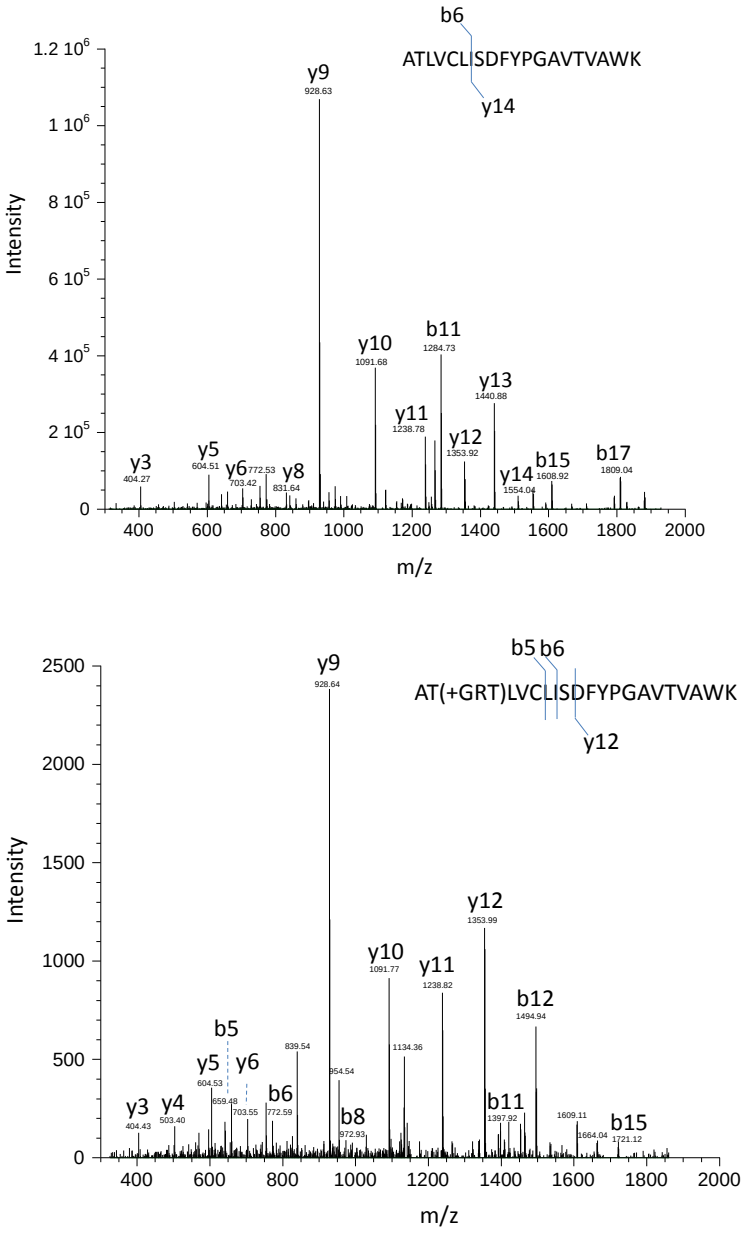

Figure 5. MS^2 spectra a GRT-derivatized carbonylation (LC T132) peptide and the corresponding wide type peptide, with assignment of the fragment ions.

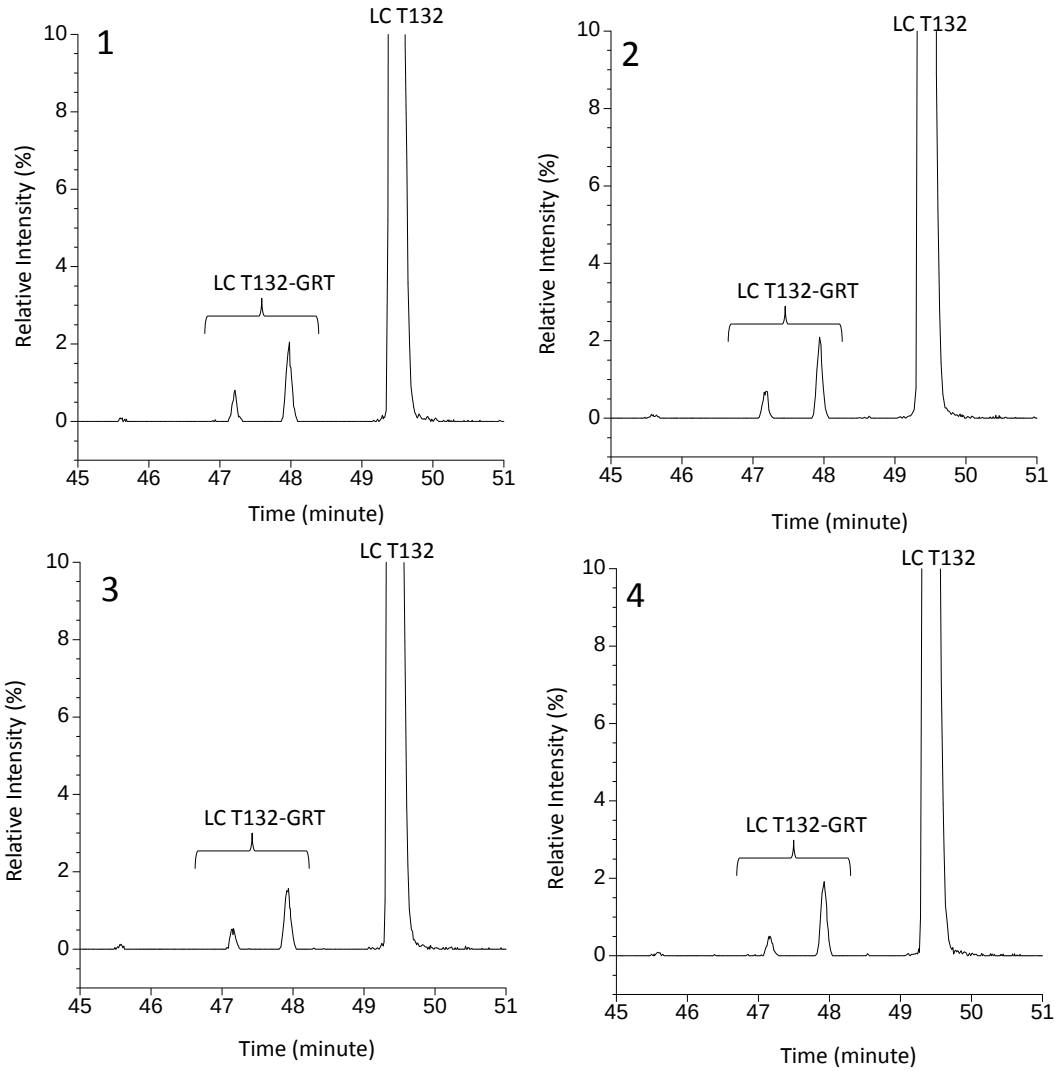

Figure 6. Extracted ion chromatograms of the GRT-derivatized carbonylation (LC T132) peptide and the corresponding wide type peptide in mAb A samples: (1) T0 (control); (2) the supernatant after 3 days of stirring in buffer A; (3) the supernatant after 1 day of stirring in buffer D; (4) the supernatant after 3 days of stirring in buffer D.

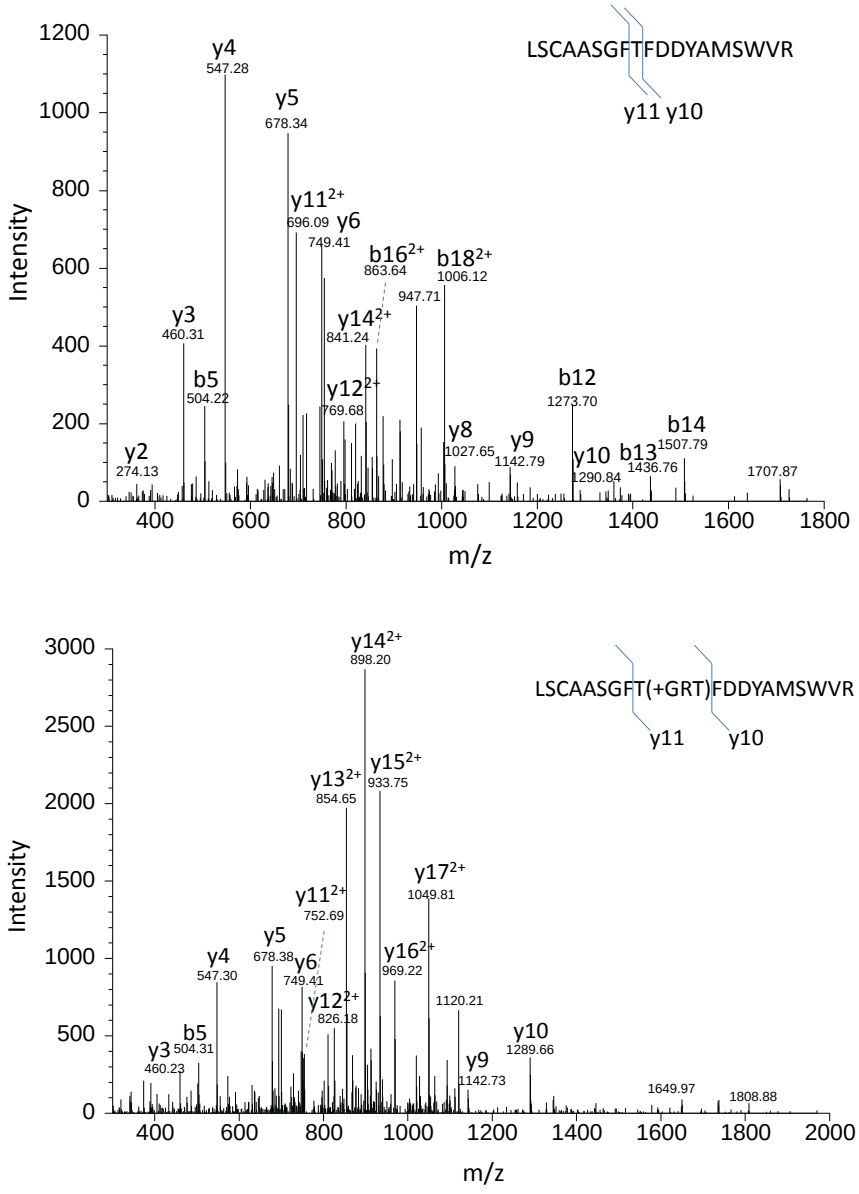

Figure 7. MS^2 spectra a GRT-derivatized carbonylation (HC T28) peptide and the corresponding wide type peptide, with assignment of the fragment ions.

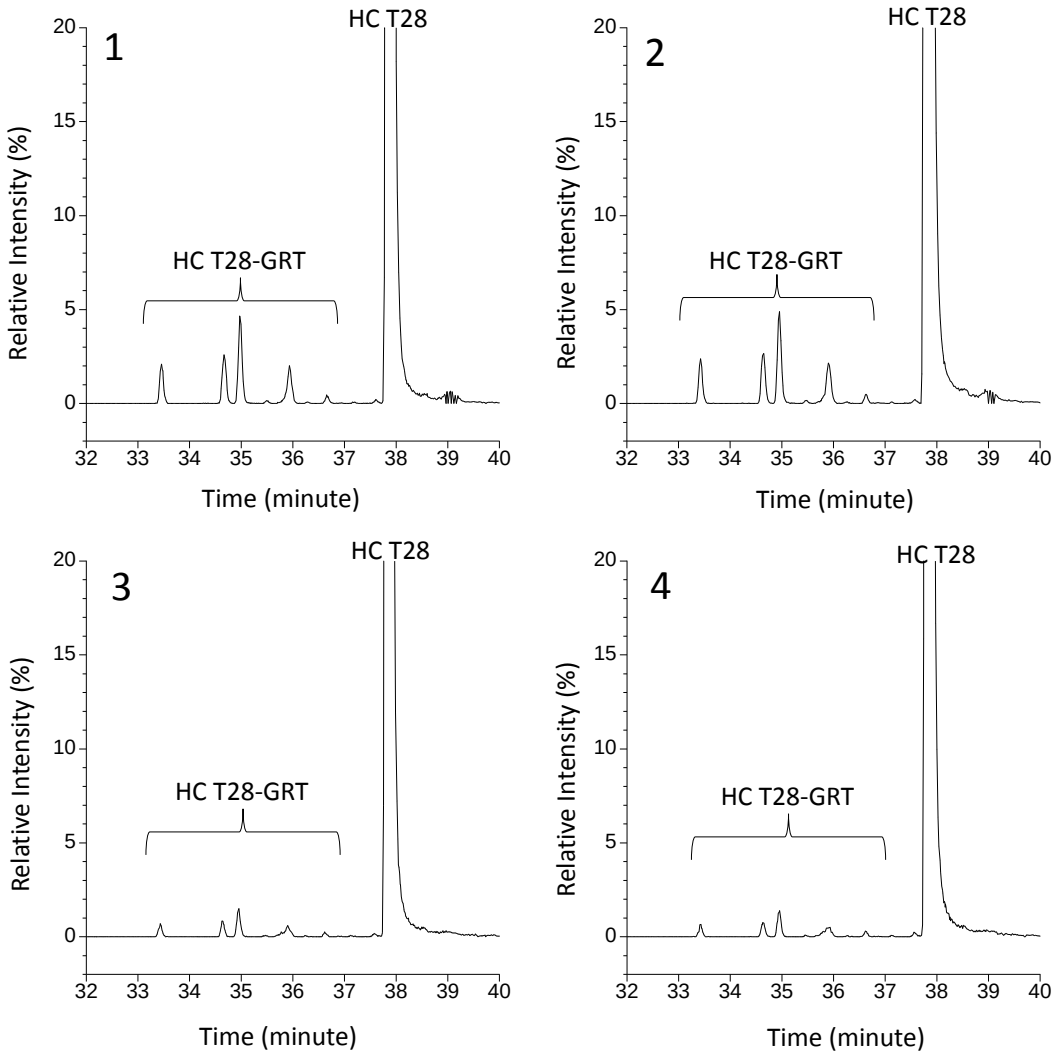

Figure 8. Extracted ion chromatograms of the GRT-derivatized carbonylation (HC T28) peptide and the corresponding wide type peptide in mAb A samples: (1) T0 (control); (2) the supernatant after 3 days of stirring in buffer A; (3) the supernatant after 1 day of stirring in buffer D; (4) the supernatant after 3 days of stirring in buffer D.

An example of type 3 carbonylation product was HC R13 carbonylation. Identification of this product was described previously in Chapter 3. The extracted ion chromatograms showed that the relative level of HC R13 carbonylation was only 0.2% at T0 (Table 2). Nevertheless, the level of HC R13 carbonylation consistently decreased in the supernatants for all buffers over the time course of stirring (Figure 9 and Table 2). A small RSD (=0.0%) was observed with three independent analyses of all the samples, which supports that the decrease was not due to assay error. Since type 1 and type 2 carbonylation products did not decrease significantly in the supernatants for buffers A, B, and C, type 3 carbonylation products may be responsible for the decrease observed in the overall mAb A carbonylation level for buffers A, B, and C. Additionally, compared to type 1 and type 2 carbonylation products, type 3 carbonylation products are least abundant. Only two products were identified, and their levels were at 0.3% or lower. The low abundance of type 3 products is consistent with the relatively small decrease (i.e., a decrease of ~1.5 nmol/mg from 16.5 nmo/mg) in the overall mAb A carbonylation level for buffers A, B, and C.

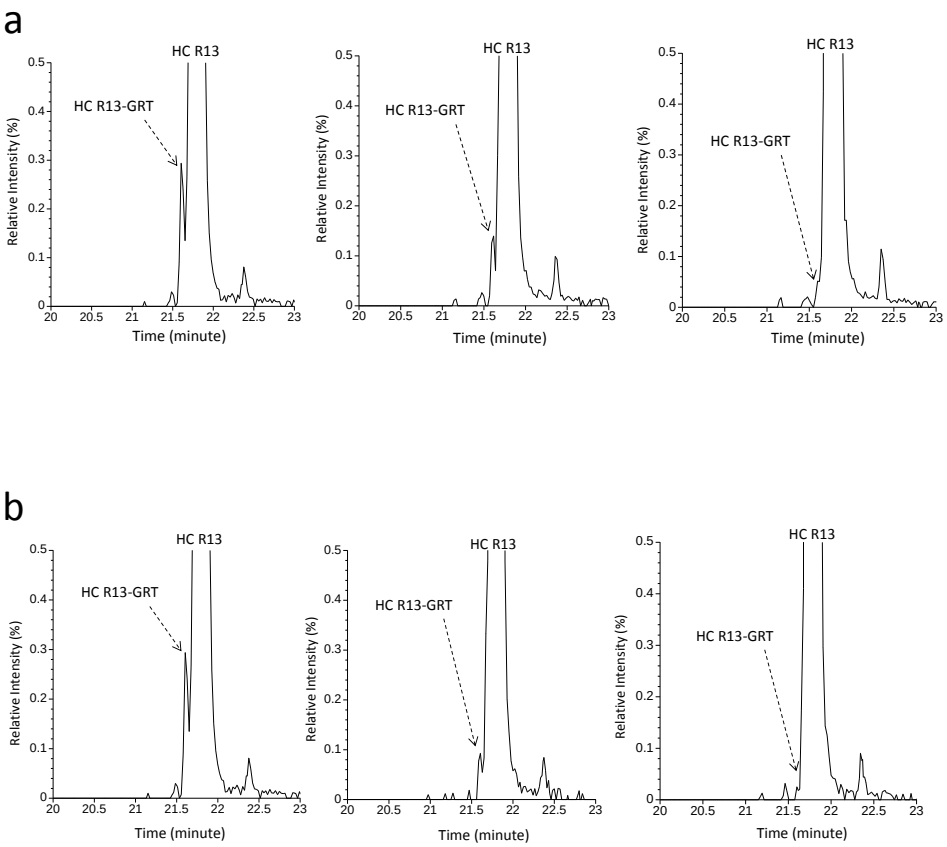

Figure 9. Extracted ion chromatograms of the GRT-derivatized carbonylation (HC R13) peptide and the corresponding wide type peptide in mAb A samples: (a) T0 (control), the supernatant after 1 day, and after 3 days of stirring in buffer A; (b) T0 (control), the supernatant after 1 day, and after 3 days of stirring in buffer D.

Characterization of Additional Degradation Products in mAb A Supernatants

It is worth noting that a decrease in mAb A carbonylation content in the supernatants may be due to enrichment of the carbonylation products in the precipitates or due to further degradation of the carbonylation products in the supernatants. For example, aldehydes (from oxidative carbonylation of Lys, Arg, and Pro residues) may react with primary amines to form Schiff bases or may be further oxidized to form carboxylic acids. To better define the effect of site-specific carbonylation on the formation of precipitates/insoluble aggregates, it is necessary to characterize these further-degraded carbonylation products in mAb A supernatants. For Schiff base products, the reactions between aldehydes and primary amines are reversible. During the peptide mapping analysis, the Schiff base products are expected to be converted to hydrazides by GRT derivatization. This is based on a consideration that the GRT derivatization reaction (while also reversible) effectively competes with the Schiff base formation reaction since the hydrazide is more stable than a Schiff base.[35] In addition, excess GRT reagent (with a GRT-to-mAb molar ratio of 8000:1) is present during the derivatization reaction, which is expected to further drive the dissociation of the Schiff base products. While it may still be necessary to confirm that Schiff base products were indeed converted to hydrazides during the peptide mapping analysis, in this study, we focused on the carboxylic acid products, which are stable during peptide mapping analysis. As shown in Table 4, two carboxylic acid products (HC R13E and LC P7E) were identified, whose levels were less than 0.1% in all the supernatant samples. These data showed that formation of carboxylic acid products is not a major pathway for the decrease of aldehyde products during the time course of stirring. Therefore, the observed decrease of aldehyde products in the supernatants is more likely due to the enrichment of these aldehyde products in the precipitates.

Besides oxidative carbonylation products, metal-catalyzed oxidation can generate other oxidation products, such as methionine sulfoxide or hydroxytryptophan.[22] To understand if the enrichment of carbonylation products in the precipitates may be due to co-precipitation with these additional oxidation products, we further characterized methionine, tryptophan, and histidine oxidation products in mAb A supernatants. As shown in Table 5, we identified four methionine oxidation products, eight tryptophan oxidation products, and two histidine oxidation products. These oxidation products behaved similarly to type 1 or type 3 carbonylation products (Tables 5 and 6). There are no type 2 Met/Trp/His oxidation products. Interestingly, the type 3 Met/Trp/His oxidation products are not located in close vicinity to the type 3 carbonylation product (HC R13) on mAb A. This distribution pattern suggests that the enrichment of carbonylation products in the precipitates was not due to co-precipitation with Met, Trp, or His oxidation products. It should also be noted that four oxidation products (on HC W47, HC W106, HC W317, and HC H228) increased slightly in the supernatants. The increase may be caused by a low degree of oxidation during the stirring experiment or enrichment of these oxidation products in the supernatants.

Carbonylation Degradation Products		Buffer A		Buffer B		Buffer C		Buffer D	
	T0	1 day	3 days	1 day	3 days	1 day	3 days	1 day	3 days
HC R13E	0.0±0.0%	0.0±0.0%	0.0±0.0%	0.0±0.0%	0.0±0.0%	0.0±0.0%	0.0±0.0%	0.0±0.0%	0.0±0.0%
LC P7E	0.0±0.0%	0.0±0.0%	0.0±0.0%	0.0±0.0%	0.0±0.0%	0.0±0.0%	0.0±0.0%	0.0±0.0%	0.0±0.0%

Table 4. Relative levels (mean ± standard deviation) of the further degradation products (aldehyde-to-carboxylic acid) in mAb A control and supernatants (determined by extracted ion chromatograms). The mean and standard deviation were obtained from three independent measurements.

Oxidation Site		Buffer A		Buffer B		Buffer C		Buffer D	
	T0	1 day	3 days	1 day	3 days	1 day	3 days	1 day	3 days
HC M256 (+16)	46.6±2.0%	46.8±1.4%	45.2±1.1%	45.5±2.8%	42.3±3.2%	44.9±1.3%	45.0±0.6%	43.5±2.0%	42.4±0.5%
HC M432 (+16)	26.2±1.3%	25.3±0.3%	24.8±0.7%	25.2±0.6%	21.8±1.1%	24.2±2.1%	24.9±1.0%	26.0±0.9%	22.0±2.2%
HC M83 (+16)	3.2±0.4%	2.7±0.6%	2.6±0.5%	2.4±0.5%	1.8±0.3%	2.2±0.3%	2.2±0.4%	1.9±0.6%	1.9±0.8%
HC M34 (+16)	61.3±3.4%	60.6±4.8%	60.8±3.4%	56.6±4.0%	54.0±2.5%	56.8±3.7%	55.7±3.6%	53.0±6.0%	53.7±6.4%
LC W149 (+4)	0.3±0.2%	0.1±0.0%	0.2±0.2%	0.2±0.1%	0.2±0.1%	0.2±0.1%	0.1±0.1%	0.2±0.1%	0.1±0.1%
LC W149 (+16)	1.4±0.4%	1.5±0.3%	1.7±0.1%	1.5±0.5%	1.5±0.5%	1.6±0.4%	1.4±0.5%	1.4±0.4%	1.3±0.4%
HC W47 (+16)	15.2±0.4%	16.2±0.3%	18.2±0.6%	16.2±0.2%	18.9±1.0%	15.5±0.2%	17.8±0.2%	18.9±0.3%	20.7±0.5%
HC W281 (+16)	1.6±0.1%	1.8±0.1%	1.5±0.1%	1.7±0.1%	1.7±0.1%	1.7±0.1%	1.6±0.1%	1.8±0.1%	1.7±0.1%
HC W106 (+16)	2.9±0.2%	3.3±0.2%	3.6±0.3%	3.1±0.3%	3.0±0.3%	3.0±0.3%	3.6±0.3%	3.0±0.2%	3.4±0.4%
LC W186 (+16)	1.3±0.1%	1.3±0.1%	1.2±0.1%	1.2±0.1%	1.4±0.1%	1.3±0.1%	1.2±0.1%	1.4±0.2%	1.4±0.1%
HC W317 (+16)	1.6±0.0%	2.0±0.1%	1.7±0.1%	2.0±0.1%	1.7±0.1%	2.0±0.1%	1.7±0.1%	2.1±0.1%	1.9±0.1%
HC W421 (+16)	68.4±3.4%	67.1±0.7%	66.4±0.8%	67.7±0.9%	63.3±1.3%	66.3±2.0%	66.3±0.6%	67.5±1.8%	63.1±3.6%
HC H272 (+16)	1.1±0.1%	1.1±0.1%	1.0±0.1%	1.0±0.1%	1.0±0.0%	1.1±0.0%	1.0±0.1%	0.9±0.0%	0.9±0.1%
HC H228 (+16)	2.6±0.1%	3.0±0.2%	2.9±0.3%	3.1±0.2%	2.8±0.3%	3.1±0.2%	2.8±0.2%	2.4±0.3%	2.5±0.2%

Table 5. Relative levels (mean ± standard deviation) of site-specific methionine, tryptophan, and histidine oxidation products in mAb A control and supernatants (determined by extracted ion chromatograms). The standard deviation was obtained from three independent measurements.

Oxidation Site	Type	Location
HC M256 (+16)	3	CH2
HC M432 (+16)	3	CH3
HC M83 (+16)	3	VH
HC M34 (+16)	3	VH
LC W149 (+4)	3	CL
LC W149 (+16)	1	CL
HC W47 (+16)	1’	VH
HC W281(+16)	1	CH2
HC W106 (+16)	1’	CL
LC W186 (+16)	1	CL
HC W317 (+16)	1’	CH2
HC W421 (+16)	3	CH3
HC H272 (+16)	1	CH2
HC H228 (+16)	1’	Hinge

Table 6. The type and location of identified methionine, tryptophan, and histidine oxidation products on the stressed mAb A. Over the time course of stirring, the product that did not show any significant decrease in the supernatants is assigned as Type 1; the product that showed decreased levels in supernatants with buffer D but not with the other buffers is assigned as Type 2 (not present in this table); the product that showed decreased levels in supernatants with all four buffers is assigned as Type 3; the product that showed increased levels in the supernatants is assigned as Type 1’.

Finally, as shown in Figures 10 and 11, we visually compared the total ion chromatograms of the digested supernatant samples from buffer D at different time points (T0, 1 day, and 3 days). Interestingly, several peaks increased over the time course of stirring. The two peaks eluted at 17.8 and 19.0 minutes are singly charged ions with m/z of 460.3112 and 504.3378, respectively. The identity of these two peaks are yet to be determined, since their MS data did not match any apparent mAb A peptides. The peak at 27.3 minutes is a doubly charged ion with m/z of 1146.1169, which came from a K/P miscleavage by trypsin. Aside from these three peaks, we did not identify any additional peptide peaks that decreased significantly during the time course of stirring.

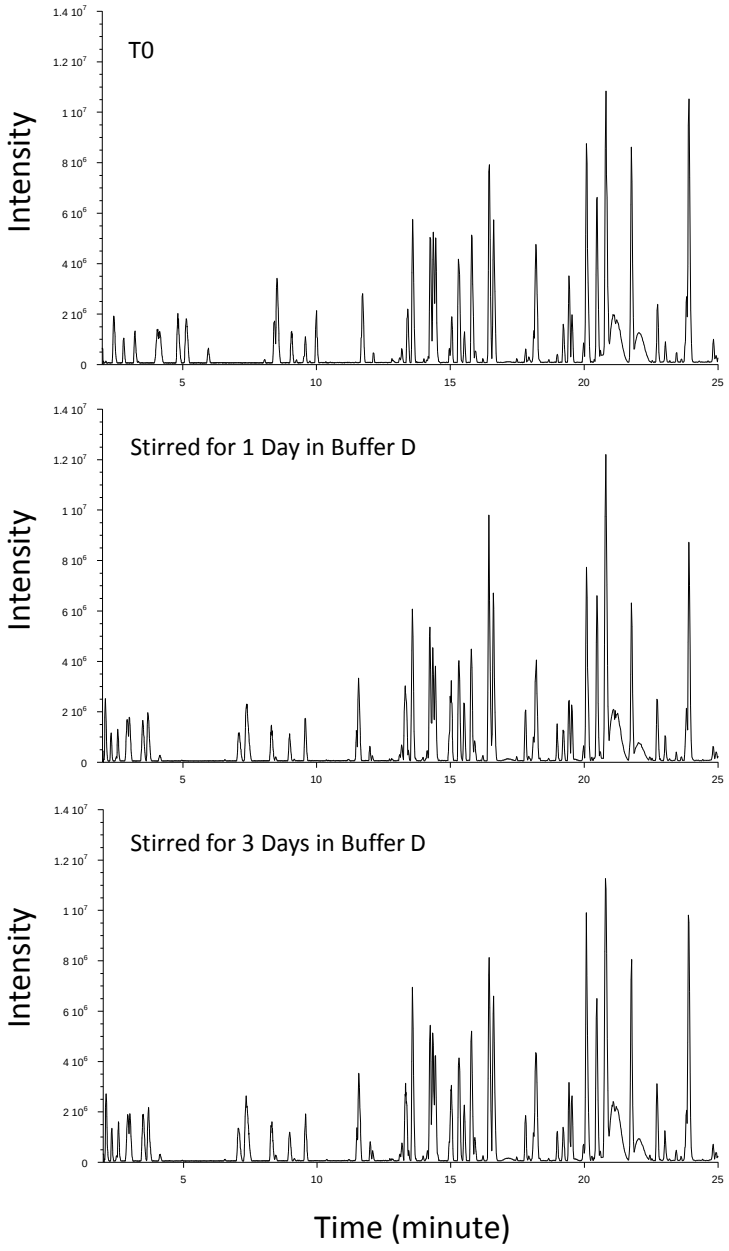

Figure 10. The total ion chromatograms of the tryptic peptide maps of the stressed mAb A samples (0-25 minutes): control (T0), the supernatant after 1 day of stirring in buffer D, and the supernatant after 3 days of stirring in buffer D.

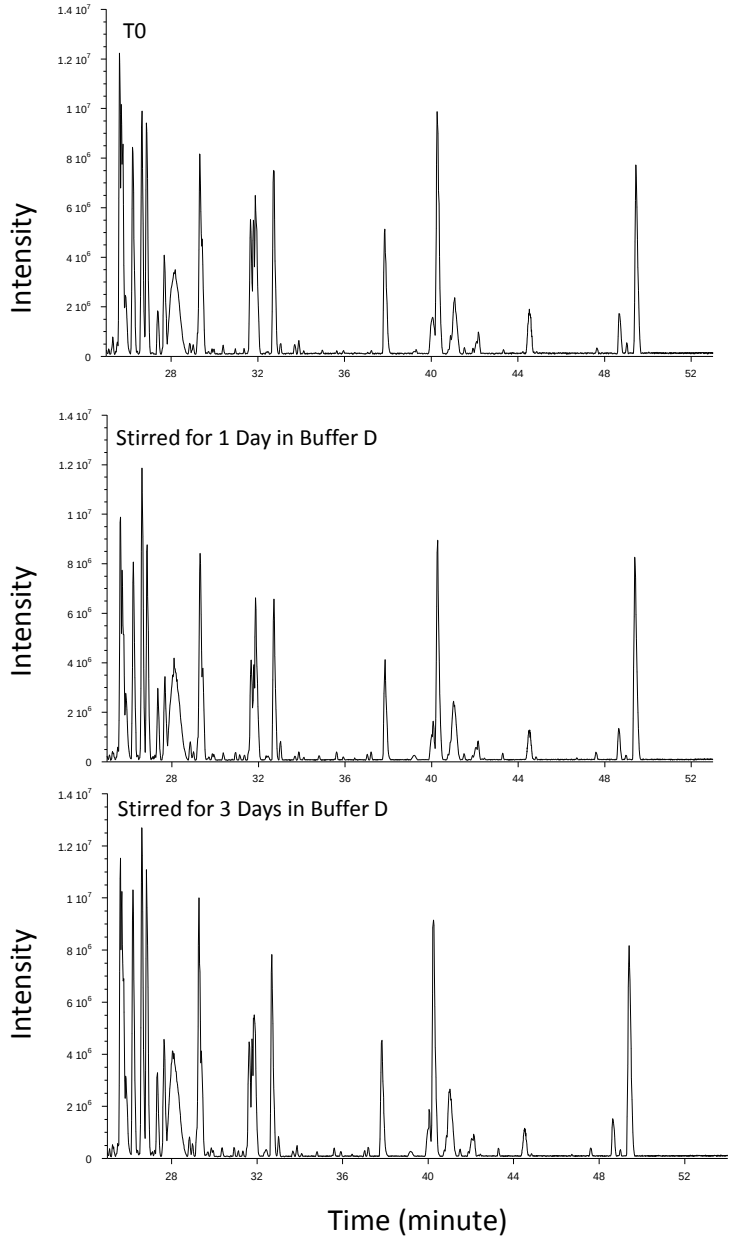

Figure 11. The total ion chromatograms of the tryptic peptide maps of the stressed mAb A samples (25-52 minutes): control (T0), the supernatant after 1 day of stirring in buffer D, and the supernatant after 3 days of stirring in buffer D.

DSC Analysis

DSC analysis was performed to understand the effects of buffer type and oxidation status on the thermal stability of mAb A, which could provide additional explanations for the formation of precipitates/insoluble aggregates and help us better interpret the effects of oxidative carbonylation. As shown in Figure 12, three thermal transitions were observed in the DSC thermograms, which likely correspond to transitions in the Fab, CH2, and CH3 domains, as seen in typical DSC thermograms of IgG1 antibodies.[36-37]

For the unstressed mAb A, as the buffer type changed from A to D, the Fab transition/denaturation shifted to lower temperatures in an order of A>B>C>D, where the lowest transition temperature was observed with buffer D. This observation shows that buffer type has a significant impact on the thermal stability of Fab, where Fab is least stable in buffer D. For CH2 and CH3, the effect of buffer type appeared to be less prominent. Only minor differences were observed in the DSC thermograms: in buffers B, C, and D, the CH2 and CH3 peaks appeared to merge with each other, while in buffer A the two peaks were resolved on the thermogram.

For the stressed mAb A, as the buffer type changed from A to D, the Fab transition/denaturation shifted in the same order as that for the unstressed mAb A. Interestingly, for each buffer, very little difference was observed in the Fab transition temperature between the unstressed and the stressed mAb A, which showed that the oxidation status has very little impact on Fab transition/denaturation temperature. On the other hand, for each buffer, Fab had a lower heat capacity (Cp) value for the stressed mAb A than for the unstressed mAb A, which indicates that the Fab domain became less ordered or structured after metal-catalyzed oxidation.[38] For CH2 and CH3, the DSC thermogram of the stressed mAb A was very similar to the respective

DSC thermogram of the unstressed mAb A. This observation indicates that the thermal stability of CH2 and CH3 was not significantly impacted by buffer type or oxidation status.

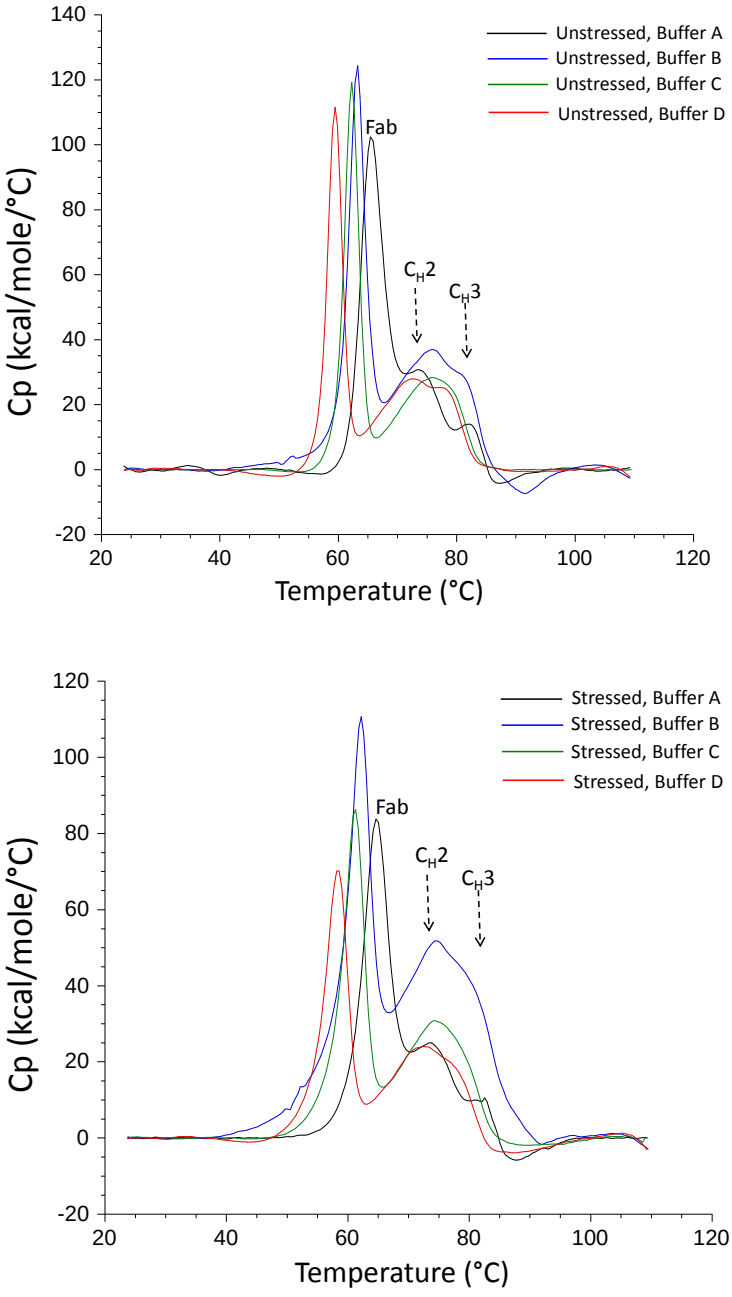

Figure 12. The DSC thermograms of unstressed and stressed mAb A in buffer A, B, C, and D.

DISCUSSION

This study applied stir stress, a model stress condition, to investigate the effect of oxidative carbonylation on the physical stability of a recombinant monoclonal antibody. The stir stress condition used in the study was largely the same as the condition used by Joubert et al.[9] and Telikepalli et al.[11] This stir stress condition is considered a harsher condition than many other stress conditions,[11] as the stir stress generates large amounts of insoluble antibody aggregates within days. For our investigation, the formation of large amounts of aggregates is beneficial in that it could help differentiate subtle changes in the effects induced by the various intrinsic and extrinsic factors. The relatively short stress time is also beneficial in that it helps to minimize the formation of other degradation products (such as deamidation) during stress studies, as degradation products concurrently generated during the study may complicate our investigation.

This study applied metal-catalyzed oxidation to generate a test sample with a moderately high level of oxidative carbonylation (approximately five times the reported normal level of plasma protein carbonylation[39]). Due to the complex nature of metal-catalyzed oxidation reactions,[22] various factors, including oxidative carbonylation, could impact mAb stability profiles. To distinguish the effect of oxidative carbonylation from those of other factors, in this study, we investigated the formation of mAb A precipitates/insoluble aggregates from multiple perspectives, with a focus on elucidating the role of oxidative carbonylation in the various mechanisms.

Taking into consideration several possible aggregation mechanisms, this study first evaluated intrinsic aggregation factors of mAb A by including the unstressed mAb A as the control, which is important for a more accurate characterization of the effect of oxidative

carbonylation. After the first day of stirring, for each buffer, there was essentially no difference in the relative amount of soluble mAb A between the unstressed and stressed mAb A samples. Clearly, it was the intrinsic aggregation factors but not oxidation-related changes that significantly contributed to the formation of precipitates/insoluble aggregates during the first day of stirring. By contrast, the effect of oxidation-related changes (including oxidative carbonylation) only became evident after additional days of stirring. This observation suggests that the effects of oxidation-related changes are not as fast-acting as those of intrinsic factors on the formation of precipitates/insoluble aggregates. This study then evaluated if the enrichment of certain carbonylation products in the precipitates may be a result of co-precipitation with other oxidation products on mAb A, based on a consideration that these oxidation products may be in close proximity with each other. By surveying a large variety of oxidation products during site-specific peptide mapping, this study showed that co-precipitation was unlikely a major mechanism, which helped establishing a direct link between oxidative carbonylation and formation of precipitates/insoluble aggregates. Finally, this study evaluated thermal stability of mAb A samples by DSC analysis. The analysis indicated that metal-catalyzed oxidation caused mAb A to become less ordered or structured than the unstressed mAb A, although the denaturation temperatures for Fab, CH2, and CH3 did not change significantly. Given that the DSC data did not rule out an effect of higher order structure on the formation of precipitates/insoluble aggregates, the effect of oxidative carbonylation could be confounded by various structural factors.

When comparing the protein carbonylation levels with the corresponding soluble mAb A levels, we observed an apparent lag between the enrichment of carbonylation products and the formation of precipitates (reflected by the relative level of soluble mAb A). As shown in Figure

4, the enrichment of carbonylation products occurred primarily within the first day of stirring. However, after the first day of stirring, very little difference in the relative level of soluble mAb A was observed between the stressed and the unstressed mAb A (Figure 1). While significant differences in the relative amount of soluble mAb A were subsequently observed between the stressed and the unstressed mAb A after additional days of stirring, the carbonylation levels either remained unchanged (presumably reached an equilibrium) or changed slightly. One explanation for the apparent lag is that other changes induced by meta-catalyzed oxidation, but not oxidative carbonylation, were responsible for the subsequently increased accumulation of precipitates (from day 1 to day 3). Another explanation is that carbonyl-containing aggregates formed during the first day of stirring may act as nuclei that drive faster formation of larger aggregates, which leads to the subsequently increased accumulation of precipitates. In either scenario, the direct effect of oxidative carbonylation on the formation of precipitates appeared to be limited. It is also interesting to note that majority of the carbonylation content (ranging from 75 to 90%) remained in the supernatants throughout the time course of stirring (Figure 4). Based on this indirect measurement, we deduce that only a small portion of the carbonylation products was preferentially enriched in the precipitates.

For the carbonylation products that demonstrated preferential enrichment in the precipitates, only one arginine carbonylation product (HC R13) can be categorized as aggregation-prone carbonylation product, given that only this carbonylation product was consistently enriched in the precipitates in all four buffers. This arginine carbonylation site is not in the conserved sequence of mAb A, which suggests that there may not be a common aggregation-prone carbonylation site on IgG1 mAbs. Seven carbonylation products, all from threonine residues, demonstrated preferential enrichment in the precipitates with buffer D but not

with buffers A, B, or C. Clearly, the iodide ion present in buffer D has a large impact on the effect of these type 2 carbonylation products. It should also be pointed out that this study did not survey all possible oxidation products from metal-catalyzed oxidation. It is likely that these other oxidation products, in particular, di-Tyr, Tyr-Trp, or di-Trp crosslinks that form covalent dimers,[40] may co-precipitate with adjacent carbonylation products. In the future, these potential crosslink products will need to be investigated by mass spectrometry and fluorescence spectroscopy, which could further distinguish the roles/effects of oxidative carbonylation from other chemical modifications on mAb aggregation.

In the anionic Hofmeister series, iodide ion ranks lower than chloride and sulfate ions based on their ability to "salt out" negatively charged proteins.[32] For positively charged proteins, the order is usually reversed, where iodide ion has a stronger "salt out" effect than chloride and sulfate ions (as is the case in this study).[33] The mechanism for the Hofmeister effect has not been fully understood yet.[29, 33] Nevertheless, it is generally believed that specific ion interaction/pairing with positively charged side chains or hydrophilic regions on protein surfaces may explain the reversed Hofmeister effect.[29, 32-33] Considering that the threonine carbonylation product is neutral in charge and is more hydrophobic than threonine, and that the formation of the threonine carbonylation product (2-Amino-3-Ketobutyric Acid, Figure 13) removes a potential hydrogen bond donor, it is unlikely that the reversed Hofmeister effect observed in this study came from interactions between Hofmeister ions and threonine carbonylation product. We hypothesiz that positively charged residues adjacent to the threonine carbonylation sites may be involved in the aggregation characteristics of the type 2 threonine carbonylation products, where these positively charged residues could have specific ion interactions with the Hofmeister ions. We further hypothesize that the local surface areas near these positively charged residues could

be less prone to aggregation due to electrostatic repulsion from the positively charged residues. For the three Hofmeister ions evaluated in this study, iodide ion could have a stronger interaction with these positively charged residues than chloride and sulfate ions, which could result in more effective shielding of these adjacent positive charges. Consequently, the reduced electrostatic repulsion would allow the threonine carbonylation product to participate in the aggregation process (due to hydrophobic interactions and/or reduced hydrogen-bonding), which may lead to the observed preferential enrichment of type 2 carbonylation products.

To evaluate the proposed hypothesis, we investigated the presence of positively charged residues near type 2 carbonylation products. Using a model IgG structure (1HZH), we examined the two carbonylation sites, HC T115 and HC T139, that are located in the conserved regions of mAb A. As shown in Figure 14, we found two lysine residues (HC K113 and HC K209) near HC T115, and one lysine residue (HC K137) near HC T139. The presence of positively charged residues near the type 2 carbonylation products is consistent with our proposed hypothesis. However, a mutagenesis study (on the adjacent lysine residues) will be needed in the future to confirm this hypothesis. It should also be pointed out that the presence of positively charged residues does not necessarily lead to preferential enrichment of an adjacent carbonylation product. For example, LC T132 is a type 1 carbonylation product, even though an adjacent lysine, LC K130, is present. It is possible that additional factors, such as orientation of the positive charge, steric constrains, and local flexibility, can also influence the aggregation propensity of carbonylation products.

The DSC analysis results of the stressed and unstressed mAb A showed that metal-catalyzed oxidation did not introduce significant structural changes in mAb A. The DSC results are consistent with the H/D exchange analysis results from our previous study in Chapter 3. On

the other hand, the DSC analysis results showed that the Hofmeiser ions did affect thermal or conformational stability of mAb A. This effect is consistent with existing literature reports.[41-43] A study by Majumdar et. al found that chloride ion decreased local flexibility in VL, CH1, and CH3 domains; sulfate ion increased local flexibility in CH1 and VL domains; thiocyanate ion increased local flexibility in the CH2 domain of an IgG1 antibody.[41] For our study, it will be interesting to understand in the future how chloride, sulfate, and iodide ions change the local flexibility of mAb A, which can provide additional explanations for the effects of carbonylation products.

In summary, this study demonstrated that the effect of oxidative carbonylation on the physical stability of mAbs is much more complicated than suggested in the existing literature.[25-27] Using a model IgG1 mAb, this study showed that the effect of oxidative carbonylation on the physical stability of mAbs can be site- and buffer-specific, which has not been previously reported. For example, using molecular dynamics simulations, Petrov and Zagrovic reported that lysine and arginine carbonylation significantly increases protein aggregation propensity via hydrophobic effects.[27] However, their study did not evaluate any buffer effect. In addition, their study did not reveal any site-specific effects for lysine and arginine carbonylation, while our study showed that not all lysine and arginine carbonylation products contribute to the formation of mAb aggregates. Similarly, in several reported mAb stability case studies,[25-26, 30] no site-specific carbonylation information was provided. Notably, this study revealed the effect of threonine carbonylation products, which has not been pointed out in the literature. To explain the buffer-dependent aggregation of type 2 carbonylation products, we provided several new potential mechanisms, which should be tested further in future investigations. Finally, this study provides new aspects of product quality evaluation of oxidative carbonylation, which can help to

identify critical carbonylation products and the development of future mAb candidates with improved physical stability.

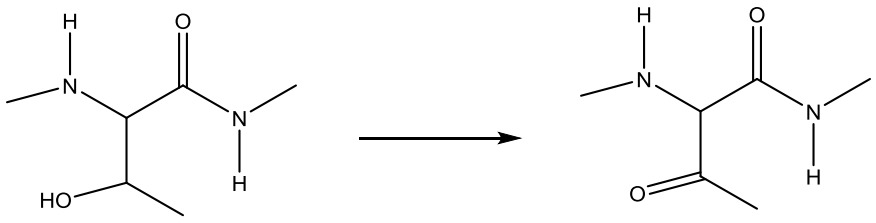

Figure 13. Threonine residue and its carbonylation product (2-Amino-3-Ketobutyric Acid)

A

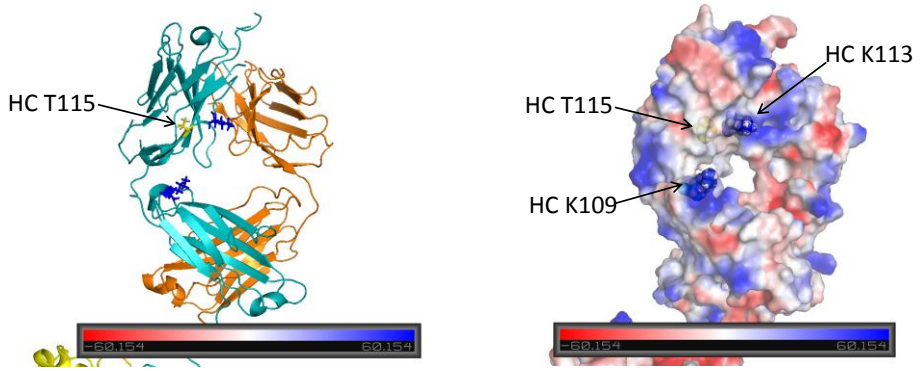

B

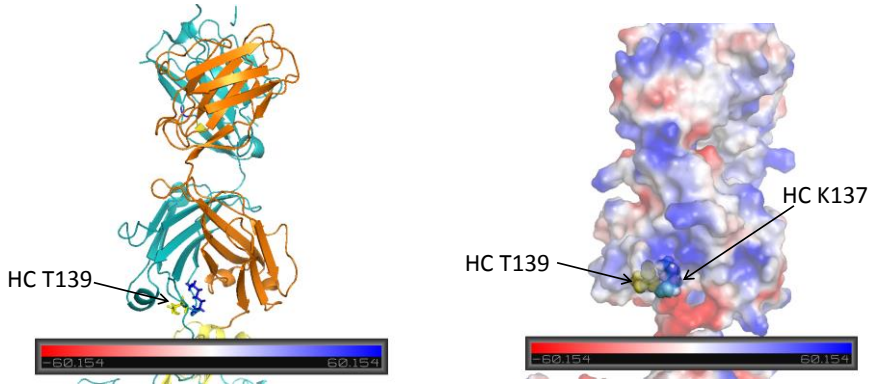

Figure 14. (A) Location of HC T115 (left) on an IgG1(PDB:1HZH) and electrostatic potential (red area: negatively charged; blue area: positively charged) distribution on the surface (right). (B) Location of HC T139 (left) on an IgG1(PDB:1HZH) and electrostatic potential (red area: negatively charged; blue area: positively charged) distribution on the surface (right).

Reference

1. Wang, W.; Singh, S.; Zeng, D. L.; King, K.; Nema, S., Antibody structure, instability, and formulation. *J Pharm Sci* **2007,** *96* (1), 1-26.

2. van der Kant, R.; Karow-Zwick, A. R.; Van Durme, J.; Blech, M.; Gallardo, R.; Seeliger, D.; Assfalg, K.; Baatsen, P.; Compernolle, G.; Gils, A.; Studts, J. M.; Schulz, P.; Garidel, P.; Schymkowitz, J.; Rousseau, F., Prediction and Reduction of the Aggregation of Monoclonal Antibodies. *J Mol Biol* **2017,** *429* (8), 1244-1261.

3. Obrezanova, O.; Arnell, A.; de la Cuesta, R. G.; Berthelot, M. E.; Gallagher, T. R.; Zurdo, J.; Stallwood, Y., Aggregation risk prediction for antibodies and its application to biotherapeutic development. *MAbs* **2015,** *7* (2), 352-63.

4. Filipe, V.; Jiskoot, W.; Basmeleh, A. H.; Halim, A.; Schellekens, H.; Brinks, V., Immunogenicity of different stressed IgG monoclonal antibody formulations in immune tolerant transgenic mice. *MAbs* **2012,** *4* (6), 740-52.

5. Moussa, E. M.; Panchal, J. P.; Moorthy, B. S.; Blum, J. S.; Joubert, M. K.; Narhi, L. O.; Topp, E. M., Immunogenicity of Therapeutic Protein Aggregates. *J Pharm Sci* **2016,** *105* (2), 417-430.

6. Joubert, M. K.; Hokom, M.; Eakin, C.; Zhou, L.; Deshpande, M.; Baker, M. P.; Goletz, T. J.; Kerwin, B. A.; Chirmule, N.; Narhi, L. O.; Jawa, V., Highly aggregated antibody therapeutics can enhance the in vitro innate and late-stage T-cell immune responses. *J Biol Chem* **2012,** *287* (30), 25266-79.

7. Rombach-Riegraf, V.; Karle, A. C.; Wolf, B.; Sorde, L.; Koepke, S.; Gottlieb, S.; Krieg, J.; Djidja, M. C.; Baban, A.; Spindeldreher, S.; Koulov, A. V.; Kiessling, A., Aggregation of human recombinant monoclonal antibodies influences the capacity of dendritic cells to stimulate adaptive T-cell responses in vitro. *PLoS One* **2014,** *9* (1), e86322.

8. Boll, B.; Bessa, J.; Folzer, E.; Rios Quiroz, A.; Schmidt, R.; Bulau, P.; Finkler, C.; Mahler, H. C.; Huwyler, J.; Iglesias, A.; Koulov, A. V., Extensive Chemical Modifications in the Primary Protein Structure of IgG1 Subvisible Particles Are Necessary for Breaking Immune Tolerance. *Mol Pharm* **2017,** *14* (4), 1292-1299.

9. Joubert, M. K.; Luo, Q.; Nashed-Samuel, Y.; Wypych, J.; Narhi, L. O., Classification and characterization of therapeutic antibody aggregates. *J Biol Chem* **2011,** *286* (28), 25118-33.

10. Luo, Q.; Joubert, M. K.; Stevenson, R.; Ketchem, R. R.; Narhi, L. O.; Wypych, J., Chemical modifications in therapeutic protein aggregates generated under different stress conditions. *J Biol Chem* **2011,** *286* (28), 25134-44.

11. Telikepalli, S. N.; Kumru, O. S.; Kalonia, C.; Esfandiary, R.; Joshi, S. B.; Middaugh, C. R.; Volkin, D. B., Structural characterization of IgG1 mAb aggregates and particles generated under various stress conditions. *J Pharm Sci* **2014,** *103* (3), 796-809.

12. Kijanka, G.; Bee, J. S.; Korman, S. A.; Wu, Y.; Roskos, L. K.; Schenerman, M. A.; Slutter, B.; Jiskoot, W., Submicron Size Particles of a Murine Monoclonal Antibody Are More Immunogenic Than Soluble Oligomers or Micron Size Particles Upon Subcutaneous Administration in Mice. *J Pharm Sci* **2018,** *107* (11), 2847-2859.

13. Roberts, C. J., Therapeutic protein aggregation: mechanisms, design, and control. *Trends Biotechnol* **2014,** *32* (7), 372-80.

14. Wang, W., Protein aggregation and its inhibition in biopharmaceutics. *Int J Pharm* **2005,** *289* (1-2), 1-30.

15. Perchiacca, J. M.; Tessier, P. M., Engineering aggregation-resistant antibodies. *Annu Rev Chem Biomol Eng* **2012,** *3*, 263-86.

16. Wang, X.; Singh, S. K.; Kumar, S., Potential aggregation-prone regions in complementarity-determining regions of antibodies and their contribution towards antigen recognition: a computational analysis. *Pharm Res* **2010,** *27* (8), 1512-29.

17. Wang, X.; Das, T. K.; Singh, S. K.; Kumar, S., Potential aggregation prone regions in biotherapeutics: A survey of commercial monoclonal antibodies. *MAbs* **2009,** *1* (3), 254-67.

18. Perchiacca, J. M.; Ladiwala, A. R.; Bhattacharya, M.; Tessier, P. M., Aggregation-resistant domain antibodies engineered with charged mutations near the edges of the complementarity-determining regions. *Protein Eng Des Sel* **2012,** *25* (10), 591-601.

19. Shire, S. J., Formulation and manufacturability of biologics. *Curr Opin Biotechnol* **2009,** *20* (6), 708-14.

20. Fesinmeyer, R. M.; Hogan, S.; Saluja, A.; Brych, S. R.; Kras, E.; Narhi, L. O.; Brems, D. N.; Gokarn, Y. R., Effect of ions on agitation- and temperature-induced aggregation reactions of antibodies. *Pharm Res* **2009,** *26* (4), 903-13.

21. Wang, S.; Wu, G.; Zhang, X.; Tian, Z.; Zhang, N.; Hu, T.; Dai, W.; Qian, F., Stabilizing two IgG1 monoclonal antibodies by surfactants: Balance between aggregation prevention and structure perturbation. *Eur J Pharm Biopharm* **2017,** *114*, 263-277.

22. Stadtman, E. R., Metal ion-catalyzed oxidation of proteins: biochemical mechanism and biological consequences. *Free Radic Biol Med* **1990,** *9* (4), 315-25.

23. Wang, G.; Wang, J.; Ma, H.; Khan, M. F., Increased nitration and carbonylation of proteins in MRL+/+ mice exposed to trichloroethene: potential role of protein oxidation in autoimmunity. *Toxicol Appl Pharmacol* **2009,** *237* (2), 188-95.

24. Rasheed, Z.; Ahmad, R.; Rasheed, N.; Ali, R., Enhanced recognition of reactive oxygen species damaged human serum albumin by circulating systemic lupus erythematosus autoantibodies. *Autoimmunity* **2007,** *40* (7), 512-20.

25. Bee, J. S.; Davis, M.; Freund, E.; Carpenter, J. F.; Randolph, T. W., Aggregation of a monoclonal antibody induced by adsorption to stainless steel. *Biotechnol Bioeng* **2010,** *105* (1), 121-9.

26. Purdie, J. L.; Kowle, R. L.; Langland, A. L.; Patel, C. N.; Ouyang, A.; Olson, D. J., Cell culture media impact on drug product solution stability. *Biotechnol Prog* **2016,** *32* (4), 998-1008.

27. Petrov, D.; Zagrovic, B., Microscopic analysis of protein oxidative damage: effect of carbonylation on structure, dynamics, and aggregability of villin headpiece. *J Am Chem Soc* **2011,** *133* (18), 7016-24.

28. Finley, E. L.; Dillon, J.; Crouch, R. K.; Schey, K. L., Identification of tryptophan oxidation products in bovine alpha-crystallin. *Protein Sci* **1998,** *7* (11), 2391-7.

29. Bostrom, M.; Tavares, F. W.; Finet, S.; Skouri-Panet, F.; Tardieu, A.; Ninham, B. W., Why forces between proteins follow different Hofmeister series for pH above and below pI. *Biophys Chem* **2005,** *117* (3), 217-24.

30. Yang, Y.; Mah, A.; Yuk, I. H.; Grewal, P. S.; Pynn, A.; Cole, W.; Gao, D.; Zhang, F.; Chen, J.; Gennaro, L.; Schoneich, C., Investigation of Metal-Catalyzed Antibody Carbonylation With an Improved Protein Carbonylation Assay. *J Pharm Sci* **2018**.

31. Yang, Y.; Stella, C.; Wang, W.; Schoneich, C.; Gennaro, L., Characterization of oxidative carbonylation on recombinant monoclonal antibodies. *Anal Chem* **2014,** *86* (10), 4799-806.

32. Okur, H. I.; Hladilkova, J.; Rembert, K. B.; Cho, Y.; Heyda, J.; Dzubiella, J.; Cremer, P. S.; Jungwirth, P., Beyond the Hofmeister Series: Ion-Specific Effects on Proteins and Their Biological Functions. *J Phys Chem B* **2017,** *121* (9), 1997-2014.

33. Paterova, J.; Rembert, K. B.; Heyda, J.; Kurra, Y.; Okur, H. I.; Liu, W. R.; Hilty, C.; Cremer, P. S.; Jungwirth, P., Reversal of the hofmeister series: specific ion effects on peptides. *J Phys Chem B* **2013,** *117* (27), 8150-8.

34. Georgiou, C. D.; Zisimopoulos, D.; Argyropoulou, V.; Kalaitzopoulou, E.; Salachas, G.; Grune, T., Protein and cell wall polysaccharide carbonyl determination by a neutral pH 2,4-dinitrophenylhydrazine-based photometric assay. *Redox Biol* **2018,** *17*, 128-142.

35. Kalia, J.; Raines, R. T., Hydrolytic stability of hydrazones and oximes. *Angew Chem Int Ed Engl* **2008,** *47* (39), 7523-6.

36. Chennamsetty, N.; Voynov, V.; Kayser, V.; Helk, B.; Trout, B. L., Design of therapeutic proteins with enhanced stability. *Proc Natl Acad Sci U S A* **2009,** *106* (29), 11937-42.

37. Ionescu, R. M.; Vlasak, J.; Price, C.; Kirchmeier, M., Contribution of variable domains to the stability of humanized IgG1 monoclonal antibodies. *J Pharm Sci* **2008,** *97* (4), 1414-26.

38. Prabhu, N. V.; Sharp, K. A., Heat capacity in proteins. *Annu Rev Phys Chem* **2005,** *56*, 521-48.

39. Rogowska-Wrzesinska, A.; Wojdyla, K.; Nedic, O.; Baron, C. P.; Griffiths, H. R., Analysis of protein carbonylation--pitfalls and promise in commonly used methods. *Free Radic Res* **2014,** *48* (10), 1145-62.

40. Torosantucci, R.; Sharov, V. S.; van Beers, M.; Brinks, V.; Schoneich, C.; Jiskoot, W., Identification of oxidation sites and covalent cross-links in metal catalyzed oxidized interferon Beta-1a: potential implications for protein aggregation and immunogenicity. *Mol Pharm* **2013,** *10* (6), 2311-22.

41. Majumdar, R.; Manikwar, P.; Hickey, J. M.; Samra, H. S.; Sathish, H. A.; Bishop, S. M.; Middaugh, C. R.; Volkin, D. B.; Weis, D. D., Effects of salts from the Hofmeister series on the conformational stability, aggregation propensity, and local flexibility of an IgG1 monoclonal antibody. *Biochemistry* **2013,** *52* (19), 3376-89.

42. Zhang, J.; Frey, V.; Corcoran, M.; Zhang-van Enk, J.; Subramony, J. A., Influence of Arginine Salts on the Thermal Stability and Aggregation Kinetics of Monoclonal Antibody: Dominant Role of Anions. *Mol Pharm* **2016,** *13* (10), 3362-3369.

43. Roberts, D.; Keeling, R.; Tracka, M.; van der Walle, C. F.; Uddin, S.; Warwicker, J.; Curtis, R., Specific ion and buffer effects on protein-protein interactions of a monoclonal antibody. *Mol Pharm* **2015,** *12* (1), 179-93.

Chapter 5

Characterization of Protein Crosslinks in a Recombinant Monoclonal Antibody After Metal-Catalyzed Oxidation

INTRODUCTION

Metal-catalyzed oxidation is a commonly observed protein degradation pathway during manufacturing of recombinant monoclonal antibody (mAb) therapeutics.[1,2,3] This type of protein degradation can negatively impact mAb product quality. First, metal-catalyzed oxidation of methionine or tryptophan residues in the complementarity-determining regions could decrease target binding of mAbs.[4] Second, metal-catalyzed oxidation of methionine residues in the Fc region could change pharmacokinetic properties of mAbs.[5] Third, certain degradation products generated by metal-catalyzed oxidation can be potentially immunogenic. For example, formation of protein carbonyls (such as 2-aminoadipic semialdehyde, glutamic semialdehyde, and 2-amino-3-butyrate) by metal-catalyzed oxidation of lysine, arginine, threonine, and proline residues in proteins, could represent a danger signal to the immune system and induce production of autoantibodies against the carbonyl-modified proteins.[6] Additionally, metal-catalyzed oxidation can drive formation of mAb aggregates,[2] which often pose an immunogenicity risk.[7-9] For example, a study by Filipe et al. showed that mAb aggregates generated by metal-catalyzed oxidation were more immunogenic than those generated by shaking, pH, or heat stress conditions in transgenic mice.[7] To date, the chemical source of the immunogenicity for aggregates generated after metal-catalyzed oxidation remains poorly understood.

Protein crosslinks, referring to covalent bonds that link amino acidic residues, could contribute to the formation of immunogenic aggregates.[10] The commonly observed crosslinks are inter-peptide crosslinks (type 2 crosslinks), intra-peptide crosslinks (type 1 crosslinks), and dead-end links (type 0 crosslinks).[11] Since inter-peptide crosslinks could directly lead to protein dimerization or oligomerization, characterization of this type of crosslinks is often a major focus in the investigation of immunogenic aggregates.[12] For metal-catalyzed oxidation, several inter-

peptide crosslinks have been discovered by Torosantucci et al. in human insulin.[13] These crosslinks occurred between amino acids with nucleophilic properties (such as lysine, histidine, phenylalanine) and tyrosine oxidation products via 1,4- or 1,6-type addition.[13] In another study, Torosantucci et al. identified similar types of crosslinks in human interferon beta-1a after oxidation with copper and ascorbate, where primary amines formed covalent bonds with oxidation products of tyrosine and phenylalanine via 1,4- or 1,6-type addition.[12] Interestingly, at the active site of a cytochrome c oxidase, a covalent bond was found between tyrosine and histidine near the ligated copper ion,[14] likely via a similar mechanism reported by Torosantucci et al.[12-13] Another tyrosine-related crosslink identified in various proteins after oxidation with copper and hydrogen peroxide is di-tyrosine.[15-17] This crosslink is formed by interactions between two tyrosine radicals, often via ortho-ortho coupling.[18] Di-tyrosine has a unique fluorescence with an excitation wavelength of 320 nm and an emission maximum wavelength of 410 nm, which is often an initial indicator of di-tyrosine crosslinks.[17]

In addition to tyrosine- and phenylalanine-related crosslinks, metal-catalyzed oxidation could generate Schiff base crosslinks, which are reversible imine bonds formed between aldehydes and primary amines.[18-19] In a study by Bardshaw et al., the presence of Schiff base crosslinks in oxidized slug proteins was first suggested by the lack of reactivity towards protein carbonyls under native conditions.[20] The decreased amount of soluble proteins after sodium borohydride treatment, which reduces the Schiff base to a more stable amine bond and lowers the solubility of protein complexes, is also consistent with the formation of a Schiff base. Additionally, the majority of primary amines were not accessible to acid anhydrides, which further supports the presence of Schiff base crosslinks in these proteins after metal-catalyzed oxidation.[20] In another study by Rysman et al., the formation of Schiff base crosslinks was

suggested in oxidized myofibrillar proteins, based on the increased fluorescence (Em 420 nm/Ex 350 nm) that may be related to Schiff base structures.[21] However, the increased fluorescence may not be specifically from Schiff base structures, since the maximum emission wavelength is close to that of di-tyrosine (Em 410 nm/Ex 325nm).[22] Interestingly, to date, there is no direct mass spectrometry analysis data that identify Schiff base crosslinks in proteins after metal-catalyzed oxidation. By contrast, Schiff base crosslink formation catalyzed by lysyl oxidase[23] was identified in collagen[24] and elastin[25] by mass spectrometry.[26-27]

For mAbs, very little is known about protein crosslinks formed after metal-catalyzed oxidation. Several analytical challenges hinder the effort to characterize protein crosslinks in mAbs by peptide mapping. First, crosslinked peptides are often in low abundance,[28] making it difficult to identify/distinguish the crosslinked peptide ions from the non-crosslinked peptide ions in a peptide map. Second, MS^2 fragments of the crosslinked peptides are often very complex, making it difficult to assign the peptide sequence and the crosslink structure, particularly when the crosslink chemistry is not known. Currently, a commonly used analytical strategy for the identification and assignment of crosslinked peptides employs enzymatic O^{18} labeling during tryptic digestion, where trypsin incorporates two O^{18} or O^{16} (as control) atoms into the C-terminus of each tryptic peptide.[29-30] A unique mass shift of +8 Da observed between tryptic peptides generated in O^{18} and O^{16} water can then allow for the detection of crosslinked peptide ions, where the non-crosslinked peptide ions show only +4 Da mass shift.[31-32] The limitation of the enzymatic O^{18} labeling is that labeling efficiency may vary for different peptides,[33] which may impact the detection. Furthermore, the +8 Da may be masked by natural isotopic distribution,[34] particularly with large peptides. Finally, the O^{18} labeling approach does not address the analytical challenge with interpreting complex MS^2 data of crosslinked peptide

ions. In addition, during MS analysis, formation of clusters in the gas phase can lead to false positive detection of crosslinks, as cluster dimers sometimes show a mass difference of +8 Da (unpublished data).

To facilitate characterization of potential inter-peptide crosslinks in mAbs after metal-catalyzed oxidation, this study applies an analytical approach to enrich crosslink peptides and then characterize these crosslinked peptides by a secondary peptide mapping method using thermolysin,[35] a protease less specific than trypsin. Enrichment of the crosslinked peptides is based on the net charge differences between the crosslinked peptides and the non-crosslinked peptides at pH 2.7, where crosslinked peptides (with ≥+4 charge) can be separated from the non-crosslinked peptides (with <=+3 charge, except those containing multiple lysine, arginine, and histidine residues) on a strong cation exchange column.[28, 36-37] After the enrichment, a secondary peptide map is used to generate complementary peptide information, which reduces the complexity of assigning the peptide sequence and the crosslink structure. To evaluate this analytical methodology, a model mAb crosslink sample was generated using an N-hydroxysuccinimide ester crosslinker, BS3, which crosslinks primary amines of proteins.[38] After demonstrating the feasibility of the new methodology to identify crosslinked peptides using the mAb crosslink sample, this approach was employed to investigate crosslinked products in a model mAb after copper-catalyzed oxidation. Copper-catalyzed oxidation instead of iron-catalyzed oxidation was used to prepare the model mAb because copper ion was found to be more effective than iron ion in generating oxidative carbonylation on mAbs and other proteins.[39-40] Therefore, it is expected that more carbonyls and the related Schiff base crosslink products will be generated using copper-catalyzed oxidation, which would facilitate/ease the crosslink identification effort. Additionally, mAbs stressed by copper-catalyzed oxidation were shown to

be highly immunogenic in a transgenic mouse model.[7] It will be interesting to understand if Schiff base crosslink products formed after copper-catalyzed oxidation may be linked to the induced immunogenicity. Finally, it was found that copper-catalyzed oxidation but not iron-catalyzed oxidation generated dityrosine crosslinks in lens proteins.[41] In addition to Schiff base crosslink products, it will be interesting to characterize dityrosine crosslink products in the model mAb, which could also be linked to the induced immunogenicity.

MATERIALS AND METHODS

Materials

The recombinant monoclonal antibody, mAb A, was manufactured at Genentech (South San Francisco, CA). Copper sulfate, hydrogen peroxide solution (30% in H_2O, w/w), ethylenediaminetetraacetic acid (EDTA), sodium phosphate (dibasic and monobasic), sodium chloride, sodium acetate, acetic acid, urea, dithiothreitol (DTT), iodoacetamide (IAM), calcium chloride, tris(hydroxymethyl) aminomethane (Tris), hydrochloric acid, formic acid (FA), and trifluoroacetic acid (TFA) were purchased from Sigma-Aldrich (St. Louis, MO, USA). Guanidine hydrochloride solution (8 M in H_2O) and BS3 (bis(sulfosuccinimidyl)suberate) were purchased from Thermo Fisher Scientific (Waltham, MA, USA). A synthetic peptide, acetylated-ALRLLIKYASQSISGVPSR, was purchased from AnaSpec (Fremont, CA, USA). The TSK G3000 SWXL (7.8x300mm) size exclusion column was purchased from Tosoh Bioscience (King of Prussia, PA, USA). Acetonitrile (ACN) was purchased from Burdick & Jackson (Muskegon, MI, USA). Thermolysin and sequencing-grade trypsin was purchased from Promega (Madison, WI, USA). The PolySULFOETHYL A column (4.6x204 mm, 5 µm) was purchased from PolyLC (Columbia, MD, USA). Zorbax Eclipse XDB-C18 Column (2.1x150 mm, 3.5 µm) was

purchased from Agilent (Milford, MA, USA). The 30-kDa Amicon centrifugal filter units were purchased from MilliporeSigma (Burlington, MA, USA).

Preparation of Crosslinked mAb A with BS3

The mAb A sample was extensively buffer exchanged into 100 mM sodium phosphate buffer, pH 7.4, which removes primary amines in mAb A storage buffer to prevent interference with the BS3 crosslink reaction. For the crosslink reaction, the BS3 stock solution (50 mM BS3 in water, prepared immediately before the crosslink reaction) was added to an mAb A solution (5 mg/mL mAb A in 100 mM sodium phosphate, pH 7.4), where the final concentration of BS3 was 2 mM. The reaction mixture was vortexed briefly and then incubated at room temperature for 40 minutes. Subsequently, Tris hydrochloride buffer (1M, pH 8.2) was added to the reaction mixture to a final concentration of 50 mM. The mixture was vortexed briefly and then incubated at room temperature for an additional 15 minutes to quench the BS3 crosslink reaction.

Copper-catalyzed Oxidation of mAb A

Copper-catalyzed oxidation of mAb A was performed in 10 mM sodium acetate buffer, pH 5.0. The final concentration of mAb A, copper sulfate, and hydrogen peroxide was 10 mg/mL, 10 mM, and 20 mM, respectively, in the reaction mixture. The reaction was carried out at room temperature for 24 hours, and was stopped by addition of EDTA (to a final concentration of 15 mM). Subsequently, the oxidized mAb A was stored at -80°C until further analysis.

Digestion of mAb A Samples by Trypsin

The unstressed, BS3-crosslinked, and oxidized mAb A samples were diluted with 8M guanidine hydrochloride to a final mAb A concentration of 2 mg/mL and a final concentration of guanidine hydrochloride of 6 M. To reduce the disulfide bonds, 15 µL of 1M DTT was added to 1 mL of these mAb A sample solutions. The samples were then incubated at 37°C for 1 hour.

Subsequently, 90 uL of IAM (0.5 M in water) was added to the samples, and the mixtures were incubated at room temperature in the dark for 15 minutes to alkylate free thiols. After the incubation, 15 uL of 1 M DTT were added to the samples to quench the alkylation reaction.

Different from the unstressed and BS3-crosslinked mAb A samples, the oxidized mAb A sample was treated with sodium borohydride prior to the DTT reduction step. The sodium borohydride treatment is necessary to stabilize any potential Schiff base products, which reduces a Schiff base to an amine. For the sodium borohydride reduction reaction, 250 µL sodium borohydride solution (1 M in 100% ethanol) and 50 µL 2M sodium phosphate buffer, pH 8.0 were added to 1 mL of the mAb A sample solution (that was prepared with 8 M guanidine hydrochloride). This mixture was incubated at room temperature for 2 hours. Subsequently, the sample was reduced by DTT and alkylated by IAM as described above.

The reduced and alkylated mAb A samples were then buffer exchanged (three times) to 6M urea, 60 mM hydroxylamine, pH 7.0, using a 30 kDa Amicon filter, where mAb A samples were concentrated to approximately 20 mg/mL after the third round of buffer exchange. These samples were then diluted to 0.3 mg/mL with 25 mM Tris, 5 mM calcium chloride, pH 8.2. To these samples, trypsin was added at an enzyme-to-substrate ratio (weight-to-weight) of 1:50. The digestion mixture was incubated at 37°C for 6 hours, and subsequently stopped by addition of TFA to a final concentration of 0.3% (v/v).

Strong Cation Exchange (SCX) Analysis of mAb A Tryptic Digests

The mAb A tryptic digests were separated on a PolySulfoethyl A strong cation column. Solvent A was 30 mM sodium phosphate, 30% acetonitrile in water, pH 2.7; solvent B was 30 mM sodium phosphate, 500 mM sodium chloride, 30% acetonitrile in water, pH 2.7. The column temperature was controlled at 40°C and the HPLC autosampler temperature was controlled at

8°C. The flow rate was 0.4 ml/min. The effluent was monitored by UV absorbance at 214 and 280 nm. A linear gradient of 0% to 95% B in 33 minutes was applied to separate mAb A tryptic peptides. On the strong cation exchange chromatograms, the two regions that contain peptides with +4 and +5 charges were fraction collected for further analysis.

LC-MS/MS analysis of the SCX Fractions

The collected SCX fractions were injected onto an Eclipse XDB-C18 Column (2.1x150 mm, 3.5 μm). Solvent A was 0.1% TFA in water (v/v). Solvent B was 0.09% TFA in 90% acetonitrile and 10% water (v/v). The column temperature was controlled at 55ºC, and the flow rate was 0.25 mL/min. A two-step gradient was used, where solvent B was first increased from 5% to 19% in 7 minutes, and then increased to 62% in 53 minutes. The eluent was monitored by absorbance at 214 nm, and was introduced to an Orbitrap Elite mass spectrometer. The mass spectrometry analysis was performed in the positive mode with an electrospray voltage of 4.0 kV and a capillary temperature of 250°C. The MS data acquisition was in a data-dependent mode, where top 5 most intense ions in the full MS spectrum was selected for MS^2 data acquisition by collision induced fragmentation. The normalized collision energy was 35% with an activation time of 10 milliseconds.

Tandem Peptide Mapping (Enzymatic MS^2) by Thermolysin

After the LC-MS/MS analysis of the SCX fractions, the peptides separated on the Eclipse XDB-C18 column were collected for tandem peptide mapping or enzymatic MS^2 (eMS^2). Different from the conventional MS^2 based on collision-induced dissociation in an MS experiment, the eMS^2 process uses non-specific proteases (such as chymotrypsin, elastase, pepsin, or thermolysin) to generate peptide fragments from parent tryptic (or Lys-C) peptides. Subsequently, these peptide fragments are analyzed by LC-MS/MS. In this study, we used

thermolysin to generate eMS^2 data on the tryptic peptides of the SCX fractions. For the thermolysin digestion, the collected peptide fractions were diluted 8-fold with 25 mM sodium phosphate buffer, pH 7.8 to adjust the pH and reduce the concentration of acetonitrile. Subsequently, 0.1 µg of thermolysin were added to the peptide sample. The mixture was incubated at 50°C for 1 hour. The thermolysin digestion was stopped by addition of formic acid to a final concentration of 0.3% (v/v). Subsequently, the themolysin digest was analyzed by LC-MS/MS using the same conditions as described for the analysis of the SCX fractions.

Identification of Crosslinked Peptides

The eMS^2 data from theromlysin peptide mapping analysis were analyzed by database search against the mAb A sequence using the Proteome Discover software (Waltham, MA, USA). For database searching, the full MS mass tolerance was 5 ppm; the CID-MS^2 mass tolerance was 0.6 Da; enzyme specificity was set as none; cysteine modification was set as carbamidomethyl (+57Da), and no other post-translational modification was included. The search results were manually investigated to identify crosslinked peptide candidates, where these peptides show partial tryptic sequence coverage in the search results.

After identification of the peptide candidates that may be crosslinked, reporter/signature fragment ions were manually selected based on the relative intensity of these fragment ions in the respective parent tryptic peptides. Typically, these reporter/signature fragment ions are the predominant b or y ions from terminal sequences, which can be also present in the CID-MS^2 spectra of the related crosslinked peptides. Additionally, since these b or y ions are from terminal sequences of the peptide candidates, their masses (m/z) do not change with different crosslink types/modifications. Subsequently, the MS^2 data from the LC-MS/MS analysis of the SCX fractions were extracted for any MS^2 spectrum that contains the reporter/signature fragment ions.

These extracted MS^2 spectra and related full MS spectra were evaluated for identification of crosslinked peptides.

RESULTS

Analytical Methodology for Identification of Crosslinked Peptides

As shown in Figure 1, a new analytical methodology using **S**trong cation exchange **E**nrichment and **E**nzymatic **MS^2** ($SEEMS^2$) was developed to identify crosslinked peptides. Sample preparation, chromatography conditions, and the identification process were designed to address the commonly encountered analytical challenges during analysis of crosslinked peptides.

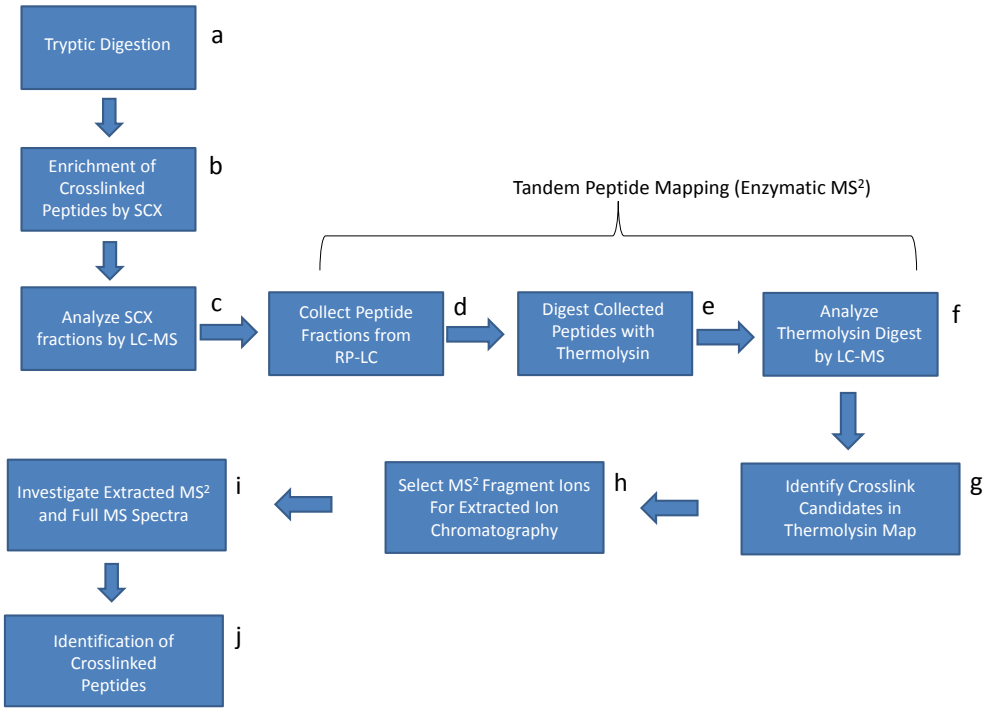

Figure 1. Workflow of the **S**trong cation exchange **E**nrichment and **E**nzymatic **MS**^{2} (SEEMS^2) approach for identification of crosslinked peptides.

For sample preparation, mAb A samples were reduced and alkylated in 6 M guanidine hydrochloride to dissolve the aggregates formed from BS3 crosslink reaction or metal-catalyzed oxidation. The solubilization of mAb A samples in 6 M guanidine hydrochloride helps improve recovery of crosslinked mAb species. Subsequently, these samples were buffer-exchanged to 6 M urea instead of the tryptic digestion buffer (25 mM Tris, 5 mM calcium chloride, pH 8.2). This was based on a concern that crosslinked mAb species are hydrophobic and could precipitate in the tryptic digestion buffer during buffer exchange. Urea was thus used since 6 M urea is an effective chaotropic reagent[42] that can keep the mAb A samples in solution during buffer exchange. Another consideration is that, upon dilution (to less than 1 M, after buffer exchange), urea does not interfere with trypsin digestion.[43] One drawback with digestion of proteins in urea solution is that urea can form isocyanic acid, which readily reacts with N-termini of peptides or Lys/Arg side chains to cause protein/peptide carbamylation.[44] To address the protein/peptide carbamylation issue, hydroxylamine was included in the urea solution;[45] subsequently, we did not detect significant carbamylation in the peptide map data (not shown) for all mAb A samples. Finally, urea is a non-ionic solute, which does not interfere with the subsequent strong cation exchange chromatography for the enrichment of crosslinked peptides.

The strong cation exchange chromatography condition was largely based on the condition described by Tinnefeld et al.[28] The mobile phase pH was 2.7, at which the N-terminus and the side chains of histidine, lysine, and arginine residues are positively charged; the side chains of aspartic acid (pKa=3.7) and glutamic acid (pKa=4.3) are predominantly neutral. Therefore, at pH 2.7, crosslinked peptides (from two tryptic peptides) have 4 or more positive charges, while non-crosslinked tryptic peptides have 2 positive charges (except for those that contain histidine or the KP/RP mis-cleavage sequence). The charge difference enables separation of the crosslinked

peptides from the non-crosslinked peptides on a strong cation exchange column. In this study, we increased the acetonitrile concentration in the mobile phase from 20% (as used by Tinnefeld et al.[28]) to 30%, which helps to improve the recovery of hydrophobic peptides.[46] After establishing the chromatography conditions, we used the tryptic digest of unstressed mAb A and a synthetic model peptide (which contains 3 positive charges at pH 2.7) to determine the regions on the strong cation exchange chromatograms for collecting +4 and +5 charged peptides. As shown in Figure 2, the synthetic peptide eluted at ~28 minutes on the chromatogram. We therefore selected the two groups of peaks (regions A and B) that eluted at between 31 to 33 minutes and between 37 to 39 minutes for fraction collection. Considering that region A likely contains +4 charged peptides and region B likely contains +5 charged peptides, these two regions are therefore the primary focus of the crosslink analysis.

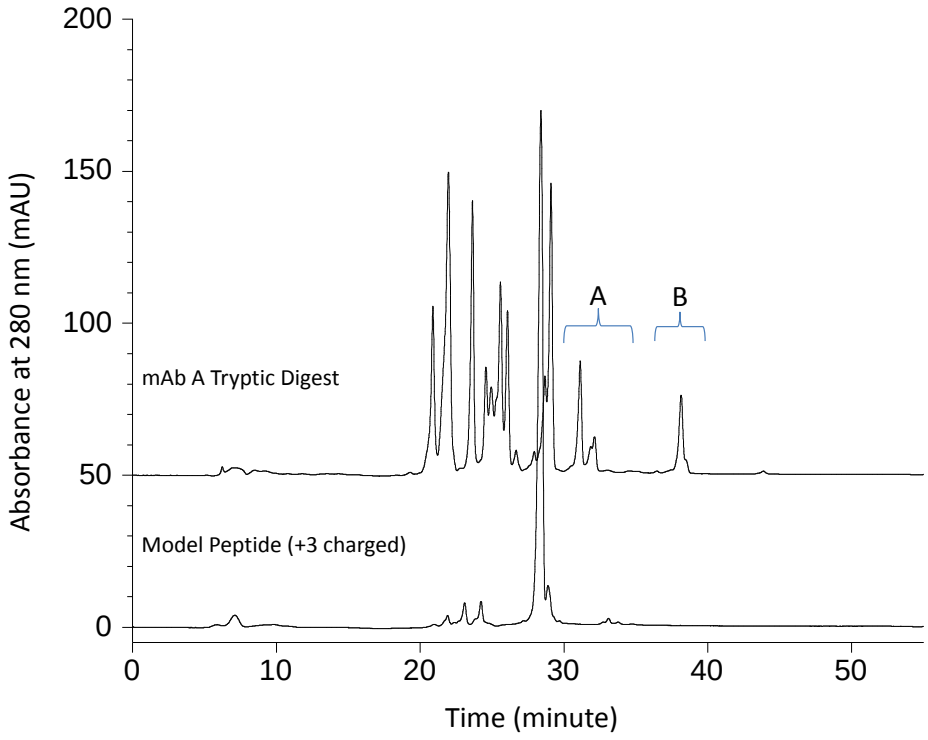

Figure 2. Strong cation exchange chromatograms of the tryptic peptides from unstressed mAb A and a model peptide (+3 charged at pH 2.5). Region A (containing +4 charged peptides) and region B (containing +5 charged peptides) were collected for further analysis.

For identification of crosslinked peptides, we rely on the information provided by tandem peptide mapping (eMS^2). The rationale is that, after thermolysin digest, the resulting peptides that contain crosslink sites are not expected to match any sequence of mAb A (as the corresponding mass shifts are not known beforehand for database search); thus, the database search result should reveal a gap in the identified peptide sequence as against an expected tryptic peptide sequence (that is not crosslinked). The information points to putative peptide candidates that may be involved in the crosslinked products. To locate the crosslinked peptides, we rely on the assumption that terminal fragment ions that do not cover the crosslink sites are likely also present in the CID-MS^2 spectra of the crosslinked peptides, in particular, for the terminal fragment ions with high intensities. Additionally, the masses of these fragment ions do not change with different crosslink types or different crosslink counterpart peptides. Therefore, by evaluating the CID-MS^2 spectra of the non-crosslinked counterpart peptides, we can identify several signature/reporter MS^2 ions, whose masses could help us extract/locate crosslinked products in the LC-MS/MS data of the collected SCX fractions. Subsequently, from the extracted CID-MS^2 and the corresponding full MS data, crosslinked peptides can be identified by manual interpretation.

Enrichment of BS3-Crosslinked Peptides by SCX

To demonstrate the capability of the $SEEMS^2$ approach to identify crosslinked peptides, we generated a model crosslinked sample using BS3. As shown in Figure 3, BS3 contains two N-hydroxysulfosuccinimide (NHS) ester groups, which can react with primary amines (such as lysine side chains) from two peptides to form crosslinks (Figure 3B). Compared to other crosslinking reagents, the BS3 crosslinking reaction is relatively fast and straightforward, and the resulting crosslinked products (amide bonds) are stable during subsequent MS analyses, which

makes BS3 a popular crosslinking reagent in crosslinking mass spectrometry.[47] In our study, after the BS3 crosslink reaction, we analyzed the unstressed and the BS3-treated mAb A sample by size exclusion chromatography, and observed that the relative level of HMWS increased from 0.8% (for the unstressed mAb A) to 65% (for the BS3-treated mAb A, Figure 4). This observation supports that the BS3-treated mAb A sample contains crosslinked species and is, thus, suitable for evaluating the capability of the SEEMS^2 approach to identify crosslinked peptides.

After tryptic digestion of the BS3-treated mAb A sample, the regions (A' and B') that likely contain +4 or +5 charged peptides were collected off the strong cation exchange column (Figure 5). On the strong cation exchange chromatograms, region B' looks very similar to region B (Figure 2) in terms of overall peak profiles and relative peak intensities. On the other hand, region A' appears to contain more peaks than region A (Figure 2). Furthermore, the percent peak area of region A' is ~7% of the total SCX peak area, while that of region A is ~10%. The low percent peak area of region A' indicates that the BS3-crosslinked peptides are in low abundance. Therefore, it is beneficial to enrich these peptides for subsequent analyses. It should be noted that the low percent peak area of region A' does not contradict with the relatively large percent peak area of HMWS (~65%) for the BS3-crosslinked mAb A sample on the SEC (Figure 4B), since a relatively low level of crosslinks at the peptide level can lead to even 100% crosslinks (i.e. containing 100% HMWS) at protein level.

LC-MS/MS analysis of the collected region A' fraction identified two +4 charged tryptic peptides. One of them is a CDR peptide, SYYASWYQQKPGQAPVLVIYGANNRPSGIPDR. The other one is the hinge peptide, THTCPPCPAPELLGGPSVFLFPPKPK. Since only these two tryptic peptides (based on a complete tryptic digestion) are +4 charged for mAb A, the SCX

condition is considered properly established for enrichment of the crosslinked peptides, and region A' should contain BS3-crosslinked peptides with +4 charges.

Analysis of the LC-MS/MS data by conventional database search against mAb A sequence showed that a large number of peptides in region A' (Figure 6) do not match any apparent sequence of mAb A, even after considering mis-cleavage caused by BS3 side chain modifications (i.e., the functional group at the other end of BS3, N-hydroxysulfosuccinimide ester, reacts with water and undergoes hydrolysis to form a carboxylic acid and a leaving product, N-hydroxysulfosuccinimide). These unmatched peptides could be BS3-crosslinked peptides. However, given that there are more than 600 possible mAb A crosslinks from the BS3 crosslinking reactions, it is difficult to survey all possible crosslink masses and identify crosslinked peptides directly from the LC-MS/MS data. The collected region A' was therefore further analyzed by the eMS^2 approach.

A

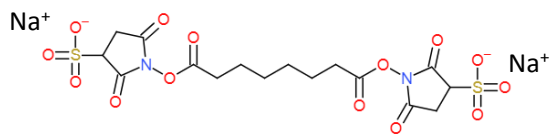

B

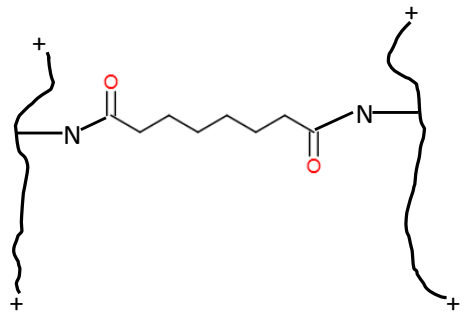

Figure 3. (A) Chemical structure of BS3 (bis(sulfosuccinimidyl)suberate). (B) Illustration of a crosslinked peptide product generated by the BS3 treatment.

A

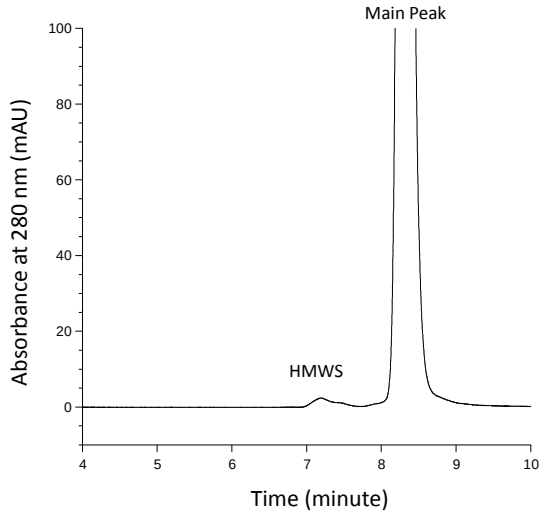

B

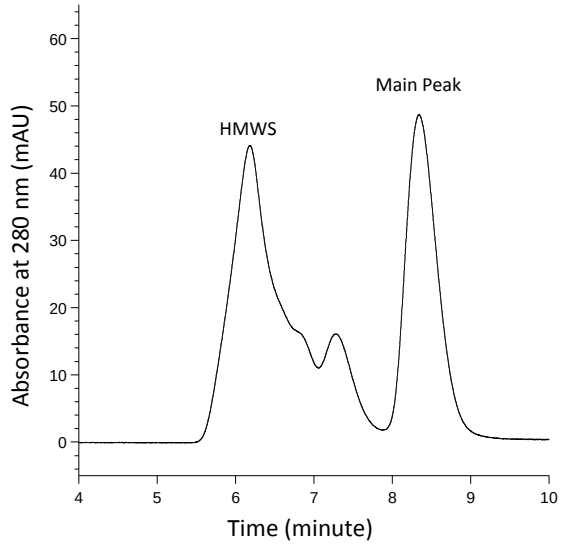

Figure 4. (A) size exclusion chromatogram of mAb A. (B) size exclusion chromatogram of the crosslinked mAb A (generated by the BS3 treatment).

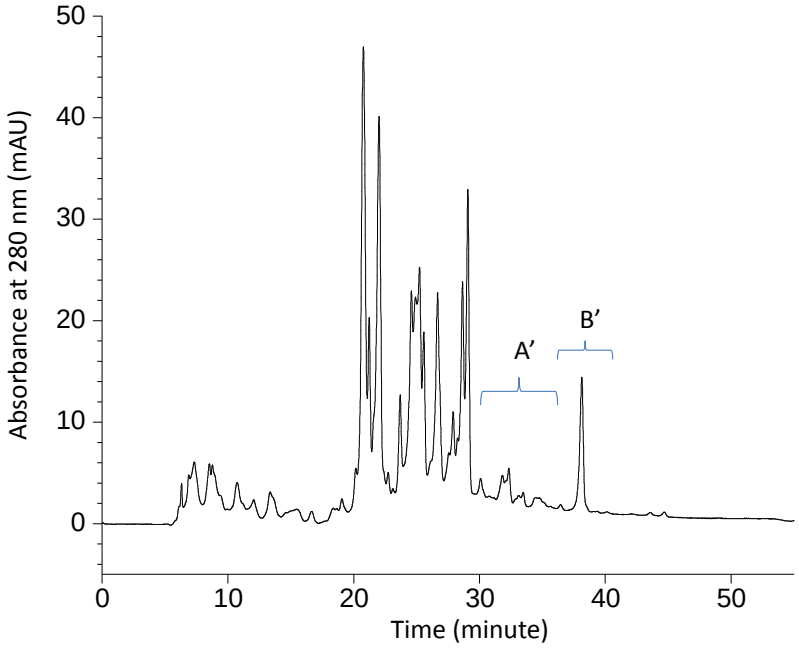

Figure 5. Strong cation exchange chromatogram of the tryptic peptides from BS3-crosslinked mAb A. Region A' (containing +4 charged peptides) and region B' (containing +5 charged peptides) were collected for further analysis.

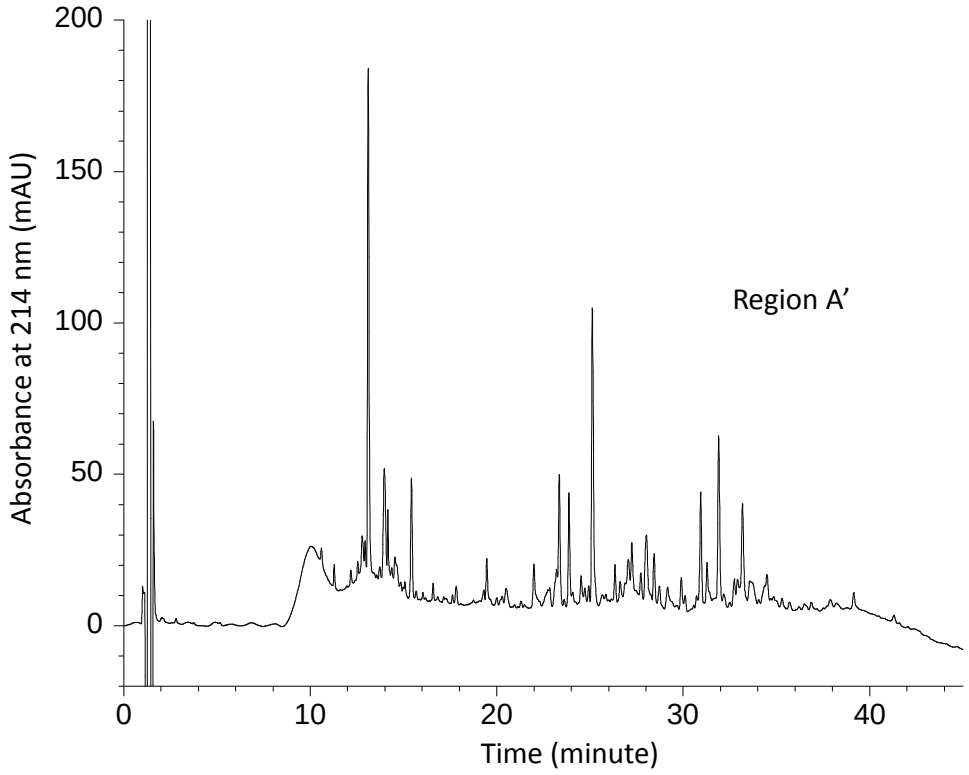

Figure 6. Analysis of the collected region A' fraction by reversed phase high performance liquid chromatography (RP-HPLC).

Identification of Crosslinked Peptides in Region A' by Tandem Peptide Mapping (eMS^2)

The peptide peaks (Figure 6) that do not match any apparent sequence of mAb A were collected and digested with thermolysin (tandem peptide mapping). The thermolysin digests were then analyzed by LC-MS/MS and database search. The database search results revealed several missing sequences in the corresponding tryptic peptides. For example, a peptide, LYLQMNSLR, was identified by the database search. However, against its corresponding tryptic peptide sequence, NS**LYLQMNSLR**, the two N-terminal residues, "NS", were not detected in the thermolysin map. After investigating the adjacent sequences, XXXR-DNAK-NS**LYLQMNSLR**-XXX, we speculated that the lysine residue next to the "NS" is a putative crosslink site. This speculation was based on a consideration that if the lysine residue were not crosslinked, we should have observed full coverage of the tryptic peptide sequence (that includes the "NS" residues). Based on this speculation and that a crosslink at the lysine residue will result in a missed cleavage from tryptic digestion, the peptide DNAKNSLYLQMNSLR was assigned as a crosslink candidate.

Considering that the crosslinked species could produce the same y ions as the peptide NSLYLQMNSLR, we investigated the CID-MS^2 spectrum of peptide NSLYLQMNSLR to look for reporter/signature y ions. Importantly, these reporter ions (if present) do not change in mass even with different crosslink counterpart peptides. As shown in Figure 7, y3, y5, y6, y7, and y8 are the dominant y ions in the spectrum. The masses of these fragment ions are not affected by any crosslink reaction that occur at the N-terminal sides of the "NS" residues. For simplicity, we selected y3, y5, y6, and y7 as the reporter MS^2 ions. Their masses were then used to extract the MS^2 spectra from region A' to find any peptide ions that could produce these fragment ions in a CID-MS^2 experiment. As shown in Figure 8, a peptide eluting at ~37.8 minutes was discovered

on the extracted MS^2 ion chromatogram. Subsequently, on the corresponding full MS spectrum, we found that the mass species is a +4 charged ion with m/z 1033.79333 (Figure 9A). The molecular mass of this species was then calculated as 4*1033.79333-4*1.007825=4131.14202 Da, which was based on the observed m/z (1033.79333), the charge state (4), and the monoisotopic mass of hydrogen (1.007825). Based on the calculated molecular mass of this crosslinked species (4131.14202 Da), the molecular mass of peptide DNAKNSLYLQMNSLR (1765.87812 Da), and the mass difference (+138.06808 Da) from BS3 crosslink modification, we inferred the other peptide in the crosslinked species as VVSVLTVLHQDWLNGKEYK, which has a molecular mass of 2227.20010 Da. From the MS^2 spectrum of the extracted ion (Figure 9B), we observed a continuous series of y ions (from y3 to y10) from the peptide NSLYLQMNSLR, and b13* ion from the peptide VVSVLTVLHQDWLNGKEYK. These observations support our assignment of the crosslinked species as shown in Figure 9B. It is worth noting that the y ions from NSLYLQMNSLR dominated the MS^2 spectrum of the crosslinked species. It is possible that the C-terminal arginine containing y ions (from NSLYLQMNSLR) were more efficient in capturing positive charges than the b ions from VVSVLTVLHQDWLNGKEYK during the CID-MS^2 process.

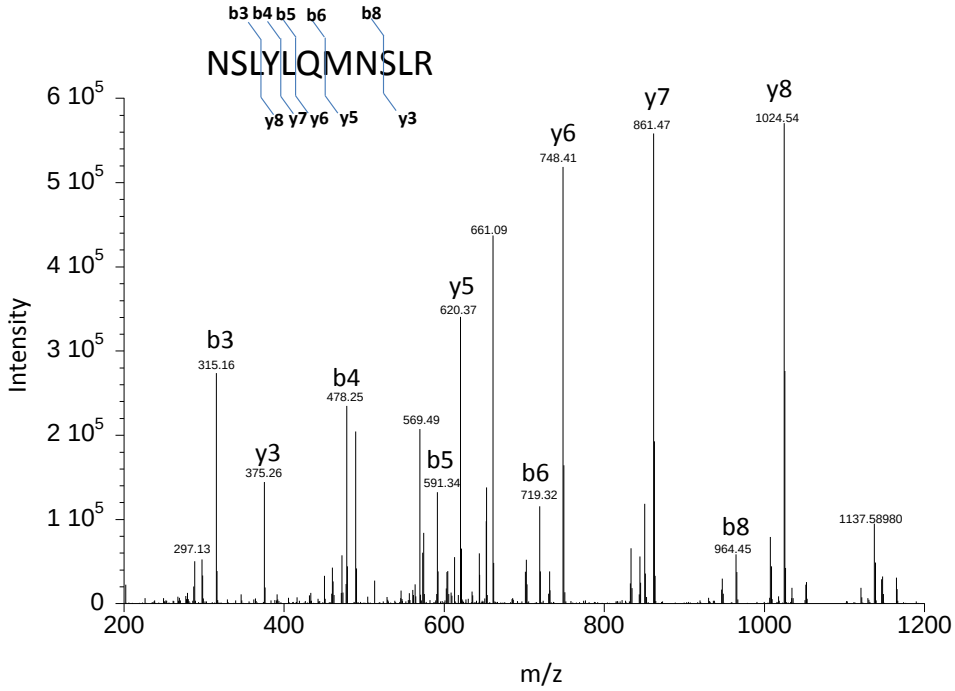

Figure 7. The CID MS^2 spectrum of a tryptic peptide (NSLYLQMNSLR) that is adjacent to a putative BS3 crosslink site. The dominant fragment ions, y3, y5, y6, and y7, were selected for extraction of any peptide ions that could produce these fragment ions in a CID experiment.

A

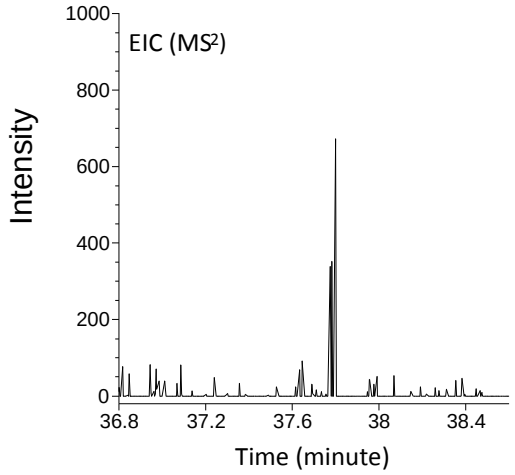

B

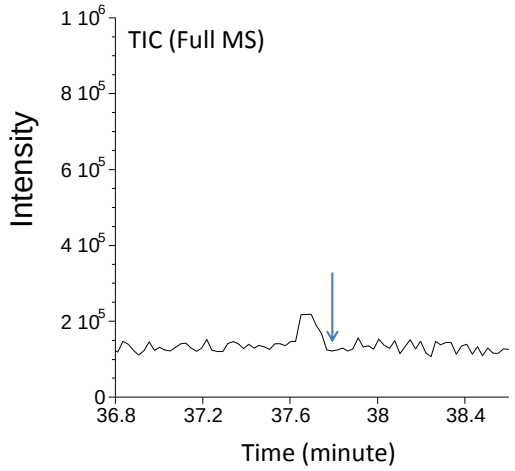

Figure 8. (A) Based on the reporter MS^2 masses (y3, y5, y6, and y7), the extracted ion chromatogram (EIC) leads to discovery of a crosslinked peptide candidate (eluted at ~37.8 minutes). (B) the corresponding region on the total ion chromatogram (TIC) of the full MS spectra.

A

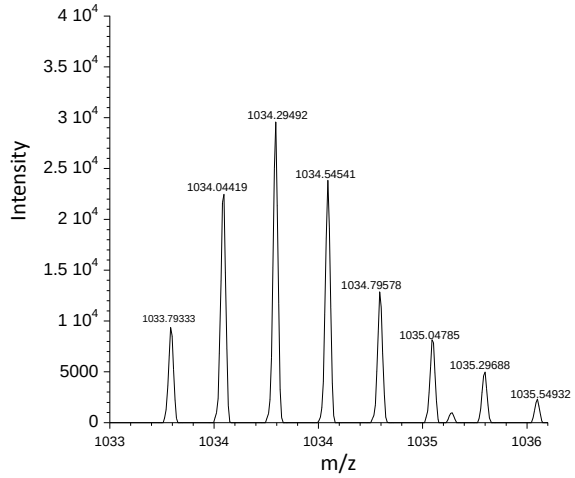

B

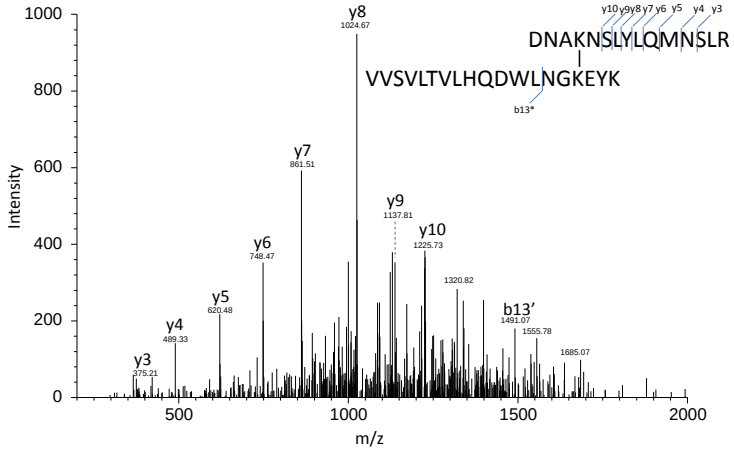

Figure 9. (A) The full MS spectrum of a BS3-crosslinked peptide. (B) The MS^2 spectrum and assignment of a BS3-crosslinked peptide that contains NSLYLQMNSLR.

Using the same approach, another peptide, LVQSGGGVERPGGSLR, was identified by database search. Against the corresponding tryptic peptide sequence, EVQLVQSGGGVERPGGSLR, three N-terminal residues, "EVQ", were not detected in the thermolysin map. Considering that this peptide is the heavy chain N-terminal tryptic peptide, we speculated that the N-terminus is a putative crosslink site. We therefore investigated the CID-MS^2 spectrum of the peptide EVQLVQSGGGVERPGGSLR to look for reporter/signature y ions. As shown in Figure 10, y6 and y7 are the dominant y ions in the spectrum, and were therefore selected as the MS^2reporter ions for extraction. After the extraction, we found a +2 charged mass species with an m/z of 1440.78174 (Figure 11A). Based on the observed molecular mass of this species (2879.54648 Da) and the mass difference (+138.068080 Da) from the BS3 crosslink modification, we inferred the other crosslinked peptide in the crosslinked species as LTVDKSR, which has a molecular mass of 817.46580 Da. From the MS^2 spectrum of the extracted ion (Figure 11B), we observed y6, y7, y11, and y13 from the peptide EVQLVQSGGGVERPGGSLR, and $b12^*$ and $b18^*$ from the crosslinked species (that contains both peptide chains). These observations support our assignment of the crosslinked species as shown in Figure 11.

Overall, a total of 13 crosslinked species were identified (Table 1). Many of the identified ion species are of low intensity. For example, the species eluting at ~37.8 minutes has an intensity of $3x10^4$, which is 1/300 of that of the most dominant peptide ion in the total ion chromatogram. Identification of these low abundant crosslinked species demonstrates the capability of the $SEEMS^2$ approach.

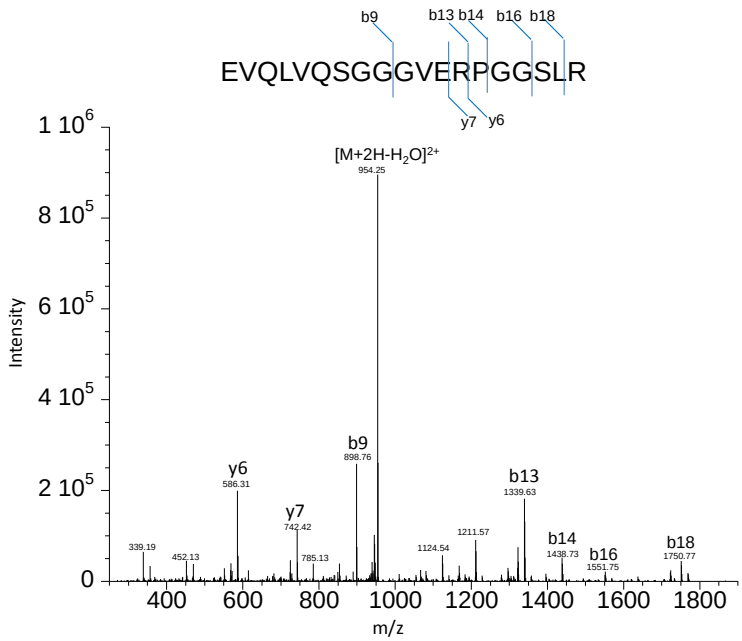

Figure 10. The CID MS^2 spectrum of a tryptic peptide (EVQLVQSGGGVERPGGSLR) that contains a putative BS3 crosslink site (N-terminus). The dominant fragment ions, y6 and y7, were selected for extraction of any peptide ions that could produce these fragment ions in a CID experiment.

A

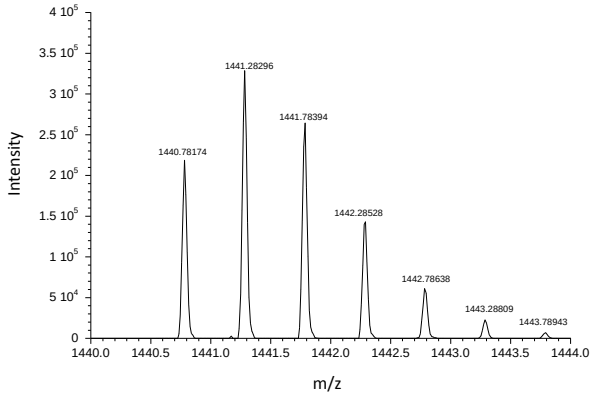

B

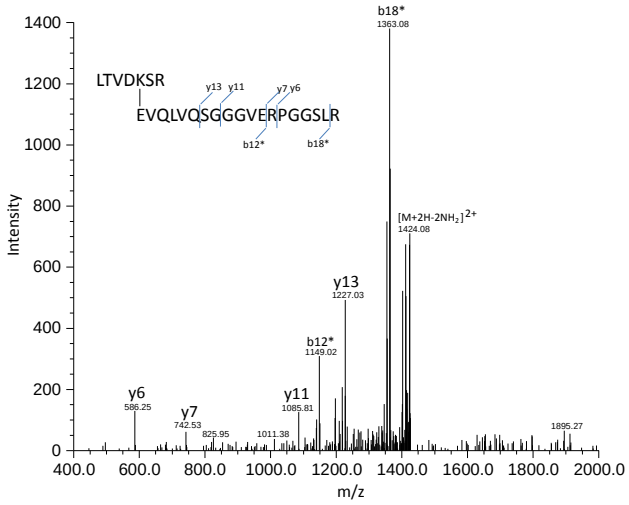

Figure 11. (A) The full MS spectrum of a BS3-crosslinked peptide. (B) The MS^2 spectrum and assignment of a BS3-crosslinked peptide that contains EVQLVQSGGGVERPGGSLR.

No.	Crosslinked Peptides	Observed m/z (charge)	Observed Mass (Da)	Theoretical Mass (Da)	Mass Error (ppm)
1	DNAKNSLYLQMNSLR VVSVLTVLHQDWLNGKEYK	1033.79333 (+4)	4131.14202	4131.14628	-1.03
2	LTVDKSR EVQLVQSGGGVERPGGSLR	1440.78174 (+2)	2879.54783	2879.54648	0.47
3	VVSVLTVLHQDWLNGKEYK ADSSPVKAGVETTTPSK	1347.37988 (+3)	4039.11617	4039.11538	0.19
4	YAASSYLSLTPEQWKSHK ADSSPVKAGVETTTPSK	1303.32544 (+3)	3906.95314	3906.95278	0.09
5	AKGQPR VVSVLTVLHQDWLNGKEYK	1007.89099 (+3)	3020.6495	3020.64478	1.50
6	AKGQPR ADSSPVKAGVETTTPSK	1234.65295 (+2)	2467.29025	2467.29188	-0.66
7	AKGQPR LTVDKSR	806.46185 (+2)	1610.90805	1610.91048	-1.50
8	AKGQPR GLEWVSGINWQGGSTGYADSVKGR	1106.56018 (+3)	3316.65706	3316.65898	-0.58
9	LTVDKSR ADSSPVKAGVETTTPSK	877.46893 (+3)	2629.38332	2629.38108	0.85
10	LTVDKSR WQQGNVFSCSVMHEALHNHYTQKSLSLSPG	1033.79333 (+4)	4397.13532	4397.13218	0.71
11	AKGQPR WQQGNVFSCSVMHEALHNHYTQKSLSLSPG	1412.69202 (+3)	4235.05258	4235.04298	2.27
12	LTVDKSR DNAKNSLYLQMNSLR	908.1451517 (+3)	2721.41198	2721.41198	0.00
13	AKGQPR DNAKNSLYLQMNSLR	854.11346 (+3)	2559.316905	2559.32278	2.30

Table 1. Summary of identified crosslinked peptides using the tandem peptide mapping approach.

Investigation of Potential Crosslinks in mAb A after Copper-catalyzed Oxidation

After tryptic digestion of the oxidized mAb A sample, the regions (A'' and B'') that likely contain +4 or +5 charged peptides were collected off the strong cation exchange column (Figure 12). On the strong cation exchange chromatogram, region A'' and region B'' represent only small percentages of the total peak area (Figure 12), which suggests that potential crosslinked species, including those from Schiff base reactions, are in low abundance.

LC-MS/MS analysis and database search of the mAb A sequence identified all of the major peaks in the chromatograms of the collected region A'' and region B' fractions (Figures 13 and 14; Tables 2 and 3). None of these peptides are inter-peptide crosslinks (type 2 crosslinks). The unidentified peaks are of very low abundance. Furthermore, even the sum of these unidentified peaks represents only a very small percentage of the total peak area. Considering that region A'' and region B'' are already in a low percentage of the tryptic digests, and that not all unidentified peaks are expected to be crosslinked peptides, we concluded that Schiff base crosslinks are not a major degradation product after copper-catalyzed oxidation/carbonylation. No further fractionation was performed to characterize these unidentified peptides by the eMS^2 analysis.

An intra-peptide dityrosine crosslink peptide was tentatively identified on the chromatogram of region A'' (peak 16 on Figure 13). The proposed crosslink occurs between two neighboring tyrosine residues, Y29 and Y30, on the mAb A light chain. From the full MS spectra, the crosslinked species is a +3 charged ion with an m/z of 1198.60107 (Table 2), whose molecular mass is 2 Da lower than that of the corresponding wild type tryptic peptide (peak 15 on Figure 13). The mass difference of -2 Da is consistent with the formation of dityrosine. From the MS^2 spectra (Figure 15), the crosslinked species showed a mass shift of - 2 Da in the b3, b4,

and b5 ions when compared with those ions of the wild type peptide. This observation supports that the -2 Da modification is located in the three residues, SYY, from the N-terminus. While carbonylation of a serine residue to form aldehyde[48] can result in a loss of 2 Da, to the best of our knowledge, such a carbonylation product is rarely observed or reported under common oxidation conditions. Therefore, the -2 Da modification was tentatively assigned to a dityrosine crosslink between LC Y29 and LC Y30. In future studies, an MS^3 experiment will be needed to confirm this crosslink product.

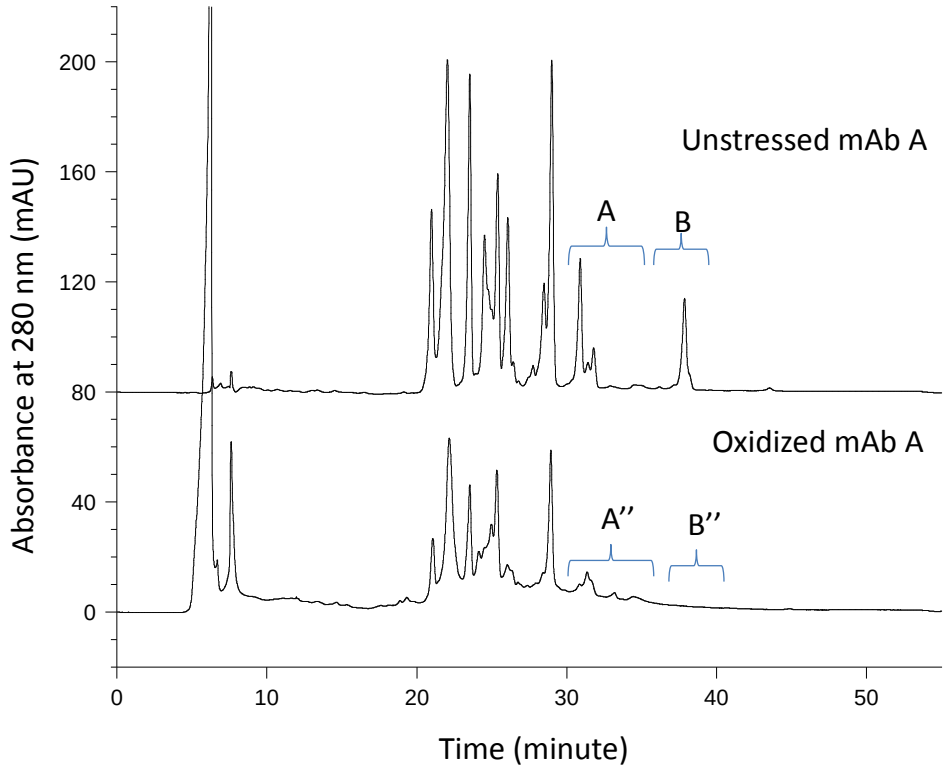

Figure 12. Strong cation exchange chromatograms of the tryptic peptides from the unstressed and oxidized mAb A. Region A'' (containing +4 charged peptides) and region B'' (containing +5 charged peptides) from the oxidized mAb A were collected for further analysis.

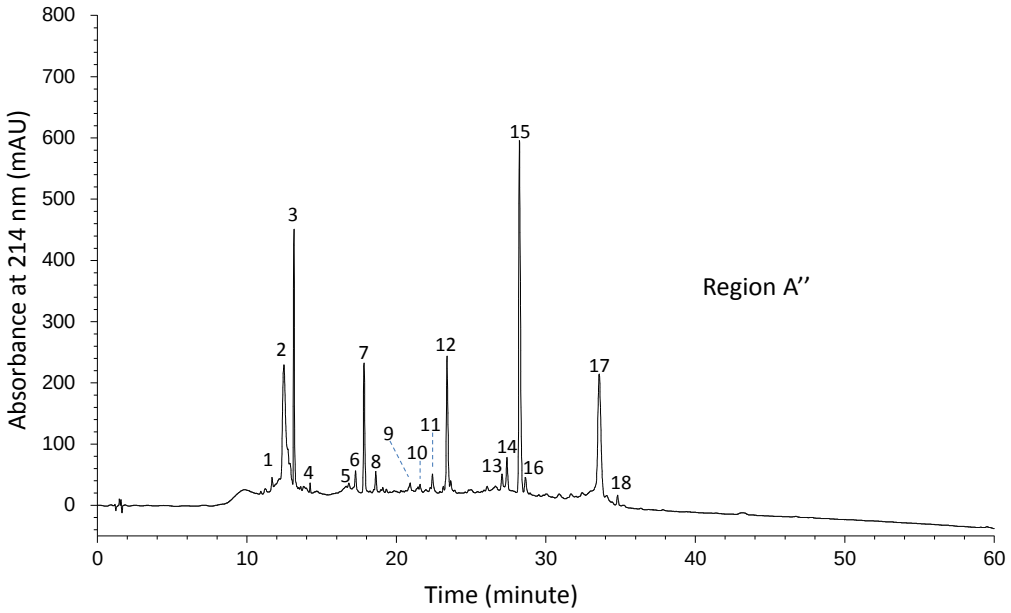

Figure 13. Analysis of collected SCX fractions of Region A'' (oxidized mAb A) by reversed-phase HPLC.

No.	Observed m/z (charge)	Observed Mass (Da)	Theoretical Mass (Da)	Mass Error (ppm)	Peptide ID
1	575.34979 (+1)	574.34196	574.33263	16.0	LTVDK
2	586.36523 (+1)	585.35740	585.35984	-4.0	ILGAGR
3	856.38324 (+2)	1710.75083	1710.75191	-0.6	SYSCQVTHEGSTVEK
4	895.33960 (+2)	1788.66355	1788.66111	1.3	SYSCQVTHEGSTVEK (+77.9 Da modification)
5	1266.62842 (+2)	2531.24119	2531.24384	1.0	VPSSSLGTQTYICNVNHKPSNTK (missed cleavage)
6	898.49109 (+2)	1794.96653	1794.97004	-1.9	VQLVQSGGGVERPGGSLR (missed cleavage)
7	963.01270 (+2)	1924.00975	1924.01264	-1.5	EVQLVQSGGGVERPGGSLR
8	963.01300 (+2)	1924.01035	1924.01264	-1.2	EVQLVQSGGGVERPGGSLR (proline isomer)
9	846.89142 (+2)	1691.76719	1691.75799	5.4	FNW(+14)YVDGVEVHN(+1)AK
10	855.39771 (+2)	1708.77977	1708.78454	-2.8	FNW(+32)YVDGVEVHNAK
11	841.40088 (+2)	1680.78611	1680.78963	-2.0	FNW(+4)YVDGVEVHNAK
12	839.40515 (+2)	1676.79465	1676.79471	0.0	FNWYVDGVEVHNAK
13	1209.93701 (+3)	3626.78755	3626.79063	-0.8	SYYASW(+32)YQQKPGQAPVLVIYGANNRPSGIPDR
14	1200.60706 (+3)	3598.79770	3598.79572	0.6	SYYASW(+4)YQQKPGQAPVLVIYGANNRPSGIPDR
15	1199.27539 (+3)	3594.802695	3594.80080	0.5	SYYASWYQQKPGQAPVLVIYGANNRPSGIPDR
16	1198.60107 (+3)	3592.77973	3592.78515	-1.5	SY(-2)YASWYQQKPGQAPVLVIYGANNRPSGIPDR
17	1422.73169 (+2)	2843.44773	2843.45020	-0.9	THTCPPCPAPELLGGPSVFLFPPKPK
18	904.50677 (+2)	1806.99789	1806.99922	-0.7	VVSVLTVLHQDWLNGK

Table 2. Summary of the identified peptides in the collected SCX fractions of Region A'' (oxidized mAb A). Peak number is as labeled in Figure 13.

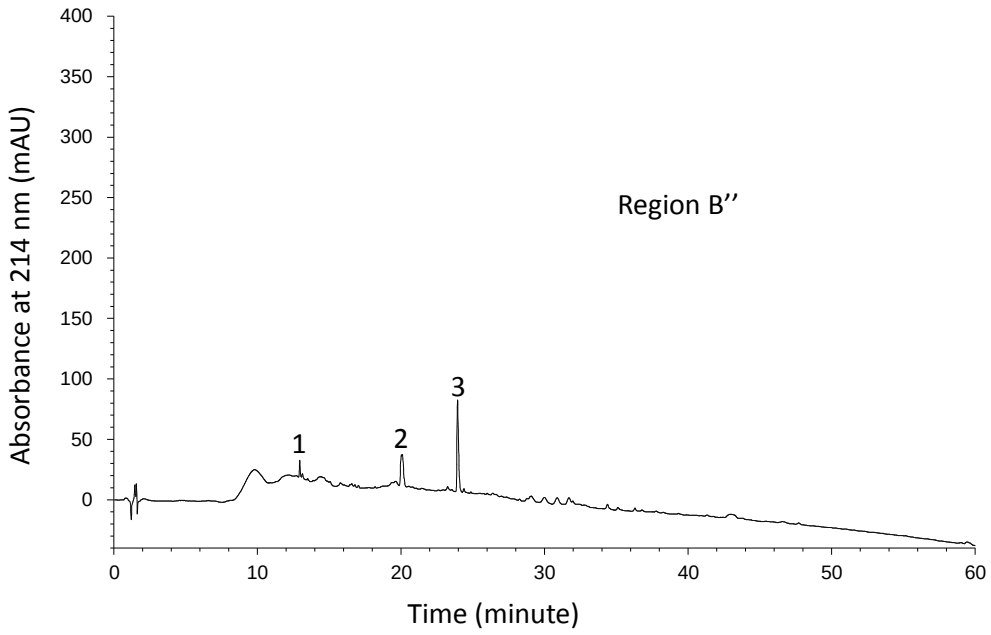

Figure 14. Analysis of collected SCX fractions of Region B'' (oxidized mAb A) by reversed-phase HPLC.

No.	Observed m/z (charge)	Observed Mass (Da)	Theoretical Mass (Da)	Mass Error (ppm)	Peptide ID
1	506.26868 (+2)	1010.52171	1010.52225	-0.54	NRPSGIPDR
2	1409.13550 (+2)	2816.24705	2816.24759	-0.19	WQQGNVFScSVM(-ox)HEALHNHYTQK
3	1401.13684 (+2)	2800.25803	2800.25858	-0.20	WQQGNVFScSVMHEALHNHYTQK

Table 3. Summary of the identified peptides in the collected SCX fractions of Region B'' (oxidized mAb A). Peak number is as labeled in Figure 14.

A

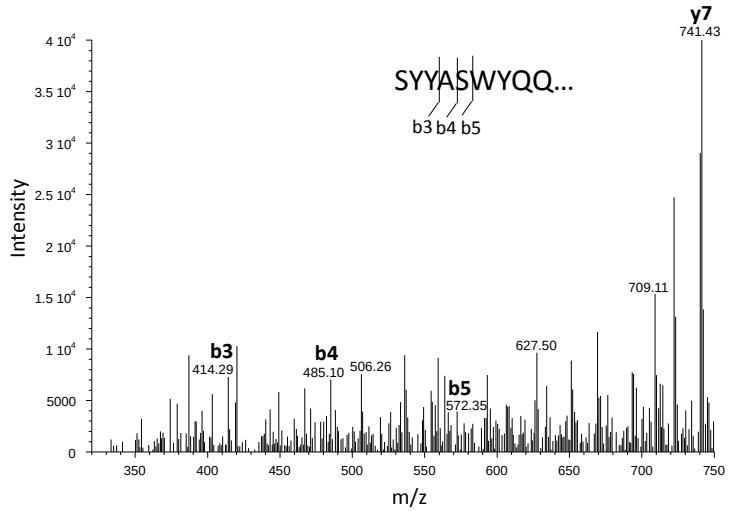

B

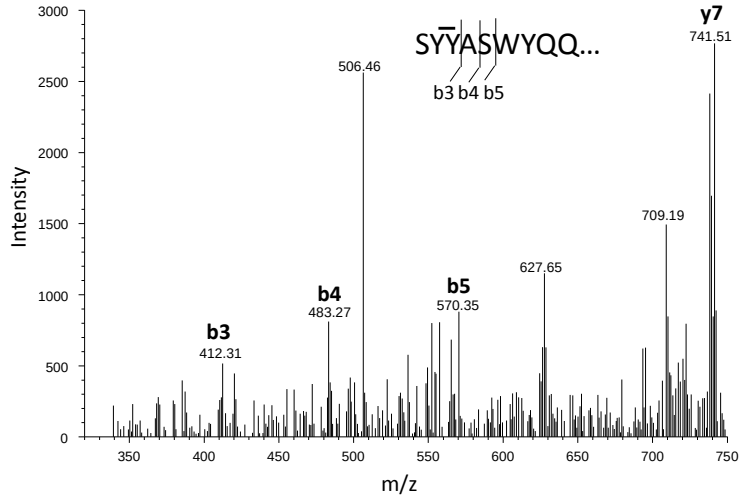

Figure 15. (A) Expanded view of the MS^2 spectrum of a tryptic peptide (wide type) that contains a potential intra-peptide dityrosine crosslink site. (B) Expanded view of the MS^2 spectrum of a tryptic peptide that could contain an intra-peptide dityrosine crosslink.

DISCUSSION

This study established a new analytical methodology, SEEMS^2, for the analysis of crosslinked peptides in complex mAb digest samples. This methodology focused on addressing several key challenges that crosslink analysis commonly faces in sample preparation and MS data analysis.[49] First, crosslinked peptides are usually in low abundance. To address this challenge, our method adopted an existing analytical strategy to enrich crosslinked peptides by strong cation exchange chromatography,[28] which has been successfully used in capturing chemically-crosslinked peptides in nuclear extracts from HeLa cells[37] and in bovine serum albumin and glutathione S-transferase.[28, 36] A benefit of this strategy is that the majority of the non-crosslinked tryptic peptides (+2 and +3 charged) are excluded from fraction collection, which reduces the complexity of the peptide samples in subsequent analyses. Second, crosslinked peptides are often hydrophobic and thus they can be lost or poorly recovered during sample preparation.[50] To address this challenge, we optimized sample preparation procedures to maximize the recovery of hydrophobic peptides. For trypsin digestion, mAb reduction, alkylation, and buffer exchange steps were in either 6 M guanidine hydrochloride or 6 M urea, which minimized mAb sample precipitation. For strong cation exchange chromatography, acetonitrile concentration in the mobile phase was 30%, a 20% increase from what was used by Fritzsche et al.,[36] and a 10% increase from what was used by Tinnefeld et al.[28] and Buncherd et al.[37] The increased acetonitrile concentration improves the recovery of large and hydrophobic peptides during strong cation exchange chromatography analysis, as demonstrated in the work by Alpert and Andrews.[46] The concentration of acetonitrile was not further increased due to a concern with the solubility of 500 mM sodium chloride in mobile phase B. It should be pointed out that the conventional O^{18} labeling method for crosslink analysis often requires lyophilization

of tryptic digests to minimize interference from residual O^{16} water and to ensure a more complete incorporation of O^{18} in the digested peptides.[29] It is not known how efficient hydrophobic peptides can be recovered after the lyophilization and reconstitution steps. By contrast, our method does not require any lyophilization in sample preparation. Therefore, from that perspective, our method should be superior to the O^{18} labeling method.

For the MS data analysis of crosslinked peptides, a major challenge is distinguishing the crosslinked peptide ions from the more abundant non-crosslinked peptide ions. To address this challenge, our method implemented the SEEMS^2 approach, where peptides of interest are fraction-collected and then digested with a non-specific protease (such as thermolysin). Subsequently, identification of crosslinked peptides relies on locating putative crosslink sites and extracting the MS^2 ions with reporter/signature masses. Compared to the O^{18} labeling strategy, the benefit of this analytical strategy is threefold. First, putative crosslink sites can be readily identified by using the commonly available database search software programs (such as proteome discover), while the O^{18} labeling method requires specialized software programs[29, 51] to survey full MS spectra in order to identify putative crosslink candidates. Second, this analytical strategy inherently generates fewer false positives since the number of non-crosslinked peptides is significantly reduced in the collected SCX fractions, while the O^{18} labeling strategy considers/surveys all peptide ions in a tryptic digest to identify putative crosslink candidates. Third, our analytical strategy provides a simplified process to interpret and decode MS^2 spectra. In particular, the reporter/signature MS^2 mass information enables a targeted investigation of the fragment ions in the MS^2 spectra, as illustrated by our case examples. By comparison, the O^{18} labeling strategy does not have such information for the analysis of the MS^2 spectra.

It should be pointed out that the use of reporter/signature MS^2 masses to extract/identify crosslinked peptide ions is not a novel concept. Iglesias et al. used signature MS^2 ions from lysine side chain rearrangement and the crosslink spacer in a precursor ion scan to identify chemically (by disuccinimidyl suberate) crosslinked peptides.[52] Barysz et al. used small fragments from cross-linker backbone and linked residues as signature MS^2 ions in their analysis of chemically crosslinked peptides.[47] Different from these reported cases, the reporter/signature MS^2 ions in our analytical strategy do not depend on the type of crosslink chemistry. In addition, the identification of the reporter/signature MS^2 masses is a simple process, which depends on the identification of a putative counterpart peptide after the digestion with a non-specific protease. Finally, our analytical strategy should be applicable to the identification of crosslinked products from different crosslinking reactions, as the terminal b or y ions from one or both linear peptide components are commonly present in the CID spectra of crosslinked peptides.[53]

Compared to many other existing analytical methods for crosslink analysis,[54-58] a key advantage of the $SEEMS^2$ approach is that this approach does not require a specialized software program for data analysis. The disadvantage of the $SEEMS^2$ approach is that this approach is labor-intensive. Nevertheless, this new approach should complement the existing analytical methods for crosslink analysis well. Future efforts to improve the $SEEMS^2$ approach will be focusing on using different non-specific proteases for generating more comprehensive peptide fragment coverage for the eMS^2 data. Another area for improvement is introducing HCD and ETD for generating reporter ions, which could help reduce false positives. Finally, it should be beneficial to use nanospray LC-MS/MS analysis for obtaining eMS^2 data, given the concern with analysis sensitivity and limited sample amount for the collected peptide fractions.

After demonstrating the feasibility of using the SEEMS^2 approach for crosslink analysis, we investigated potential crosslinked products in mAb A after copper-catalyzed oxidation. Selection of the copper oxidation condition instead of the iron oxidation conditions (as used in previous chapters) for our investigation was based on the following considerations. First, the study performed by Filipe et al. reported immunogenicity in an antibody stressed after copper-catalyzed oxidation.[7] We were interested in identifying crosslinked products under similar conditions to help elucidate potential sources of the immunogenicity. Second, copper-catalyzed oxidation was found to be the strongest stress condition among nine different metals evaluated for inducing carbonylation and aggregation on IgG and other proteins.[39-40] Potential crosslinked products (including Schiff base crosslinks, if present) are, therefore, expected to be more abundant with copper-catalyzed oxidation than with other stress conditions, which is beneficial to our investigation. Third, copper/hydrogen peroxide is more effective in causing dityrosine formation in lens proteins than iron/hydrogen peroxide.[41] In addition to investigating Schiff base crosslinked products, we were interested in understanding if copper/hydrogen peroxide can induce dityrosine crosslinks in mAbs.

Our study showed that Schiff base crosslinks are not a major degradation product of mAb A even after applying a harsh stress condition with copper ion and hydrogen peroxide. It is possible that the aldehyde products (from carbonylation of lysine, arginine, and proline residues) are not the major degradation products of mAb A. Additionally, the copper-catalyzed oxidation condition, such as copper concentration or incubation time, may not be optimal for the formation of Schiff base crosslinks. Nevertheless, our finding indicates that Schiff base crosslinks are unlikely a major source for the oxidation-induced acidic charge heterogeneity or aggregation propensity as hypothesized in previous chapters, although this will still need to be confirmed in

future studies with additional oxidation conditions. Our study tentatively identified a type 1 dityrosine crosslink product, which is consistent with existing reports in the literature showing that tyrosine crosslinks are major crosslink products after copper-catalyzed oxidation. To the best of our knowledge, dityrosine crosslink products have not been well characterized in mAbs. In future studies, it should be interesting to apply the $SEEMS^2$ approach to confirm and investigate such dityrosine crosslinked products of mAb A under various oxidation conditions.

Reference

1. Purdie, J. L.; Kowle, R. L.; Langland, A. L.; Patel, C. N.; Ouyang, A.; Olson, D. J., Cell culture media impact on drug product solution stability. *Biotechnol Prog* **2016,** *32* (4), 998-1008.

2. Bee, J. S.; Davis, M.; Freund, E.; Carpenter, J. F.; Randolph, T. W., Aggregation of a monoclonal antibody induced by adsorption to stainless steel. *Biotechnol Bioeng* **2010,** *105* (1), 121-9.

3. Yang, Y.; Mah, A.; Yuk, I. H.; Grewal, P. S.; Pynn, A.; Cole, W.; Gao, D.; Zhang, F.; Chen, J.; Gennaro, L.; Schoneich, C., Investigation of Metal-Catalyzed Antibody Carbonylation With an Improved Protein Carbonylation Assay. *J Pharm Sci* **2018**.

4. Dashivets, T.; Stracke, J.; Dengl, S.; Knaupp, A.; Pollmann, J.; Buchner, J.; Schlothauer, T., Oxidation in the complementarity-determining regions differentially influences the properties of therapeutic antibodies. *MAbs* **2016,** *8* (8), 1525-1535.

5. Stracke, J.; Emrich, T.; Rueger, P.; Schlothauer, T.; Kling, L.; Knaupp, A.; Hertenberger, H.; Wolfert, A.; Spick, C.; Lau, W.; Drabner, G.; Reiff, U.; Koll, H.; Papadimitriou, A., A novel approach to investigate the effect of methionine oxidation on pharmacokinetic properties of therapeutic antibodies. *MAbs* **2014,** *6* (5), 1229-42.

6. Kirkham, P. A.; Caramori, G.; Casolari, P.; Papi, A. A.; Edwards, M.; Shamji, B.; Triantaphyllopoulos, K.; Hussain, F.; Pinart, M.; Khan, Y.; Heinemann, L.; Stevens, L.; Yeadon, M.; Barnes, P. J.; Chung, K. F.; Adcock, I. M., Oxidative stress-induced antibodies to carbonyl-modified protein correlate with severity of chronic obstructive pulmonary disease. *Am J Respir Crit Care Med* **2011,** *184* (7), 796-802.

7. Filipe, V.; Jiskoot, W.; Basmeleh, A. H.; Halim, A.; Schellekens, H.; Brinks, V., Immunogenicity of different stressed IgG monoclonal antibody formulations in immune tolerant transgenic mice. *MAbs* **2012,** *4* (6), 740-52.

8. Joubert, M. K.; Hokom, M.; Eakin, C.; Zhou, L.; Deshpande, M.; Baker, M. P.; Goletz, T. J.; Kerwin, B. A.; Chirmule, N.; Narhi, L. O.; Jawa, V., Highly aggregated antibody therapeutics can enhance the in vitro innate and late-stage T-cell immune responses. *J Biol Chem* **2012,** *287* (30), 25266-79.

9. Rombach-Riegraf, V.; Karle, A. C.; Wolf, B.; Sorde, L.; Koepke, S.; Gottlieb, S.; Krieg, J.; Djidja, M. C.; Baban, A.; Spindeldreher, S.; Koulov, A. V.; Kiessling, A., Aggregation of human recombinant monoclonal antibodies influences the capacity of dendritic cells to stimulate adaptive T-cell responses in vitro. *PLoS One* **2014,** *9* (1), e86322.

10. Qian, F.; Reiter, K.; Zhang, Y.; Shimp, R. L., Jr.; Nguyen, V.; Aebig, J. A.; Rausch, K. M.; Zhu, D.; Lambert, L.; Mullen, G. E.; Martin, L. B.; Long, C. A.; Miller, L. H.; Narum, D. L., Immunogenicity of self-associated aggregates and chemically cross-linked conjugates of the 42 kDa Plasmodium falciparum merozoite surface protein-1. *PLoS One* **2012,** *7* (6), e36996.

11. Schilling, B.; Row, R. H.; Gibson, B. W.; Guo, X.; Young, M. M., MS2Assign, automated assignment and nomenclature of tandem mass spectra of chemically crosslinked peptides. *J Am Soc Mass Spectrom* **2003,** *14* (8), 834-50.

12. Torosantucci, R.; Sharov, V. S.; van Beers, M.; Brinks, V.; Schoneich, C.; Jiskoot, W., Identification of oxidation sites and covalent cross-links in metal catalyzed oxidized interferon Beta-1a: potential implications for protein aggregation and immunogenicity. *Mol Pharm* **2013,** *10* (6), 2311-22.

13. Torosantucci, R.; Mozziconacci, O.; Sharov, V.; Schoneich, C.; Jiskoot, W., Chemical modifications in aggregates of recombinant human insulin induced by metal-catalyzed oxidation: covalent cross-linking via michael addition to tyrosine oxidation products. *Pharm Res* **2012,** *29* (8), 2276-93.

14. Rauhamaki, V.; Baumann, M.; Soliymani, R.; Puustinen, A.; Wikstrom, M., Identification of a histidine-tyrosine cross-link in the active site of the cbb3-type cytochrome c oxidase from Rhodobacter sphaeroides. *Proc Natl Acad Sci U S A* **2006,** *103* (44), 16135-40.

15. Huggins, T. G.; Wells-Knecht, M. C.; Detorie, N. A.; Baynes, J. W.; Thorpe, S. R., Formation of o-tyrosine and dityrosine in proteins during radiolytic and metal-catalyzed oxidation. *J Biol Chem* **1993,** *268* (17), 12341-7.

16. Yoburn, J. C.; Tian, W.; Brower, J. O.; Nowick, J. S.; Glabe, C. G.; Van Vranken, D. L., Dityrosine cross-linked Abeta peptides: fibrillar beta-structure in Abeta(1-40) is conducive to formation of dityrosine cross-links but a dityrosine cross-link in Abeta(8-14) does not induce beta-structure. *Chem Res Toxicol* **2003,** *16* (4), 531-5.

17. Al-Hilaly, Y. K.; Biasetti, L.; Blakeman, B. J.; Pollack, S. J.; Zibaee, S.; Abdul-Sada, A.; Thorpe, J. R.; Xue, W. F.; Serpell, L. C., The involvement of dityrosine crosslinking in alpha-synuclein assembly and deposition in Lewy Bodies in Parkinson's disease. *Sci Rep* **2016,** *6*, 39171.

18. Stadtman, E. R.; Levine, R. L., Free radical-mediated oxidation of free amino acids and amino acid residues in proteins. *Amino Acids* **2003,** *25* (3-4), 207-18.

19. Hassib, H. B.; Abdel-Kader, N. S.; Issa, Y. M., Kinetic Study of the Hydrolysis of Schiff Bases Derived from 2-Aminothiophenol. *J Solution Chem* **2012,** *41* (11), 2036-2046.

20. Bradshaw, A.; Salt, M.; Bell, A.; Zeitler, M.; Litra, N.; Smith, A. M., Cross-linking by protein oxidation in the rapidly setting gel-based glues of slugs. *J Exp Biol* **2011,** *214* (Pt 10), 1699-706.

21. Rysman, T.; Utrera, M.; Morcuende, D.; Van Royen, G.; Van Weyenberg, S.; De Smet, S.; Estevez, M., Apple phenolics as inhibitors of the carbonylation pathway during in vitro metal-catalyzed oxidation of myofibrillar proteins. *Food Chem* **2016,** *211*, 784-90.

22. Giulivi, C.; Davies, K. J., Dityrosine and tyrosine oxidation products are endogenous markers for the selective proteolysis of oxidatively modified red blood cell hemoglobin by (the 19 S) proteasome. *J Biol Chem* **1993,** *268* (12), 8752-9.

23. Siegel, R. C.; Pinnell, S. R.; Martin, G. R., Cross-linking of collagen and elastin. Properties of lysyl oxidase. *Biochemistry* **1970,** *9* (23), 4486-92.

24. Page, R. C.; Benditt, E. P.; Kirkwood, C. R., Schiff base formation by the lysyl and hydroxylysyl side chains of collagen. *Biochem Biophys Res Commun* **1968,** *33* (5), 752-7.

25. Akagawa, M.; Suyama, K., Mechanism of formation of elastin crosslinks. *Connect Tissue Res* **2000,** *41* (2), 131-41.

26. Gineyts, E.; Borel, O.; Chapurlat, R.; Garnero, P., Quantification of immature and mature collagen crosslinks by liquid chromatography-electrospray ionization mass spectrometry in connective tissues. *J Chromatogr B Analyt Technol Biomed Life Sci* **2010,** *878* (19), 1449-54.

27. Naffa, R.; Holmes, G.; Ahn, M.; Harding, D.; Norris, G., Liquid chromatography-electrospray ionization mass spectrometry for the simultaneous quantitation of collagen and elastin crosslinks. *J Chromatogr A* **2016,** *1478*, 60-67.

28. Tinnefeld, V.; Venne, A. S.; Sickmann, A.; Zahedi, R. P., Enrichment of Cross-Linked Peptides Using Charge-Based Fractional Diagonal Chromatography (ChaFRADIC). *J Proteome Res* **2017,** *16* (2), 459-469.

29. Liu, M.; Zhang, Z.; Zang, T.; Spahr, C.; Cheetham, J.; Ren, D.; Zhou, Z. S., Discovery of undefined protein cross-linking chemistry: a comprehensive methodology utilizing 18O-labeling and mass spectrometry. *Anal Chem* **2013,** *85* (12), 5900-8.

30. Liu, M.; Zhang, Z.; Cheetham, J.; Ren, D.; Zhou, Z. S., Discovery and characterization of a photo-oxidative histidine-histidine cross-link in IgG1 antibody utilizing (1)(8)O-labeling and mass spectrometry. *Anal Chem* **2014,** *86* (10), 4940-8.

31. Gao, Q.; Xue, S.; Doneanu, C. E.; Shaffer, S. A.; Goodlett, D. R.; Nelson, S. D., Pro-CrossLink. Software tool for protein cross-linking and mass spectrometry. *Anal Chem* **2006,** *78* (7), 2145-9.

32. Back, J. W.; Notenboom, V.; de Koning, L. J.; Muijsers, A. O.; Sixma, T. K.; de Koster, C. G.; de Jong, L., Identification of cross-linked peptides for protein interaction studies using mass spectrometry and 18O labeling. *Anal Chem* **2002,** *74* (17), 4417-22.

33. Xie, F.; Liu, T.; Qian, W. J.; Petyuk, V. A.; Smith, R. D., Liquid chromatography-mass spectrometry-based quantitative proteomics. *J Biol Chem* **2011,** *286* (29), 25443-9.

34. Fenselau, C.; Yao, X., 18O2-labeling in quantitative proteomic strategies: a status report. *J Proteome Res* **2009,** *8* (5), 2140-3.

35. Tronrud, D. E.; Roderick, S. L.; Matthews, B. W., Structural basis for the action of thermolysin. *Matrix Suppl* **1992,** *1*, 107-11.

36. Fritzsche, R.; Ihling, C. H.; Gotze, M.; Sinz, A., Optimizing the enrichment of cross-linked products for mass spectrometric protein analysis. *Rapid Commun Mass Spectrom* **2012,** *26* (6), 653-8.

37. Buncherd, H.; Roseboom, W.; Ghavim, B.; Du, W.; de Koning, L. J.; de Koster, C. G.; de Jong, L., Isolation of cross-linked peptides by diagonal strong cation exchange chromatography for protein complex topology studies by peptide fragment fingerprinting from large sequence databases. *J Chromatogr A* **2014,** *1348*, 34-46.

38. Schmidt, C.; Robinson, C. V., A comparative cross-linking strategy to probe conformational changes in protein complexes. *Nat Protoc* **2014,** *9* (9), 2224-36.

39. Kryndushkin, D.; Rao, V. A., Comparative Effects of Metal-Catalyzed Oxidizing Systems on Carbonylation and Integrity of Therapeutic Proteins. *Pharm Res* **2016,** *33* (2), 526-39.

40. Kryndushkin, D.; Wu, W. W.; Venna, R.; Norcross, M. A.; Shen, R. F.; Rao, V. A., Complex Nature of Protein Carbonylation Specificity After Metal-Catalyzed Oxidation. *Pharm Res* **2017,** *34* (4), 765-779.

41. Kato, Y.; Kitamoto, N.; Kawai, Y.; Osawa, T., The hydrogen peroxide/copper ion system, but not other metal-catalyzed oxidation systems, produces protein-bound dityrosine. *Free Radic Biol Med* **2001,** *31* (5), 624-32.

42. Peach, M.; Marsh, N.; Macphee, D. J., Protein solubilization: attend to the choice of lysis buffer. *Methods Mol Biol* **2012,** *869*, 37-47.

43. Kim, S. C.; Chen, Y.; Mirza, S.; Xu, Y.; Lee, J.; Liu, P.; Zhao, Y., A clean, more efficient method for in-solution digestion of protein mixtures without detergent or urea. *J Proteome Res* **2006,** *5* (12), 3446-52.

44. Kollipara, L.; Zahedi, R. P., Protein carbamylation: in vivo modification or in vitro artefact? *Proteomics* **2013,** *13* (6), 941-4.

45. Sun, S.; Zhou, J. Y.; Yang, W.; Zhang, H., Inhibition of protein carbamylation in urea solution using ammonium-containing buffers. *Anal Biochem* **2014,** *446*, 76-81.

46. Alpert, A. J.; Andrews, P. C., Cation-exchange chromatography of peptides on poly(2-sulfoethyl aspartamide)-silica. *J Chromatogr* **1988,** *443*, 85-96.

47. Barysz, H. M.; Malmstrom, J., Development of Large-scale Cross-linking Mass Spectrometry. *Mol Cell Proteomics* **2018,** *17* (6), 1055-1066.

48. Mark A. Blaskovich, a. G. A. L., Synthesis of a Chiral Serine Aldehyde Equivalent and Its Conversion to Chiral-Amino Acid Derivatives. *J. Am. Chem. Soc.* **1993,** *115*, 5021-5030.

49. Maes, E.; Dyer, J. M.; McKerchar, H. J.; Deb-Choudhury, S.; Clerens, S., Protein-protein cross-linking and human health: the challenge of elucidating with mass spectrometry. *Expert Rev Proteomics* **2017,** *14* (10), 917-929.

50. Rappsilber, J., The beginning of a beautiful friendship: cross-linking/mass spectrometry and modelling of proteins and multi-protein complexes. *J Struct Biol* **2011,** *173* (3), 530-40.

51. Gao, Q.; Xue, S.; Shaffer, S. A.; Doneanu, C. E.; Goodlett, D. R.; Nelson, S. D., Minimize the detection of false positives by the software program DetectShift for 18O-labeled cross-linked peptide analysis. *Eur J Mass Spectrom (Chichester)* **2008,** *14* (5), 275-80.

52. Iglesias, A. H.; Santos, L. F.; Gozzo, F. C., Identification of cross-linked peptides by high-resolution precursor ion scan. *Anal Chem* **2010,** *82* (3), 909-16.

53. Giese, S. H.; Fischer, L.; Rappsilber, J., A Study into the Collision-induced Dissociation (CID) Behavior of Cross-Linked Peptides. *Mol Cell Proteomics* **2016,** *15* (3), 1094-104.

54. Hoopmann, M. R.; Zelter, A.; Johnson, R. S.; Riffle, M.; MacCoss, M. J.; Davis, T. N.; Moritz, R. L., Kojak: efficient analysis of chemically cross-linked protein complexes. *J Proteome Res* **2015,** *14* (5), 2190-8.

55. Fan, S. B.; Meng, J. M.; Lu, S.; Zhang, K.; Yang, H.; Chi, H.; Sun, R. X.; Dong, M. Q.; He, S. M., Using pLink to Analyze Cross-Linked Peptides. *Curr Protoc Bioinformatics* **2015,** *49*, 8 21 1-19.

56. Yu, F.; Li, N.; Yu, W., ECL: an exhaustive search tool for the identification of cross-linked peptides using whole database. *BMC Bioinformatics* **2016,** *17* (1), 217.

57. Yilmaz, S.; Drepper, F.; Hulstaert, N.; Cernic, M.; Gevaert, K.; Economou, A.; Warscheid, B.; Martens, L.; Vandermarliere, E., Xilmass: A New Approach toward the Identification of Cross-Linked Peptides. *Anal Chem* **2016,** *88* (20), 9949-9957.

58. Chu, F.; Baker, P. R.; Burlingame, A. L.; Chalkley, R. J., Finding chimeras: a bioinformatics strategy for identification of cross-linked peptides. *Mol Cell Proteomics* **2010,** *9* (1), 25-31.

Chapter 6

Conclusions and Future Work

6.1: Investigation of Antibody Carbonylation during Process Development (Chapter 2)

This chapter reviewed the current analytical assays for measuring total protein carbonylation levels, and then focused on developing a new protein carbonylation assay, CALY, to address the analytical challenges/drawbacks with the conventional protein carbonylation assays. After demonstrating that CALY is more robust and precise than the conventional assays, we applied CALY to investigate antibody carbonylation under production, storage, and stress conditions and showed that iron, hydrogen peroxide, and polysorbate 20 at pharmaceutically relevant levels critically influence the extent of mAb carbonylation. In addition, we investigated the impact of carbonylation on antibody product quality. We found that carbonylation cannot be used as a general indicator for aggregation, even though carbonylation correlates with antibody aggregation in several cases. We also found that antibody carbonylation level can decrease during storage, which indicates that carbonylation products may not be stable. Finally, we report for the first time a positive correlation between carbonylation and acidic charge heterogeneity of antibodies that underwent metal-catalyzed oxidation. This finding shows that the impact of protein carbonylation on product quality for antibodies is not limited to aggregation but also extends to charge heterogeneity.

For future study, CALY can be used to investigate additional cell culture factors that impact antibody carbonylation and related product quality. For example, recently, Vijayasankaran et al. reported the use of hypotaurine, hydrocortisone, peptone, and cysteine as cell culture additives to reduce antibody coloration and acidic charge variants.[1] It will be interesting to understand if the reduction in acidic charge variants was actually achieved through reduction of antibody carbonylation, and if so, how these cell culture additives interact with iron ions or hydrogen peroxide to reduce antibody carbonylation. Specifically, among these additives,

hydrocortisone is known to reduce hydrogen peroxide production in cells.[2-3] It is plausible that the hydrocortisone reduces hydrogen peroxide production in CHO cells, which could lead to decreased antibody carbonylation. Answering these questions can further elucidate the mechanisms of antibody carbonylation in the cell culture environment and help better control antibody carbonylation during production. Another cell culture factor worth investigating is the effect of ambient light on antibody carbonylation during cell culture production. Mallaney et al. reported that antibody acidic variant level increased when the cell culture production was exposed to ambient light.[4] The cause for the increased acidic variants was attributed to light-induced oxidation, as the antibody showed a similar increase in the acidic variants under ICH light stress conditions.[4] However, since many cell culture medium components are known photosensitizers[5] and can generate hydrogen peroxide upon light exposure, it is possible that ambient light promotes antibody carbonylation by increasing hydrogen peroxide levels during cell culture production. Clearly, CALY will be a very useful analytical tool to help discern the different mechanisms that lead to the increased acidic charge variants during cell culture process development.

6.2: Characterization of Acidic Charge Heterogeneity of Antibodies Induced by Metal-Catalyzed Oxidation (Chapter 3)

Our research findings from Chapter 2 strongly suggest that metal-catalyzed carbonylation may represent a general degradation mechanism for inducing acidic charge heterogeneity in mAbs. In particular, carbonylation of positive residues, such as lysine and arginine, can lead to loss of the positive charge, which should contribute to the increased acidic charge variants. However, to date, the induced acidic charge heterogeneity has not been well characterized. This chapter therefore focused on studying the mechanism and the related degradation products that

account for the induced acidic charge variants after metal-catalyzed oxidation. With a model IgG1 antibody, we fraction collected the acidic charge variants generated after metal-catalyzed oxidation. We then characterized the collected fractions with a large variety of analytical methods, such as SEC, intact/reduced mass analysis, and peptide mapping. Specifically, we analyzed antibody carbonylation products at both protein and peptide levels. We showed that the commonly observed methionine and tryptophan oxidation products cannot satisfactorily explain the formation of oxidation-induced acidic charge variants. On the other hand, carbonylation products were found to be enriched in the acidic fractions at both protein and peptide levels. Surprisingly, a threonine carbonylation product, but not lysine and arginine carbonylation products, was found to be a major component enriched in the acidic fractions. Additionally, our characterization identified several novel degradation products that have not been previously reported in mAbs. One of these products is the carboxylic acid product formed after further oxidation of arginine and proline carbonylation products. Another product is the pyroglutamate product from oxidation of proline residues in the hinge region, whose formation also leads to hinge fragmentation. Finally, H/D exchange analysis of the acidic and main peak fractions showed that metal-catalyzed oxidation did not induce any significant change in mAb conformation, which suggests that the induced acidic charge variants is likely not caused by conformational factors.

For future study, it will be interesting to understand the mechanism(s) for the enrichment of threonine carbonylation product (2-amino-3-ketobutyrate), a ketone, in the acidic fraction. One hypothesis is the deprotonation of alpha hydrogen in 2-amino-3-ketobutyrate. This hypothesis is based on an observation that beta-diketone compounds have unusually acidic alpha hydrogens (with a pKa of 9 or lower[6]), where deprotonation of their alpha hydrogens becomes

easier due to stabilization of the deprotonated species through multiple resonance structures.[6] It is possible that, in certain protein structures, a similar mechanism may exist, which could partially contribute to the enrichment of the threonine carbonylation product in the acidic fraction. In the future, we will perform a pH titration study to determine the pKa of threonine carbonylation product to understand if this could be the source of the apparent increase in antibody acidic charge heterogeneity. Another topic worth investigating is the formation of the pyroglutamate product from oxidation of proline residues in the hinge region, which also causes hinge fragmentation. To the best of our knowledge, such a hinge fragmentation mechanism has not been reported in the literature. To evaluate our proposed mechanism, we will conduct the oxidation reaction in O^{18} or O^{16} water and with O^{18} or O^{16} molecular oxygen. This experiment will reveal the source of the oxygen introduced to the pyroglutamate product and into the carboxylic acid (C-terminus of the other fragment peptide), which can confirm or rule out the mechanism we proposed. Finally, based on the relative quantitation of the site-specific carbonylation products on mAb 1, we identified a carbonylation hotspot on LC T29, which is adjacent to two aspartic acid residues. Considering that aspartic acid could be a metal-binding site,[7] it is possible that the TXDD sequence represents a motif for a carbonylation hotspot. In future studies, we will study model peptides, such as XXTDD, XXTXDD, XXTXXDD, XXTXXXDD, that have different numbers of residues between the carbonylation site (T) and the two DD residues, to understand the role/effect of adjacent aspartic acid residues on metal-catalyzed carbonylation. This study could help us gain more insight on site-specific carbonylation and design mAbs that are more stable against metal-catalyzed carbonylation in the future.

6.4: Physical Instability of Antibody induced by Metal-Catalyzed Carbonylation (Chapter 4)

Existing experimental observations suggested that metal-catalyzed carbonylation may drive formation of protein aggregates.[8-10] A theoretical study using molecular dynamics simulations also indicated that lysine and arginine carbonylation can significantly increase intrinsic aggregation propensity of proteins, and that the formation of these carbonylation products is equivalent of introducing charge-neutral hydrophobic residues on proteins.[11] To gain a better understanding on how metal-catalyzed carbonylation impacts mAb physical stability, this chapter studied the aggregation/precipitation of a carbonylated IgG1 antibody in buffers containing various Hofmeister anions.[12] A commonly used stir stress condition was applied to generate the mAb aggregates/precipitates. The extent of mAb carbonylation in the supernatants was then studied at both protein and peptide levels to assess the effect of carbonylation on the induced physical instability. We showed that mAb intrinsic aggregation propensity plays a more dominant role than carbonylation (even at a relatively high level) in the formation of mAb aggregates/precipitates. More critically, for the first time, we showed that the effect of carbonylation on physical instability of mAbs depends on the type of the carbonyls, the location of the carbonyls on antibodies, and the type of Hofmeister anion. In particular, for type 2 carbonylation products, their effect on mAb aggregation/precipitation appeared to depend on specific ion-pairing interactions between the Hofmeister anions and the positively charged residues that are adjacent to the carbonylation site.

For future study, it will be interesting to apply similar buffer/stress conditions to additional antibodies or other proteins (such as BSA). These investigations will help us understand if the effects of carbonylation that we discovered from the model IgG1 antibody are generally

applicable to other proteins. Additionally, for the type 2 carbonylation products, it will be interesting to test our hypothesis regarding the effect of the adjacent positively charged residues by performing site-directed mutagenesis. If our hypothesis is confirmed, it could provide a new approach to designing mAbs with improved stability against metal-catalyzed oxidation. Finally, The stability of mAb carbonylation in biological systems may differ significantly from that in buffers. For example, intracellularly, mildly carbonylated proteins are targeted for turn-over by proteolysis, while extensively carbonylated proteins may escape proteolysis by forming high molecular weight species.[13] In addition, a thiol-dependent decarbonylation mechanism was reported in biological systems.[14] Therefore, it will be interesting to study chemical and physical consequences of carbonylated mAbs in additional in vitro (such as plasma) and in vivo systems. In particular, it will be interesting to understand if any decarbonylation process may exist when relevant biological factors are present. For an initial assessment, a time course study by incubating carbonylated mAbs in plasma and PBS will be performed to characterize specific physiochemical changes to mAb carbonylation, which can provide insights into the consequence of mAb carbonylation under in vivo conditions.

6.5: Investigation of Antibody Crosslinks after Metal-Catalyzed Oxidation (Chapter 5)

Our research findings in Chapters 3 and 4 suggest that formation of Schiff base crosslinks could contribute to the formation of acidic charge variants and aggregates. To help investigate if Schiff base crosslinks represent a major factor for the induced chemical and physical instability of mAbs after metal-catalyzed oxidation, this chapter developed a new analytical method, SEEMS^2, for enriching and identifying crosslinked peptides. Compared to the existing methods, our method significantly reduces the difficulties with interpreting the MS^2 spectra of crosslink

peptides and our method does not require any specialized software program to identify crosslinked peptides. To demonstrate the feasibility of the SEEMS^2 approach, we successfully identified more than a dozen crosslinked peptides from a BS3-crosslinked mAb. We subsequently applied this approach to investigate mAb crosslinks after copper-catalyzed oxidation. Our data showed that, even under a harsh oxidation condition, no significant Schiff base crosslink was observed in the tested mAb sample. This finding suggests that Schiff base crosslinks are not a major factor for the induced chemical and physical instability of mAbs after metal-catalyzed oxidation, at least for the tested mAb sample under the copper-catalyzed oxidation condition. Interestingly, we tentatively identified a di-tyrosine intra-peptide crosslink in the tested mAb sample, which is consistent with the crosslink products that occurred on other proteins after copper-catalyzed oxidation.[15-16]

For future study, it will be interesting to further confirm that Schiff base crosslinks are not a significant degradation product by evaluating additional metal-catalyzed oxidation conditions. It will be also interesting to apply the SEEMS^2 approach to study mAb crosslinks after light stress or Maillard reactions. Finally, the SEEMS^2 method provides a new tool for chemical crosslinking mass spectrometry.[17-20] It will be interesting to apply the SEEMS^2 method to structural and functional analysis of proteins in the future.

Reference

1. Vijayasankaran, N.; Varma, S.; Yang, Y.; Meier, S.; Kiss, R., Effect of cell culture medium additives on color and acidic charge variants of a monoclonal antibody. *Biotechnol Prog* **2018,** *34* (5), 1298-1307.

2. Mandell, G. L.; Rubin, W.; Hook, E. W., The effect of an NADH oxidase inhibitor (hydrocortisone) on polymorphonuclear leukocyte bactericidal activity. *J Clin Invest* **1970,** *49* (7), 1381-8.

3. Levine, P. H.; Hardin, J. C.; Scoon, K. L.; Krinsky, N. I., Effect of corticosteroids on the production of superoxide and hydrogen peroxide and the appearance of chemiluminescence by phagocytosing polymorphonuclear leukocytes. *Inflammation* **1981,** *5* (1), 19-27.

4. Mallaney, M.; Wang, S. H.; Sreedhara, A., Effect of ambient light on monoclonal antibody product quality during small-scale mammalian cell culture process in clear glass bioreactors. *Biotechnol Prog* **2014,** *30* (3), 562-70.

5. McElearney, K.; Ali, A.; Gilbert, A.; Kshirsagar, R.; Zang, L., Tryptophan oxidation catabolite, N-formylkynurenine, in photo degraded cell culture medium results in reduced cell culture performance. *Biotechnol Prog* **2016,** *32* (1), 74-82.

6. John W. Bunting, J. P. K., Raymond Nelander, Zhennan Wu, The acidity and tautomerism of beta-diketones in aqueous solution *Can. J. Chem.* **1995,** *73*, 1305-1311.

7. Yamashita, M. M.; Wesson, L.; Eisenman, G.; Eisenberg, D., Where metal ions bind in proteins. *Proc Natl Acad Sci U S A* **1990,** *87* (15), 5648-52.

8. Purdie, J. L.; Kowle, R. L.; Langland, A. L.; Patel, C. N.; Ouyang, A.; Olson, D. J., Cell culture media impact on drug product solution stability. *Biotechnol Prog* **2016,** *32* (4), 998-1008.

9. Bee, J. S.; Davis, M.; Freund, E.; Carpenter, J. F.; Randolph, T. W., Aggregation of a monoclonal antibody induced by adsorption to stainless steel. *Biotechnol Bioeng* **2010,** *105* (1), 121-9.

10. Yang, Y.; Mah, A.; Yuk, I. H.; Grewal, P. S.; Pynn, A.; Cole, W.; Gao, D.; Zhang, F.; Chen, J.; Gennaro, L.; Schoneich, C., Investigation of Metal-Catalyzed Antibody Carbonylation With an Improved Protein Carbonylation Assay. *J Pharm Sci* **2018**.

11. Petrov, D.; Zagrovic, B., Microscopic analysis of protein oxidative damage: effect of carbonylation on structure, dynamics, and aggregability of villin headpiece. *J Am Chem Soc* **2011,** *133* (18), 7016-24.

12. Okur, H. I.; Hladilkova, J.; Rembert, K. B.; Cho, Y.; Heyda, J.; Dzubiella, J.; Cremer, P. S.; Jungwirth, P., Beyond the Hofmeister Series: Ion-Specific Effects on Proteins and Their Biological Functions. *J Phys Chem B* **2017,** *121* (9), 1997-2014.

13. Nystrom, T., Role of oxidative carbonylation in protein quality control and senescence. *EMBO J* **2005,** *24* (7), 1311-7.

14. Wong, C. M.; Marcocci, L.; Das, D.; Wang, X.; Luo, H.; Zungu-Edmondson, M.; Suzuki, Y. J., Mechanism of protein decarbonylation. *Free radical biology & medicine* **2013,** *65*, 1126-33.

15. Kato, Y.; Kitamoto, N.; Kawai, Y.; Osawa, T., The hydrogen peroxide/copper ion system, but not other metal-catalyzed oxidation systems, produces protein-bound dityrosine. *Free Radic Biol Med* **2001,** *31* (5), 624-32.

16. Atwood, C. S.; Perry, G.; Zeng, H.; Kato, Y.; Jones, W. D.; Ling, K. Q.; Huang, X.; Moir, R. D.; Wang, D.; Sayre, L. M.; Smith, M. A.; Chen, S. G.; Bush, A. I., Copper mediates dityrosine cross-linking of Alzheimer's amyloid-beta. *Biochemistry* **2004,** *43* (2), 560-8.

17. Rappsilber, J., The beginning of a beautiful friendship: cross-linking/mass spectrometry and modelling of proteins and multi-protein complexes. *J Struct Biol* **2011,** *173* (3), 530-40.

18. Sinz, A., Cross-Linking/Mass Spectrometry for Studying Protein Structures and Protein-Protein Interactions: Where Are We Now and Where Should We Go from Here? *Angew Chem Int Ed Engl* **2018,** *57* (22), 6390-6396.

19. Yu, C.; Huang, L., Cross-Linking Mass Spectrometry: An Emerging Technology for Interactomics and Structural Biology. *Anal Chem* **2018,** *90* (1), 144-165.

20. Leitner, A.; Faini, M.; Stengel, F.; Aebersold, R., Crosslinking and Mass Spectrometry: An Integrated Technology to Understand the Structure and Function of Molecular Machines. *Trends Biochem Sci* **2016,** *41* (1), 20-32.